

BULGARIAN CHEMICAL COMMUNICATIONS

2013 Volume 45/ Number 3

*Journal of the Chemical Institutes
of the Bulgarian Academy of Sciences
and of the Union of Chemists in Bulgaria*

Novel enantioselective synthesis and dissolution studies on enteric coated pellets of (*S*)-duloxetine hydrochloride

R. Venkatram*, V.K. Pai, S. Nagaraj

Department of Studies in Industrial Chemistry, Kuvempu University, Shankargatta, India

Received July 2, 2011; Revised June 4, 2012

The enantioselective hydrogenation of 2-bromo-1-(thiophen-2-yl)ethanone and further elaboration of the cyclic carbamate derived from γ -aminoalcohol to provide a facile synthesis of (*S*)-duloxetine, a potent dual inhibitor of serotonin and norepinephrine reuptake, is described. Enteric coated pellets with polymer load of 25% and 30% failed to provide the required acid resistance of the pellets. Very insignificant amount of drug was leached from the coated tablets with polymer load 35% and 40% in the acidic phase, whereas almost the whole amount of drug was released in the buffer phase. The results generated in this study showed that the proper selection of polymeric materials based on their physicochemical properties, as well as the polymer load is important in designing delayed release pellets dosage form with acceptable dissolution profile.

Keywords: Enantioselective synthesis, Eudragit L30 D 55, duloxetine hydrochloride, enteric coated pellets, powder layering.

INTRODUCTION

Duloxetine, a medication with effects on both serotonin and noradrenaline transporter molecules, has recently been approved for the treatment of generalized anxiety disorder. Serotonin and norepinephrine neurotransmitters are intimately involved in a number of neurochemical and physiological processes, such as depression and pain disorders. Selective serotonin or norepinephrine reuptake inhibitors are currently an important class of antidepressants, which includes fluoxetine, nisoxetine, tomoxetine, and duloxetine [1]. They have been already approved as racemates, but some of them are since being redeveloped as 'chiral switches' derived from the established racemates [2]. While fluoxetine and nisoxetine are currently available as racemates, (*S*)-duloxetine [(*S*)-*N*-methyl-3-(1-naphthoxy)-3-(2-thienyl)-1-propanamine] has gained acceptance in the market because it inhibited serotonin reuptake in rat synaptosomes two times more potently than the (*R*)-enantiomer [3]. The (*S*)-duloxetine, a dual inhibitor of both serotonin and norepinephrine reuptake, is effective for the treatment of major depressive disorders and is being considered for treatment of stress-related urinary incontinence. Several different approaches have been reviewed for the synthesis of duloxetine as a racemate or an enantiomerically enriched form [4]. However, there

are only a few reports on the asymmetric and catalytic synthesis of duloxetine. One of the methods employs asymmetric reduction of β -aminoketone or α -cyanoketone/ β -chloroketone with a chiral modified LAH complex [5] or an oxazaborolidine-catalyzed borane, respectively [6]. The other involves chemoenzymatic synthesis, for the most part, lipase-mediated resolution of β -cyano-, γ -chloro-, and γ -azidoalcohols [7].

Recently, the application of asymmetric-transfer hydrogenation has been extended to enantioselective hydrogenation of unsaturated carbonyl and imine groups [8]. The asymmetric-transfer hydrogenation, rather, offers operational simplicity, since the reaction does not involve molecular hydrogen and is insensitive to air oxidation, and thus is particularly valuable in scale-up syntheses of active pharmaceutical ingredients. In continuation of our earlier efforts towards the preparation of biologically important compounds, particularly possessing a chiral aminoalcohol unit [9] we herein report asymmetric-transfer hydrogenation of 2-tosyloxy-1-(2-thiophenyl)ethanone and further elaboration of a cyclic carbamate to access the facile synthesis of duloxetine.

The enteric film coat is a special film coat designed to resist gastric fluids and disrupt or dissolve in small intestine. The enteric coat is used to protect drug from degrading in stomach or to minimize the gastric distress caused by some drugs. Enteric coated pellets must empty from stomach

* To whom all correspondence should be sent:
E-mail: hurulihalli@yahoo.com

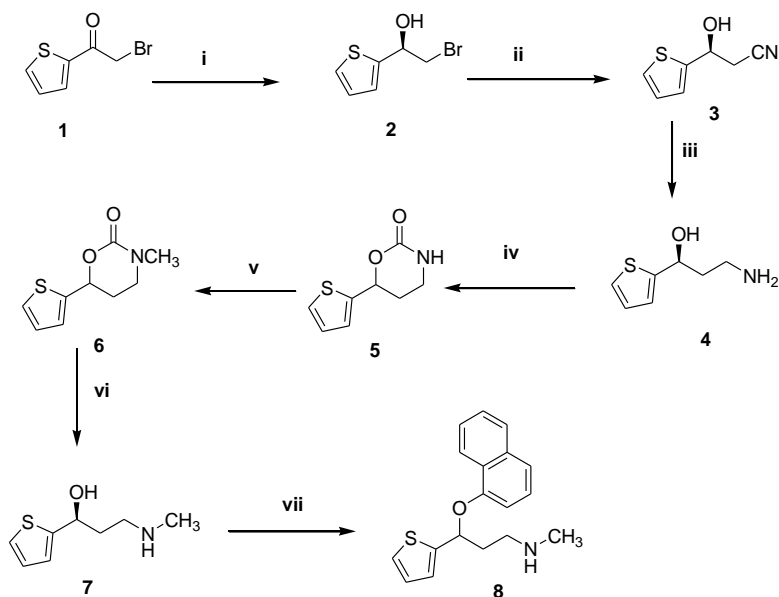
before absorption begins. The rate of appearance of blood after giving the enteric coated tablets is the function of gastric emptying. The differences in the gastric emptying from one patient to another or in the same patient with different administration were found to be largely variable in absorption commonly found in this dosage form. The enteric coated tablets approximately require 0.8 to 5 h to travel from stomach to duodenum but enteric coated pellets dispersed in the stomach pass through pyloric sphincter after a mean residence time in the stomach similar to that of a suspension dosage form [10]. The synthesized (*S*)-duloxetine hydrochloride was formulated as enteric tablets and was evaluated for various characteristics including dissolution rate. The possibility of increasing the dissolution rate of duloxetine through formulated enteric coated pellets was investigated.

RESULTS AND DISCUSSION

The starting material, 2-bromo-1-(thiophen-2-yl) ethanone **1** was prepared by photochemical reaction of *n*-bromo succinamide in carbon tetrachloride in the presence of catalytic amount of benzoyl peroxide. The catalytic reaction of **1** (substrate/catalyst molar ratio 500) with Cp*RhCl[(*S,S*)-TsDPEN] [11] where Cp* = pentamethylcyclopentadienyl, was effectively performed with an azeotropic mixture of formic acid/triethylamine (molar ratio 5/2) in ethyl acetate to produce (*S*)-2-tosyloxy-1-(2-thiophenyl)ethanol **2**, $[\alpha]_{\text{D}}^{27} = -31.3$ (*c* 1.08, CHCl₃), in 95% yield with 95% *ee*. It should be noted that the observed enantioselectivity was similar to that reported for the corresponding α -chloroketone [12] and thus represented a first successful application of α -tosyloxy heteroaryl ketone in transfer hydrogenation with high enantioselectivity. The *ee* value was measured by chiral HPLC analysis using Daicel Chiralcel OD-H column. The racemic alcohol (\pm)-**2** was prepared by sodium borohydride reduction of **1** in THF, and was used as a standard for *ee* determination.

In turn, most approaches to the synthesis of *N*-methylamine **7** routinely adopted lithium aluminum hydride reduction in refluxing THF of the ethyl carbamate derived from the aminoalcohol **4** with ethyl chloroformate, or mono-demethylation of the reduced Mannich product with 2,2,2-trichloroethyl formate with Zn in toluene. In order to circumvent these harsh conditions, we supposed that the formation of a cyclic carbamate [13] would offer a facile route to the introduction of an *N*-methyl

group into the γ -aminoalcohol, as shown in Scheme 1. It was envisioned that the required aminoalcohol **4** can be easily prepared from the tosylate **2**, a versatile chiral building block. Thus, the tosylate (*S*)-**2** was readily converted into the nitrile **3** without loss of chirality, $[\alpha]_{\text{D}}^{20} = -39.7$ (*c* 0.45, CHCl₃); lit.[7b] $[\alpha]_{\text{D}}^{30} = -33.5$ (*c* 1, CHCl₃), by the treatment of sodium cyanide in DMSO. Subsequently, the nitrile **3** was reduced with borane-dimethyl sulfide in refluxing THF to give the γ -aminoalcohol which was directly cyclized using *N,N*-carbonyldiimidazole (CDI) in the presence of catalytic amount of DMAP to obtain the corresponding cyclic carbamate **5** in 71% yield for the two steps. Indeed, this allowed a facile introduction of the *N*-methyl group, by the treatment of methyl iodide with sodium hydride in THF to give the *N*-methyl oxazinanone **6**. Hydrolysis of the oxazinanone **6** by refluxing with lithium hydroxide in aqueous methanol afforded the aminoalcohol **7**. The final installation was then carried out by nucleophilic aromatic substitution with 1-fluoronaphthalene by means of sodium hydride in DMSO to afford (*S*)-duloxetine **8** in 78% yield with 95% *ee* [14]. Duloxetine hydrochloride powder, mannitol and disodium hydrogen phosphate were blended and sieved through 250 micron screen mesh to prepare dusting powder. Disodium hydrogen phosphate and sodium hydroxide were dissolved in purified water. HPMC 5 cps was then dispersed using a stirrer to prepare the binding solution. NPS (710 micron – 1.0 mm) was taken in a conventional coating pan and dusting powder was applied on it. The pan rotated at 40 rpm and simultaneously binding solution was sprayed onto the NPS. After completion of drug loading, the nuclei were dried in an oven at 100°C for 5 h. The dried nuclei were sieved in a 1.18 mm screen mesh followed by 850 mm screen mesh to get the desired size (850 micron to 1.18 mm). The under- and oversized nuclei were discarded. Seal coating suspension was prepared containing HPMC 5 cps, PEG-6000, titanium dioxide, sodium hydroxide pellets with the use of a Silverson stirrer (UK). The dried uncoated nuclei were taken in a fluid bed coater and seal coating suspension was sprayed onto it. The sealed coated pellets were dried at 60°C for 3 h. Dried seal coated pellets were sieved through 1.18 mm and 850 micron to get 850 micron to 1.18 mm seal coated pellets. Under- and oversized nuclei were discarded. Enteric coated suspension was prepared by Eudragit L 30 D 55 (ammonium methacrylate



Scheme 1. Asymmetric synthesis of (S)-duloxetine. Reagents and conditions: i) 10 mmol of 1 (S/C=500), Cp*RhCl[(S,S)-TsDPEN], HCO₂H/Et₃N (molar ratio 5/2, 2 ml), EtOAc, 3h, 95%, 95%ee; ii) NaCN, DMSO, 20h, 88%; iii) BH₃SMe₂, THF, reflux, 2h; iv) CDI, cat. DMAP, CH₂Cl₂, 8h, 71% (for 2 steps); v) MeI, NaH, THF, ice-bath, 6h, 89%; vi) LiOH, MeOH-H₂O, reflux, 8h, 84%; vii) 1-fluoronaphthalene, Nah, DMSO, 8h, 78%.

copolymer dispersion), talc, triethyl citrate, titanium dioxide and purified water with the use of a Silverson stirrer. The seal coated pellets were coated using lab coater with Eudragit L 30 D 55 to a thickness equivalent to a theoretical polymer load of 25%, 30%, 35% and 40% w/w on dry basis.

Table 1. Composition of nuclei and seal coated pellets (weights are expressed in grams)

Nuclei	Quantity	Seal coating	Quantity
Duloxetine hydrochloride	256.24	Nuclei	800.00
Disodium hydrogen phosphate	5.53	HMPC	50.42
HMPC	38.30	PEG-6000	6.824
Mannitol	21.56	Sodium hydroxide pellets	0.060
		Titanium dioxide	10.48
Sodium hydroxide pellets	0.452	Weight of seal coated pellets	836.00
NPS	677.90	Potency of seal coated nuclei	23.00
Weight of nuclei	920.00		
Potency of nuclei	25.30		

The enteric coated pellets were dried in a fluid bed coater at 60°C for 5 h and then sieved through 1.40 mm and 850 micron mesh to get 850 micron - 1.40 mm size enteric coated pellets by discarding under- and oversized pellets. In this way all lots of pellets were coated according to the formula for F-1 to F-4 (Table 2). The compositions of nuclei and seal pellets are shown in Tables 1 and 2. Machine parameters during fluid coating are shown in Table 3.

Table 2. Codes and formulation of duloxetine enteric coated tablets

Materials	Formulation codes			
	F1	F2	F3	F4
Seal coated pellets	200.00	200.00	200.00	200.00
Sodium hydroxide pellets	0.590	0.702	0.826	0.942
Titanium dioxide	2.250	3.024	3.524	4.212
Methacrylic acid copolymer dispersion	166.67	200.00	233.23	265.65
Purified talc	1.889	2.645	2.657	3.021
Triethyl dispersion	8.062	9.673	11.28	12.900
Weight of the enteric coated pellets	237.00	240.00	256.34	266.43
Potency of enteric coated pellets	17.52	16.72	15.75	15.23

Table 3. Machine parameters during fluid bed coating

Parameters	Fluid bed coating	
	Seal coating	Enteric coating
Batch size	800 g	200 g
Inlet air temperature	40-45°C	40-45°C
Outlet air temperature	30-35°C	30-35°C
Product temperature	37-40°C	37-40°C
Chamber humidity	55%-60%	55%-60%
Air flow	90m ³ /h	90m ³ /h
Spraying pressure	1.20 bar	1.20 bar
Spraying rate	2.0 g/min	3.0 g/min
Secondary drying	60°C /180 min	60°C /300 min

EXPERIMENTAL

The dissolution of duloxetine hydrochloride enteric coated pellets was studied in a dissolution tester (En/veka, Germany) using USP apparatus II

(Paddle method). An appropriate amount of duloxetine hydrochloride enteric coated pellets containing 20 mg of duloxetine in total was used in 900 ml of dissolution medium (0.1 N hydrochloric acid) at 370°C and 100 rpm for 2 h. After 1 h 25 ml sample was withdrawn from each vessel and was replaced with fresh medium so that the volume remains constant. At the end of the 2nd h 25 ml sample was withdrawn from each vessel. The drug content of the sample solution, i.e., the quantity of drug release was determined by high-performance liquid chromatography (HPLC) method. Then by replacing the acid medium after the 2nd h, 900 ml of dissolution medium (KH₂PO₄ buffer, pH 6.8) was added in each vessel. Then again the machine was operated at a rotation of 100 rpm at 370°C for the next 1 h. Thereafter 25 ml sample was withdrawn from each vessel. After appropriate dilution, the drug content of the collected samples, i.e., the quantity of drug release was determined by HPLC method. The HPLC system consisted of a pump (Waters, USA), an auto sampler (Waters), and a UV detector (Waters). The reverse-phase column (C18) O(terra, 5 µm, 4.6 mm × 25 cm, Waters) was used at ambient temperature. The mobile phase consisted of acetonitrile (40%) and the flow rate was 1 ml/min. The injection volume was 20 µl and the signal was observed at 218 nm.

The reactions were monitored by TLC using silica gel plates and the products were purified by flash column chromatography on silica gel (230–400 mesh). Melting points were measured on an Electrothermal apparatus and were uncorrected. NMR spectra were recorded at 300 MHz for ¹H and at 75 MHz for ¹³C. Mass spectra were recorded on a GC/MS operating system at an ionization potential of 70 eV. Optical rotations were measured on a high resolution digital polarimeter. The *ee* values of the samples were determined by HPLC analysis using Daicel Chiralcel OD–H chiral column.

(S)-Duloxetine (8)

To a solution of **7** (171 mg, 1 mmol) in DMSO (5 ml), were added sodium hydride (36 mg 1.5 mmol) and then 1-fluoronaphthalene (190 mg, 1.3 mmol). After stirring for 8 h, the reaction mixture was partitioned with ethyl acetate and water. After extractive workup, the combined organic layers were dried over sodium sulfate and then concentrated *in vacuo*. The residue was purified by flash chromatography (ammonium hydroxide/methanol/ dichloromethane, 0.1/1/4) to yield 232 mg (78%) of **8**: ¹H NMR (300 MHz, CDCl₃) δ 8.37–8.33 (m, 1H), 7.79–7.74 (m, 1H), 7.50–7.44

(m, 2H), 7.39–7.37 (m, 1H), 7.28–7.18 (m, 2H), 7.05–7.04 (m, 1H), 6.93–6.90 (m, 1H), 6.86–6.84 (m, 1H), 5.78 (dd, 1H, *J* 7.6 and 5.3 Hz), 2.86–2.78 (m, 2H), 2.50–2.39 (m, 4H), 2.27–2.16 (m, 1H); ¹³C NMR (75 MHz, CDCl₃) δ 153.3, 145.2, 134.5, 127.4, 126.5, 126.2, 126.1, 125.7, 125.2, 124.6, 124.5, 122.1, 120.5, 106.9, 74.7, 48.3, 39.0, 36.5; EIMS (70eV) *m/z* (rel. intensity) 297 (M⁺, 4), 187 (80), 153 (69), 144 (100); [α]_D²⁰ = +110.5 (*c* 1.1, MeOH); lit. ^{7b} [α]_D³⁰ = +114 (*c* 1, MeOH); lit. ^{15b} [α]_D²⁰ = +112 (*c* 1, MeOH); HPLC analysis: 95% *ee* (Chiralcel OD-H, hexane/Pr OH, 85/15, 0.5 ml/min; t_R (S) 18 min, t_R (R) 25 min.

CONCLUSION

The (S)-duloxetine hydrochloride was successfully synthesized using enantioselective hydrogenation of 2-bromo-1-(thiophen-2-yl)ethanone and further elaboration of cyclic carbamate derived from γ-aminoalcohol. Duloxetine hydrochloride loaded pellets were prepared by powder-layering technology. Acid resistant coating with acrylic polymer was done using fluid bed coater at different coating loads and the *in vitro* release of drug was investigated. The release of drug was found to be a function of polymer load. The results indicated that it is possible to prevent the release of drug in the upper GI tract where the environment is acidic and the release of drug in the intestinal region by developing a multiparticulate system coated with suitable pH dependent polymer.

Acknowledgements: The authors thank the Department of studies in industrial chemistry for the laboratory support.

REFERENCES

1. Z. Chen, P. Skolnick. *Expert Opin. Investig. Drugs*, **16**, 1365 (2007).
2. I. Agranat, H. Caner, I. J. Caldwell. *Nature Rev. Drug Discov.*, **1**, 753 (2002)
3. F.P. Bymaster, E.E. Beedle, J. Findlay, P.T. Gallagher, J.H. Krushinski, *Bioorg. Med. Chem. Lett.*, **13**, 4477 (2003).
4. L.A. Sorbera, R.M. Castaner, J. Castaner, *Drugs Future*, **25**, 907 (2000).
5. J. Deeter, J. Frazier, G. Staten, M. Staszak, L. Weigel, *Tetrahedron Lett.*, **31**, 7101 (1990).
6. W.J. Wheeler, F. Kuo, J. Label. *Compd. Radiopharm.*, **36**, (1995) 213.
7. H. Liu, B.H. Hoff, T. Anthonson, *Chirality*, **12**, 26 (2000).

8. R. Noyori, S. Hashiguchi, *Acc. Chem. Res.*, **30**, 97 (1997).
9. D. Lee, J. C. Lee, N. Jeong, K. I. Lee, *Tetrahedron Asymmetry*, **18**, 2662 (2007).
10. M. Gibaldi, *Biopharmaceutics and clinical pharmacology*, 4th ed., Lee and Feddiger, USA. p. 68. 1991.
11. K. Mashima, T. Abe, K. Tani. *Chem. Lett.* Vol. **27** No. 12. p. 1199 (1998).
12. T. Hamada, T. Torii, Izawa, T. Ikariya, *Tetrahedron*, **7411**, 60 (2000).
13. J. R. Dehli, V. Gotor, *Tetrahedron Asymmetry*, **12**, 1485 (2001).
14. Martindale, *The complete drug reference*, 32nd edition, 2002, London: Pharmaceutical Press p. 291.

НОВА ЕНАНТИОСЕЛЕКТИВНА СИНТЕЗА И РАЗТВАРЯНЕ НА ФИЛМОВИ ТАБЛЕТКИ ОТ (S)-ДУЛОКСЕТИН ХИДРОХЛОРИД С ЕНТЕРО-ПРИЛОЖЕНИЕ

Р. Венкатрам, В. К. Паи, С. Нагарадж

Изследователски департамент по индустриална химия, Университет Кувемпу, Шанкаргата, Индия

Постъпила на 2 юли, 2011 г.; Коригирана на 4 юни, 2012 г.

(Резюме)

Описано е енантиселективното хидриране на 2-бромо-1-(тиофен-2-ил)етанон и следващото третиране с цикличен карбамат, получен от γ -аминоалкохол за получаването на (S)-дулоксетин. Последният е потенциален двоен инхибитор за резорбцията на серотонин и норепинефрин. Таблетките с ентеро-приложение и филмово покритие от 25 и 30% полимер нямат нужната устойчивост в кисела среда. Незначително количество от лекарството се освобождава от таблетките при съдържание на полимера от 35% до 40% в кисела среда, докато почти цялото количество лекарство се освобождава в среда на буфер. Получените резултати показват, че подходящият избор на полимерния материал, основан на физико-химичните му свойства, както и количеството му са важни за създаването на таблетки със забавено освобождаване с приемлив профил на разтваряне.

Synthesis and antimicrobial evaluation of novel derivatives of 1,3,4-thiadiazine incorporated with pyrazole-4-carboxylic acid moiety

K. Shubakar¹, K. B. Umesh^{1*}, N. Srikantamurthy¹, J. Chethan²

¹Department of Chemistry, Yuvaraja's College, University of Mysore, Mysore-570 005, India.

²Department of Studies in Biotechnology, Manasagangotri, University of Mysore, Mysore-570 006, India.

Received February 2, 2012; Revised June 14, 2012

2-Amino-5-phenyl-6*H*-[1,3,4]-thiadiazine (**5a-c**) condense with pyrazole-4-carboxylate (**1a-e**) using alcohol as a solvent to give 5-methyl-1,3-diphenyl-1*H*-pyrazole-4-carboxylic acid-(5-phenyl-6*H*-[1,3,4]-thiadiazin-2-yl)-amide (**6a-i**) in 30% yield. The same product is obtained from pyrazole-4-acid (**2a-e**) in presence of HOBt (1-hydroxybenzotriazole) and EDC (*N*-ethyl-*N'*-(3-dimethyl-aminopropyl)-carbodiimide hydrochloride) in triethyl amine using CHCl₃ as a solvent, in 75-85% yields. The structures of these compounds (**6a-i**) were characterized by FT-IR, ¹H NMR, mass spectroscopic techniques and elemental analysis. All synthesized pyrazole-1,3,4-thiadiazine (**6a-i**) derivatives were found to exhibit antimicrobial activities.

Key words: 2-amino-1,3,4-thiadiazine, pyrazole-4-carboxylic acid, antimicrobial.

INTRODUCTION

Heterocyclic compounds containing five- and six-membered ring systems are successfully used as drugs. Synthesis of such compounds containing condensed rings or more than one heterocyclic nucleus is gaining more and more popularity due to their specific use in medicine.

1,3,4-Thiadiazines may exist in three different tautomeric forms. Spectroscopic investigations suggest that the 6*H*-form is preferred. The 4*H*-form represents a potentially anti-aromatic 8π-system which can be transformed by valence isomerization to a thiahomopyrazole and by subsequent extrusion of sulfur to a pyrazole [1]. In addition, 1,3,4-thiadiazines exhibit a broad spectrum of biological activity, which includes matrix metalloproteinase inhibition, tuberculostatic activity against *Mycobacterium tuberculosis*, antiplatelet and antithrombotic properties, antiarrhythmic activity, cardiostonic and hypertensive activities, phosphodiesterase inhibition, and spasmolytic activity. In addition, compounds containing thiadiazine moieties are being used as anti-inflammatory, nonsteroidal contraception agents for females and also for the treatment of erectile dysfunction. Recent reports reveal that 1,3,4-thiadiazine derivatives are used as anesthetics, cardiovascular and hypometabolic agents, for prevention and/or treatment of anemia, for treating

deficient bone growth, tumors and acquired immune deficiency syndrome (AIDS), heart failure, asthma, allergies. 1,3,4-Thiadiazine derivatives are also being used in agriculture as herbicides, fungicides, pesticides, insecticides and plant-growth regulators [2].

The 1,3,4-thiadiazine system was first reported by Bose [3], employing a reaction of α-bromoacetophenone with thiosemicarbazide. Bose isolated two reaction products, 2-amino-5-phenyl-1,3,4-thiadiazine and 2-hydrazino-4-phenylthiazole, by heating phenacyl bromide/chloride with TSC in methanol in yields of 70–80%. But 2-amino-1,3,4-thiadiazines are formed in higher yields (up to 96%) in acidic media (acetic acid and concentrated hydrochloric and hydrobromic acids). Also 2-amino-5-phenyl-6*H*-1,3,4-thiadiazines, 2-amino-5-(4-methylphenyl)-6*H*-1,3,4-thiadiazines and 2-amino-5-(4-bromophenyl)-6*H*-1,3,4-thiadiazines were prepared [4] from appropriate α-haloacetophenones and thiosemicarbazide.

Synthesis of *N*-haloacyl and *N*-hetarylthioacyl derivatives [5] of 2-amino-5-aryl-6*H*-1,3,4-thiadiazine were synthesized by *N*-acylation of 2-amino-5-aryl-6*H*-1,3,4-thiadiazines with trifluoroacetic anhydride and halogen-substituted carboxylic acid halides with retention of the initial heterocyclic system 2-haloacylamino-5-aryl-6*H*-1,3,4-thiadiazines in preparative yields. The obtained 2-haloacylamino-5-aryl-6*H*-1,3,4-thiadiazines can alkylate heterocyclic thiols under mild conditions to give the corresponding 5-aryl-2-hetarylthioacetyl(butyryl)amino-6*H*-1,3,4-

* To whom all correspondence should be sent:
E-mail: kbu68umesh@rediffmail.com

thiadiazine derivatives containing pharmacophore groups.

A new series [6] of novel bis[1,2,4]triazolo[3,4-*b*][1,3,4]-thiadiazines has been synthesized by the reaction of [5,5'-methylenebis(3-methylbenzofuran-7,5-diyl)]bis[(4-amino-5-thioxo-4,5-dihydro-1*H*-1,2,4-triazol-3-yl)methanone] with a variety of phenacyl bromides in ethanol under reflux for 6 h. All newly synthesized compounds were tested for *in vitro* activity against certain strains of bacteria and fungi.

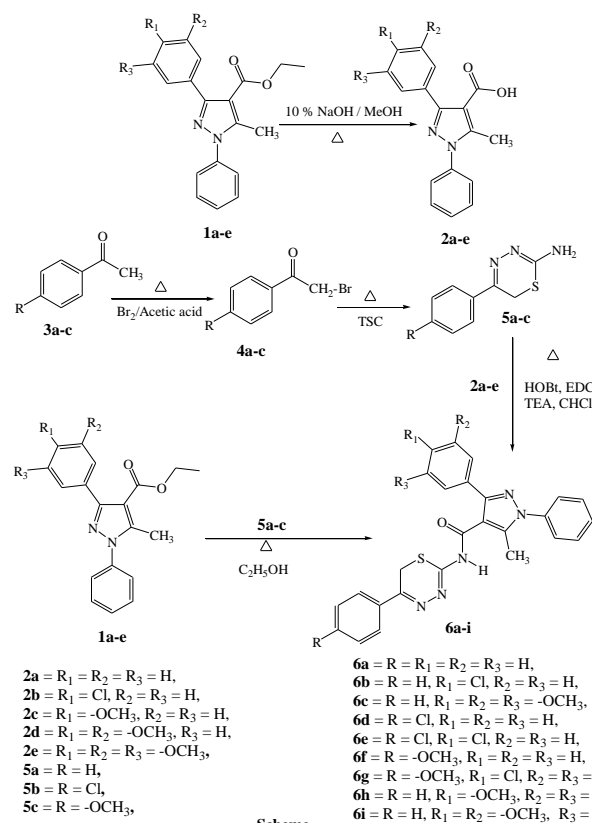
Synthesis of 3,6-diaryl-1,2,4-triazolo[3,4-*b*] – 1,3,4-thiadiazines by condensation of appropriate 5- (3,4-dichlorophenyl)-2-(aroylmethyl)thio-1,3,4-oxadiazoles and hydrazine hydrate in acetic acid is described [7]. All compounds were evaluated for anti-inflammatory activity by determining their ability to provide protection against carrageenan-induced edema in rat paw. In addition, ulcerogenic activities of the compounds were determined. New route for the synthesis of pyrimido[4,5-*e*][1,3,4]thiadiazine derivatives [8] from 5-bromo-2-chloro-4-methyl-6-(1-methylhydrazino)pyrimidine with carbon disulfide was used and several alkyl halides gave an intermediate which was successfully converted to its corresponding derivatives in basic acetonitrile.

A series of heterocycle-substituted phthalimide derivatives [9] with various heterocyclic rings, such as furan, imidazo[1,2-*a*]pyridine, 1,3,4-thiadiazine, imidazo[2,1-*b*][1,3,4]thiadiazine, pyrazole, 1,2,4-triazolo[3,4-*b*][1,3,4]thiadiazine, thiazole and thiazoline can be rapidly synthesized from α -bromoketone intermediate. Their cytotoxic activity was also *in vitro* evaluated against five human cancer cell lines.

Pyrazole and its synthetic analogues have been found to exhibit antidepressant, anticonvulsant, antimicrobial, analgesic, and antitumor activity, as well as human acyl-Co A:cholesterol acyltransferase inhibitor activity. In fact, the pyrazole derivative celecoxib is now widely used in the market as anti-inflammatory drug [10, 11]. We have synthesized 1-(5-methyl-1,3-diphenyl-1*H*-pyrazol-4-yl)-ethanone [12] and ethyl 5-methyl-1,3-diphenyl-1*H*-pyrazole-4-carboxylate [13] *via* 1,3-dipolar cycloaddition of the enol form of acetyl acetone and ethyl acetoacetate with *in situ* generated nitrile imines by catalytic dehydrogenation of diphenyl hydrazone using chloramine-T. In view of these observations we report herein the synthesis of 1,3,4-thiadiazine with incorporated pyrazole-4-carboxylic acid moiety and the study of its antimicrobial activities.

RESULTS AND DISCUSSION

The synthesis of 5-methyl-1,3-diphenyl-1*H*-pyrazole-4-carboxylic acid (**2a-e**) obtained from 5-methyl-1,3-diphenyl-1*H*-pyrazole-4-carboxylate **1(a-e)** [13] refluxed with 10% NaOH solution in presence of methanol as a solvent for about 3-4 hours is described. On the other hand, 2-amino-5-phenyl-6*H*-[1,3,4]-thiadiazines (**5a-c**) [3,4] are synthesized from acetophenone with bromine in acetic acid to give phenacyl bromide (α -bromocarbonyl compounds) (**4a-c**). The obtained phenacyl bromide (**4a-c**) is treated with thiosemicarbazide (TSC) to produce a cyclocondensation product (**5a-c**). The obtained pyrazole-4-acid (**2a-e**) is condensed with 2-amino-5-phenyl-6*H*-[1,3,4]-thiadiazine (**5a-c**) in presence of HOBt and EDC in triethyl amine using CHCl_3 as a solvent to produce the respective 5-methyl-1,3-diphenyl-1*H*-pyrazole-4-carboxylic acid-(5-phenyl-6*H*-[1,3,4]-thiadiazin-2-yl)-amide (**6a-i**) in good yield [Scheme].



Scheme

Synthesis of 5-methyl-1,3-diphenyl-1*H*-pyrazole-4-carboxylic acid (**2a-e**) obtained from 5-methyl-1,3-diphenyl-1*H*-pyrazole-4-carboxylate (**1a-e**) is performed by reflux with 10% NaOH solution in the presence of methanol for about 3-4 h. The structural proof for pyrazole-4-carboxylic acid is given by IR, ^1H NMR, ^{13}C NMR, MS studies and elemental analysis. For instance, the ^1H

NMR spectra show the absence of a quartet in the region δ 4.12–4.31 ppm, (2H for $-\text{OCH}_2-$ group), and a triplet in the region δ 1.18–1.30 ppm, (3H for $-\text{OCH}_2-\text{CH}_3$ group) and the presence of carboxylic acid peak at 9.10–9.86 ppm. In the ^{13}C NMR spectra the peaks δ 13.58–13.84 ppm (for $-\text{OCH}_2-\text{CH}_3$) and δ 58.72–58.96 ppm (for $-\text{OCH}_2-$) were absent and the peak δ 169.36–173.40 ppm (for $-\text{COOH}$) was seen. All pyrazole-4-carboxylic acids showed MH^+ as a base peak in the mass spectra and significantly stable molecular ion peaks with a relative abundance of 20–90%, which strongly favors the formation of pyrazole-4-carboxylic acid.

The obtained pyrazole-4-carboxylic acid (**2a–e**) was condensed with 2-amino-5-phenyl-6*H*-[1,3,4]-thiadiazine (**5a–c**) in cold by slowly adding HOBt, then EDC and triethyl amine using chloroform as solvent. The resulting solution was stirred at room temperature in nitrogen atmosphere for about 5–6 h to give 5-methyl-1,3-diphenyl-1*H*-pyrazole-4-carboxylic acid-(5-phenyl-6*H*-[1,3,4]-thiadiazin-2-yl)-amide (**6a–i**). The obtained pyrazole-1,3,4-thiadiazines (**6a–i**) were confirmed by IR, ^1H NMR, MS studies and elemental analysis. The IR spectra showed amide $-\text{NH}-$ frequency in the region 3328.88–3388 cm^{-1} and $-\text{C}=\text{O}$ stretching frequency in the region 1670.20–1690.50 cm^{-1} . In the ^1H NMR spectra there was no carboxylic acid peak at 9.10–9.86 ppm, but the single peak due to $-\text{CO}-\text{NH}-$ protons appeared in the region δ 7.90–8.34 ppm. All pyrazole-1,3,4-thiadiazines (**6a–i**) showed $\text{M}+1$ as a base peak in the mass spectra. Further, the elemental analysis supported the formation of the products.

Antimicrobial activity

The synthesized pyrazole-1,3,4-thiadiazines (**6a–i**) were tested (dose of 100 μg) for their *in vitro* antimicrobial activity against the human pathogenic bacterial strain *Bacillus cereus* (*B. cereus*), *Escherichia coli* (*E. coli*), *Klebsiella pneumonia* (*K. pneumonia*) and *Shigella flexneri* (*S. flexneri*) by the disc diffusion method [14, 15]. Plates were inoculated into 25 ml of N-broth (Nutrient Broth) and incubated for 24 h in an incubator at 37°C and chloramphenicol was used as a standard drug. All compounds **6a** were also screened (dose of 100 μg) for their antifungal activity against *Candida albicans* (*C. albicans*) and *Aspergillus flavus* (*A. flavus*) using Fluconazole as a standard drug. After the period of incubation the inhibition zones were measured in mm and the results obtained are shown in Table 1.

Table 1. Antibacterial activity of synthesized 1,3,4-thiadiazine derivatives (**6a–i**). (Zone of inhibition in mm).

Compound	Antibacterial activity				Antifungal activity	
	B. cereus	E. coli	K. pneumonia	S. flexneri	C. albicans	A. flavus
6a	08	14	09	10	12	18
6b	08	12	12	14	14	14
6c	12	14	16	14	16	12
6d	08	12	10	08	14	10
6e	09	10	12	16	18	20
6f	09	12	14	10	12	14
6g	08	10	08	08	10	12
6h	10	14	10	10	10	12
6i	09	12	08	12	10	12
Chloramphenicol	14	18	20	24		
Fluconazole					28	30

The screening results revealed that the test compounds (**6a–i**) exhibited significant activity, but with a degree of variation. Among all synthesized compounds, the compound **6c** exhibited a pronounced activity against all four bacterial strains and **6e** showed higher antifungal activity. The compounds **6a–i** showed good activity against *E. coli*. The compounds **6a–i** showed moderate activity against both *C. albicans* and *A. flavus*.

EXPERIMENTAL SECTION

All melting points were measured in open capillaries and are uncorrected. IR spectra (nujol) were recorded on a Bruker Ft-IR spectrometer. ^1H NMR and ^{13}C NMR spectra (CDCl_3 as a solvent) were obtained on a Varian Gemini 400MHz spectrometer. TMS as internal standard, chemical shifts in (ppm); mass spectra: Agilent mass spectrometer operating at 70 eV; elemental analysis was performed on a Jusco microanalytical data unit at Mysore University, India.

General procedures for the synthesis of 5-methyl-1,3-diphenyl-1*H*-pyrazole-4-carboxylic acid (2a): The solution of ethyl 5-methyl-1,3-diphenyl-1*H*-pyrazole-4-carboxylate (**1a**, 3.06g, 10.0 mmol) was treated with 10 ml of 10% NaOH solution in the presence of absolute methanol for about 3–4 h to give 5-methyl-1,3-diphenyl-1*H*-pyrazole-4-carboxylic acid (**2a**, 2.78g). The progress of the reaction was monitored by TLC (chloroform:acetone = 7 : 1 v/v). After the completion of the reaction the solvent was evaporated and the solution was acidified with dilute HCl to give a crude white precipitate. The obtained solid was filtered, dried and recrystallized from methanol to give a white solid (80% yield), m.p. 136°C. The pyrazole-4-acid showed IR bands

(Nujol) ν : 1678 cm^{-1} (-COOH); ^1H NMR (CDCl_3) δ : 2.7 (s, 3H, -CH₃), 7.45–7.62 (m, 5H, Ar), 7.35–7.9 (m, 5H, Ar¹), 9.6 (s, 1H, -COOH); ^{13}C NMR (CDCl_3) δ : 0.56 (q, 1C, H₃C), 108.32 (s, 1C), 118.08 (d, 2C), 126.42 (d, 1C), 128.66 (d, 2C), 128.22 (d, 2C), 128.74 (d, 2C), 130.28 (s, 1C), 131.08 (d, 1C), 132.42 (s, 1C), 148.6 (s, 1C, C-CH₃), 161.12 (s, 1C -C=N), 173.4* (s 1C, -COOH). MS (relative intensity) m/e for C₁₇H₁₄N₂O₂: 279 (M+1, 100), 260 (62), 233 (48). Anal. Calcd: C, 73.37; H, 5.07; N, 10.07%. Found: C, 73.78; H 5.19; N: 10.21%.

General procedures for the synthesis of 2-amino-5-phenyl-6H-[1,3,4]-thiadiazine (5a-c): 2-amino-5-phenyl-6H-[1,3,4]-thiadiazine (**5a**) was synthesized from acetophenone (2.0 g) with bromine in acetic acid (30 ml) to give phenacyl bromide (α -bromocarbonyl compound). The obtained phenacyl bromide was refluxed with thiosemicarbazide (TSC) in 20 ml of conc. HCl for about 30 min and the resulting solution was allowed to stand at room temperature to produce pale yellow solid. The obtained solid was filtered, washed with chloroform, dried and recrystallized from methanol to give pale yellow solid (85% yield), m.p. 126-128°C. ^1H NMR spectra of **5a** (CDCl_3) δ : 3.32 (s, 2H, -CH₂-), 7.26–7.42 (m, 5H, Ar-H), 8.1-8.8 (bs, 2H, -NH₂); ^{13}C NMR (CDCl_3) δ : 25.8 (s, 1C, -CH₂-), 128.8 (d, 2C, C-2 and C-6 phenyl), 130.2 (d, 2C, C-3 and C-5 phenyl), 131.6 (s, 1C, C-4 phenyl), 132.4 (s, 1C, C-1 phenyl), 163.60* (s, 1C, C-NH₂), 164.4* (s, 1C, -C=N). MS (relative intensity) m/e for C₉H₉N₃S: 192 (M+1, 100), Anal. Calcd: C, 56.45; H, 4.68; N, 21.74; S, 16.70%. Found: C, 56.36; H, 4.52; N, 21.66; S, 16.64%.

Typical procedure for the synthesis of 5-methyl-1,3-diphenyl-1H-pyrazole-4-carboxylic acid-(5-phenyl-6H-[1,3,4]-thiadiazin-2-yl)-amide (6a): 2-amino-5-phenyl-6H-[1,3,4]-thiadiazine (**5a**, 0.19 g, 10 mmol) was dissolved in 15 ml of CHCl_3 and stirred at 0°C. Then 0.22 g of HOBt (15 mmol) was slowly added to the solution, after 15 min 0.20 g of EDC (15 mmol), 0.05ml of triethyl amine (15 mmol) and pyrazole-4-acid (**2a** 0.27g, 10 mmol) were added, the resulting solution was stirred at room temperature in nitrogen atmosphere for about 6–7 h. The progress of the reaction was monitored by TLC. After the completion of reaction the residue was extracted with CHCl_3 (30 ml), washed successively with 5% NaHCO_3 solution and 5% HCl solution. Finally, the solution was washed with water (2×30 ml), and dried over anhydrous Na_2SO_4 . The solvent was evaporated to give yellow solid

which was recrystallized from methanol to give pale yellow solid in 76% yield (0.33 g), m.p. 146-148 °C. The obtained pyrazole-thiadiazine **6a** showed IR bands (nujol) ν : 1670.20 cm^{-1} (-C=O), 1595.84 cm^{-1} (-C=N-), 3357.90 cm^{-1} (-NH-); ^1H NMR (CDCl_3): δ 2.72 (s, 3H, CH₃), 3.56 (s, 2H, -CH₂-), 7.25–7.68 (m, 15H, Ar-H), 7.90 (d, 1H, -NH-CO-); MS (relative intensity) m/e for C₂₆H₂₁N₅OS: 452 (M+1, 100); Anal. Calcd: C, 69.16, H, 4.69, N, 15.51%. Found: C, 68.96, H, 4.60, N, 15.44%.

3-(4-Chloro-phenyl)-5-Methyl-1-phenyl-1H-pyrazole-4-carboxylic acid-(5-phenyl-6H-[1,3,4]-thiadiazin-2-yl)-amide (6b): Obtained from 2-amino-5-phenyl-6H-[1,3,4]-thiadiazine (**5a**, 0.19g, 10 mmol), 0.22g HOBt, 0.20g of EDC, 0.05ml triethyl amine and pyrazole-4-acid (**2b**, 0.30g, 10 mmol). Pale yellow solid, yield 78%, m.p. 158-160 °C. IR bands (nujol) ν : 1676.04 cm^{-1} (-C=O), 1562.02 cm^{-1} (-C=N-), 3328.88 cm^{-1} (-NH-); ^1H NMR (CDCl_3): δ 2.70 (s, 3H, CH₃), 3.60 (s, 2H, -CH₂-), 7.20–7.66 (m, 14H, Ar-H), 8.21 (d, 1H, -NH-CO-); MS (relative intensity) m/e for C₂₆H₂₀ClN₅OS: 486 (M+1, 100); Anal. Calcd: C, 64.26, H, 4.15, N, 14.40%. Found: C, 64.08, H, 4.04, N, 14.34%.

5-Methyl-1-phenyl-3-(3,4,5-trimethoxy-phenyl)-1H-pyrazole-4-carboxylic acid-(5-phenyl-6H-[1,3,4]-thiadiazin-2-yl)-amide (6c): Obtained from 2-amino-5-phenyl-6H-[1,3,4]-thiadiazine (**5a**, 0.19 g, 10 mmol), 0.22 g HOBt, 0.20 g of EDC, 0.05ml triethyl amine and pyrazole-4-acid (**2c**, 0.37g, 10 mmol). Pale yellow solid, yield 82%, m.p. 152-154 °C. IR bands (nujol) ν : 1684.04 cm^{-1} (-C=O), 1558.38 cm^{-1} (-C=N-), 3364.78 cm^{-1} (-NH-); ^1H NMR (CDCl_3): δ 2.79 (s, 3H, CH₃), 4.06 (s, 2H, -CH₂-), 3.84 (s, 9H, -OCH₃), 7.22–7.96 (m, 12H, Ar-H), 8.34 (d, 1H, -NH-CO-); MS (relative intensity) m/e for C₂₉H₂₇N₅O₄S: 542 (M+1, 100); Anal. Calcd: C, 64.30, H, 5.00, N, 12.89%. Found: C, 64.24, H, 4.96, N, 12.80%.

5-Methyl-1,3-diphenyl-1H-pyrazole-4-carboxylic acid-(5-(4-chloro-phenyl)-6H-[1,3,4]-thiadiazin-2-yl)-amide (6d): Obtained from 2-amino-5-(4-chloro-phenyl)-6H-[1,3,4]-thiadiazine (**5b**, 0.22 g, 10 mmol), 0.22 g HOBt, 0.20 g of EDC, 0.05 ml triethyl amine and pyrazole-4-acid (**2a**, 0.27 g, 10 mmol). Pale yellow solid, yield 84%, m.p. 160-162 °C. IR bands (Nujol) ν : 1676 cm^{-1} (-C=O), 1560.32 cm^{-1} (-C=N-), 3360.64 cm^{-1} (-NH-); ^1H NMR (CDCl_3): δ 2.68 (s, 3H, CH₃), 3.92 (s, 2H, -CH₂-), 7.28-7.82 (m, 14H, Ar-H), 8.26 (d, 1H, -NH-CO-); MS (relative intensity) m/e for C₂₆H₂₀ClN₅OS: 486 (M+1, 100); Anal. Calcd: C,

64.25, H, 4.08, N, 14.38%. Found: C, 64.22, H, 4.00, N, 14.34%.

3-(4-Chloro-phenyl)-5-methyl-1-phenyl-1H-pyrazole-4-carboxylic acid-(5-(4-chloro-phenyl)-6H-[1,3,4]-thiadiazin-2-yl)-amide (6e): Obtained from 2-amino-5-(4-chloro-phenyl)-6H-[1,3,4]-thiadiazine (**5b**, 0.22 g, 10 mmol), 0.22 g HOBt, 0.20 g of EDC, 0.05 ml triethyl amine and pyrazole-4-acid (**2b**, 0.30 g, 10 mmol). Pale yellow solid, yield 80%, m.p. 144-146 °C. IR bands (nujol) v: 1672 cm⁻¹ (-C=O), 1566.24 cm⁻¹ (-C=N-), 3380.52 cm⁻¹ (-NH-); H¹ NMR (CDCl₃): δ 2.72 (s, 3H, CH₃), 3.84 (s, 2H, -CH₂-), 7.28-7.82 (m, 13H, Ar-H), 8.08 (d, 1H, -NH-CO-); MS (relative intensity) m/e for C₂₆H₁₉Cl₂N₅O₂S: 520 (M+1, 100); Anal. Calcd: C, 60.00, H, 3.68, N, 13.62%. Found: C, 59.96, H, 3.64, N, 13.60%.

5-Methyl-1,3-diphenyl-1H-pyrazole-4-carboxylic acid-(5-(4-methoxy-phenyl)-6H-[1,3,4]-thiadiazin-2-yl)-amide (6f): Obtained from 2-amino-5-(4-methoxy-phenyl)-6H-[1,3,4]-thiadiazine (**5c**, 0.22 g, 10 mmol), 0.22 g HOBt, 0.20 g of EDC, 0.05 ml triethyl amine and pyrazole-4-acid (**2a**, 0.26g, 10 mmol). Pale yellow solid, yield 85%, m.p. 132-134 °C. IR bands (nujol) v: 1684 cm⁻¹ (-C=O), 1572 cm⁻¹ (-C=N-), 3356.04 cm⁻¹ (-NH-); H¹ NMR (CDCl₃): δ 2.64 (s, 3H, CH₃), 4.14 (s, 2H, -CH₂-), 3.72 (s, 3H, -OCH₃), 7.32-7.92 (m, 14H, Ar-H), 8.12 (d, 1H, -NH-CO-); MS (relative intensity) m/e for C₂₇H₂₃N₅O₂S: 482 (M+1, 100); Anal. Calcd: C, 67.34, H, 4.81, N, 14.54%. Found: C, 67.30, H, 4.78, N, 14.50%.

3-(4-Chloro-phenyl)-5-methyl-1-phenyl-1H-pyrazole-4-carboxylic acid-(5-(4-methoxy-phenyl)-6H-[1,3,4]-thiadiazin-2-yl)-amide (6g): Obtained from 2-amino-5-(4-methoxy-phenyl)-6H-[1,3,4]-thiadiazine (**5c**, 0.22 g, 10 mmol), 0.22g HOBt, 0.20 g of EDC, 0.05 ml triethyl amine and pyrazole-4-acid (**2b**, 0.30 g, 10 mmol). Pale yellow solid, yield 78%, m.p. 172-174 °C. IR bands (nujol) v: 1672 cm⁻¹ (-C=O), 1560 cm⁻¹ (-C=N-), 3358 cm⁻¹ (-NH-); H¹ NMR (CDCl₃): δ 2.76 (s, 3H, CH₃), 4.22 (s, 2H, -CH₂-), 3.68 (s, 3H, -OCH₃), 7.20-8.06 (m, 13H, Ar-H), 8.22 (d, 1H, -NH-CO-); MS (relative intensity) m/e for C₂₇H₂₂ClN₅O₂S: 516 (M+1, 100); Anal. Calcd: C, 62.84, H, 4.30, N, 13.57%. Found: C, 62.78, H, 4.28, N, 13.52%.

3-(4-Methoxy-phenyl)-5-methyl-1-phenyl-1H-pyrazole-4-carboxylic acid-(5-phenyl-6H-[1,3,4]-thiadiazin-2-yl)-amide (6h): Obtained from 2-amino-5-phenyl-6H-[1,3,4]-thiadiazine (**5a**, 0.22 g, 10 mmol), 0.19 g HOBt, 0.20 g of EDC, 0.05 ml triethyl amine and pyrazole-4-acid (**2c**, 0.30 g, 10 mmol). Pale yellow solid, yield 80%, m.p. 154-156

°C. IR bands (nujol) v: 1682 cm⁻¹ (-C=O), 1574 cm⁻¹ (-C=N-), 3388 cm⁻¹ (-NH-); H¹ NMR (CDCl₃): δ 2.80 (s, 3H, CH₃), 3.82 (s, 2H, -CH₂-), 3.58 (s, 3H, -OCH₃), 7.28-8.12 (m, 14H, Ar-H), 8.20 (d, 1H, -NH-CO-); MS (relative intensity) m/e for C₂₇H₂₃N₅O₂S: 482 (M+1, 100); Anal. Calcd: C, 67.34, H, 4.80, N, 14.54%. Found: C, 67.30, H, 4.78, N, 14.50%.

3-(3,4-Dimethoxy-phenyl)-5-methyl-1-phenyl-1H-pyrazole-4-carboxylic acid-(5-phenyl-6H-[1,3,4]-thiadiazin-2-yl)-amide (6i): Obtained from 5-(4-methoxy-phenyl)-6H-[1,3,4]-thiadiazine-2-yl amine (**5a**, 0.19 g, 10 mmol), 0.22 g HOBt, 0.20 g of EDC, 0.05 ml triethyl amine and pyrazole-4-acid (**2d**, 0.33 g, 10 mmol). Pale yellow solid, yield 75%, m.p. 174-176 °C. IR bands (nujol) v: 1690 cm⁻¹ (-C=O), 1564 cm⁻¹ (-C=N-), 3366 cm⁻¹ (-NH-); H¹ NMR (CDCl₃): δ 2.72 (s, 3H, CH₃), 4.16 (s, 2H, -CH₂-), 3.58 (s, 6H, -OCH₃), 7.28-8.08 (m, 13H, Ar-H), 8.16 (d, 1H, -NH-CO-); MS (relative intensity) m/e for C₂₈H₂₅N₅O₃S: 512 (M+1, 100); Anal. Calcd: C, 65.74, H, 4.93, N, 13.68%. Found: C, 65.70, H, 4.88, N, 13.60%.

REFERENCES

1. W. D. Pfeiffer in: "Methods of Organic Chemistry" (Houben-Weyl), *Thiadiazines* (review), 4th ed. (1998); K. H. Büchel, J. Falbe, H. Hagemann, M. Hanack, D. Klamann, R. Kreher, H. Kropf, M. Regitz, E. Schaumann, Eds.; Georg Thieme Verlag, Stuttgart, E9c, pp. 483-529.
2. W.D. Pfeiffer, "1,3,4-Oxadiazines and 1,3,4-Thiadiazines", *Chem. Rev.*, (2008) Elsevier Ltd., University of Greifswald, Greifswald, Germany.
3. P.K. Bose, (Thiodiazines. Part 1. Condensation of thiosemicarbazide with α-bromo-acetophenone), *J. Indian Chem. Soc.* **1**, 51 (1924).
4. A.P. Novikova, N.M. Petrova, L.G. Egorova, I.E. Bragina, *Khim. Geterotsikl. Soedin.*, 843 (1991); [*Chem. Heterocycl. Compd.*, **37**, 6 (1991), (Engl. Transl.)].
5. L.B. Kulikova, G.I. Ezhova, N.E. Kravchenko, O.V. Dorofeeva, A.S. Kulikov, A.G. Zavozin, *Russian Chemical Bulletin, International Edition*, **56**, 1631 (2007).
6. C. Sanjeeva Reddy, D. Chandrasekhar Rao, V. Yakub, A. Nagaraj, *Acta Chim. Slov.*, **58**, 582 (2011).
7. M. Koksai, I. Ozkan, M. Yarim, S. S. Bilge, A. Bozkurt, D. D. Erol., *Rev. Chim. (Bucharest)*, **62**, 1069 (2011).
8. M. Rahimizadeh, M. Nikpour, M. Bakavoli., *Journal of Heterocyclic Chemistry*, **44**, 463 (2007).
9. Y.J. Yang, Y.N. Yang, J.S. Jiang, Z.M. Feng, H.Y. Liu, X.D. Pan, P.C. Zhang, *Chinese Chemical Letters*, **21**, 902 (2010).
10. C. Sharma, B. Thadhaney, G. Pemawat, G. L. Talesara, (Synthesis of some novel ethoxyphthalimide

- derivatives of pyrazolo[3,4-c]pyrazoles) *Indian Journal of Chemistry*, **47B**, 1892 (2008).
11. P. Caramella, P. Grunanger in: 1,3-Dipolar Cycloaddition chemistry, A. Padwa (ed.), Wiley Interscience, New York, 1984, vol. 1, pp. 337.
 12. B. Umesh, K. M. L. Rai, K. Ajaykumar, *Indian J. Chem., Sec. B*, **41B**, 1450 (2002).
 13. K. B. Umesh, K. M. L. Rai, *Bulg. Chem. Commun.*, **42(1)**, pp.11-15 (2010).
 14. A. Simmons, *Practical Medical Microbiology*, 14th Edn. (Churchill Livingstone, Edinburgh), **11**, 163 (1996).
 15. P. S. Bisen, K. Verma, *Hand Book of Microbiology*, 1st Edn.(CBS Publishers and Distributors, New Delhi), (1996).

СИНТЕЗА И АНТИМИКРОБНИ СВОЙСТВА НА НОВИ ПРОИЗВОДНИ НА 1,3,4-ТИАДИАЗИН ВКЛЮЧЕНИ В СРЕДА ОТ ПИРАЗОЛ-4-КАРБОНОВА КИСЕЛИНА

К. Шубакар¹, К. Б. Умеша¹ Н. Срикантамурти¹, Дж. Четхан²

¹Департамент по химия, Колеж Ювраджа, Университет в Майсор, Индия.

²Департамент по биотехнологични изследвания, Манасаганготри, Университет в Майсор, Индия

Постъпила на 2 февруари, 2012 г.; коригирана на 14 юли, 2012 г.

(Резюме)

2-амино-5-фенил-6H-[1,3,4]-тиадиазин (**5a-c**) се кондензира с пиразол-4-карбоксилат (**1a-e**) при алкохол като разтворител за получаването на 5-метил-1,3-дифенил-1H-пиразол-4-карбонова киселина-(5-фенил-6H-[1,3,4]-тиадиазин-2-ил)-амид (**6a-i**) с 30% добив. Същият продукт се получава от пиразол-4-киселина (**2a-e**) в присъствие на HOBT (1-хидрокси-бензотриазол) и EDC (*N*-етил-*N'*-(3-диметил-аминопропил)-карбодиимид хидрохлорид) в триетиламин използвайки CHCl₃ като разтворител с добиви 75-85%. Структурите на тези съединения (**6a-i**) са характеризирани чрез FT-IR, ¹H NMR, мас-спектрометрия и елементен анализ. За всички производни на пиразол-1,3,4-тиадиазина (**6a-i**) са установени антибактериални свойства.

Hydrogen sorption properties of a MgH₂ - V₂O₅ composite prepared by ball milling

E. Grigorova^{1*}, M. Khristov¹, P. Peshev¹, D. Nihtianova^{1,2}, N. Velichkova¹, G. Atanasova¹

¹ Institute of General and Inorganic Chemistry, Bulgarian Academy of Sciences, bl.11, Acad. G. Bonchev str., 1113 Sofia, Bulgaria

² Institute of Mineralogy and Crystallography, Bulgarian Academy of Sciences, Acad. G. Bonchev Str., bl. 107, 1113 Sofia, Bulgaria

Received April 9, 2012; Revised November 7, 2012

A 90 wt.% MgH₂ – 10 wt.% V₂O₅ composite was obtained by ball milling of a mixture of magnesium hydride and vanadia for 60 min under argon. Hydrogen sorption properties of the composite were determined volumetrically with a Sieverts-type device. Absorption was studied at temperatures of 473 and 573 K and pressure of 1 MPa, while desorption was investigated at T = 573 and 623 K and P = 0.15 MPa. Structure, phase and surface composition of the starting compounds and the composite before and after hydriding were determined by XRD, thermal analysis, TEM and XPS. After hydriding the composite at 573 K, a high absorption capacity value of 6.3 wt.% H₂ was attained. However, fast hydrogen desorption was observed only at temperatures higher than those needed for practical use. Some ideas about further studies to be performed in view to improving the performance of vanadia-containing magnesium composites for hydrogen storage were discussed.

Keywords: hydrogen storage materials; composite materials; electron microscopy; photoelectron spectroscopy

INTRODUCTION

Owing to its high energy density, possibility of its production from various renewable sources, low weight and low environmental impact, hydrogen is considered as a promising energy carrier and a basis of the so-called hydrogen economy of the future. However, the key factor for the use of hydrogen as a clean fuel remains the development of safe and efficient materials for its storage. The requirements towards these materials are: suitable thermodynamic properties, favorable hydriding and dehydriding kinetics, high absorption capacity at relatively low temperature and pressure, good cycling properties and low price.

At present, there is no material capable to answer all these requirements. This also concerns the recently developed metal-organic frameworks [1], nanoporous polymers [2] and graphene nanostructures [3] which physisorbed not more than 1–2 wt.% of hydrogen, a capacity being far from the U.S. Department of Energy (DOE) target of 6–6.5 wt.% for hydrogen storage tanks. In a recent report on hydrogen clathrate hydrate [4] it is shown that hydrogen can be trapped under high pressure in the clathrate cavities reaching a mass ratio close to that defined by DOE, but such a material is only

stable under high pressure or at very low temperature. It is also worth noting, that the DOE target is largely exceeded by some B-N compounds. Thus, the simplest one, ammonia borane (borazane), H₃NBH₃, which is a nontoxic nonflammable solid, has a record potential of 19.6 wt.% H₂ storage capacity, but unfortunately it irreversibly releases hydrogen [6].

Chronologically, bulk metal hydrides were, since the 1970-ies, the first substances subject to systematic studies as potential storage materials. At present it is worth pointing out that only low-weight metal hydrides and especially MgH₂ and materials on its basis present a real perspective of usage for automotive applications. This is due to the high absorption capacity (7.6 wt.% H₂ theoretical capacity) of magnesium, its availability and low cost. However, along with these advantages, Mg has a series of disadvantages, such as poor hydriding/ dehydriding kinetics and high temperature of reversible hydrogen absorption. Two principal approaches are applied to their overcoming. The first one consists in tailoring the properties through size restriction, most often by ball milling. In this way the crystallite size is reduced, fresh surface area is created and both thermodynamics and kinetics can be effectively controlled at a molecular level [7]. With the second approach, nanocrystalline composites of Mg (or MgH₂) with certain additives (catalysts) are

* To whom all correspondence should be sent:
E-mail: egeorg@svr.igic.bas.bg

prepared by high energy ball milling under inert (Ar) or reactive (H₂) atmosphere with a view to preserving the high absorption capacity of magnesium, simultaneously reaching suitable sorption characteristics under milder hydriding/dehydriding conditions [8–11]. A great variety of substances (mainly transition metals and their oxides, intermetallics, carbon materials, SiC etc.) exhaustively summarized in the above reviews [8, 10, 11] have been used as additives in the Mg-composites. As is pointed out in a recent paper of Borgschulte *et al.* [12], the exact phase of the additive, its promoting role and mechanism are still remaining unclear, which leads to a controversial debate on the origin of the effects observed. Probably, many interpretation inconsistencies are due to the complex character of the kinetic phenomena.

Recently, brittle MgH₂ was used quite often instead of the ductile magnesium powder as a starting substance for the preparation of Mg-based composite materials. This reduces the occurrence of cold welding during milling, thus increasing the efficiency and productivity of the process.

For many years in the past, the research activity of our laboratory in the field of hydrogen storage was devoted to studies on mechanically alloyed composites of magnesium with 3d-metal oxides. Thus, in papers published in 1987–1989 [13, 14] it was shown that mixtures of Mg with 10% TiO₂ or V₂O₅ obtained by ball milling had improved hydrogen absorption-desorption properties compared to those of pure magnesium. In a XPS study [15] the presence of elemental Ti and Ti³⁺ favoring dissociative chemisorption of hydrogen was established on the surface of the TiO₂-containing composite. The catalytic effect of TiO₂, V₂O₅, as well as of other transition metal oxides in which the metal can appear at different oxidation degrees, on improving the hydriding/dehydriding kinetics of Mg-based composites was confirmed by Oelerich *et al.* [16]. In a recent paper Croston *et al.* [17] demonstrated the decisive role played by the TiO₂ preparation procedure on the hydriding-dehydriding kinetics of the MgH₂-TiO₂ composite. It was shown that the anatase form was more effective at lowering the dehydrogenation onset temperature of MgH₂ than the rutile modification. According to these authors, such a behavior corresponds to two different mechanisms of dehydrogenation, changing from one of surface control followed by volume contraction to a two-dimensional Johnson-Mehl-Avrami nucleation and growth mechanism. Du *et al.* using the results of *ab*

initio DFT calculations attempted to explain the catalytic role of V₂O₅ for MgH₂ destabilization with an elongation and weakening of the Mg-H bond length when MgH₂ clusters are positioned on single, two and three coordinated oxygen sites on the V₂O₅ (001) surface [18].

During the last years Nb₂O₅ proved to be a very effective catalyst for improving the hydrogen sorption kinetics of magnesium [19–21]. It was shown that during heating and cycling of MgH₂ ball milled with Nb₂O₅ additive, reduction of the oxide to metallic niobium occurred, accompanied by the appearance of a ternary MgNb₂O_{3.67} phase [22]. According to a model proposed in ref. [23], these products are working as catalysts, reducing the activation barrier of the reactions controlling the hydrogen sorption kinetics. Another model of the same authors is based on the fact that the products of Nb₂O₅ reduction embedded in an MgH₂ matrix emerge on the surface during hydrogenation, thus bringing up a possibility to generate gateways for further hydrogen diffusion. The effect of microstructure and the catalytic role of Nb₂O₅ on the hydriding /dehydriding kinetics of MgH₂ were studied in [24–26]. The decrease of the activation energy of dehydriding caused by the Nb₂O₅ was observed after 15 min of ball milling only [24]. It was demonstrated that the reduction of grain and particle size enhances substantially the hydriding/dehydriding kinetics. In addition to the results mentioned above, it is worth noting a recent study of Dolci *et al.* [27] who reported the existence, besides MgNb₂O_{3.67}, of a number of other ternary Mg-Nb-O phases.

In the light of the brief review given above and taking into consideration that vanadium belongs to the same group of d-transition metals as niobium, it seemed interesting to the authors of the present paper to reexamine in some details the hydrogen sorption properties of a MgH₂-V₂O₅ composite with a view to enlarge the understanding of the role of oxide promoters in MgH₂-based hydrogen storage materials.

EXPERIMENTAL

Powdery MgH₂ (99.8% purity, Alfa Aesar) and specpure V₂O₅ (Alfa Aesar) were used for preparing the composite 90 wt.% MgH₂ – 10 wt.% V₂O₅. It was obtained by mechanical alloying in a Fritsch Pulverisette 6 planetary ball mill under argon. The ball-to-sample weight ratio was 10:1, the rotation speed 200 rpm and the time of milling, 60 min. This duration was chosen in order to avoid sticking of the particles and formation of

agglomerates, which was often observed as a result of prolonged grinding. Messer GmbH argon and hydrogen gases with purity of 99.998% and 99.999%, respectively, were used in the experiments.

The sorption characteristics of the composite were determined volumetrically using a Sieverts-type device described elsewhere [28]. Hydrogen absorption was investigated at temperatures of 473 and 573 K and pressure of 1 MPa, while desorption was studied at $T = 573$ and 623 K and $P = 0.15$ MPa.

The phase composition of the starting compounds, the initial, hydrided and dehydrided composites was controlled with the use of a Bruker D8 Advance X-ray diffractometer (CuK_{α} radiation).

Additional characterization of the samples was performed by thermal analysis, transmission electron microscopy (TEM) and X-ray photoelectron spectroscopy (XPS). All procedures during these characterizations as well as the X-ray measurements were carried out in air. As demonstrated in a very recent paper of Vincent and Huot [29], air contamination is not as detrimental as often expected.

A combined DTA/TG apparatus (LABSYSTEM EVO, SETARAM, France) with a gas analyzer (Omnistar TM – type) was used in thermal analysis studies of the samples before and after ball milling and after 10 hydriding-dehydriding cycles. The investigations were carried out in a flow of 20 ml Ar/min with a heating rate of 10K/min.

The TEM studies were performed on a JEOL 2100 instrument at an accelerating voltage of 200 kV. The specimens were prepared by grinding and dispersing them in ethanol followed by an ultrasonic treatment for 6 min. The suspensions were dripped on standard holey carbon/Cu grids.

The XPS surface characterization of the composite before and after hydriding at $T = 573$ K and $P = 1$ MPa was carried out with the use of a VG ESCALAB II spectrometer. The spectra were recorded by means of unmonochromatized AlK_{α} radiation ($h\nu = 1486.6$ eV) with a total instrument resolution of 1 eV. Binding energy (BE) values were referenced to the C1s line of carbon at 285 eV. The C1s, Mg1s, Mg2s, Mg2p, O1s+V2p and V2p_{1/2} photoelectron spectra were obtained.

RESULTS AND DISCUSSION

The X-ray diffraction pattern of the as-received commercial MgH_2 powder revealed only the presence of its polymorphic modification stable at ambient conditions and having a rutile-type

tetragonal structure (S.G. $P4_2/mnm$, No 136) [30, 31]. Similarly, only peaks corresponding to the widely known orthorhombic α - V_2O_5 (S.G. $Pmmn$, No 59) [32, 33] were observed on the XRD pattern of the starting oxide. Both patterns are trivial and are not presented here.

The results of the thermal analysis of magnesium hydride used are given in Fig. 1. It is evident that the decomposition reaction accompanied by hydrogen evolution starts at around 703 K. The weight loss of 6.35% is much lower than the theoretical (7.6%) which indicates incomplete decomposition of MgH_2 under the experimental conditions chosen, as well as the presence of some unhydrided magnesium.

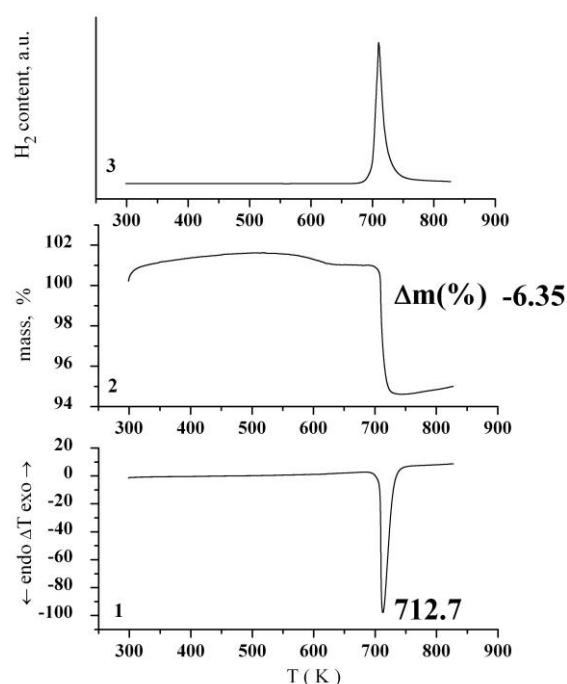


Fig. 1. DTA (1), TG (2) and evolved H_2 (3) curves of the as-received commercial MgH_2

The X-ray phase analysis of the composite obtained after ball milling of magnesium hydride with vanadia showed the presence of tetragonal MgH_2 , orthorhombic α - V_2O_5 and some traces of Mg (Fig. 2). Appearance of polymorphic modifications of the components was not registered. The thermal analysis curves presented in Fig. 3 reveal that hydrogen evolution from the composite after ball milling took place at a lower temperature than from the hydrided sample with a simultaneous decrease of the H_2 percentage. Comparison showed that the decomposition of the composite after hydriding was probably more complex and proceeded in a broader temperature range.

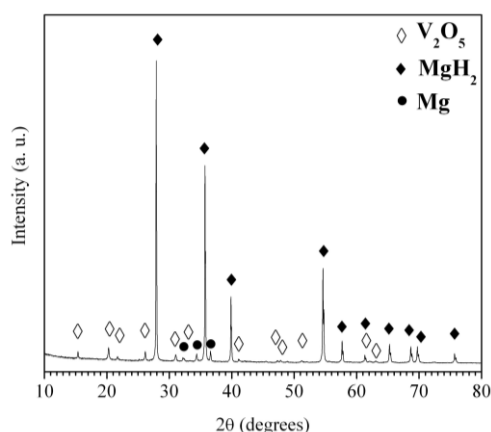


Fig. 2 X-ray diffraction pattern of the composite 90 wt. % MgH_2 - 10 wt. % V_2O_5 obtained by ball milling.

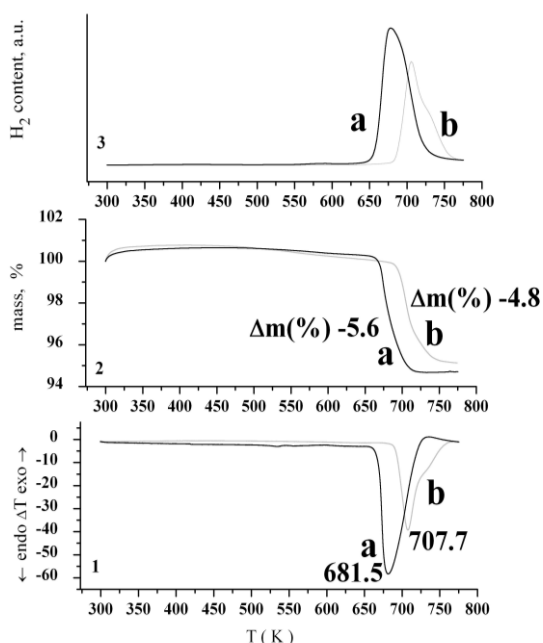


Fig. 3 DTA (1), TG (2) and evolved H_2 (3) curves of the composite 90 wt. % MgH_2 - 10 wt. % V_2O_5 : (a) obtained by ball milling and (b) after hydriding at $T = 573$ K and $P = 1$ MPa.

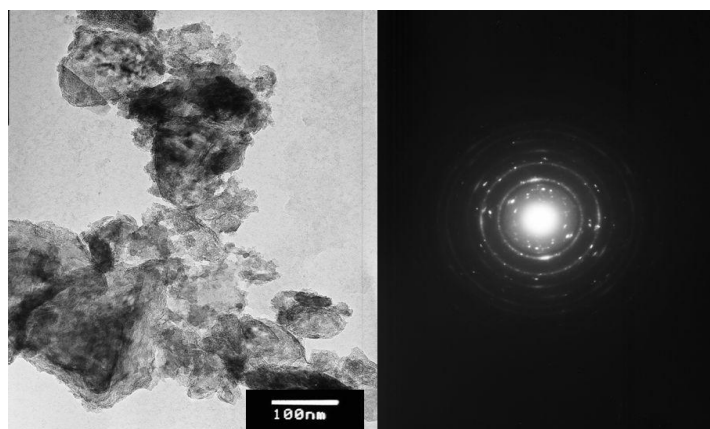


Fig. 4. TEM bright field micrograph and electron diffraction pattern of the composite 90 wt. % MgH_2 - 10 wt. % V_2O_5 obtained by ball milling

A TEM image of the composite is presented in Fig. 4. It is evident that the sample consists of crystallites sized in a wide range, two principal groups of small and large particles, respectively, being observed. The polycrystalline electron diffraction pattern revealed, in contrast to the XRD data, a much richer phase composition of the ball milled composite. Thus, along with the tetragonal MgH_2 , the presence of some orthorhombic γ - MgH_2 with α - PbO_2 type structure (S.G. *Pbcn*, No 60) [31, 34] was detected. This polymorph is, as a rule, a high pressure phase, but some authors observed its formation induced by lattice strains after prolonged milling of the tetragonal hydride [35, 36]. The present results show that even a relatively short milling time is sufficient for the tetragonal-orthorhombic MgH_2 -transition to occur at a level which usually cannot be detected by X-ray measurements. Thus, a possible explanation of the observed lower temperature of hydrogen evolution from the ball milled sample (Fig. 3) compared to that from pure magnesium hydride consists in the presence of the less stable orthorhombic MgH_2 polymorph.

Electron diffraction permitted to establish that a small amount of the high-pressure β - V_2O_5 phase was also present in the MgH_2 - V_2O_5 composite studied. Kusaba *et al.* [37] ascribed to β - V_2O_5 an orthorhombic structure, while according to Balog *et al.* [33] the phase with the same lattice parameters was monoclinic.

Finally, it is worth noting that, in accordance with the electron diffraction results, the ball milled composite contained a certain amount of metallic vanadium.

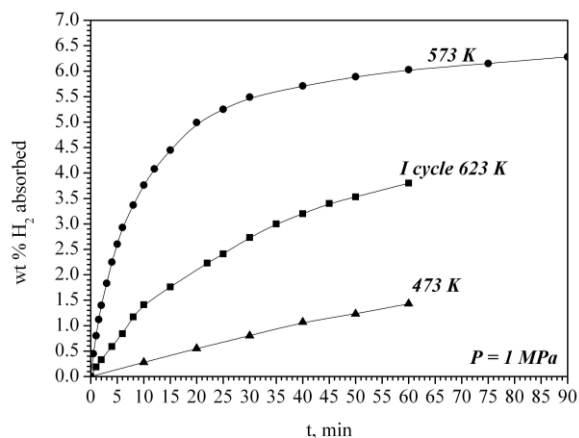


Fig. 5. Kinetic curves of hydrogen absorption by the composite 90 wt.% MgH_2 - 10 wt.% V_2O_5 at $P = 1$ MPa and different temperatures

The kinetic curves of hydrogen absorption by the ball milled composite at temperatures of 473 and 573 K and pressure of 1 MPa, along with the first cycle (cycle of activation) curve are given in Fig. 5. At 573 K, high absorption capacity of 6.3 wt.% H_2 was attained after 60 min hydriding. However, with a temperature decrease by 100 K the capacity drastically dropped down.

Desorption of hydrogen from the hydrided composite proceeded at $T = 573$ K and $P = 0.15$ MPa very slowly. After 1h of dehydriding only less than 0.5 wt.% H_2 was desorbed. When increasing the temperature to 623 K, desorption became much faster and was completed in 25 min attaining a capacity of about 5.4 wt.% H_2 (Fig. 6).

Hydriding of the 90 wt.% MgH_2 -10 wt.% V_2O_5 composite was accompanied by a particle size decrease, as is evident from the comparison of the TEM pictures in Figs. 4 and 7. Simultaneously, an

increased homogeneity of the crystallite size is observed in the hydrided sample due to recrystallization. The electron diffraction pattern showed that orthorhombic γ - MgH_2 was no more present, the sample being composed of tetragonal magnesium hydride, both polymorphs of vanadia and metallic vanadium. It is worth noting that, even after ten hydriding/dehydriding cycles, complete reduction of V_2O_5 to V was not attained.

The $\text{Mg}2p$ and $\text{O}1s$ X-ray photoelectron spectra of composite samples 90 wt.% MgH_2 - 10 wt.% V_2O_5 after ball milling and hydriding at $T = 573$ K and $P = 1$ MPa are shown in Fig. 8, the peaks positions being marked on the spectra. The slight shift of the $\text{Mg}2p$ peak to a lower binding energy value suggests that magnesium is present on the sample surface mainly in oxidized form. Even after

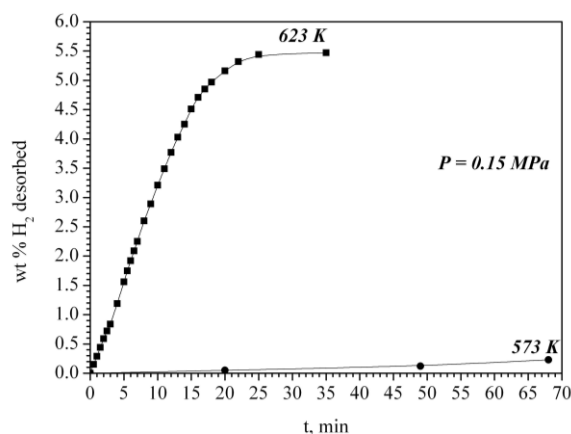


Fig. 6. Kinetic curves of hydrogen desorption from the composite 90 wt. % MgH_2 - 10 wt. % V_2O_5 at $P = 0.15$ MPa and different temperatures

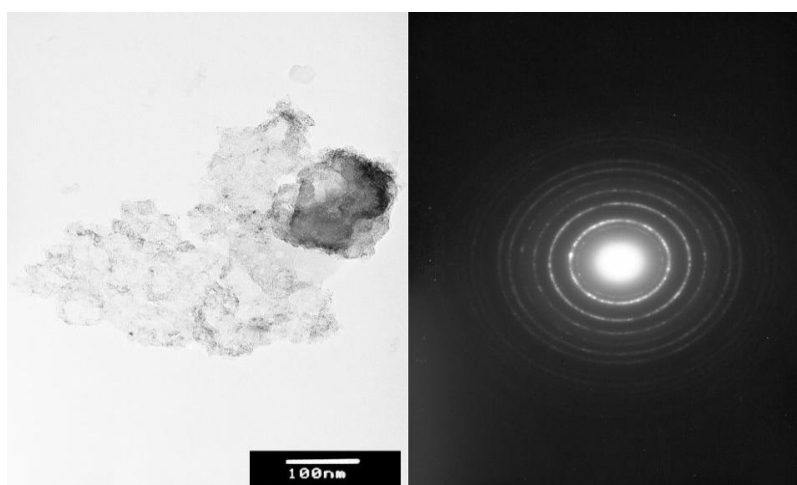


Fig. 7. TEM bright field micrograph and electron diffraction pattern of the composite 90 wt. % MgH_2 - 10 wt. % V_2O_5 after 60 min hydriding at $T = 573$ K and $P = 1$ MPa.

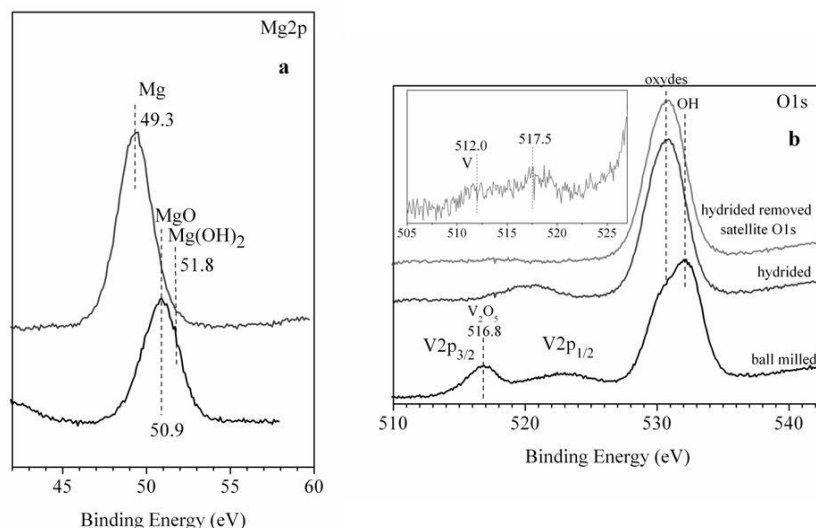


Fig. 8 XPS Mg2p (a) and O1s (b) spectra of the 90 wt. % MgH₂ - 10 wt. % V₂O₅ composite after ball milling and hydriding.

removal of the oxygen satellite, it is difficult to collect XPS data for vanadium, especially in the case of a hydrided specimen. This is probably due to the high reactivity of the samples and the low volume fraction of V₂O₅ in them. Broadened peaks were observed for V2p_{1/2}.

CONCLUSIONS

High absorption capacity of the composite 90 wt.% MgH₂ - 10 wt.% V₂O₅ (ca. 6.3 wt.% H₂) was attained after hydriding at 573 K, but at the same temperature hydrogen desorption proceeded very slowly. As a whole, however, the kinetic hydriding/dehydriding parameters of the vanadia-containing composite studied are, from a practical point of view, inferior as compared to the most performed magnesium-based hydrogen storage materials with oxide catalysts (e.g. Nb₂O₅ or TiO₂).

In the case of magnesium hydride composites with niobia, it has been found [12] that the enhanced hydrogen sorption kinetics are correlated to the presence of a substoichiometric MgH_{2-δ} phase recently established by neutron diffraction experiments [38]. This phase can appear in nanostructured samples usually obtained after prolonged ball milling. It is less stable than the stoichiometric one and acts as a gateway through which hydrogen released from magnesium hydride is flowing. It is also assumed [22] that some favorable influence on the hydrogen sorption kinetics can be exerted by oxygen deficient Mg-Nb-O phases (like MgNb₂O_{3.67}) formed during hydriding of MgH₂ - Nb₂O₅ composites.

In the context of the aforementioned, further studies of the authors will be focused on enhancing the hydrogen sorption kinetics of vanadia-containing MgH₂-composites by providing conditions for: (i) appearance of hydrogen depleted MgH₂ and (ii) formation of Mg_xV_yO_z, the more so as such phases are known as hydrogenation catalysts in petrochemistry [39].

It is generally accepted that the catalytic activity depends, to an important extent, on the catalyst biography. With the exception of a few papers (e.g. [17]) or the recently published study [40] there are no systematic studies on the hydriding/ dehydriding characteristics of magnesium-based composites as a function of the methods of preparation of their oxide or binary oxide-metal additives. In this aspect, a research work of authors is in progress, with special emphasis on vanadia.

Acknowledgement: Thanks are due to Dr. D. Rabadzhieva for her help in performing the thermal analysis measurements. Authors are grateful to the financial support of the National Centre for New Materials UNION (Contract No DO-02-82/2008).

REFERENCES

1. L.J. Murray, M. Dinča, J.R. Long, *Chem. Soc. Rev.*, **38** 1294 (2009).
2. J. Germain, J.M. Fréchet, F. Svec, *Small*, **5** 1098 (2009).
3. S. Patchkowskii, J.S. Tse, S.N. Yurchenko, L. Zhechkov, T. Heine, G. Seifert, *Proc. Natl. Acad. Sci. USA*, **102** 10439 (2005).
4. W.L. Mao, H.-K. Mao, A.F. Goncharov, V.V. Struzhkin, Q. Guo, J. Hu, J. Shu, R.J. Hemley, M. Somayazulu, Y. Zhao, *Science*, **297**, 2247 (2002).

5. C.W. Hamilton, R.T. Baker, A. Staubitz, I. Manners *Chem. Soc. Rev.*, **38**, 279 (2009).
6. S. Harder, J. Spielmann, J. Intermann, H. Bandmann, *Angew. Chem. Int. Ed.* **50** 4156 (2011).
7. K.-F. Aguey-Zinsou, J.-R. Ares-Fernández, *Energy Environ. Sci.*, **3**, 526 (2010).
8. J. Huot, G. Liang, R. Schulz, *Appl. Phys.*, **A 72**, 187 (2001).
9. M. Dornheim, N. Eigen, G. Barkhordarian, T. Klassen, R. Bormann, *Adv. Eng. Mater.*, **8**, 377 (2006).
10. M. Dornheim, S. Doppiu, G. Barkhordarian, U. Boesenberg, T. Klassen, O. Gutfleisch, R. Bormann, *Scripta Mater.*, **56**, 841 (2007).
11. I.P. Jain, C. Lal, A. Jain, *Int. J. Hydrogen Energy*, **35**, 5133 (2010).
12. A. Borgschulte, U. Bösenberg, G. Barkhordarian, M. Dornheim, R. Bormann, *Catal. Today*, **120**, 262 (2007).
13. M. Khrussanova, M. Terzieva, P. Peshev, E. Yu. Ivanov, *Mater. Res. Bull.*, **22**, 405 (1987).
14. M. Khrussanova, M. Terzieva, P. Peshev, I. Konstantchuk, E. Ivanov, *Z. Phys. Chem. (N.F.)*, **164**, 1261 (1989).
15. P. Peshev, M. Khrussanova, D. Chakarov, M. Terzieva, Ts. Marinova, *Mater. Res. Bull.*, **24**, 207 (1989).
16. W. Oelerich, T. Klassen, R. Bormann, *J. Alloys Compd.*, **315**, 237 (2001).
17. D.L. Croston, D.M. Grant, G.S. Walker, *J. Alloys Compd.*, **492**, 251 (2010).
18. A. J. Du, C. S. Sean, X. D. Yao, C. H. Sun, L. Li, G. Q. Lu, *Appl. Phys. Lett.*, **92**, 163106 (2008).
19. G. Barkhordarian, T. Klassen, R. Bormann, *Scripta Mater.*, **49**, 213 (2003).
20. G. Barkhordarian, T. Klassen, R. Bormann, *J. Alloys Compd.*, **364**, 242 (2004).
21. N. Hanada, T. Ichikawa, S. Hino, H. Fujii, *J. Alloys Compd.*, **420**, 46 (2006).
22. O. Friedrichs, F. Aguey-Zinsou, J.R. Ares-Fernández, J.C. Sánchez-López, A. Justo, T. Klassen, R. Bormann, A. Fernández, *Acta Mater.*, **54**, 105 (2006).
23. O. Friedrichs, T. Klassen, J.C. Sánchez-López, R. Bormann, A. Fernández, *Scripta Mater.*, **54**, 1293 (2006).
24. D. Fátay, A. Révész, T. Spassov, *J. Alloys Compd.*, **399**, 237 (2005).
25. A. Révész, D. Fátay, T. Spassov, *J. Mater. Res.*, **22**, 3144 (2007).
26. A. Révész, D. Fátay, T. Spassov, *J. Alloys Compd.*, **434-435**, 725 (2007).
27. F. Dolci, M. Di Chio, M. Baricco, E. Giamello *Mater. Res. Bull.*, **44**, 194 (2009).
28. B. Tanguy, J.-L. Soubeyroux, M. Pezat, J. Portier, P. Hagenmuller, *Mater. Res. Bull.*, **11**, 1441 (1976).
29. S. D. Vincent, J. Huot, *J. Alloys Compd.*, **509**, L175 (2011).
30. W.H. Zachariasen, C.E. Holley Jr., J.F. Stamper Jr, *Acta Crystallogr.*, **16**, 352 (1963).
31. T. Moriwaki, Y. Akahama, H. Kawamura, S. Nakano, K. Takemura, *J. Phys. Soc. Japan*, **75**, 074603 (2006).
32. R. Enjalbert, J. Galy *Acta Crystallogr.*, **C42**, 1467 (1986).
33. P. Balog, D. Orosel, Z. Cancarevic, C. Schön, M. Jansen, *J. Alloys Compd.*, **429**, 87 (2007).
34. M. Bortz, B. Bertheville, G. Böttger, K. Yvon, *J. Alloys Compd.*, **287**, L4 (1999).
35. N. Hanada, T. Ichikawa, S. I. Orimo, H. Fujii *J. Alloys Compd.*, **366**, 269 (2004).
36. S. Gialanella, R. Ceccato, F. Casari, G. Ischita, A. Molinari, *CALPHAD*, **33**, 82 (2009).
37. K. Kusaba, E. Ohshima, Y. Syono, T. Kikegawa, *J. Cryst. Growth*, **229**, 467 (2001).
38. H. G. Schimmel, J. Huot, L. C. F. Chapon, D. Tichelaar, F. M. Mulder *J. Am. Chem. Soc.*, **127**, 14348 (2005).
39. S. R. G. Carrazán, C. Peres, J. P. Bernard, M. Ruwet, P. Ruiz, B. Delmon, *J. Catal.*, **158**, 452 (1996).
40. Y. Jia, L. Cheng, N. Pan, J. Zou, G. Lu, X. Yao, *Adv. Energy Mater.*, **1**, 387 (2011).

СОРБЦИОННИ СВОЙСТВА ПО ОТНОШЕНИЕ НА ВОДОРОД НА КОМПОЗИТ MgH₂ - V₂O₅ ПОЛУЧЕН ЧРЕЗ МЕХАНОАКТИВИРАНЕ

Е. Григорова¹, М. Христов¹, П. Пешев¹, Д. Нихтянова^{1,2}, Н. Величкова¹, Г. Атанасова¹

¹⁾ *Институт по обща и неорганична химия, Българска академия на науките, бул. Акад. Г. Бончев, блок 11, София 1113*

²⁾ *Институт по минералогия и кристалография, Българска академия на науките, бул. Акад. Г. Бончев., блок 107, София 1113*

Постъпила на 9 април, 2012 г.; коригирана на 7 ноември, 2012 г.

(Резюме)

Композит със състав 90 мас.% MgH₂ – 10 мас.% V₂O₅ беше получен чрез механоактивиране за 60 мин. под аргон на смес от MgH₂ и V₂O₅. Сорбционните свойства по отношение на водород бяха определени чрез апаратура базирана на обемен метод или метод на Сиверт. Абсорбцията беше проведена при температури 473 и 573 К и налягане 1 МРа, а десорбцията при Т = 573 и 623 К и Р = 0.15 МРа. Структурата, фазовият и повърхностният състав на изходните съединения и композита преди и след хидриране бяха изследвани чрез рентгеноструктурен фазов анализ, термичен анализ, трансмисионна електронна микроскопия и рентгенова фотоелектронна спектроскопия. След хидрирането на композита при 573 К беше достигнат висок абсорбционен капацитет от 6.3 мас.% H₂. Бърза десорбция беше наблюдавана при температури по-високи отколкото се изискват за практическо приложение. Някои идеи за бъдещи изследвания на композити на базата на магнезий съдържащи V₂O₅ са обсъдени с оглед подобряване на свойствата.

Systematic approach for designing and activities' scheduling of supply chain network

R. Adonyi¹, E. G. Kirilova^{2*}, N. Gr. Vaklieva-Bancheva²

¹Department of Computer Science and Systems Technology, University of Pannonia, Egyetem u. 10, 8200 Veszprem, Hungary

²Institute of Chemical Engineering, Bulgarian Academy of Sciences, Acad. G. Bonchev Str., bl. 103, 1113 Sofia, Bulgaria

Received April 14, 2012; Revised May 23, 2012

The present work introduces a two-level systematic approach for optimal Supply Chain (SC) Management. At the first level the SC design problem is solved by applying the mathematical programming; while at the second level the scheduling of the SC activities is modeled and solved by the S-graphs framework. The proposed systematic approach is tested on a tree echelon supply chain example. As a result both, the network of the supply chain corresponding to the optimal total site products portfolio is obtained and the optimal schedule ensuring fleet's assignments so as to implement the portfolio within the production horizon.

Key words: design, activities scheduling, supply chain, S-graph, mathematical programming

INTRODUCTION

Market globalization and increased competitiveness press plant management for a best use of available resources, efficient manufacturing, and looking for a best market position. The current manufacturing environment for process industry has changed from a traditional single-site, single market to a more integrated global production mode where multiple sites are serving a global market with multiple products. Later requires coordination of the planning across sites in terms of cost and market effectiveness [1].

In a way the correct product to be produced and delivered on time on the market, a sequence of functions called Supply Chain has to be performed. It encompasses purchasing of raw materials, transformation of these materials into intermediate and target products and distribution of these products to the customers. Some of these functions in most of the companies are performed by separated organizations which have own objectives and operate independently. Supply chain management is a strategy through which an integration of these functions is achieved. It also coordinates all input/output flows (of materials, information and funds) so that products are produced and distributed in the right quantities, to the right locations, and at the right time. Its main objective is to achieve acceptable financial returns

together with the desired consumers' satisfaction.

The Supply Chain Management (SCM) problem may be considered at different levels depending on the types of decisions which should be made. The strategic decisions are made typically over a longer time horizon. These are closely linked to the corporate strategy and guide supply chain policies from a design perspective. On the other hand operational decisions are made over a day-to-day basis in short-term scheduling the SC activities.

In order to provide quantitative support for making these decisions numerous model-based approaches and algorithms have been developed. They are heuristic [2] or mathematical programming approaches [3, 4]. The proposed various deterministic models of the supply chain are formulated in terms of MINLP [5–10] or MILP [11–13]. In the case of the uncertainty in the supply chain optimization stochastic analytical models [14, 15] and scenario planning [16, 17] are used.

Usually, the SCM problem considers both, the design and scheduling decision levels. The design problem arises from the network characteristics of SC and is connected with a production planning, while the scheduling one comes from the production control.

Considered SCM problem comprises three echelons SC, i.e. sets of suppliers of raw materials, the production complex with a given number of plants manufacturing the same group of products and the group of markets (see Figure 1). The management process involves conducting the following activities: purchase of the raw materials

* To whom all correspondence should be sent:
E-mail: eshopova@mail.bg

from suppliers and their transportation to the plants, production of target products and their shipment to the markets and selling.

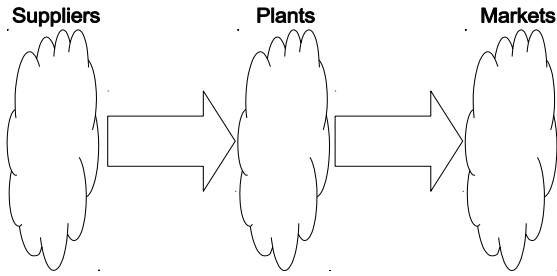


Fig.1. The considered three echelon SC.

Accounting for the considered set of target products, the SC design problem is connected with definition of these production routes through the SC from the suppliers to the markets that results in optimal product portfolios for the entire production complex, i.e. that maximize a total income of the complex and fulfill predetermined conditions for suppliers, plants and markets in a given time horizon, Figure 2.

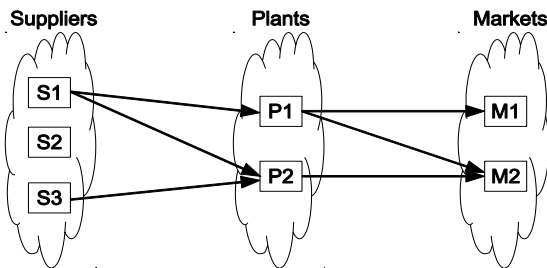


Fig. 2. Material flows in the SC network (design).

The scheduling of the SC activities comes into account after the selection of the SC network. The scheduling of the SC resources, e.g. transportation, units, is based on the parameters of the selected SC network (see Figure 3). Scheduling controls the activities of the SC elements through the transportation of raw materials and target products.

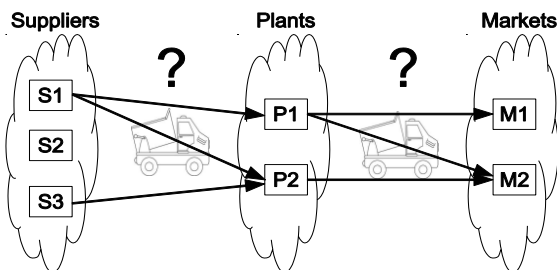


Fig.3. Scheduling the SC activities.

The major challenge of the SCM problem is that it becomes computationally intractable when the number of production sites, markets, and products

increase in the supply chain network. A good way to deal effectively with the increasing complexity is application of a sequential solution approach by using specific hierarchical methods and techniques.

The main aim of this paper is developing of two-level systematic approach for short-term SC designing and scheduling of supply chain activities, embedding continuous plant complex. The proposed approach is based on the applications of the mathematical programming approach and S-graphs framework. Firstly, for the SC design purpose, the mathematical model is built and used in an optimization framework to determine the network for the optimal total site product portfolio together with respective flow rates of the raw materials and the products. Then the S-graph framework is used for scheduling of SC activities.

FIRST LEVEL – SUPPLY CHAIN DESIGN

Firstly using a mathematical programming approach a SC design problem, is solved, defining the network with regard to the optimal total site production portfolio, and accounting for distribution of raw materials to the plants, products processing, distribution and selling of the manufactured products to the markets.

To formulate the SC design problem the alternative production routes for the demands must be considered (see Figure 1 and 2). The decision problem determines the flow rates of the raw materials and the products that have a maximal profit.

2.1. Problem description

A complex of continuous plants, set I , is considered. Range of products, set p , could be manufactured in each plant using separate production lines. Respective production rates are known. Production costs for products are constant over the time but different for each plant.

Set J contains the required raw materials (e.g. $j1, j2$). The products can be manufactured by alternative raw materials. However, only one raw material type is taken into account in manufacturing of each product but each raw material can be used for production of more than one products. No stocks and raw materials accumulations are permitted in the plants. The raw materials are provided by suppliers, set S , the products are transported to the markets defined by set M .

The distances between suppliers, plants and markets are known. Transportation costs depend on the raw materials and products. Transportation costs, products and raw materials costs are also

known and constant over the planning horizon H . Market demands and raw materials provisions are fixed for the horizon.

Assuming that a structure of the supply chain under consideration is constant over the horizon H the goal of this step is to design it in such a way so as to define the optimal products portfolio for the total site and its distribution on the involved plants; and to determine respective routes of products from the suppliers to the markets.

2.2. Data required

To define the problem following set of data must be given:

$PRC_{i,p}$ - production cost of product p in plant i , [CU / ton];

$MDem_{m,p}$ - demand of product p on market m for the horizon H , [tons];

$Cost_{m,p}$ - cost of product p on market m , [CU per ton];

$MSup_{s,j}$ - capacity of the supply center s with regard to raw material j for the horizon H , [tons];

$CRM_{s,j}$ - cost of raw material j in the supply center s , [CU per ton];

$MDis_{i,m}$ - distance between plant i and market m , [km];

$TMC_{p,i,m}$ - transportation cost of product p between plant i and market m , [CU per ton per km];

$SDis_{i,s}$ - distance between plant i and supply center s , [km];

$TRC_{j,i,s}$ - transportation cost of raw material j from the supply centre s to plant i , [CU per ton per km].

Following additional data, concerning production rate of each plant to each product and average products yield of each product, must be given:

$PR_{i,p}$ - production rate of product p in plant i , [ton/hour].

$YF_{p,j}$ - average yield of product p in plant i from a unit mass of raw material j , [ton product /ton raw material].

2.3. Mathematical modeling of Supply Chain Control Variables

To describe the problem we introduce next groups of control variables:

Purposing to determine the structure of the supply chain two sets of binary variables are set up. Variables χ to structure the SC between the plants and markets:

$$\chi_{m,i} = \begin{cases} 1 - \text{if market } m \text{ is connected} \\ \quad \text{with plant } i \\ 0 - \text{otherwise} \end{cases}, \quad (1)$$

and variables γ to structure the SC between the plants and supply centers for raw materials:

$$\gamma_{s,i} = \begin{cases} 1 - \text{if the supply center } s \text{ is connected} \\ \quad \text{with the plant } i \\ 0 - \text{otherwise} \end{cases}. \quad (2)$$

Additionally, purposing to follow for the product flows from plants to markets and for the raw materials flows from supply centers to plants we introduce following two groups of continuous variables. Variables $X_{i,p,m}$ track for the amount of product p processed in plant i and sold on market m , to be in the following boundaries:

$$0 \leq X_{i,p,m} \leq MDem_{p,m}, \quad \forall i, \forall p, \forall m, \quad (3)$$

and variables $Y_{i,j,s}$ accounting for the amount of raw material j bought by plant i from the supply center s , varying in:

$$0 \leq Y_{i,j,s} \leq MSup_{j,s}, \quad \forall i, \forall j, \forall s. \quad (4)$$

Mathematical description of Supply Chain design problem

The mathematical description of SC design problem involves a set of aggregated plants models and a set of constraints. Accounting for relations between plants and other elements (markets and supply centers) of the SC, the aggregated plants' models aim to describe the proper boundaries of the feasible product portfolio for each plant. The posed set of constraints has to track for keeping the posed conditions on the markets and in the supply centers.

Aggregated Plants' Models. To define the products portfolio for each plant i , the variables $QP_{i,p}$ are introduced to calculate the amount of each product p processed in the plant within the horizon H :

$$QP_{i,p} = \sum_{m=1}^M X_{i,p,m} \chi_{m,i}, \quad \forall p, \forall i. \quad (5)$$

From the other side, equations (5) present the condition that no stocks accumulation takes place in each plant:

Using the average yield for each product p , the amount of raw material $QRM_{i,j}$ required for its processing in the plant i is determined:

$$QRM_{i,j} = \sum_{p=1}^P \frac{1}{YF_{p,j}} QP_{i,p}, \quad \forall i, \forall j. \quad (6)$$

Moreover, calculated amount of raw materials $QRM_{i,j}$ must be:

$$QRM_{i,j} = \sum_{s=1}^S Y_{i,j,s} \gamma_{s,i}, \quad \forall i, \forall j. \quad (7)$$

Equations (7) describe pre-posed condition for no raw materials accumulation in the plants.

Constraints. Aggregated plants' models are completed with sets of constraints tracking for product portfolio feasibility and for feasibility of the connected with the plants flows.

The product portfolio feasibility constraints ensure that the amount of each product p manufactured during the horizon H in each plant i corresponds to the plant's capacity:

$$0 \leq QP_{i,p} \leq PR_{i,p} H, \quad \forall p, \forall i. \quad (8)$$

The flows feasibility constraints guarantee that the assigned to a given plant i product ($X_{i,p,m}$) and the raw material ($Y_{i,j,s}$) flows are really existing, i.e. the respective connections between the plant i and market m and supply center s exist:

$$0 \leq X_{i,p,m} \leq MDem_{p,m} \chi_{m,i}, \quad \forall i, \forall p, \forall m, \quad (9)$$

$$0 \leq Y_{i,j,s} \leq MSup_{j,s} \gamma_{s,i}, \quad \forall i, \forall j, \forall s. \quad (10)$$

Posed on each market m constraints ensure that the amount of product p processed in all plants and sold on it is less or equal to its demand:

$$0 \leq \sum_{i=1}^I X_{i,p,m} \chi_{m,i} \leq MDem_{p,m}, \quad \forall p, \forall m, \quad (11)$$

Similarly, the constraints posed on each supply center guarantee that the raw material- j bought by plants from the supply center s is less or equal of its capacity:

$$0 \leq \sum_{i=1}^I Y_{i,j,s} \gamma_{s,i} \leq MSup_{j,s}, \quad \forall j, \forall s. \quad (12)$$

Objective Function

The profit of the production complex is used as an objective function. It is determined as a difference between the incomes from products sale on the markets and expenditures for products processing, transportation and raw materials:

$$F = \sum_{i=1}^I \left[\sum_{m=1}^M \sum_{p=1}^P X_{i,p,m} \chi_{m,i} \cdot Cost_{m,p} - \sum_{p=1}^P \sum_{m=1}^M X_{i,p,m} \chi_{m,i} \cdot PRC_{i,p} - \left(\sum_{s=1}^S \sum_{j=1}^J CRM_{j,s} \cdot Y_{i,j,s} \cdot \gamma_{s,i} + \sum_{j=1}^J \sum_{s=1}^S Y_{i,j,s} \cdot \gamma_{s,i} \cdot TRC_{j,s} \cdot SDis_{i,s} + \sum_{p=1}^P \sum_{m=1}^M X_{i,p,m} \chi_{m,i} \cdot TMC_{p,i,m} \cdot MDis_{i,m} \right) \right] \quad (13)$$

Thus formulated objective function is subject to maximization:

$$MAX(F)_{X,Y,\chi,\gamma} \quad (14)$$

Thus formulated deterministic SC model, comprises the plants aggregated models (5–8), set of constraints (9–12), sets of control variables (1-4) and the objective function (13), and results in a Mixed Integer Non-Linear Programming (MINLP) problem. Its solution gives the optimal profit of the production complex and provides the conditions at which will be reached. Moreover, using optimal values of control variables and the set of equations (5), the respective optimal product portfolios for each involved plant is determined. Values of integer variables provide the generalized structure of looked for production routes.

SECOND LEVEL – SCHEDULING THE SUPPLY CHAIN ACTIVITIES

Based on the results of the mathematical programming the S-graph framework is used to generate the optimal fleet's assignments with regard to transportation of the obtained amounts of raw materials and products between the supply centers, the plants and the markets which results in schedule with minimal makespan.

The S-graph framework [19–21] originally was developed for scheduling of production units aiming minimization of makespan. However, using the S-graph framework for SC activities scheduling the terms equipment units and tasks lose their conventional meaning. In the SC network three consecutive operations are represented. First the raw material is transported from the supplier to the plant, second the plant manufactures the product,

and third the product is transported from the plant to the market. The transportation is realized by using fleets which have different speed and cost. The order of the fleet selection can affect the required free time between two transportation jobs. The manufacturing step is performed by dedicated production lines at any given plants. This SC structure can be modeled with S-graph with three consecutive tasks, representing the transportation needs and the production. Thus, in S-graph terminology, the fleets, for the transportation tasks, and the production lines, for the manufacturing task, will represent the alternative equipment units.

The mathematical programming model determines the products portfolio of the plants and the flow rates of the supply chain network. The flow rates and the available transportation fleet capacities conclude the required number of batches to be scheduled. For example, based on the solution of the mathematical programming model, raw material *r1* from supplier *S1* is transported to plant *P1*, and the product *p1* is transported from plant *P1* to market *M1*. Plant *P2* produces from the raw material from suppliers *S1* and *S3* the required products for market *M2*. If the transportation cannot be fulfilled by any of the available fleets by itself, multiple batches are required to be scheduled.

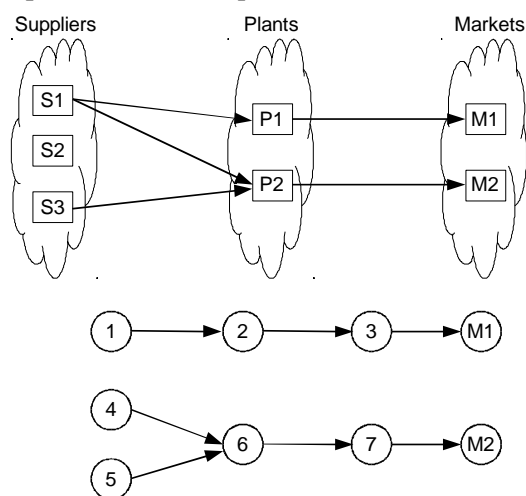


Fig.4. Transformation of the S-graph from the results of the mathematical programming.

In Figure 4, tasks 1, 4, and 5 represent the transportations from the suppliers to the plants. Tasks 3 and 7 represent the transportation from the plants to the markets. Tasks 2 and 6 denote the production.

CASE STUDY

The efficiency of proposed approached is proved on the case study of manufacturing of four products *A*, *B*, *C* and *D* in two plants *P1* and *P2*

operating in continuous mode. The products sell at two markets *M1* and *M2*. Table 1 and 2 represent demands and the incoming of the products at the markets.

Table 1. Required demands from the products at the markets.

Demands (t)				
	A	B	C	D
M1	1400	55	53	110
M2	400	20	28	65

Table 2. Incomings of the product at the markets.

Incomings (CU/t)				
	A	B	C	D
M1	790	1430	4530	3260
M2	900	2800	6320	3950

Two raw materials *R1* and *R2* are used for products manufacturing, which could be purchased by two suppliers *S1* and *S2*. Table 3 contains the available stocks from the raw materials at the suppliers, and Table 4 contains the prices for them.

Table 3. Available stock from the raw materials.

Raw material stock (t)		
	R1	R2
S1	1800	1600
S2	850	1200

Table 4. Price of the raw materials at the suppliers.

Price of the raw materials (CU/t)		
	R1	R2
S1	200	160
S2	180	140

Tables 5 – 7 contain the production rates, the cost of the production and the required raw materials for product *A*, *B*, *C*, and *D*. Plants *P1* and *P2* can manufacture the products with different cost and efficacy parameters.

Table 5. Production rates for products *A*, *B*, *C*, and *D*.

Production rate (t/h)				
	A	B	C	D
P1	1	0.06	0.05	0.12
P2	0.95	0.05	0.06	0.12

Table 6. Production costs for products *A*, *B*, *C*, and *D*.

Production cost (CU/t)				
	A	B	C	D
P1	165	230	165	112
P2	180	200	150	134

Table 7. Required raw materials for the manufacturing of products A, B, C, and D.

Raw material consumption (t/t)				
	A	B	C	D
R1	1.02	4.54	0	0
R2	0	0	20	8.33

Table 8 contains the distances between the suppliers, plants and markets. These data will be required for the calculation of the time for the transportations. For the transportations four different fleets are available with different capacities and average velocities (see Table 9). The transportation cost is based on the distance between the suppliers and plants and between the plants and markets (see Tables 10 and 11.).

Table 8. Distances between the plants, the markets and the suppliers.

Distance (km)		
	P1	P2
M1	226	238
M2	92	89
S1	41	31
S2	36	61

Table 9. Capacity and velocity of the available fleets for the transportation.

Fleet	Capacity (t)	Velocity (km/h)
Fleet #1	100	100
Fleet #2	300	80
Fleet #3	500	80
Fleet #4	800	60

Table 10. Transportation costs of the raw materials between the suppliers and the plants.

Transportation cost of the raw mat. (CU/t)			
Raw material	Plant	Supply centre	
		S1	S2
R1	P1	41	28.8
R2	P1	36.9	32.4

Table 11. Transportation costs of the products between the plants and the markets.

Transportation cost of the products (CU/t)			
Product	Plant	Market	
		M1	M2
A	P1	339	184
B	P1	339	184
C	P1	271.2	165.6
D	P1	271.2	165.6

RESULTS

Solution of the case study considered is carried out by using mathematical programming approach along with BASIC GA [18] optimization technique on the design level. As a result the flow rates of the raw materials and the products ensuring the

maximal total site profit are obtained. Based on these results on the scheduling level S-graph framework coupled with branch and bound solution technique [19-21] is applied in order to be obtained the optimal fleet's assignments with regard to transportation of the obtained amounts of raw materials and products between the supply centers, the plants and the markets corresponding to a schedule with minimal makespan.

Besides both plants, the designed supply chain involves both markets and both distribution centers. The distribution of the materials flows between the suppliers the plants and the first and the second markets are listed in Table 12 and Table 13. On particular, they are represented the data for the purchased by the suppliers amounts of raw materials for products manufacturing and the amounts of the produced products sold at the selected markets.

Table 12. Material flows in the supply chain (products for market M1).

Supplier	Raw mat. (t)	Plant	Product to M1 (t)
S2	R1 (326)	P1	A (320)
S1	R1 (678.9)	P2	A (684)
S2	R1 (32.7)	P1	B (7.2)
S1	R2 (55.1)	P1	C (3)
S1	R2 (502)	P2	C (25.1)
S2	R2 (178.3)	P1	D (21.4)
S1	R2 (719.9)	P2	D (86.4)

Table 13. Material flows in the supply chain (products for market M2).

Supplier	Raw mat. (t)	Plant	Product to M2 (t)
S2	R1 (408)	P1	A (400)
S2	R1 (43.8)	P1	B (16.8)
S2	R1 (14.53)	P2	B (3.2)
S2	R2 (368)	P1	C (18.4)
S1	R2 (85.5)	P2	C (9.6)
S2	R2 (541.4)	P1	D (65)

Analyzing the above listed results, it can be seen that the market demands of the second market M2 that proposes higher incomings of the products and is situated closer to both plants are completely satisfied (100%) for all four products – A, B, C and D. On a contrary, market demands of the first market are satisfied on 72% for the first product and on 13% and 53% and 98% for the second, third and the fourth products. Also greater part (60%) of the raw materials (R1 and R2) required in the plant complex must be provided by the second supplier S2. In this way the capacity of S2 is completely fulfilled (843.83 t from R1 and 1200 t from R2) and

this one of the first supplier *S1* is fulfilled up to 61%.

The optimal fleet allocation is generated by the transportations and plants scheduling. The makespan of the optimal schedule is 723.8 h. The optimal fleet assignment is given in Table 14. It can be seen that the most frequency selected fleet for transportation of raw materials and products between suppliers, plants and the markets is fleet 1 – 63%. The fleet 2 – 27% is the next one. The fleet 3 is used just one time and fleet 4 - two times.

CONCLUDING REMARKS

This study proposes two-level hierarchical approach for sequential short-term design of SC and scheduling of the activities in the Supply Chain network with embedded production complex of

continuous plants. At the first level, the SC mathematical model is formulated involving aggregated plants model accounting for the connections with markets and suppliers and also for the portfolio feasibility. The model is used to determine the optimal flow rates of the raw materials and the products with regard to the maximal total site profit. From the planning level a scheduling problem is generated. S-graph framework is applied for its solution. As a result the optimal fleet's assignments with regard to transportation of the obtained amounts of raw materials and products between the supply centers, the plants and the markets corresponding to a schedule with minimal makespan are obtained.

Table 14. Scheduling the fleet.

Supplier	Raw material (t)	Plant	Product (t)	Market	
S2	R1 (326)	P1	A (320)	M1	Fleet #1
S1	R1 (678.9)	P2	A (684)	M1	Fleet #2
S2	R1 (18.8)				Fleet #3
S2	R1 (32.7)	P1	B (7.2)	M1	Fleet #4
S1	R2 (55.1)	P1	C (3)	M1	
S2	R2 (5.8)				
S1	R2 (502)	P2	C (25.1)	M1	
S2	R2 (178.3)	P1	D (21.4)	M1	
S1	R2 (719.9)	P2	D (86.4)	M1	
S2	R1 (408)	P1	A (400)	M2	
S2	R1 (43.8)	P1	B (16.8)	M2	
S1	R1 (32.5)				
S2	R1 (14.53)	P2	B (3.2)	M2	
S2	R2 (368)	P1	C (18.4)	M2	
S1	R2 (85.5)	P2	C (9.6)	M2	
S2	R2 (106.5)				
S2	R2 (541.4)	P1	D (65)	M2	

The efficiency of the proposed approach is illustrated on a case study of manufacturing of four products in production complex comprising two plants, two suppliers, and two markets. Obtained results are discussed in details.

Acknowledgements: *The study has been carried out with the financial support of the Bulgarian-Hungarian Bilateral Project Chem20 2010/2012.*

REFERENCES

1. S. J. Wilkinson, A. Cortier, N. Shah, C.C. Pantelides, *Computers&Chem.Eng.*, **S20**, S1275 (1996).
2. J. F. Williams, *Manag. Sci.*, **27**, 336 (1981).
3. C.E. Bodington, D.E. Sorbys, *Hydrocarbon Processing*, **75**, 55, (1996).
4. H. L. Lee, C. Billington, *Sloan Management Review*, Spring, 65 (1992).
5. M. A. Cohen, H.L. Lee, *J. Manufact.Operations Manag.*, **2**, 81 (1989).
6. B. B. Ivanov, K.I. Mintchev, *Bulg.Chem. Commun.*, **39**, 106 (2007).
7. B. Ivanov, D. Dobrudzhaliev, Proc.International Conference on Information Technologies – Info Tech 2008, (Plovdiv, Bulgaria, September 19th–20th, 2008), Volume 2, pp. 267-274.
8. B. B. Ivanov, D. Dobrudzhaliev, *J.Inform. Control Manag. Syst.*, **8**, 157 (2010).

9. B. Ivanov, D. Dobrudzhaliev, A. Angelov, Proc. 7th Int. Conf. *ICOSECS7*, (Bucharest, Romania, September 15th–17th, 2010), **CD**.
10. N. G. Vaklieva-Bancheva, E. G. Shopova, A. España, L. Puigjaner, Proc.Int. Mediterranean Modelling Multiconference, (Barcelona, Spain, October 4th-6th, 2006), pp. 101-110.
11. J. Pooly, *Interface*, **24**, 113 (1994).
12. H. Pirkul, V. Jayarama, *Transport. Sci.*, **30**, 291 (1996).
13. K. S. Hindi, K. Pienkosz, *J. Operat. Soc.*, **50**, 268 (1999).
14. D. F. Pyke, M.A. Cohen, *Eur.J.Operat. Res.*, **68**, 23 (1993).
15. H. L. Lee, C. S. Tang, *Manag. Sci.*, **43**, 40 (1997).
16. F. Mobasheri, L. H. Orren, F. P. Sioshansi, *Interface*, **19**, 31 (1989).
17. J. M. Mulvey, *Interface*, **26**, 1, (1996).
18. E. G. Shopova, G. Vaklieva-Bancheva, *Computers & Chem. Eng.*, **30**, 1293 (2006).
19. E. Sanmarti, T. Holczinger, L. Puigjaner, F. Friedler, *AIChE J.*, **48(11)**, 2557 (2002).
20. T. Holczinger, J. Romero, L. Puigjaner, F. Friedler, *Hung. J. Ind. Chem.*, **30**, 305 (2002).
21. R. Adonyi, G. Biros, T. Holczinger, F. Friedler, *J. Cleaner Productn*, **16 (2)**, 225 (2008).

НА ПИКОВИТЕ ВЪЗДЕЙСТВИЯ ОТ ЗАМЪРСИТЕЛИ ВЪРХУ ОКОЛНАТА СРЕДА ЗА МНОГОЦЕЛЕВИ ПЕРИОДИЧНИ ХИМИЧНИ И БИОХИМИЧНИ ПРОИЗВОДСТВА

Р. Адоньи¹, Е.Г. Кирилова², Н.Гр. Ваклиева-Банчева²,

¹Департамент по компютърни науки и системно инженерство, Панонски университет, ул. Едъетем 10,
8200 Веспрем, Унгария

²Институт по инженерна химия, Българска академия на науките, ул. "Акад. Г. Бончев", бл. 103, София 1113,
България

Постъпила на 14 април, 2012 г.; коригирана на 23 май, 2012 г.

(Резюме)

Това изследване представя един системно-ориентиран подход за редуциране на пиковите въздействия от замърсители върху околната среда за периодични химични и биохимични производства чрез подходящо управление на стартовите времена за производство на продуктите в производствените системи. Този подход въвежда оригинални екологични оценки за въздействие на пиковете, които отчитат само тези от моментни стойности на въздействие, които надвишават определено гранично ниво и позволяват обединяването на различни типове замърсители чрез средата, в която се излъчват. Тези оценки са използвани като оптимизационни критерии във формулираната задача за редуциране на пиковите въздействия върху околната среда от периодични химични и биохимични производствени системи.

В резултат на нейното решаване са получени най-подходящите стартови времена за производство на продуктите в даден времеви хоризонт. Ефективността на подхода е показана на пример от млечната индустрия.

Assessing the nano scale variation of the ferritin and iron level following two months of progressively increasing interval physical activity

M. J. Pourvaghari

Department of Physical Education, University of Kashan, Kashan, I.R. Iran

Received January 22, 2012; Accepted October 18, 2012

Variation of the serum blood ferritin and iron level leads to considerable changes in the body metabolism that eventually results in decrease of vital activity in the body. The purpose of this research was to examine the changes in iron level and its stored form, ferritin, in the subjects measured in nano scale level after participating in two months of physical activity. For this purpose, 20 healthy male subjects were randomly assigned to two groups of experimental and control groups. The subjects' fasting blood sample was collected. They participated in two months of progressively increasing aerobic exercise twice per week. Following two months of exercise, blood sample was collected again. The results of analysis showed that there was a significant difference between the mean values of iron serum blood level of the subjects after two months of interval training ($P=0.003$). There was also a significant difference between the control and the experimental group after two months of interval training ($P=0.005$). In addition, there was a significant difference between the mean values of ferritin serum blood level of the subjects after two months of interval training ($P=0.019$). There was a significant difference between the control and the experimental group after two months of interval training ($P=0.04$). It was concluded that 8 weeks of interval running activity can mobilize ferritin from its local store, that is, liver, bone marrow and muscle and as a result increase the level of serum ferritin and following that increase the iron level in the blood.

Keywords: Ferritin, Iron, Increasing Intensity Interval Exercise.

INTRODUCTION

Minerals are essential for a wide variety of metabolic and physiologic processes in the human body. Some of the physiologic roles of minerals important for the athletes are their involvement in: muscle contraction, normal heart rhythm, nerve impulse conduction, oxygen transport, oxidative phosphorylation, enzyme activation, immune functions, antioxidant activity, bone health, and acid-base balance of the blood [1].

Iron is one of the most critical minerals with implications for sports performance. Iron is a component of hemoglobin, myoglobin, cytochromes, and various enzymes in the muscle cells, all of which are involved in the transport and metabolism of oxygen for aerobic energy production during endurance exercise [1].

Ferritin has been the most frequently used indicator of iron stores in the body. Low ferritin levels are an indication of decreased or exhausted iron stores. Namely, ferritin is an acute phase protein and may thus cover actual iron deficiency [2, 3].

About 30% of the body's total iron in a healthy young adult male (and about 10% in females) is stored in the form of ferritin (known as storage iron) located in such areas as the liver, bone marrow, muscle, and other body organs. From these locations, iron is transported throughout the body via the blood stream [4]. Serum ferritin levels in the range of 20–30 nanograms per milliliter have been considered markers of iron deficiency [1].

Iron deficiency is fairly common in athletes, especially in the endurance athletes [5, 6]. It commonly appears in latent form, the iron deficiency-induced anemia being, however, infrequent [5, 7, 8, 9, 10, 11]. Detecting the deficiency in physically active individuals is difficult due to possible exercise-induced changes in iron metabolism indices, especially ferritin. Increased ferritin levels were reported immediately post-exercise states [12] and even several days following strenuous exertions [12]. The detection of latent iron deficiency in athletes is not easy and requires the use of appropriate indices [12]. Although ferritin is the basic indicator of iron stores, its use as the single index of iron status may not be sufficient, especially in disorders, due to the fact that ferritin is an acute-phase protein [5, 13, 14].

* To whom all correspondence should be sent:
E-mail: vaghar@kashanu.ac.ir.

Serum ferritin concentrations decrease during training, and it has been assumed that this reflects an induction of iron deficiency following physical activity. Although serum ferritin concentrations in elite athletes are usually low, frank iron deficiency is unusual; nevertheless, obligatory daily iron losses are often increased, but this is usually compensated by enhanced absorption of dietary iron [15].

The purpose of this research was to examine the changes in iron level and its stored form, ferritin, after participating in two months of physical activity. The likely variations in such change will be associated with disruption of oxygen carrying activity, carbon dioxide, metabolic activity, performing physical activity and other metabolism events.

EXPERIMENTAL

The present research was a quasi experimental research in which 20 healthy male volunteer subjects were randomly assigned into two equal groups (n=10) of experimental and control conditions. The subjects completed a health questionnaire form. The subjects did not consume any medication within the last month nor had a history of participation in a heavy regular aerobic physical activity. Such activity can disrupt iron and ferritin metabolism regulation within the body [16]. In addition, a physician performed a general physical examination in order to approve physical and mental readiness of the subjects to participate in the project. The presence of any infection or inflammation was also ruled out since such condition result in increase in the ferritin level [16]. The systolic and diastolic blood pressure as well as Body Mass Index (BMI) of the participants was measured. Other characteristics of the subjects are presented in Table 1.

Table 1: Characteristics of the exercise and control groups.

Variables	Experimental		Control	
	Mean	Standard deviation	Mean	Standard deviation
Age (Yr.)	22.23	3.2	21.5	2.5
Height (Cm)	174.5	4.6	175.3	4.8
Systolic blood pressure(mm/Hg)	110	2.6	115	2.1
Diastolic blood pressure(mm/Hg)	76	2.2	85	2.7
Maximum oxygen consumption (VO _{2max}), (ml.min ⁻¹ .kg ⁻¹)	49.06	4.4	48.4	3.2
Body Mass Index (BMI), (kg/m ²)	24.3	3.3	25.2	4.3

For the purpose of having a homogenous group of participants, Maximum Oxygen Consumption (VO_{2max}) of the subjects was measured by running-walking test [17]. The running-walking program was employed to measure it a week prior and one week after the termination of the protocol in order to eliminate the effect of training protocol on the VO_{2max} of the participants.

TRAINING PROTOCOL

The fasting subjects in both groups attended the pathology lab at 8 am. Four milliliters of elbow venous blood sample was collected. The exercise protocol included increasing interval running program at a track and field path. They ran 4 consecutive distances of 200 meters with rest interval between each distance in the first week. Then, on the second week, 400 meters was added to the running distance on the first week. Such increase continued weekly and finally at the eighth week, the subjects ran approximately 35 Km. The running intensity was set to 60 to 75 percent of reserved heart rate [18] monitored by a polar watch provided to the subjects. At the end of 8th week, fasting blood sample was collected and analyzed by the same lab. The ferritin and iron were measured to see whether ferritin serum is released in interval physical activity in two months to supply blood iron. After reduction, iron changes to iron (II) and makes the colorful complex of ferrozine, which can show iron level [16]. These elements were analyzed by biochemistry analyzer Hitachi 717 machine. The amounts of serum iron concentration was measured according to nanogram per micro liter (ng/mic l), and ferritin level was measured according to nanogram per milliliter (ng/ml).

SPSS: PC 13.0 was used to analyze the data. Paired as well as independent t-test was used to compare the means of the pre test and post test results as well as the control and the experimental groups.

RESULTS

Kolmogrov-Smirinov was used to test the normality of the independent variables of this research. The results indicated that the variables of iron and ferritin showed normal distribution; therefore, parametric statistical procedures such as dependent and independent t-test were employed to analyze the data. These results are presented in Table 2 and Figs 1, 2.

The means and standard deviations of serum blood ferritin and iron is presented in Table 2.

Table 2: Comparing the mean values of iron (ng/micl) and ferritin (ng/ml) levels of the exercise and control groups in pre and post test

Variables-stage	Condition	Stage		t-valve	P-value
		Pre test	Post test		
		Mean± (SD)	Mean± (SD)		
Iron (ng/micl)	Experimental	1.105±0.152	1.417±0.210	3.97	0.003
	Control	1.186± 0.153	1.174±0.119	0.806	0.44
Post test-Iron	Experimental	-	1.417±0.210	3.17	0.005
	Control	-	1.174±0.119		
Ferritin (ng/ml)	Experimental	30.94±10.94	39.86±8.33	2.86	0.019
	Control	32.76±8.56	32.29±6.89	0.166	0.872
Post test- Ferritin	Experimental	-	39.86±8.33	2.213	0.04
	Control	-	32.29 ±6.89		
Weight (Kg)	Intermittent	82.7±4.2	78.4±4.7	2.15	0.044
	control	81.5±4.6	82.9±4.16	0.63	0.53
	Intermittent	-	78.4±4.7	2.26	0.035
	control	-	82.9±4.16		

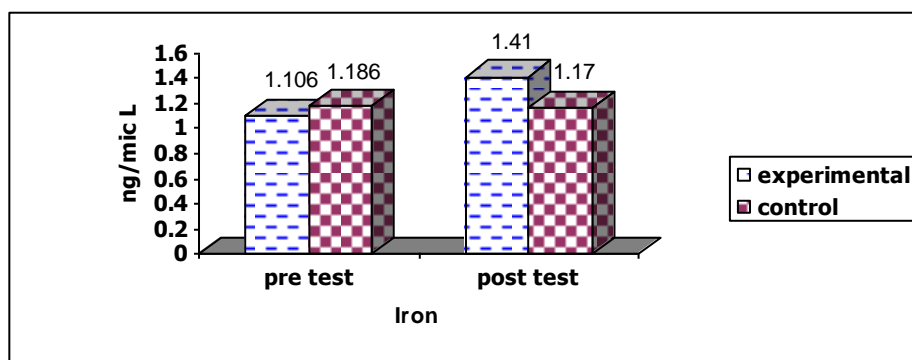


Figure 1: Comparing iron level changes (ng/micl) in experimental and control groups

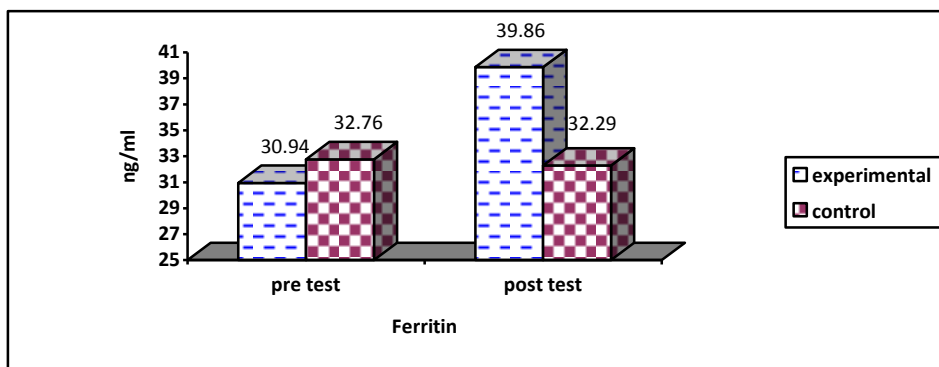


Figure 2: Comparing ferritin level changes (ng/ml) in experimental and control groups

The mean value of iron in the aerobic exercising condition prior to the start of the protocol was 1.105 ng/micl and increased to 1.417 ng/micl after two months of training. The results of analysis indicated that the increase was statistically significant (P=0.003). No significant changes was observed in the blood level of the control group after two months of their regular activity without participating in any exercise program (P=0.44).

Comparing the mean value of serum ferritin in the experimental and control condition indicated that there was a significant difference between these two groups (P=0.005).

In addition, the result of comparing the mean of pre test level of serum ferritin (30.94 ng/ml) with the post value of this variable after the aerobic intermittent activity (39.86 ng/ml) revealed that there was a significant difference between these two stages (P=0.019).

The result of comparing the mean of pre test level of serum ferritin (32.76 ng/ml) with the post test value of this variable in the control group (32.29 ng/ml) indicated that there was no significant differences between these two stages ($P=0.872$).

The result of analysis showed that there was a significant difference between the mean of serum ferritin of the control and the experimental group after the termination of the exercise protocol ($P=0.04$). In addition, the results of analysis using Pearson correlation test indicated that there was a significant association between the iron and ferritin of the subjects ($r=0.63$, $P=0.04$).

Also, participation in the exercise program resulted to a significant weight loss in the exercising group. The mean value of weight from the pre test condition (82.7 kg) decreased significantly (78.4 kg) - a 3.4 kg loss ($P=0.44$).

DISCUSSION

This study was designed to examine the changes in iron and ferritin level of serum blood measured in nano gram scale following two months of aerobic physical activity. The subjects participating in this research protocol performed two months of progressively increasing running exercise. The mean value of iron level of the subjects increased 0.313 ng/micl, a 28.23 per cent change that was also statistically significant. When compared this changes to the control group, the amount of increase was 0.243 ng/ micl equal to 20.7 percent rise. Thus, two months of aerobic running exercise resulted in a significant increase in the exercising group compared to the control group. The level of serum ferritin of the subjects changed from 30.94 to 39.86 ng/ml (28.82 percent increase) following the exercise program. The amount of increase in the exercise condition compared to the control group at the end of project was 23.63 percent.

The changes of iron level was associated with the changes of ferritin level and this association was evident in the correlation coefficient equal to 0.63 ($P=0.04$).

The findings of the present research was in agreement with the results of researches conducted by Chatard (2002) and Roecker (2002) to examine the changes in iron level following the participation of their subject in aerobic endurance activity [5, 6]. However, the result of this research did not support the findings of Zoller and associates (2004) that reported a decrease in the value of ferritin and consequently iron in athlete subjects [15]. Such discrepancy in the findings may be attributed to the

fact that the participants in the present research were sedentary subjects whereas the subjects in Zoller et. al were athletes.

Gray and associates (1993) examined the density of serum ferritin in male athletes following an interval exercise program. They reported that no significant change occurred in the ferritin value whereas the level of iron increased [19]. In this regard, the findings of the present research are similar to the alteration in the iron changes but not to the changes in ferritin value since iron in both researches increased.

Iron is stored in the form of ferritin in muscles, bone marrow, liver, and other body organs. When there is no infection or inflammation within the body, an individual uses iron for particular needs such as physical activity for the purpose of carrying oxygen, muscle contractions, nerve impulse conduction, enzyme activity, immune functions and acid-base balance [1]. On the other hand, the energy required during physical activity originates the mitochondrial iron centers. The cells may use their ferritin and iron to make mitochondrial used by mitochondrial.

Therefore, ferritin can compensate for the insufficiency of iron during the interval physical activity programs. In this research, it seemed like the iron in the serum blood was mobilized for physiological purpose and its value increased in the subjects engaged in physical activity. Such condition resulted in the release of ferritin storage including muscle and bone marrow in the blood stream. This condition in turn increased the value of ferritin in blood significantly. Following this release and increase of ferritin, iron concentration increased as well. This chain of associated changes was statistically evident. The correlation coefficient between iron and ferritin was 0.63, ($P=0.04$). Apparently, various types of physical activity can cause different responses in the concentration of mineral substances such as iron and ferritin. In addition, different intensity of exercise program, different durations or different volumes of physical activity can produce different research results. Thus, the research findings in any research may be explainable in regard to the type of responses produced by the participants.

In summary, the findings of this research indicated that participation in two months of intermittent physical activity covering approximately 35 kilometers can increase significantly the concentration of iron and ferritin of serum blood to carry oxygen, perform muscle contraction, enhance enzyme activity and immune

responses and produce anti oxidation activity during the physical activity.

Acknowledgement: The research of author was partially supported by the University of Kashan under grant No. 159233/1.

REFERENCES

1. H.W. Melvin, *J. Int. Soc. Sports Nutr.*, **2**, 43 (2005).
2. N. Ahluwalia, *Nutr. Rev.*, **56**, 133 (1998).
3. R.D. Baynes, *Clin. Biochem.*, **29**, 209 (1996).
4. V. Deakin, L. Burke, V. Deakin, *Clinical Sports Nutrition*, Sydney: McGraw-Hill, 2000, pp. 273-311.
5. J. C. Chatard, I. Mujika, C. Guy, J. R. Lacour, *Sports Med.*, **27**, 229 (1999).
6. L. Roecker, K. Hinz, K. Holland, H-CH. Gunga, J. Vogelgesang, H. Kiesewetter, *Clin. Lab.*, **48**, 307 (2002).
7. J. Malczewska, B. Raczynska, D. Siwińska, B. Szczepańska, *Biol. Sport.*, **13**, 21 (1996).
8. J. Malczewska, B. Szczepańska, R. Stupnicki, W. Sendekci, *Int. J. Sport Nutr. Exerc. Metab.*, **11**, 2 (2001).
9. K.W. Mercer, J.J. Densmore, *Clin. Sports Med.*, **24**, 599 (2005).
10. Y.O. Schumacher, A. Schmid, D. Grathwohl, D. Bültermann, A. Berg, *Med. Sci. Sports Exerc.*, **34**, 869 (2002).
11. J. Malczewska-Lenczowska, R. Stupnicki, T. Gabryś, *Biol. Sport.*, **27**, 241 (2010).
12. J.D. Cook, C.H. Flowers, B. S. Skikne, *Blood.*, **101**, 3359 (2003).
13. R.S. Gibson, Assessment of iron states. In: *Principles of Nutritional Assessment*, 2nd Edition, Oxford University Press; 2005, pp.443-476.
14. P. Peeling, B. Dawson, C. Goodman, G. Landers, D. Trinder, *Eur. J. Appl. Physiol.*, **103**, 381 (2008).
15. H. Zoller, W. Vogel, *Nutrition*, **20**, 615 (2004).
16. A.C. Guyton, E. Hall, *John Textbook of Medical Physiology*. Elsevier Inc, 2006.
17. R.W. Earle T.R. Baechle, *Essentials of Personal Training National Strength and Conditioning Association*, NSCA's Human Kinetic 2004.
18. V.F. Froelicher, J. Myers, *Exercise and the Heart*, 5th Ed. Saunders, Elsevier 2006.
19. A.B. Gray, *Medicine and Science in Sport and Exercise*, **25**, 778 (1993).

ОПРЕДЕЛЯНЕ НА НИВАТА НА ФЕРИТИН И НА ЖЕЛЯЗО В НАНОМАЩАБИ СЛЕД ДВУМЕСЕЧНО ПРОГРЕСИВНО ФИЗИЧЕСКО НАТОВАРВАНЕ

М. Дж. Пурвагар

Департамент по физическо възпитание, Университет в Кашан, Кашан, Иран

Постъпила на 22 януари, 2012 г.; приета на 18 октомври, 2012 г.

(Резюме)

Измененията на феритина и желязото в кръвния серум води до значителни промени в телесния метаболизъм, водещи в крайна сметка до намаляване на жизнената активност. Цел на тази работа е се изследват измененията на нивото в наномасштаби на желязото и неговата съхранена форма (феритинът) при хора след двумесечна физическа активност. За тази цел двадесет здрави мъже-доброволци бяха разделени на две групи (тестова и контролна) на случаен принцип. От тях са взимани кръвни проби на гладно. Те участваха в продължение на два месеца в прогресивно нарастващи аеробни упражнения два пъти седмично. Бяха взимани кръвни проби след два месеца. Резултатите от анализите показват, че е налице значителна разлика между средните концентрации на желязото в доброволците след двумесечни тренировки ($P=0.003$). Освен това е налице и значителна разлика между контролната и тестовата група след двумесечните тренировки ($P=0.005$). Освен това, налице е и значима разлика между средните стойности на феритина преди и два месеца след упражненията ($P=0.019$). Има и значима разлика между показанията на контролната и тестовата група два месеца след упражненията ($P=0.04$). Следва изводът, че 8 седмици на физическа дейност могат да мобилизират феритина от неговите естествени депа, като черен дроб, костен мозък и мускули. В резултат се повишава нивото на серумния феритин и следващото повишаване на нивото на желязото в кръвта.

Synthesis and crystal structure of an ammonium salt of 4-hydroxy-3-[(2-oxo-2H-chromen-3-yl)-(3,4,5-trimethoxyphenyl)-methyl]chromen-2-one

S. Dochev¹, A. Penkova², P. Retailleau³, I. Manolov^{4*}

¹Research Group Mihovilovic, Research Division of Organic Chemistry, Institute of Applied Synthetic Chemistry, Faculty of Technical Chemistry, Vienna University of Technology, A-1060 Vienna, Austria

²University of Southern California, Los Angeles, California, USA, 90089-1453; Rostislav Kaischew Institute of Physical Chemistry, Bulgarian Academy of Sciences, Acad. G. Bonchev str., 1113 Sofia, Bulgaria

³Service de Cristallochimie, Institut de Chimie des Substances Naturelles - CNRS, UPR2301 Bât 27 – 1, avenue de la Terrasse, 91198 Gif-sur-Yvette Cédex, France–

⁴Department of Pharmaceutical Chemistry, Faculty of Pharmacy, Medical University, 2, Dunav St., 1000 Sofia, Bulgaria

Received February 7, 2012; Revised March 23, 2013

The structure of ammonium salt of 4-hydroxy-3-[(2-oxo-2H-chromen-3-yl)-(3,4,5-trimethoxyphenyl)-methyl]chromen-2-one was determined by X-ray crystallography. The compound crystallizes as a colourless prism in the monoclinic crystal system, space group $P2_1/c$ (#14) with cell constants: $a = 16.3834(3)$ Å, $b = 10.7529(2)$ Å, $c = 14.7635(3)$ Å, $\beta = 108.287(1)^\circ$, $\alpha = \gamma = 90^\circ$, $V = 2469.52(8)$ Å³, $Z = 4$. The crystal structure was solved by direct methods and refined by full-matrix least-square on F^2 to a final $R1$ of 0.00467. The 4-hydroxycoumarins are intra molecularly hydrogen bonded between hydroxyls and carbonyls. The salt and the acid form of the title compound have slight differences between the bond lengths and the bond angles.

Key words: 4-Hydroxy-3-[(2-oxo-2H-chromen-3-yl)-(3,4,5-trimethoxyphenyl)-methyl] chromen-2-one, crystal structure, coumarin derivatives, Knoevenagel reaction, Hantzsch reaction and Pechmann condensation.

INTRODUCTION

The coumarins constitute an important class of compounds, with several types of pharmacological agents possessing anticancer [1], anti-HIV [2,3], anticoagulant [4-6], spasmolytic [7,8] and antibacterial activity among others. A large number of structurally novel coumarin derivatives have ultimately been reported to show substantial cytotoxic activity in vitro and in vivo [9,10].

Biscoumarin derivatives possess anticoagulant, spasmolytic, bacteriostatic rodenticidal, antioxidant, and antimetastatic activities. Some of them can be used as herbicides. By chemical modifications it is possible to obtain a compound with good biological activity, but with lower toxicity and fewer side effects. The products synthesized by the reaction of Knoevenagel are in an acid form of the molecules.

We studied the possibility for converting the hydroxy derivatives of the polysubstituted 1,4-dihydropyridine (structure analogues of well known Ca-channel blockers) to the corresponding

coumarine products by Pechmann condensation. The synthesis were realized with agreement of the reaction conditions of the Hantzsch reaction and Pechmann condensation.

EXPERIMENTAL

All hydroxyl- and methoxy substituted aromatic aldehydes, ethyl acetoacetate, ammonium acetate, 4-hydroxycoumarin, 4-methyl acetophenone and solvents were reagent grade and were purchased from Sigma-Aldrich and Merck. Melting points were measured on Boetius hot plate microscope (Germany) and were uncorrected. IR spectra (nujol) were recorded on an IR-spectrometer FTIR-8101M Shimadzu. ¹H-NMR spectra were recorded at ambient temperature on a Bruker 250 WM (250 MHz) spectrometer in [d₆]-acetone, CDCl₃. Chemical shifts are given in ppm (δ) relative to TMS used as an internal standard. Mass spectra were recorded on a Jeol JMS D 300 double focusing mass spectrometer coupled to a JMA 2000 data system. The compounds were introduced by direct inlet probe, heated from 50 °C to 400 °C at a rate of 100 °C/min. The ionization current was 300 mA, the accelerating voltage 3 kV and the chamber temperature 150°C. TLC was performed on

* To whom all correspondence should be sent:
E-mail: imanolov@gmx.net

precoated plates Kieselgel 60 F₂₅₄ Merck (Germany) with layer thickness 0.25 mm and UV detection (254 nm). Yields of TLC-homogeneous isolated products are given. Results of elemental analyses indicated by the symbols of the elements were within $\pm 0.4\%$ of the theoretical values.

The crystal-structure determination was mounted on a glass fibre and used for a low-temperature X-ray structure determination. All measurements were made on a *Nonius KappaCCD* area-detector diffractometer [11] using graphite-monochromated Mo K α radiation ($\lambda = 0.71073 \text{ \AA}$) and an *Oxford Cryosystems Cryostream 700* cooler. The unit cell constants and an orientation matrix for data collection were obtained from a least-squares refinement of the setting angles of 5908 reflections in the range $4^\circ < 2\theta < 55^\circ$. The mosaicity was $0.390(1)^\circ$. A total of 299 frames were collected using ϕ and ω scans with κ offsets, 80 seconds exposure time and a rotation angle of 2.0° per frame, and a crystal-detector distance of 30.0 mm.

Data reduction was performed with HKL Denzo and Scalepack [12]. The intensities were corrected for Lorentz and polarization effects, but not for absorption. The space group was uniquely determined by the systematic absences. Equivalent reflections were merged. The data collection and refinement parameters are given in Table 1. A view of the molecule is shown in the Figs. 3 and 4.

The structure was solved by direct methods using *SIR92* [13], which revealed the positions of all non-hydrogen atoms. The non-hydrogen atoms were refined anisotropically. The hydroxyl and ammonium H-atoms were placed in the positions indicated by a difference electron density map and their positions were allowed to refine together with individual isotropic displacement parameters (Tables 7-9). All remaining H-atoms were placed in geometrically calculated positions and refined by using a riding model where each H-atom was assigned a fixed isotropic displacement parameter with a value equal to $1.2U_{\text{eq}}$ of its parent C-atom ($1.5U_{\text{eq}}$ for the methyl groups). The refinement of the structure was carried out on F^2 by using full-matrix least-squares procedures, which minimised the function $\sum w(F_o^2 - F_c^2)^2$. The weighting scheme was based on counting statistics and included a factor to downweight the intense reflections. Plots of $\sum w(F_o^2 - F_c^2)^2$ versus $F_c/F_c(\text{max})$ and resolution showed no unusual trends. A correction for secondary extinction was applied.

Neutral atom scattering factors for non-hydrogen atoms were taken from Maslen, Fox and O'Keefe [14a], and the scattering factors for H-atoms were taken from Stewart, Davidson and Simpson [15]. Anomalous dispersion effects were included in F_c [16]; the values for f' and f'' were those of Creagh and McAuley [14b]. The values of the mass attenuation coefficients are those of Creagh and Hubbel [14c]. The *SHELXL97* program [17] was used for all calculations.

Synthesis of 1,4-dihydropyridines

3,4,5-Trimethoxybenzaldehyde (1.96 g, 10 mmol), 4-hydroxycoumarin (3.24 g, 10 mmol), 4-methoxyacetophenone (1.5 g, 10 mmol), ammonium acetate (30.8 g, 40 mmol), 40 mL of water were added and the reaction mixture refluxed and vigorously stirring for nearly 2 h. Usually the product must be well known 1,4-dihydropyridine (Hantzsch reaction). Yield 3.5 g (67 %), m. p. $174.8\text{--}177^\circ\text{C}$ [18].

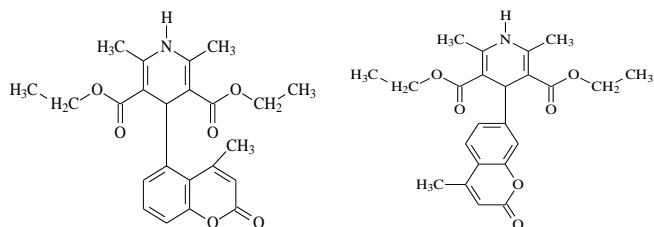
Synthesis of biscoumarins

4-Hydroxycoumarin (6.48 g, 40 mmol), 3,4,5-trimethoxybenzaldehyde (3.92 g, 20 mmol), 75 mL ethanol were mixed under stirring and heating at reflux for 10 min. After cooling the product was filtered and was recrystallized from acetonitrile (Knoevenagel reaction). Yield 5.4 g (54 %), m.p. $241\text{--}243^\circ\text{C}$. TLC (hexane/chloroform/acetone 5:3:1) R_f 0.26. Anal. C₂₈H₂₂O₉ (502) (C, H) (Calcd/found): % C = 66.93 / 67.11 ; % H = 4.38 / 4.57. IR (nujol) cm⁻¹: 1661, 1620, 1266, 1211, 1129, 760. ¹H-NMR (DMSO-d₆) 3.2-3.6 d (9H), 4.4-4.6 s (1H), 5.0-5.5 s (1H), 6.0-6.4 d (1H), 6.8-7.8 m (10H). MS (FAB NEG): 502 (7.5), 501 (29), 306 (17.5), 305 (40), 199 (79), 161 (100). The other technique of mass spectral investigation led to another way of fragmentation. The condensation process lasted for 2 h in glacial acetic acid medium at reflux [19-25].

RESULTS AND DISCUSSION

We would like to synthesized dihydropyridine derivatives and pyridine derivatives of 2H-chromen-2-one (coumarin). The synthesis were realized with agreement of the reaction conditions of the Hantzsch reaction and Pechmann condensation (Fig. 1). Usually the product must be well known 1,4-dihydropyridine. But in this case (Hantzsch reaction) instead of dihydropyridine derivative the product is ammonium salt of 4-hydroxy-3-[(2-oxo-2H-chromen-3-yl)-(3,4,5-trimethoxyphenyl)-methyl]chromen-2-one, i.e.

biscoumarin derivative. We proved that this is a new way for producing biscoumarin derivatives. Anal. $C_{28}H_{25}NO_9$ (519) (C, H, N) (Calcd/found): % C = 64.74 / 64.81; % H = 4.82 / 4.76; % N = 2.70 / 2.58. Crystallographic data of the investigated crystal are listed in Table 1. The solid state structure of one molecule is shown in Figures 2, 3 and 4.



Diethyl 2,6-dimethyl-4-(4-methyl-2-oxo-2-chromen-5-yl)-1,4-dihydropyridine-3,5-dicarboxylate (1)

Diethyl 2,6-dimethyl-4-(4-methyl-2-oxo-2-chromen-7-yl)-1,4-dihydropyridine-3,5-dicarboxylate (2)

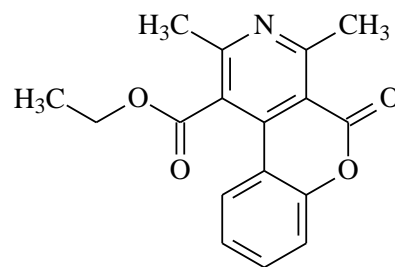


Fig. 1b. Pyridine derivative of coumarin (3)

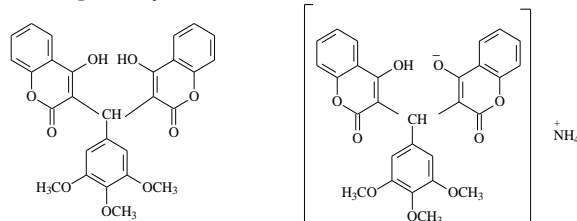


Fig. 2. Unexpected ammonium salt of biscoumarin derivative

Fig. 1a. Expected 1,4-dihydropyridine derivatives and Pyridine derivative of coumarin

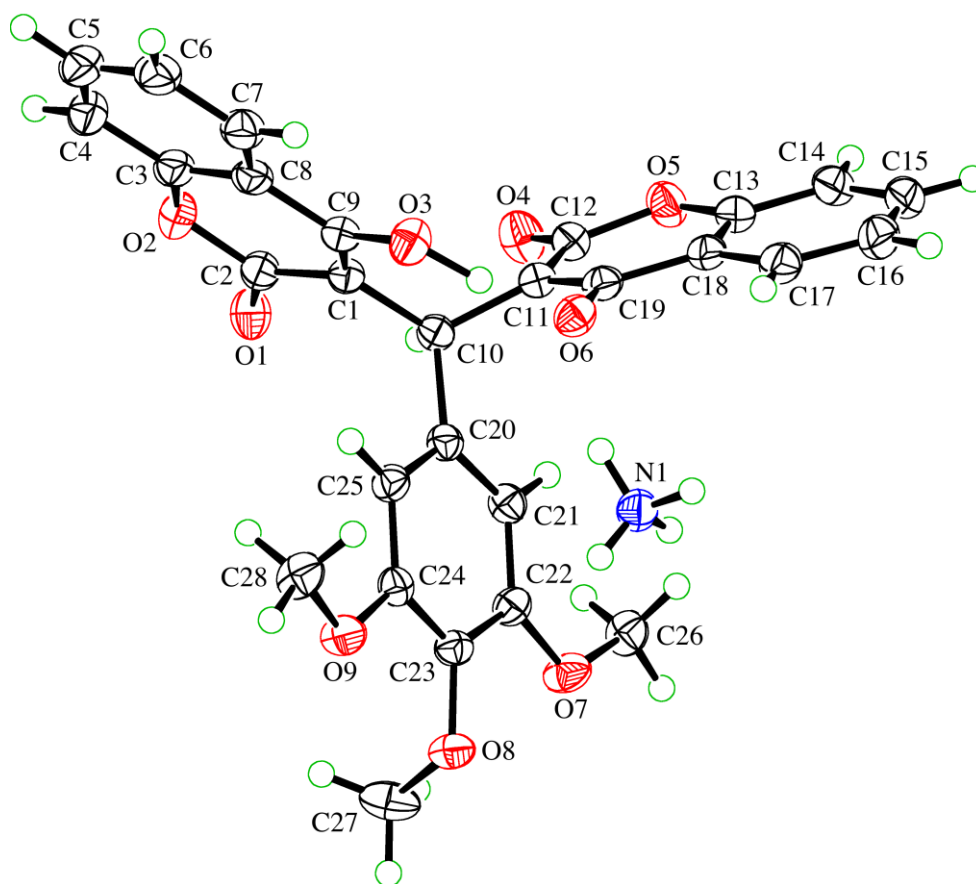


Fig. 3. ORTEP representation of the molecule (50 % probability ellipsoids; H-atoms given arbitrary displacement parameters for clarity) [30].

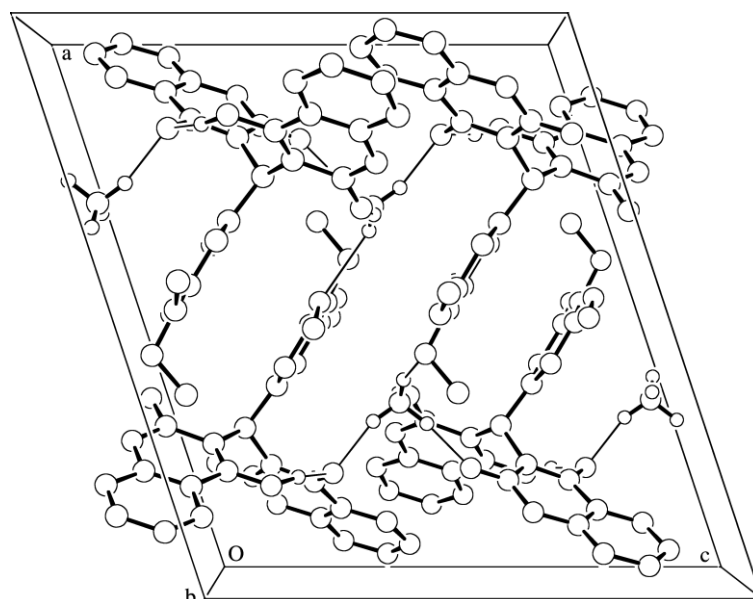


Fig. 4. Molecular packing projected down the a -axis showing the hydrogen bonding scheme (equivalent isotropic sphere for atoms; uninvolved H-atoms omitted for clarity).

Table 1. Crystal data and structure refinement

Empirical formula	$C_{28}H_{25}NO_9$	
Formula weight [$g\ mol^{-1}$]	519.51	
Crystal colour, habit	colourless, prism	
Crystal dimensions [mm]	$0.10 \times 0.15 \times 0.33$	
Temperature [K]	160(1)	
Crystal system	monoclinic	
Space group	$P2_1/c$ (#14)	
Z	4	
Reflections for cell determination	5908	
2θ range for cell determination [°]	4–55	
Unit cell parameters	a [Å]	16.3834(3), α [°] = 90
	b [Å]	10.7529(2), β [°] = 108.287(1)
	c [Å]	14.7635(3), γ [°] = 90
	V [Å ³]	2469.52(8)
$F(000)$	1088	
D_x [$g\ cm^{-3}$]	1.397	
μ (Mo $K\alpha$) [mm^{-1}]	0.105	
Scan type	φ and ω	
$2\theta_{(max)}$ [°]	55	
Total reflections measured	54740	
Symmetry independent reflections	5651	
R_{int}	0.062	
Reflections with $I > 2\sigma(I)$	4091	
Reflections used in refinement	5651	
Parameters refined	367	
Final $R(F)$	0.0467	
[$I > 2\sigma(I)$ reflections]		
$wR(F^2)$ (all data)	0.1215	
Weights: $w = [\sigma^2(F_o^2) + (0.0570P)^2 + 0.4821P]^{-1}$		
where $P = (F_o^2 + 2F_c^2)/3$		
Goodness of fit	1.050	
Secondary extinction coefficient	0.0056(7)	
Final Δ_{max}/σ	0.001	
$\Delta\rho$ (max; min) [$e\ \text{Å}^{-3}$]	0.23; -0.26	
$\sigma(d(C-C))$ [Å]	0.002 - 0.003	

The structure of $NH_4^+ C_{28}H_{21}O_9^-$ has been solved and refined successfully. Within the anion, the hydroxyl group forms a very strong intramolecular hydrogen bond with the adjacent oxide O-atom. The ammonium cation forms five hydrogen bonds with surrounding anions. These interactions link the ions into an extended two-dimensional network which lies parallel to the (100) plane. Data reduction was performed with *HKL Denzo* and *Scalepack* [12]. The intensities were corrected for Lorentz and polarization effects, but not for absorption. The space group was uniquely determined by the systematic absences. Equivalent reflections were merged. The data collection and refinement parameters and other data are given in Tables 1–9.

Two 4-hydroxycoumarin moieties are linked through a methylene bridge on which one hydrogen atom has been replaced with a 3,4,5-trimethoxyphenyl residue. The bond distances and angles are given in Tables 3 and 4. Most of the bond distances are of the expected length. The C10–C20 distance of 1.539(2) Å is longer than an unstrained $C(sp^3)$ – $C(Ar)$ bond. We established that nearly all of the bonds are shorter than those in the unsubstituted aromatic nucleus in analogous biscoumarin derivative. In spite of the presence of ammonium cation two 4-hydroxycoumarin residues are arranged in a position which permits the formation of two intramolecular hydrogen bonds between a hydroxyl group of one coumarin fragment and a lacton carbonyl group of the other coumarin fragment. The space group $P2_1/c$ (#14) and the cell

Table 2. Fractional atomic coordinates and equivalent isotropic displacement parameters (\AA^2) with standard uncertainties in parentheses.

Atom	x	y	z	U_{eq}^*
N 1	0.6775(1)	0.6144(2)	0.5363(1)	0.0328(3)
O 1	0.66958(7)	0.6285(1)	1.01337(8)	0.0366(3)
O 2	0.74348(7)	0.4595(1)	1.06661(8)	0.0351(3)
O 3	0.82305(7)	0.4302(1)	0.82995(8)	0.0355(3)
O 4	0.79762(8)	0.8925(1)	0.94087(9)	0.0411(3)
O 5	0.87690(7)	0.9271(1)	0.84912(8)	0.0363(3)
O 6	0.80640(7)	0.5951(1)	0.70960(8)	0.0320(3)
O 7	0.48572(7)	0.8400(1)	0.59333(8)	0.0359(3)
O 8	0.41413(6)	0.6138(1)	0.54350(8)	0.0321(3)
O 9	0.49328(7)	0.4084(1)	0.62328(8)	0.0341(3)
C 1	0.75099(9)	0.5503(1)	0.9183(1)	0.0257(3)
C 2	0.7194(1)	0.5515(2)	0.9986(1)	0.0292(4)
C 3	0.7945(1)	0.3623(2)	1.0569(1)	0.0320(4)
C 4	0.8161(1)	0.2748(2)	1.1302(1)	0.0405(4)
C 5	0.8664(1)	0.1750(2)	1.1220(1)	0.0447(5)
C 6	0.8937(1)	0.1612(2)	1.0427(1)	0.0428(5)
C 7	0.8714(1)	0.2486(2)	0.9706(1)	0.0366(4)
C 8	0.82144(9)	0.3520(2)	0.9772(1)	0.0308(4)
C 9	0.79740(9)	0.4493(2)	0.9049(1)	0.0280(4)
C 10	0.72522(9)	0.6624(1)	0.8522(1)	0.0256(3)
C 11	0.79614(9)	0.7343(1)	0.8281(1)	0.0263(3)
C 12	0.8210(1)	0.8504(2)	0.8759(1)	0.0304(4)
C 13	0.9015(1)	0.9006(2)	0.7702(1)	0.0331(4)
C 14	0.9493(1)	0.9911(2)	0.7423(1)	0.0404(4)
C 15	0.9727(1)	0.9707(2)	0.6621(1)	0.0458(5)
C 16	0.9492(1)	0.8606(2)	0.6101(1)	0.0460(5)
C 17	0.9032(1)	0.7700(2)	0.6396(1)	0.0389(4)
C 18	0.87829(9)	0.7895(2)	0.7209(1)	0.0313(4)
C 19	0.82578(9)	0.7011(2)	0.7536(1)	0.0290(3)
C 20	0.64695(9)	0.6419(1)	0.7630(1)	0.0252(3)
C 21	0.60766(9)	0.7485(1)	0.7157(1)	0.0276(3)
C 22	0.53078(9)	0.7406(1)	0.6412(1)	0.0275(3)
C 23	0.49343(9)	0.6242(1)	0.6135(1)	0.0262(3)
C 24	0.53504(9)	0.5173(1)	0.6573(1)	0.0260(3)
C 25	0.61187(9)	0.5257(1)	0.7328(1)	0.0268(3)
C 26	0.5215(1)	0.9609(1)	0.6204(1)	0.0332(4)
C 27	0.3451(1)	0.6449(2)	0.5803(1)	0.0454(5)
C 28	0.5402(1)	0.2948(2)	0.6493(1)	0.0381(4)

* U_{eq} is defined as one third of the trace of the orthogonalized

U^{ij} tensor

constants $a = 16.3834(3) \text{ \AA}$, $b = 10.7529(2) \text{ \AA}$, $c = 14.7635(3) \text{ \AA}$, $\beta = 108.287(1)^\circ$, $\alpha = \gamma = 90^\circ$, $V = 2469.52(8) \text{ \AA}^3$ are different from the analogous data of the acid form of the molecule.

The compound was tested for *in vivo* activity on blood coagulation time using mice. It was assayed for acute toxicity after intra peritoneal and oral administration. Warfarin was used as a reference compound. The studies were approved by the authors' institutional committee on animal care [26].

Table 3. Bond lengths (\AA) with standard uncertainties in parentheses

O 1 - C 2	1.228(2)	C 6 - C	1.381(2)
O 2 - C 3	1.374(2)	C 7 - C 8	1.401(2)
O 2 - C 2	1.376(2)	C 8 - C 9	1.458(2)
O 3 - C 9	1.318(2)	C 10 - C 11	1.528(2)
O 4 - C 12	1.226(2)	C 10 - C 20	1.539(2)
O 5 - C 13	1.377(2)	C 11 - C 19	1.381(2)
O 5 - C 12	1.378(2)	C 11 - C 12	1.429(2)
O 6 - C 19	1.301(2)	C 13 - C 18	1.388(2)
O 7 - C 22	1.363(2)	C 13 - C 14	1.390(2)
O 7 - C 26	1.431(2)	C 14 - C 15	1.371(3)
O 8 - C 23	1.388(2)	C 15 - C 16	1.397(3)
O 8 - C 27	1.440(2)	C 16 - C 17	1.382(2)
O 9 - C 24	1.370(2)	C 17 - C 18	1.400(2)
O 9 - C 28	1.430(2)	C 18 - C 19	1.462(2)
C 1 - C 9	1.375(2)	C 20 - C 25	1.389(2)
C 1 - C 2	1.435(2)	C 20 - C 21	1.390(2)
C 1 - C 10	1.525(2)	C 21 - C 22	1.390(2)
C 3 - C 8	1.384(2)	C 22 - C 23	1.397(2)
C 3 - C 4	1.393(2)	C 23 - C 24	1.388(2)
C 4 - C 5	1.381(3)	C 24 - C 25	1.398(2)
C 5 - C 6	1.387(3)		

Table 4. Bond angles ($^\circ$) with standard uncertainties in parentheses.

C 3-O 2-C 2	121.1(1)	O 4-C 12-O 5	113.7(1)
C 13-O 5-C 12	121.1(1)	O 4-C 12-C 11	126.7(2)
C 22-O 7-C 26	117.4(1)	O 5-C 12-C 11	119.6(1)
C 23-O 8-C 27	111.3(1)	O 5-C 13-C 18	121.1(1)
C 24-O 9-C 28	117.8(1)	O 5-C 13-C 14	116.7(2)
C 9-C 1-C 2	119.0(1)	C 18-C 13-C 14	122.2(2)
C 9-C 1-C 10	126.0(1)	C 15-C 14-C 13	118.7(2)
C 2-C 1-C 10	114.9(1)	C 14-C 15-C 16	120.4(2)
O 1-C 2-O 2	114.2(1)	C 17-C 16-C 15	120.5(2)
O 1-C 2-C 1	125.8(1)	C 16-C 17-C 18	119.9(2)
O 2-C 2-C 1	120.0(1)	C 13-C 18-C 17	118.2(2)
O 2-C-C 8	121.1(1)	C 13-C 18-C 19	118.6(1)
O 2-C 3,- C 4	116.6(2)	C 17-C 18-C 19	123.1(2)
C 8-C 3,- C 4	122.3(2)	O 6-C 19-C 11	122.2(1)
C 5 - C 4 - C 3	118.1(2)	O 6-C 19-C 18	118.8(1)
C 4 - C 5 - C 6	121.1(2)	C 11 - C 19 - C 18	119.0(2)
C 7 - C 6 - C 5	120.0(2)	C 25 - C 20 - C 21	120.0(1)
C 6 - C 7 - C 8	120.4(2)	C 25 - C 20 - C 10	123.6(1)
C 3 - C 8 - C 7	118.1(2)	C 21 - C 20 - C 10	116.3(1)
C 3 - C 8 - C 9	118.7(2)	C 20 - C 21 - C 22	120.6(1)
C 7 - C 8 - C 9	123.2(2)	O 7 - C 22 - C 21	124.8(1)
O 3 - C 9 - C 1	125.5(1)	O 7 - C 22 - C 23	115.8(1)
O 3 - C 9 - C 8	114.8(1)	C 21 - C 22 - C 23	119.4(1)
C 1 - C 9 - C 8	119.8(1)	O 8 - C 23 - C 24	119.2(1)
C 1 - C 10 - C 11	118.1(1)	O 8 - C 23 - C 22	120.8(1)
C 1 - C 10 - C 20	151.1(1)	C 24 - C 23 - C 22	120.0(1)
C 11 - C 10 - C 20	111.3(1)	O 9 - C 24 - C 23	114.9(1)
C 19 - C 11 - C 12	120.1(1)	O 9 - C 24 - C 25	124.7(1)
C 19 - C 11 - C 10	122.5(1)	C 23 - C 24 - C 25	120.3(1)
C 12 - C 11 - C 10	116.6(1)	C 20 - C 25 - C 24	119.5(1)

Table 5. Torsion angles (°) with standard uncertainties in parentheses.

C 3 - O 2 - C 2 - O 1	175.8(1)	C 18 - C 13 - C 14 - C 15	1.5(2)
C 3 - O 2 - C 2 - C 1	-3.1(2)	C 13 - C 14 - C 15 - C 16	0.5(2)
C 9 - C 1 - C 2 - O 1	-171.6(1)	C 14 - C 15 - C 16 - C 17	-0.9(3)
C 10 - C 1 - C 2 - O 1	5.8(2)	C 15 - C 16 - C 17 - C 18	1.3(2)
C 9 - C 1 - C 2 - O 2	7.2(2)	O 5 - C 13 - C 18 - C 17	178.1(1)
C 10 - C 1 - C 2 - O 2	-175.5(1)	C 14 - C 13 - C 18 - C 17	-1.1(2)
C 2 - O 2 - C 3 - C 8	-1.7(2)	O 5 - C 13 - C 18 - C 19	0.9(2)
C 2 - O 2 - C 3 - C 4	179.3(1)	C 14 - C 13 - C 18 - C 19	-178.3(1)
O 2 - C 3 - C 4 - C 5	179.1(1)	C 16 - C 17 - C 18 - C 13	-0.3(2)
C 8 - C 3 - C 4 - C 5	0.1(2)	C 16 - C 17 - C 18 - C 19	176.7(1)
C 3 - C 4 - C 5 - C 6	-0.8(3)	C 12 - C 11 - C 19 - O 6	178.4(1)
C 4 - C 5 - C 6 - C 7	0.6(3)	C 10 - C 11 - C 19 - O 6	-12.2(2)
C 5 - C 6 - C 7 - C 8	0.3(2)	12 - C 11 - C 19 - C 18	-3.8(2)
O 2 - C 3 - C 8 - C 7	-178.2(1)	C 10 - C 11 - C 19 - C 18	165.7(1)
C 4 - C 3 - C 8 - C 7	.7(2)	13 - C 18 - C 19 - O 6	177.7(1)
O 2 - C 3 - C 8 - C 9	2.4(2)	C 17 - C 18 - C 19 - O 6	5.3(2)
C 4 - C 3 - C 8 - C 9	178.7(1)	13 - C 18 - C 19 - C 11	.4(2)
C 6 - C 7 - C 8 - C 3	0.9(2)	17 - C 18 - C 19 - C 11	172.7(1)
C 6 - C 7 - C 8 - C 9	78.4(2)	1 - C 10 - C 20 - C 25	12.6(2)
C 2 - C 1 - C 9 - O 3	73.1(1)	C 11 - C 10 - C 20 - C 25	125.2(2)
C 10 - C 1 - C 9 - O 3	4.0(2)	1 - C 10 - C 20 - C 21	163.2(1)
C 2 - C 1 - C 9 - C 8	6.5(2)	11 - C 10 - C 20 - C 21	-59.1(2)
C 10 - C 1 - C 9 - C 8	76.5(1)	25 - C 20 - C 21 - C 22	3.5(2)
C 3 - C 8 - C 9 - O 3	177.8(1)	10 - C 20 - C 21 - C 22	172.4(1)
C 7 - C 8 - C 9 - O 3	.9(2)	26 - O 7 - C 22 - C 21	.7(2)
C 3 - C 8 - C 9 - C 1	.8(2)	26 - O 7 - C 22 - C 23	79.4(1)
C 7 - C 8 - C 9 - C 1	-177.5(1)	20 - C 21 - C 22 - O 7	77.0(1)
C 9 - C 1 - C 10 - C 11	-55.4(2)	20 - C 21 - C 22 - C 23	0.6(2)
C 2 - C 1 - C 10 - C 11	127.5(1)	27 - O 8 - C 23 - C 24	02.0(2)
C 9 - C 1 - C 10 - C 20	79.4(2)	27 - O 8 - C 23 - C 22	-77.0(2)
C 2 - C 1 - C 10 - C 20	-97.7(2)	7 - C 22 - C 23 - O 8	1.8(2)
C 1 - C 10 - C 11 - C 19	.6(2)	21 - C 22 - C 23 - O 8	76.0(1)
C 20 - C 10 - C 11 - C 19	-49.8(2)	7 - C 22 - C 23 - C 24	79.2(1)
C 1 - C 10 - C 11 - C 12	-103.6(2)	C 21 - C 22 - C 23 - C 24	-3.0(2)
C 20 - C 10 - C 11 - C 1	20.0(1)	28 - O 9 - C 24 - C 23	66.4(1)
C 13 - O 5 - C 12 - O 4	172.4(1)	28 - O 9 - C 24 - C 25	16.2(2)
C 13 - O 5 - C 12 - C 11	7.5(2)	O 8 - C 23 - C 24 - O 9	2.2(2)
C 19 - C 11 - C 12 - O 4	77.9(2)	22 - C 23 - C 24 - O 9	-178.8(1)
C 10 - C 11 - C 12 - O 4	7.8(2)	8 - C 23 - C 24 - C 25	-175.3(1)
C 19 - C 11 - C 12 - O 5	2.0(2)	22 - C 23 - C 24 - C 25	3.7(2)
C 10 - C 11 - C 12 - O 5	172.1(1)	C 21 - C 20 - C 25 - C 24	-2.8(2)
C 12 - O 5 - C 13 - C 18	-6.9(2)	C 10 - C 20 - C 25 - C 24	172.8(1)
C 12 - O 5 - C 13 - C 14	72.3(1)	9 - C 24 - C 25 - C 20	178.0(1)
O 5 - C 13 - C 14 - C 15	177.7(1)	23 - C 24 - C 25 - C 20	0.8(2)

Table 6. Anisotropic atomic displacement parameters (\AA^2).

Atom	U ¹¹	U ²²	U ³³	U ²³	U ¹³	U ¹²
N 1	0.0354(8)	0.0330(9)	0.0288(8)	-0.0013(6)	0.0085(7)	-0.0043(7)
O 1	0.0449(7)	0.0328(6)	0.0381(7)	-0.0008(5)	.0219(5)	-0.0001(5)
O 2	0.0450(7)	0.0327(6)	0.0291(6)	0.0042(5)	0.0138(5)	-0.0014(5)
O 3	0.0405(6)	0.0351(7)	0.0350(7)	0.0042(5)	0.0176(5)	0.0084(5)
O 4	0.0479(7)	0.0368(7)	0.0432(7)	-0.0105(6)	0.0208(6)	-0.0103(5)
O 5	0.0361(6)	0.0339(6)	0.0401(7)	-0.0015(5)	.0136(5)	0.0088(5)
O 6	0.0351(6)	0.0342(6)	0.0270(6)	-0.0006(5)	0.0101(5)	0.0024(5)
O 7	0.0374(6)	0.0230(6)	0.0387(7)	0.0037(5)	-0.0006(5)	0.0032(5)
O 8	0.0282(5)	0.0319(6)	0.0300(6)	-0.0014(5)	0.0001(5)	0.0014(5)
O 9	0.0359(6)	0.0228(6)	0.0369(7)	-0.0004(5)	0.0019(5)	-0.0017(5)
C 1	0.0251(7)	0.0267(8)	0.0236(8)	0.0003(6)	0.0052(6)	-0.0029(6)
C 2	0.0305(8)	0.0286(9)	0.0269(8)	-0.0009(7)	0.0067(6)	-0.0047(7)
C 3	0.0292(8)	0.0303(9)	0.0316(9)	0.0023(7)	0.0023(7)	-0.0045(7)
C 4	0.0421(9)	0.040(1)	0.036(1)	0.0094(8)	.0065(8)	-0.0071(8)
C 5	0.0378(9)	0.041(1)	0.046(1)	0.0158(9)	0.0004(8)	-0.0032(8)
C 6	0.0315(9)	0.036(1)	0.055(1)	0.0108(9)	0.0052(8)	0.0008(7)
C 7	0.0297(8)	0.0340(9)	0.043(1)	0.0052(8)	0.0066(7)	0.0003(7)
C 8	0.0254(8)	0.0289(9)	0.0333(9)	0.0013(7)	0.0021(6)	-0.0043(6)
C 9	.0239(7)	0.0310(9)	0.0271(8)	0.0003(7)	0.0051(6)	-0.0032(6)
C 10	0.0252(7)	0.0254(8)	0.0259(8)	-0.0014(6)	0.0078(6)	-0.0006(6)
C 11	0.0239(7)	0.0287(8)	0.0246(8)	0.0023(6)	0.0052(6)	0.0001(6)
C 12	0.0273(8)	0.0314(9)	0.0312(9)	0.0034(7)	0.0072(7)	-0.0024(6)
C 13	0.0246(8)	0.039(1)	0.0343(9)	0.0079(7)	0.0067(7)	0.0015(7)
C 14	0.0271(8)	0.042(1)	0.049(1)	0.0126(8)	0.0076(8)	-0.0014(7)
C 15	0.0278(9)	0.055(1)	0.054(1)	0.025(1)	0.0114(8)	0.0020(8)
C 16	0.0330(9)	0.067(1)	0.042(1)	0.020(1)	0.0172(8)	0.0081(9)
C 17	0.0309(8)	0.051(1)	0.036(1)	0.0090(8)	0.0118(7)	0.0065(8)
C 18	0.0230(7)	0.041(1)	0.0292(8)	0.0085(7)	0.0067(6)	0.0046(7)
C 19	0.0244(7)	0.0333(9)	0.0268(8)	0.0035(7)	0.0045(6)	0.0040(7)
C 20	0.0241(7)	0.0279(8)	0.0247(8)	-0.0004(6)	0.0090(6)	-0.0003(6)
C 21	0.0288(8)	0.0236(8)	0.0305(8)	-0.0013(6)	0.0097(6)	-0.0013(6)
C 22	0.0292(8)	0.0248(8)	0.0281(8)	0.0026(6)	0.0081(6)	0.0037(6)
C 23	0.0251(7)	0.0287(8)	0.0235(8)	-0.0012(6)	0.0057(6)	0.0002(6)
C 24	0.0275(8)	0.0245(8)	0.0270(8)	-0.0011(6)	0.0101(6)	-0.0026(6)
C 25	0.0269(8)	0.0257(8)	0.0275(8)	0.0031(6)	0.0080(6)	0.0029(6)
C 26	0.0399(9)	0.0224(8)	0.0365(9)	0.0000(7)	0.0109(7)	0.0009(7)
C 27	0.0269(9)	0.046(1)	0.056(1)	-0.0102(9)	0.0033(8)	0.0064(8)
C 28	0.048(1)	0.0227(8)	0.039(1)	-0.0001(7)	0.0066(8)	0.0012(7)

The anisotropic displacement parameter exponent takes the form:

$$-2\pi^2(h^2a^2U^{11} + k^2b^2U^{22} + \dots + 2hka^*b^*U^{12})$$

Table 7. Hydrogen atom coordinates and displacement parameters

Atom	x	y	z	U _{iso}
H 11	0.716(1)	0.607(2)	0.497(1)	0.045(5)
H 12	0.662(1)	0.699(2)	0.533(2)	0.065(7)
H 13	0.712(1)	0.596(2)	0.599(2)	0.064(7)
H 14	0.635(2)	0.559(2)	0.514(2)	0.063(7)
H 3	0.810(2)	0.502(2)	0.776(2)	0.086(8)
H 4	0.797	0.284	1.184	0.049
H 5	0.882	0.115	1.172	0.054
H 6	0.928	0.091	1.038	0.051
H 7	0.890	0.239	0.916	0.044
H 10	0.704	0.723	0.891	0.031
H 141	0.965	1.065	0.778	0.049
H 15	1.005	1.032	0.642	0.055
H 16	0.965	0.848	0.554	0.055
H 17	0.888	0.695	0.605	0.047
H 21	0.634	0.827	0.734	0.033
H 25	0.640	0.452	0.763	0.032
H 261	0.529	0.975	0.688	0.050
H 262	0.483	1.024	0.582	0.050
H 263	0.577	0.967	0.609	0.050
H 271	0.347	0.590	0.634	0.068
H 272	0.290	0.635	0.530	0.068
H 273	0.351	0.731	0.602	0.068
H 28	0.593	0.299	0.632	0.057
H 282	0.505	0.225	0.615	0.057
H 283	0.554	0.282	0.718	0.057

Table 8. Selected bond lengths (Å) and angles (°) involving H-atoms.

N 1 - H 11	0.98(2)	N 1 - H 14	0.90(2)
N 1 - H 12	0.94(2)	O 3 - H 3	1.08(3)
N 1 - H 13	0.94(2)	O 6 - H 3	.39(3)
H 11 - N 1 - H 12	105(2)	H 12 - N 1 - H 14	117(2)
H 11 - N 1 - H 13	106(2)	H 13 - N 1 - H 14	112(2)
H 12 - N 1 - H 13	109(2)	C 9 - O 3 - H 3	118(1)
H 11 - N 1 - H 14	108(2)	C 19 - O 6 - H 3	109(1)

Table 9. Hydrogen bonding geometry (Å, °).

D	H	A	D-H	H...A	D...A	D-H...A
O 3	H 3	O 6	1.08(3)	1.39(3)	2.464(2)	172(2)
N 1	H 11	O 4'	0.98(2)	1.78(2)	2.758(2)	171(2)
N 1	H 12	O 1'	0.94(2)	1.89(2)	2.783(2)	158(2)
N 1	H 13	O 6	0.94(2)	1.87(2)	2.768(2)	159(2)
N 1	H 14	O 8''	0.90(2)	2.10(2)	2.924(2)	153(2)
N 1	H 14	O 9''	0.90(2)	2.44(2)	3.049(2)	125(2)

Primed atoms refer to the molecule in the following symmetry related positions:

$$' \quad x, 1', -2-y, -1', -2+z \quad " \quad 1-x, 1-y, 1-z$$

This compound showed an effect on HIV replication in acutely infected cells by microtiter infection assay. The same substance demonstrated no impact on early stages of HIV-1 replication cycle [27, 28]. The structure of the title compound was solved and published previously [29].

REFERENCES

1. B. Hagmar, *Pathol. Eur.* **4**, 283 (1969).
2. Zhao H., N. Neamati, H. Hong, A. Mazumder, S. Wang, S. Sunder, G. W. A. Milne, Y. Pommier, T. R. Burke Jr., *J. Med. Chem.* **40**, 242 (1997).
3. Markal de Queroz P Italy PCT Int. Appl. WO 98 25,608 (1998).
4. Nagashima R., R. O'Reilly, G. Levy. *Clin. Pharm. Ther.* **1**, 22 (1969).
5. R. O'Reilly, J. Ohms, C. Motley. *J. Biol. Chem.*, **244**, 1303 (1969).
6. N. Numamoto, T. Yamamoto, A. Yamashita, T. Hatano, J. Kurahara. *Jpn Kokai Tokkyo Koho JP 02 36,178* (1990).
7. E. Boshetti, D. Molho, L. Fontaine. *S. African* **68** 01, 383 (1968).
8. C. Stacchino, R. Spano, A. Pettiti, *Bull. Chim. Pharm.*, **122**, 158 (1983).
9. Lu H. D. et al. *Ann. N. Y. Acad. Sci.*, **833**, 147 (1997).

10. C.L. Laprinzi et al., *N. Eng. J. Med.*, **340**, 346 (1999).
11. R. Hoofdt, KappaCCD Collect Software, Nonius BV, Delft, The Netherlands, 1999.
12. Z. Otwinowski, W. Minor, in: *Methods in Enzymology*, Vol. 276, *Macromolecular Crystallography, Part A* (eds. C.W. Carter Jr., R.M. Sweet), Academic Press, New York, 1997, p. 307.
13. A. Altomare, G. Cascarano, C. Giacovazzo, A. Guagliardi, M.C. Burla, G. Polidori, M. Camalli, SIR92, *J. Appl. Crystallogr.*, **27**, 435 (1994).
14. a) E.N. Maslen, A.G. Fox, M.A. O'Keefe, in *International Tables for Crystallography*, Ed. A.J.C. Wilson, Kluwer Academic Publishers, Dordrecht, 1992, Vol. C, Table 6.1.1.1, p. 477; b) D.C. Creagh, W.J. McAuley, *ibid.* Table 4.2.6.8, p. 219; c) D.C. Creagh, J.H. Hubbell, *ibid.* Table 4.2.4.3, p. 200.
15. R.F. Stewart, E.R. Davidson, W.T. Simpson, *J. Chem. Phys.*, **42**, 3175 (1965).
16. J.A. Ibers, W.C. Hamilton, *Acta Crystallogr.* **17**, 781 (1964).
17. G.M. Sheldrick, SHELXL97, *Acta Crystallogr., Sect A*, **64**, 112 (2008).
18. S. Dochev, Diploma work, Medical University, Faculty of Pharmacy, Department of Organic Chemistry, Sofia, 2010.
19. A.K. Mitra, A. De, N. Karchaudhuri, S. K. Misra, A. K. Mukhopadhyay, *J. Indian Chem. Soc.*, **75**, 526 (1998).
20. A. Grussner, Jubilee Vol Emil Barell **238** (1946).
21. P. Desnoyers, K. Binovic, *Therapie*, **22**, 207 (1967).
22. E. Perola, K. Xu, T. M. Kollmeyer, S. H. Kauffman, F. G. Prendergast, Y.-P. Pang, *J. Med. Chem.*, **43**, 401 (2000).
23. R. Griffith, R. Chanphen, S.P. Leach, P.A. Keller, *Bioorg. Med. Chem. Lett.*, **12**, 539 (2002).
24. P.A. Keller, C. Birch, S.P. Leach, D. Tyssen, R. Griffith, *J. Mol. Graphics & Modelling*, **21**, 365 (2003).
25. K.M. Khan, S. Iqbal, M.A. Lodhi, G.M. Maharvi, S. Perveen, M.I. Choudhary, Atta-Ur-Rahman, Z.H. Zahid, C.T. Supuran, *J. Enzyme Inhib. Med. Chem.*, **19**, 367 (2004).
26. I. Manolov, C. Maichle-Moessmer, N. Danchev, *Eur. J. Med. Chem.*, **41**, 882 (2006).
27. S. Raleva, A. Savov, L. Froloshka, D. Dundarova, I. Manolov, R. Argirova. *Biotechnol. & Biotechnol. Eq.*, **19**, 11 (2005).
28. P. Genova, D. Dundarova, S. Raleva, R. Argirova, I. Manolov. *Farmacya (Sofia)*. **LII**, 74 (2005).
29. I. Manolov, M. Ströbele, H.-Jürgen Meyer. *Anal. Sci. - X-Ray Struct. Anal. Online*, **24**, 135 (2008).
30. C. K. Johnson, ORTEP II, Report ORNL-5138, Oak Ridge National Laboratory, Oak Ridge, Tennessee, 1976.

СИНТЕЗ И КРИСТАЛНА СТРУКТУРА НА АМОНИЕВА СОЛ НА 4-ХИДРОКСИ-3-[(2-ОКСО-2Н-ХРОМЕН-3-ИЛ)-(3,4,5-ТРИМЕТОКСИФЕНИЛ)МЕТИЛ]ХРОМЕН-2-ОН

С. Дочев¹, А. Петкова², П. Ретайльо³, И. Манолов⁴

¹Изследователска група Миховилович, Научен отдел по органична химия, Институт по приложна синтетична химия, Факултет по техническа химия, Университет по технология Виена, А-1060 Виена, Австрия

²Южнокалифорнийски Университет, Лос Анджелис, Калифорния, САЩ, 90089-1453; Институт по физикохимия „Акад. Р. Каишев“, БАН, ул. „Акад. Г. Бончев“, 1113 София, България

³Лаборатория по кристалография, Институт по Химия на природните продукти – ЦНРС, УПР2301, 91198-седекс, Жиф-сюр-Ивет, Франция

⁴Катедра по Фармацевтична химия, Фармацевтичен факултет, Медицински университет, ул. „Дунав“ 2, 1000 София, България

Постъпила на 7 февруари, 2012 г.; коригирана на 23 март, 2013 г.

(Резюме)

Структурата на амониевата сол на 4-хидрокси-3-[(2-оксо-2Н-хромен-3-ил)-(3,4,5-триметоксифенил)метил]хромен-2-он е определена с помощта на рентгеноструктурен анализ. Съединението кристализира в моноклинната система във вид на безцветни призматични кристали, пространствена група P2₁/c (#14) с константи a = 16.3834(3) Å, b=10.7529(2)Å, c=14.7635(3) Å, β=108.287(1)°, α=γ=90° V=2469.52(8) Å³, Z=4. Кристалната структура е доказана с директни методи и точно определена с помощта на метода на най-малките квадрати за F² до стойност R1 = 0.00467. Двата 4-хидроксикумаринови фрагмента в молекулата са свързани с вътрешномолекулни водородни връзки между хидроксилните и карбонилните групи. Солта и киселинната форма на съединението показват слаби различия в дължините на химичните връзки и валентните ъгли.

Permutation symmetry of fullerene isomers of C₈₂

Morteza Yavari

Department of Physics, Islamic Azad University, Kashan Branch, Kashan, Iran

Received March 13, 2012; Revised September 30, 2012

A fullerene is a cubic planar graph, all faces of which consist of 5- or 6- cycles. The symmetry of these molecules is important with a view to counting their isomers. In this article the permutation symmetry group of the isomers of a C₈₂ fullerene is calculated.

Keywords: Fullerene, C₈₂, symmetry, isomers.

INTRODUCTION

A fullerene is any molecule composed entirely of carbon, in the form of a hollow sphere, ellipsoid, or tube. Since their discovery in 1985 by Kroto et al., the fullerenes have been the objects of interest of scientists all over the world [1,2]. Symmetry of these macromolecules is important in spectroscopy and also in some part of nanoscience.

The molecular symmetry group is first defined by Longuet-Higgins [3]. Although there have been earlier works that suggested the need for such a framework. Bunker and Papoušek [4] extended the definition of the molecular symmetry group to linear molecules using extended molecular symmetry.

A graph is a collection of vertices and a collection of edges that connect pairs of vertices. It may be undirected, meaning that there is no distinction between the two vertices associated with each edge. Graphs are one of the prime objects of study in Discrete Mathematics. Refer to Glossary of graph theory for basic definitions in graph theory.

The symmetry of a graph means the automorphism group symmetry and it does not need to be isomorphic to the molecular point group symmetry. However, it does represent the maximal symmetry which the geometrical realization of a given topological structure may possess.

By symmetry we mean the automorphism group symmetry of a graph. Randić [5,6] showed that a graph can be depicted in different ways, such that its point group symmetry or three-dimensional (3D) perception may differ, but the underlying

connectivity symmetry is still the same, as characterized by the automorphism group of the graph.

Balasubramanian [7-9] in some leading papers considered the Euclidean matrix of a chemical graph to find its symmetry. He proved that for computing the symmetry of a molecule, it is sufficient to solve the matrix equation

$$P^t E P = E,$$

where E is the Euclidean matrix of the molecule under consideration and P varies on the set of all permutation matrices with the same dimension as E. He computed the Euclidean graphs and automorphism group for benzene, eclipsed and staggered forms of ethane and eclipsed and staggered forms of ferrocene.

Ashrafi and his co-workers [10-20] in a series of papers applied a computational method for computing symmetry of fullerenes. We continue the mentioned method to compute the permutation symmetry of the isomers of C₈₂ fullerenes. Our calculations were done by computer algebra system GAP [21]. Here, GAP stands for Groups, Algorithms and Programming. The name was chosen to reflect the aim of the system, which is a group theoretical software for solving computational problems in computational group theory. This software was constructed by the GAP team in Aachen.

2. RESULTS AND DISCUSSION

In this section, we first describe a notation which will be kept throughout. Suppose X is a set. The set of all permutations on X, denoted by S_X, is a group which is called the symmetric group on X. In the case that X = {1, 2, ..., n}, we denote S_X by S_n or Sym(n). Also, for a group G

* To whom all correspondence should be sent:
E-mail: yavari@iaukashan.ac.ir

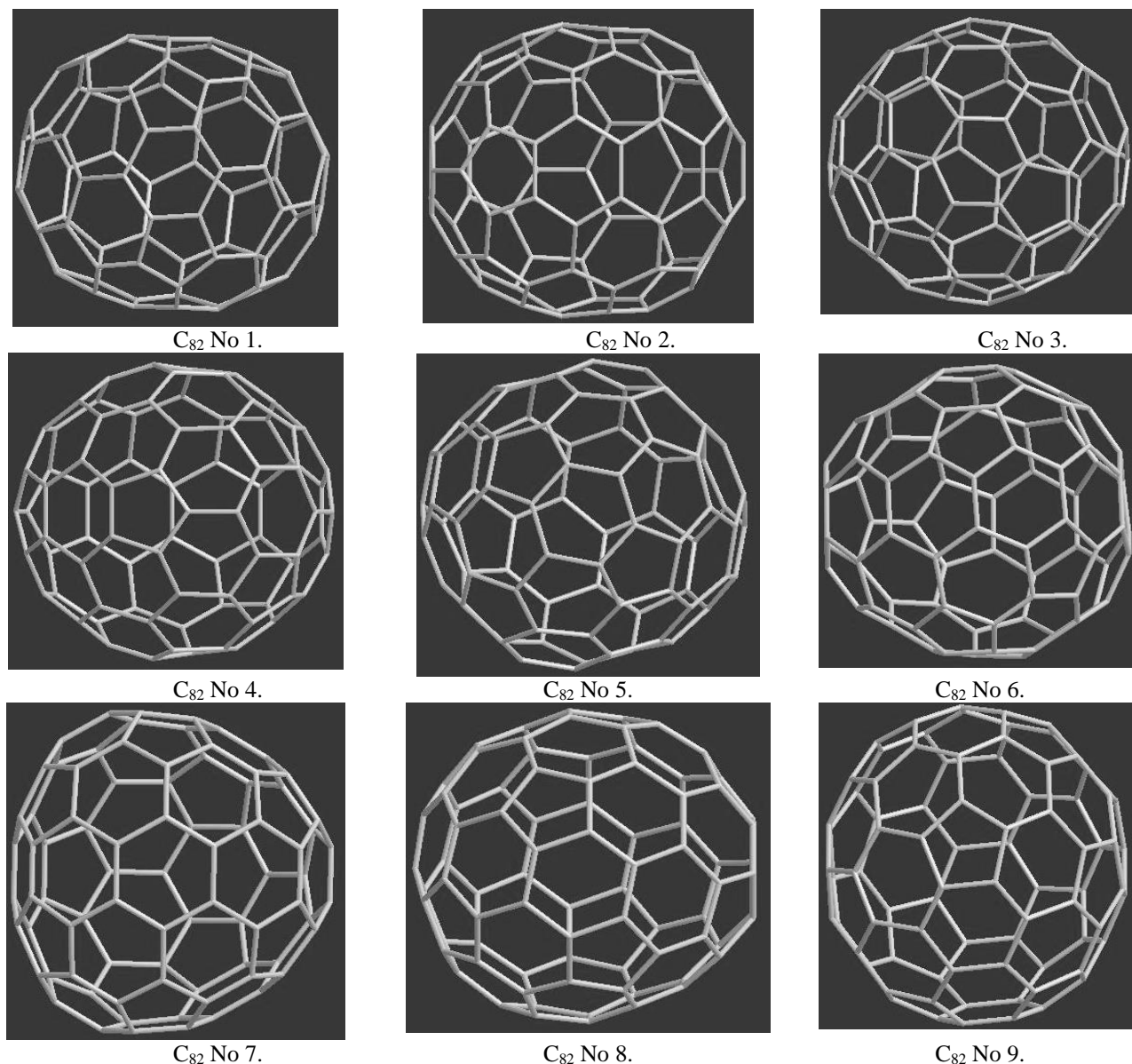


Figure 1. The isomers of C_{82} fullerene.

and a subset A of G , $\langle A \rangle$ is the subgroup of G generated by A .

In this section, we apply some GAP programs to calculate a generating set for the automorphism group of the isomers of the fullerene molecule C_{82} . We name these molecules $C_{82}[1]$, $C_{82}[2]$, ... and $C_{82}[9]$ which are depicted in Figure 1. By some calculations, we can see that the symmetry group of $C_{82}[2]$, $C_{82}[6]$, $C_{82}[7]$ and $C_{82}[8]$ is a trivial group.

The symmetry group of $C_{82}[1]$, $C_{82}[3]$, $C_{82}[4]$ and $C_{82}[9]$ is a group of order 2 generated by A_1 , A_3 , A_4 and A_9 , respectively. Finally, the symmetry group of A_5 is isomorphic to the symmetric group on 3 symbols. The symmetry elements of this group are denoted by $A_5[1]$, $A_5[2]$, $A_5[3]$, $A_5[4]$ and $A_5[5]$.

These permutations are calculated by GAP as follows.

Generators of Permutational Isomer Groups of C_{82} Fullerenes

$A_1 :=$
 $(1,82)(2,81)(3,80)(4,79)(5,78)(6,77)(7,12)(8,13)(9,14)(10,57)(11,56)(15,62)$
 $(16,63)(17,65)(18,64)(19,61)(20,58)(21,59)(22,60)(23,53)(24,54)(25,55)(26,66)$
 $(27,67)(28,69)(29,68)(30,49)(31,46)(32,47)(33,48)(34,43)(35,44)(36,45)(37,42)$
 $(38,70)(39,71)(40,73)$
 $(41,72)(50,74)(51,75)(52,76)$.

$A_3 :=$
 $(1,42)(2,43)(3,44)(4,45)(5,76)(6,75)(7,74)(8,39)(9,40)(10,38)(11,41)(12,71)$

(13,67)(14,60)(15,61)(16,59)(17,68)(18,69)(19,70)(
20,37)(21,35)(22,34)(23,36)
(24,46)(25,49)(26,47)(27,48)(28,55)(29,56)(30,57)(
31,51)(32,50)(33,52)(53,72)
(54,73)(58,79)(62,82)(63,77)(64,78)(65,80)(66,81).

$A_4 :=$

(1,11)(2,9)(3,10)(4,8)(5,14)(6,15)(7,16)(17,31)(18,
30)(19,29)(20,50)
(21,48)(22,49)(23,47)(24,54)(25,55)(26,53)(27,52)(
28,51)(32,35)(36,39)
(40,57)(41,58)(42,56)(43,59)(44,61)(45,60)(46,64)(
62,67)(63,66)(65,68)
(69,79)(70,73)(71,78)(72,82)(74,75)(76,81)(77,80).

$A_5[1] :=$

(1,13)(2,14)(3,15)(4,12)(5,20)(6,19)(7,21)(10,11)(1
6,82)(17,18)(22,24)
(26,36)(27,37)(28,35)(29,34)(30,49)(31,47)(32,48)(
33,46)(38,44)(39,45)
(40,43)(41,42)(50,79)(51,78)(52,77)(53,75)(54,76)(
55,67)(56,72)(57,71)
(58,70)(59,69)(60,74)(61,73)(62,63)(64,65)(80,81),

$A_5[2] :=$

(1,30,39)(2,31,40)(3,32,38)(4,33,41)(5,79,59)(6,78,
61)(7,77,60)(8,27,37)
(9,28,35)(10,26,34)(11,29,36)(12,42,46)(13,45,49)(
14,43,47)(15,44,48)
(16,70,55)(17,71,56)(18,72,57)(19,73,51)(20,69,50)
(21,74,52)(22,25,24)
(53,75,68)(54,76,66)(58,82,67)(62,64,81)(63,80,65)

$A_5[3] :=$

(1,39,30)(2,40,31)(3,38,32)(4,41,33)(5,59,79)(6,61,
78)(7,60,77)(8,37,27)
(9,35,28)(10,34,26)(11,36,29)(12,46,42)(13,49,45)(
14,47,43)(15,48,44)
(16,55,70)(17,56,71)(18,57,72)(19,51,73)(20,50,69)
(21,52,74)(22,24,25)
(53,68,75)(54,66,76)(58,67,82)(62,81,64)(63,65,80)

$A_5[4] :=$

(1,45)(2,43)(3,44)(4,42)(5,69)(6,73)(7,74)(8,27)(9,
28)(10,29)(11,26)
(12,33)(13,30)(14,31)(15,32)(16,67)(17,72)(18,71)(
19,78)(20,79)(21,77)
(24,25)(34,36)(38,48)(39,49)(40,47)(41,46)(50,59)(
51,61)(52,60)(53,68)
(54,66)(55,58)(56,57)(62,80)(63,64)(65,81)(70,82),

$A_5[5] :=$

(1,49)(2,47)(3,48)(4,46)(5,50)(6,51)(7,52)(8,37)(9,
35)(10,36)(11,34)
(12,41)(13,39)(14,40)(15,38)(16,58)(17,57)(18,56)(
19,61)(20,59)(21,60)
(22,25)(26,29)(30,45)(31,43)(32,44)(33,42)(55,82)(
62,65)(63,81)(64,80)
(66,76)(67,70)(68,75)(69,79)(71,72)(73,78)(74,77)

$A_9 :=$

(2,15)(4,13)(5,17)(6,16)(7,19)(8,18)(9,28)(10,29)(1
1,27)(12,48)(14,47)(20,23)
(21,22)(24,53)(25,51)(26,54)(30,52)(31,49)(32,50)(
33,45)(34,46)(35,44)(36,64)
(37,63)(38,56)(39,57)(40,55)(41,82)(42,81)(43,80)(
58,61)(62,75)(65,73)(66,74)
(67,70)(71,76)(72,79)(77,78).

3. CONCLUDING REMARKS

The GAP SYSTEM is a useful software for research and education in chemistry. In this article, this package is applied to compute the symmetry of C_{82} fullerenes. There are several examples showing that the symmetry group of a molecule critically depends to the accuracy in computing the Cartesian coordinates of atoms in the molecule under consideration.

Acknowledgment. The author is indebted to Professor A.R. Ashrafi for some discussion about the symmetry of fullerenes. This work was supported in part by the Islamic Azad University-Kashan Branch.

REFERENCES

1. H.W. Kroto, J.R. Heath, S.C. O'Brien, R.F. Curl, R.E. Smalley, *Nature*, **318**, 162 (1985).
2. H.W. Kroto, J.E. Fichier, D.E. Cox, *The Fullerene*, Pergamon Press, New York, 1993.
3. H.C. Longuet-Higgins, *Mol. Phys.*, **6**, 445 (1963).
4. P.R. Bunker, D. Papoušek, *J. Mol. Spectrosc.*, **32**, 419 (1969).
5. M. Randić, *Chem. Phys. Letters.*, **42**, 283 (1976).
6. M. Randić, *J. Chem. Phys.*, **60**, 3920 (1974).
7. K. Balasubramanian, *Chem. Phys. Letters.*, **232**, 415 (1995).
8. K. Balasubramanian, *J. Chem. Phys.*, **72**, 665 (1980).
9. K. Balasubramanian, *Int. J. Quant. Chem.*, **21**, 411 (1982).
10. A.R. Ashrafi, *Chem. Phys. Letters.*, **403**, 75 (2005).
11. A.R. Ashrafi, *MATCH Commun. Math. Comput. Chem.*, **53**, 161 (2005).
12. A.R. Ashrafi, M. Hamadani, *Croat. Chem. Acta.*, **76**, 299 (2003).
13. M. Hamadani, A.R. Ashrafi, *Croat. Chem. Acta.*, **76**, 305 (2003).
14. A.R. Ashrafi, *Chinese J. Chem.*, **23**, 829 (2005).
15. M.R. Darafsheh, A.R. Ashrafi, A. Darafsheh, *Int. J. Quant. Chem.*, **105**, 485 (2005).
16. M.R. Darafsheh, A.R. Ashrafi, A. Darafsheh, *Acta Chim. Slov.*, **52**, 282 (2005).
17. M.R. Darafsheh, Y. Farjami, A.R. Ashrafi, *Bull. Chem. Soc. Japan.*, **78**, 996 (2005).

18. M.R. Darafsheh, Y. Farjami, A.R. Ashrafi, *MATCH Commun. Math. Comput. Chem.*, **54**, 53 (2005).
19. M. Yavari, A.R. Ashrafi, *Asian J. Chem.*, **20**, 5119 (2008).
20. M. Yavari, A.R. Ashrafi, *Asian J. Chem.*, **20**, 409 (2008).
21. The GAP Team, 'GAP, Groups, Algorithms and Programming', Lehrstuhl D für Mathematik, RWTH: Aachen, Germany, 1995.

ПЕРМУТАЦИОННА СИМЕТРИЯ НА ИЗОМЕРИ НА ФУЛЕРЕН С 82 ВЪГЛЕРОДНИ АТОМА

Мортеза Явари

Департамент по физика, Ислямски университет "Азад", клон Кашан, Кашан, Иран

Постъпила на 13 март, 2012 г.; коригирана на 30 септември, 2012 г.

(Резюме)

Фулеренът е кубичен планарен граф, на който всички страни се състоят от 5 или 6 пръстена. Симетрията на тези молекули е важна с оглед броя на нейните изомери. В настоящата работа е определена пермутационната симетрия на изомерите на фулкерен C₈₂.

A catalytic crossed-aldol condensation of ketones with aromatic and non-aromatic aldehydes by silica supported Preyssler heteropolyacids catalyst

Ali Gharib^{1,2*}, Nader Noorozi Pesyan³, Manouchehr Jahangir¹, Mina Roshani¹, J. (Hans) W. Scheeren⁴

¹Department of Chemistry, Islamic Azad University, Mashhad, IRAN

²Agricultural Researches and Services Center, Mashhad, IRAN

³Department of Chemistry, Faculty of Science, Urmia University, 57159 Urmia, Iran

⁴Cluster for Molecular Chemistry, Department of Organic Chemistry, Radboud University Nijmegen, The Netherlands

Received March 4, 2012; Revised September 17, 2012

Synthesis of α,β -unsaturated aldol products by crossed-aldol condensation of aromatic aldehydes in the presence of heteropolyacids (HPAs) catalyst under reflux conditions and free of organic solvent is reported. Aldol condensation of 2-acetylthiophene, 2-acetylpyrrole and 2-acetylpyridine with different aromatic aldehydes was carried out in water in the presence of a silica supported Preyssler HPAs catalyst at room temperature. All reactions occur in a short time with excellent yields of cycloalkanones in water as an environmentally friendly solvent.

Keywords: α,β -unsaturated aldol, catalysts, aldehyde, ketone, condensation

INTRODUCTION

Aldol condensations are important in organic synthesis, providing a good way to form carbon-carbon bonds. The Robinson annulation reaction sequence features an aldol condensation; the Wieland-Miescher ketone product is an important starting material for many organic syntheses. In its usual form, it involves nucleophilic addition of a ketone enolate to an aldehyde to form a β -hydroxy ketone, a structural unit found in many naturally occurring molecules and pharmaceuticals [1–3]. Chalcones are α,β -unsaturated ketones and they have great abundance in the plant kingdom. It is well known that most of natural and synthetic chalcones are highly biologically active with multiple pharmaceutical and medicinal applications [4]. Recently they are used as anti-AIDS [5], cytotoxic with antiangiogenic activity [6,7], antimalarial [8,9], anti-inflammatory [10,11] and antitumor agents [12,13]. Recently, water has been considered as an attractive medium for many organic reactions [14]. With respect to organic solvents aqueous media are less expensive, healthy, safe and environmentally friendly. Also, water allows pH control and use of surfactants as micro aggregates. The hydrophilic effect and the large cohesive energy of water [15] are considered to be the main factors responsible for increasing

reactivity and selectivity of the reactions [16]. Bis(p-methoxyphenyl) telluroxide and $\text{KF-Al}_2\text{O}_3$ have been used for crossed-condensation of cycloalkanones with aromatic aldehydes under microwave irradiation [17]. Anhydrous RuCl_3 and $\text{TiCl}_3(\text{SO}_3\text{CF}_3)$ have also been used for this purpose under solvent-free conditions [18]. The use of expensive and toxic reagents, long reaction times, low yields, and the formation of a mixture of products are among the drawbacks of the reported methods. Recently, more attention has been paid to the synthesis of α,α' -bis(substituted benzylidene) cycloalkanones [19]. Aldol condensation is a powerful tool for the formation of a carbon-carbon bond in many classes of carbonyl compounds [20]. Due to the importance of the methylene structural unit which is found in many naturally occurring compounds and antibiotics, and the use of α,α' -bis(substituted benzylidene)cycloalkanones as precursors for the synthesis of bioactive pyrimidine derivatives [21], condensation of cycloalkanones with aldehydes and ketones is of special interest and crossed-aldol condensation is an effective pathway for these preparations. However, traditional acid- or base-catalyzed reactions suffer from the reverse reaction [22], and from self-condensation of the starting materials [23]. Heteropolyacids (HPAs) are well defined molecular clusters that are remarkable for their molecular and electronic structural diversity and their significance in many areas, e.g., catalysis, medicine, and materials science [24,25]. The applications of

* To whom all correspondence should be sent:

E-mail: : aligharib5@yahoo.com

HPAs in the field of catalysis are continuously growing. These compounds possess unique properties such as Brønsted acidity, possibility to modify their acid/base and redox properties by changing their chemical composition (substituted HPAs), ability to accept and release electrons, high proton mobility, easy work-up procedures, easy filtration, and minimization of cost and waste generation due to reuse and recycling of these catalysts [26-30]. Because of their stronger acidity, they generally exhibit higher catalytic activity than conventional catalysts such as mineral acids, ion exchange resins, mixed oxides, zeolites, etc. [31]. In the context of Green Chemistry, the substitution of harmful liquid acids by solid reusable HPAs as catalysts in organic synthesis is the most promising application of these acids [32,33]. HPAs are applied both in bulk or supported forms, homogeneous and heterogeneous catalysis being possible. HPAs have many advantages that make them environmentally attractive in the academic, industrial and economical signification. These are useful acids and oxidation catalysts in various reactions since their catalytic features can be varied at a molecular level [34]. Among them, the Keggin-type HPAs have long been known to be good catalysts for oxidation reactions [35]. They exhibit great advantages: for example, their catalytic properties can be tuned by changing the identity of the charge-compensating counter cations, heteroatoms and framework metal atoms [35]. Being stronger acids, heteropolyacids will have significantly higher catalytic activity than the conventional catalysts such as mineral acids, mixed oxides, zeolites, etc. In particular, in organic media, the molar catalytic activity of a heteropolyacid is often 100-1000 times higher than that of H_2SO_4 [34,36].

EXPERIMENTAL

Materials and Methods

All chemicals were obtained from Merck and used as received.

Instruments

1H NMR spectra were recorded on a FT NMR Bruker 400 MHz spectrometer at 298 K. Melting points were recorded on an Electrothermal type 9100 melting point apparatus and were uncorrected. Chemical shifts were reported in ppm (δ -scale) relative to internal standard TMS (0.00 ppm) using $CDCl_3$ as a reference solvent. IR spectra were obtained with a Buck 500 scientific spectrometer (KBr pellets). The mass spectra (EI) were obtained on a Jeol JMS D-300 spectrometer operating at 70

eV. The products were identified by comparison of their mp., IR and NMR spectra with those of authentic samples. Elemental analyses were performed on a Perkin Elmer 2400, series II microanalyzer.

Catalyst Preparation

Preyssler catalyst, $H_{14}[NaP_5W_{30}O_{110}]$ was prepared by passage of a solution of the potassium salt (30 mL) in water (30 mL) through a column (50 cm \times 1 cm) of Dowex 50W \times 8 in the H^+ form. The eluent was evaporated to dryness under vacuum [37,38]. Silica-supported Preyssler $H_{14}[NaP_5W_{30}O_{110}]/SiO_2$ catalysts were prepared by impregnating Aerosil 300 silica with a methanolic solution of $H_{14}[NaP_5W_{30}O_{110}]/SiO_2$ [39].

General procedure for crossed-aldol condensation of ketones with aromatic aldehydes:

Ketones (2.5 mmol), aromatic aldehydes (5 mmol), water (5 mL) and silica-supported Preyssler HPAs catalyst (0.05 g) were mixed. The mixture was refluxed for 3 h (Table 1). After complete conversion of the ketone, as monitored by TLC, the mixture was cooled to room temperature. Dichloromethane (30 mL) was added and heated for few minutes. The reagent was removed by filtration. The filtrate was concentrated, then the solid products were filtered off, washed with water (3 \times 25 mL) and the solid residue was recrystallized from ethanol to afford the pure product. The catalyst was filtered off and recycled using a Buechner funnel ($\varnothing = 6.0$ cm) and washed with 20 mL dichloromethane followed by drying in an oven (90 $^\circ C$) for 1 h.

Spectral data for selected compounds:

Compound (**15a**): Anal. Calcd for $C_{19}H_{12}C_{14}O$: C 57.32, H 3.04; Found C 57.21, H 3.14;

IR (KBr, cm^{-1}): 3060, 2932, 1705, 1635, 1578, 1553; 1H -NMR (400 MHz, $CDCl_3$, δ/ppm): 7.53 (s, 2H), 7.38 (m, 4H), 7.24 (m, 2H), 2.61 (s, 4H); ^{13}C -NMR (75 MHz, $CDCl_3$, δ/ppm): 29.5, 126.3, 128.7, 132.2, 143.3, 146.5, 196.8.; MS (m/z , (relative abundance, %)): 361 (M+, 39.5), 325 (22.1), 291 (45.0), 226 (39.3), 161 (28.7).

Compound (**16a**): Anal. Calcd for $C_{23}H_{20}O_3$: C 80.21, H 5.85; Found C 80.17, H 5.88;

IR (KBr, cm^{-1}): 2908, 1683, 1632, 1614, 1599; 1H -NMR (400 MHz, $CDCl_3$, δ/ppm): 7.35 (s, 2H), 7.24 (d, 4H, $J = 8.8$ Hz), 7.04 (d, 2H, $J = 7.6$ Hz), 6.12 (s, 4H), 3.05 (s, 4H); ^{13}C -NMR (75 MHz, $CDCl_3$, δ/ppm): 29.5, 74.5, 125.2, 127.4, 132.2, 134.5, 139.9, 144.1, 197.2. MS (m/z , (relative

abundance, %)): 344 (M+, 41.3), 273 (56.4), 251 (62.3), 212 (41.6).

Compound (**17a**): Anal. Calcd for C₁₉H₁₄Br₂O: C 54.58, H 3.38; Found C 54.52, H 3.43;

IR (KBr, cm⁻¹): 3058, 2925, 1686, 1624, 1603, 1555, 1180; ¹H-NMR (400 MHz, CDCl₃, δ/ppm): 7.75 (s, 2H), 7.53 (m, 6 H), 7.33 (t, 2 H, *J* = 8.0 Hz), 3.12 (s, 4H); ¹³C-NMR (75 MHz, CDCl₃, δ/ppm): 29.7, 124.1, 127.9, 130.7, 132.9, 144.2, 196.4; MS (*m/z*, (relative abundance, %)): 416 (M+, 54.5), 345 (67.4), 337 (57.6), 339 (78.5), 326 (48.9), 325 (51.3), 311 (66.4), 129 (69.9).

Compound (**18a**): Anal. Calcd for C₂₁H₂₀O: C, 87.46; H, 6.98; Found: C, 87.31; H, 7.02;

IR (KBr, cm⁻¹): 3023, 2962, 2927, 1660, 1605, 1572, 1485, 1442, 1240, 1144 cm⁻¹; ¹H-NMR (400 MHz, CDCl₃, δ/ppm): 7.80 (2H, dbr, *J* = 1.6 Hz), 7.45 (10H, Ar), 3.10 (2H, dbr, *J* = 3.5, 15.8 Hz), 2.53 (2H, ddd, *J* = 2.6, 11.4, 15.8 Hz), 1.90 (1H, m), 1.10 (3H, d, *J* = 6 Hz). ¹³C-NMR (75 MHz, CDCl₃, δ/ppm): 21.63, 29.40, 36.48, 128.35, 128.55, 130.37, 135.36, 135.95, 137.12, 190.15; MS (*m/z*, (relative abundance, %)): 288 (M+, 36.5), 217 (73.0), 197 (37.6), 191 (54.6), 183 (70.4).

Compound (**19a**): Anal. Calcd for C₂₃H₂₄O: C, 87.29; H, 7.64; Found: C, 86.39; H, 7.69;

IR (KBr, cm⁻¹): 3025, 2964, 2930, 1663, 1596, 1575, 1514, 1243, 1180, 1146 cm⁻¹; ¹H-NMR (400 MHz, CDCl₃, δ/ppm): 7.78 (2H, dbr, *J* = 1.6 Hz), 7.32 (8H, Ar), 3.10 (2H, dbr, *J* = 3.5, 15.7 Hz), 2.52 (2H, ddd, *J* = 2.4, 11.3, 15.7 Hz), 2.37 (3H, s), 1.85 (1H, m), 1.06 (3H, d, *J* = 6.3 Hz). ¹³C-NMR (75 MHz, CDCl₃, δ/ppm): 21.38, 21.65, 29.40, 36.55, 129.10, 130.45, 133.19, 134.66, 137.05, 138.77, 190.19; MS (*m/z*, (relative abundance, %)): 316 (M+, 42.5), 301 (46.7), 225 (76.5), 219 (81.4), 211 (38.7).

Compound (**20a**): Anal. Calcd for C₂₃H₂₄O₃: C, 83.14; H, 7.22; Found: C, 82.39; H, 7.18;

IR (KBr, cm⁻¹): 2956, 2927, 1665, 1595, 1511, 1296, 1260, 1183, 1175, 1147 cm⁻¹; ¹H-NMR (400 MHz, CDCl₃, δ/ppm): 7.76 (2H, dbr, *J* = 1.6 Hz), 7.40 (8H, Ar), 3.83 (3H, s), 3.04 (2H, dbr, *J* = 3.5, 15.7 Hz), 2.50 (2H, ddd, *J* = 2.4, 11.3, 15.7 Hz), 1.89 (1H, m), 1.12 (3H, d, *J* = 6.5 Hz); ¹³C-NMR (75 MHz, CDCl₃, δ/ppm): 21.75, 29.39, 36.57, 55.30, 113.86, 128.72, 132.20, 133.55, 136.70, 159.84, 190.05; MS (*m/z*, (relative abundance, %)): 348 (M+, 43.2), 317 (58.7), 254 (44.7), 251 (85.1), 243 (63.2), 240 (38.6).

Compound (**21a**): Anal. Calcd for C₂₁H₁₈C₁₂O: C, 70.63; H, 5.04; Found: C, 70.54; H, 5.09; IR (KBr, cm⁻¹): 2960, 2927, 2870, 1662, 1604, 1571,

1485, 1405, 1247, 1148; ¹H-NMR (400 MHz, CDCl₃, δ/ppm): 7.75 (2H, dbr, *J* = 1.6 Hz), 7.39 (8H, Ar), 2.97 (2H, dbr, *J* = 3.5, 15.7 Hz), 2.49 (2H, ddd, *J* = 2.6, 11.2, 15.7 Hz), 1.90 (1H, m), 1.06 (3H, d, *J* = 6.5 Hz); ¹³C-NMR (75 MHz, CDCl₃, δ/ppm): 21.60, 29.25, 36.34, 128.68, 131.55, 134.26, 134.57, 135.59, 135.99, 189.61; MS (*m/z*, (relative abundance, %)): 356 (M+, 35.5), 321 (57.5), 266 (68.4), 265 (45.4), 259 (42.2), 251 (41.4).

Compound (**2b**): Anal. Calcd for C₁₆H₂₅O: C, 82.20; H, 11.36; Found: C, 82.16; H, 11.33;

IR (KBr, cm⁻¹): 1620, 1605; ¹H-NMR (400 MHz, CDCl₃, δ/ppm): 6.50 (2H, d, *J* = 9.7 Hz), 2.40 (4H, m), 2.09 (2H, m), 1.66 (14 H, m), 1.19 (8H, m); ¹³C-NMR (75 MHz, CDCl₃, δ/ppm): 185.59, 144.25, 134.40, 40.21, 36.73, 31.75, 26.65, 23.70, 23.34; MS (*m/z*, (relative abundance, %)): 248 (M+, 21.3), 223 (63.2), 169 (35.6), 166 (49.8).

Compound (**3b**): Anal. Calcd for C₁₁H₁₆O: C, 80.44; H, 9.82; Found: C, 80.40; H, 9.87;

IR (KBr, cm⁻¹): 1620; ¹H-NMR (400 MHz, CDCl₃, δ/ppm): 6.50 (2H, d, *J* = 9.7 Hz), 2.49 (4H, m), 2.09 (2H, m), 1.69 (14 H, m), 1.18 (8H, m); ¹³C-NMR (75 MHz, CDCl₃, δ/ppm): 185.56, 144.25, 134.40, 40.20, 36.72, 31.74, 26.65, 23.70, 23.35; MS (*m/z*, (relative abundance, %)): 164 (M+, 21.0), 135 (64.3), 82 (58.6).

Compound (**4b**): Anal. Calcd for C₁₃H₁₆O: C, 81.20; H, 10.48; Found: C, 81.01; H, 10.30;

IR (KBr, cm⁻¹): 1621; ¹H-NMR (400 MHz, CDCl₃, δ/ppm): 6.50 (2H, d, *J* = 9.7 Hz), 2.48 (4H, m), 2.10 (2H, m), 1.67 (14H, m), 1.20 (8H, m); ¹³C-NMR (75 MHz, CDCl₃, δ/ppm): 185.57, 144.24, 134.40, 40.21, 36.73, 31.71, 26.65, 23.70, 23.35; MS (*m/z*, (relative abundance, %)): 192 (M+, 19.1), 149 (49.9), 136 (67.8).

Compound (**1c**): Anal. Calcd for C₁₃H₁₁NO (197.24); calcd.: C, 79.16; H, 5.62; N, 7.10; found: C, 79.07; H, 5.54; N, 7.13; IR (KBr, cm⁻¹): 1641 (C=O), 2850, 2916, 3025 (CH), 3268 (NH). ¹H-NMR (400 MHz, CDCl₃, δ/ppm): 6.36 (m, 1H), 7.05 (d, 1H), 7.18 (d, 1H), 7.30 (d, 1H, C₂-H; *J* = 15.60), 7.58 (m, 5H), 7.85 (d, 1H, C₃-H; *J* = 15.58), 10.30 (s, 1H). ¹³C-NMR (75 MHz, CDCl₃, δ/ppm): 35.2, 42.1, 110.7, 117.6, 125.2, 127.4, 128.0, 190.4. MS (*m/z*, (relative abundance, %)): 197 (M+, 29.4), 120 (52.4), 107 (49.9), 103 (52.6), 106 (32.9), 94 (43.0), 92 (41.4), 41 (44.6), 39 (23.1), 28 (38.7).

Compound (**2c**): Anal. Calcd for C₁₄H₁₃NO (211.26); calcd.: C, 79.60; H, 6.20; N, 6.63; found: C, 79.51; H, 6.13; N, 6.57; IR (KBr, cm⁻¹): 1642

(C=O), 2993 (CH), 3255 (NH). ¹H-NMR (400 MHz, CDCl₃, δ/ppm): 2.40 (s, 3H), 6.36 (m, 1H), 7.12 (d, 1H), 7.25 (s, 1H), 7.28 (d, 2H), 7.35 (d, 1H, C₂-H; *J*=15.62), 7.55 (d, 2H), 7.85 (d, 1H, C₃-H; *J*=15.68), 10.32 (s, 1H). ¹³C-NMR (75 MHz, CDCl₃, δ/ppm): 22.2, 34.5, 41.5, 111.0, 127.8, 129.1, 135.4, 138.2, 190.2. MS (*m/z*, (relative abundance, %)): 211 (M⁺, 20.5), 196 (53.3), 120 (46.4), 117 (36.9), 106 (39.7), 92 (44.1), 41 (51.0), 39 (31.8), 28 (32.0).

Compound (3c): Anal. Calcd for C₁₃H₁₀ClNO (231.68); calcd.: C, 67.40; H, 4.35; N, 6.05; found: C, 67.32; H, 4.30; N, 5.97; IR (KBr, cm⁻¹): 1645 (C=O), 2875, 2984 (CH), 3272 (NH). ¹H-NMR (400 MHz, CDCl₃, δ/ppm): 6.35 (m, 1H), 6.93 (d, 1H), 7.12 (s, 1H), 7.25 (s, 1H), 7.26 (d, 1H), 7.33 (d, 1H, C₂-H; *J*=15.69), 7.46 (d, 1H), 7.75 (t, 1H), 8.21 (d, 1H, C₃-H; *J*=15.69), 10.12 (s, 1H). ¹³C-NMR (75 MHz, CDCl₃, δ/ppm): 24.4, 40.8, 110.8, 117.3, 125.9, 133.0, 146.5, 190.1. MS (*m/z*, (relative abundance, %)): 231 (M⁺, 18.3), 196 (23.6), 137 (35.3), 126 (46.8), 107 (34.7), 41 (31.6), 39 (53.7), 28 (44.6).

Compound (4c): Anal. Calcd for C₁₃H₁₀ClNO (231.68); calcd.: C, 67.40; H, 4.35; N, 6.05; found: C, 67.32; H, 4.30; N, 5.97; IR (KBr, cm⁻¹): 1645 (C=O), 2873, 2984 (CH), 3275 (NH). ¹H-NMR (400 MHz, CDCl₃, δ/ppm): 6.35 (m, 1H), 7.12 (s, 1H), 7.15 (s, 1H), 7.34 (d, 1H, C₂-H; *J*=15.78), 7.40 (d, 2H), 7.55 (d, 2H), 7.80 (d, 1H, C₃-H; *J*=15.72), 10.36 (s, 1H). ¹³C-NMR (75 MHz, CDCl₃, δ/ppm): 111.33 (CH), 117.12 (CH), 122.83 (CH), 124.40 (CH), 128.12 (CH), 129.65 (C), 131.40 (2xCH), 134.17 (C₂-H), 134.67 (C), 137.23 (C), 142.30 (C₃-H), 179.79 (C=O). MS (*m/z*, (relative abundance, %)): 231 (M⁺, 16.2), 196 (39.8), 137 (31.5), 126 (49.7), 107 (63.3), 41 (50.7), 39 (28.9), 28 (41.4).

Compound (5c): Anal. Calcd for C₁₃H₁₁NO₂ (213.23); calcd.: C, 73.23; H, 5.20; N, 6.57; found: C, 73.11; H, 5.14; N, 6.50; IR (KBr, cm⁻¹): 1630 (C=O), 2851, 2921 (CH), 3256 (NH), 3455 (OH). ¹H-NMR (400 MHz, CDCl₃, δ/ppm): 6.27 (m, 1H), 6.61 (m, 1H), 6.84 (d, 1H), 7.09 (m, 1H), 7.12 (d, 1H), 7.25 (d, 1H, C₂-H; *J*=15.58), 7.36 (d, 1H), 7.65 (m, 1H), 8.16 (d, 1H, C₃-H; *J*=15.66), 10.07 (s, 1H), 10.36 (s, 1H). ¹³C-NMR (75 MHz, CDCl₃, δ/ppm): 25.6, 40.9, 110.6, 115.6, 117.3, 121.4, 125.3, 28.0, 130.3, 133.1, 154.4, 190.4. MS (*m/z*, (relative abundance, %)): 213 (M⁺, 19.7), 122 (36.8), 119 (49.6), 108 (21.6), 94 (28.9), 41 (48.6), 39 (37.6), 28 (50.9).

Compound (6c): Anal. Calcd for C₁₄H₁₃NO₂ (227.26); calcd.: C, 73.99; H, 5.77; N, 6.16; found: C, 73.86; H, 5.71; N, 6.05; IR (KBr, cm⁻¹): 1642

(C=O), 2844, 2970 (CH), 3262 (NH). ¹H-NMR (400 MHz, CDCl₃, δ/ppm): 3.87 (s, 3H), 6.35 (m, 1H), 6.95 (d, 2H), 7.12 (d, 1H), 7.17 (d, 1H), 7.26 (d, 1H, C₂-H; *J*=15.62), 7.60 (d, 2H), 7.80 (d, 1H, C₃-H; *J*=15.59), 10.45 (s, 1H). ¹³C-NMR (75 MHz, CDCl₃, δ/ppm): 57.85 (CH₃), 111.74 (CH), 115.33 (2xCH), 117.15 (CH), 118.96 (C), 121.60 (CH), 126.41 (C), 130.25 (2xCH), 131.76 (C₂-H), 143.81 (C₃-H), 163.20 (C), 180.95 (C=O). MS (*m/z*, (relative abundance, %)): 227 (M⁺, 23.3), 196 (71.6), 133 (67.0), 94 (58.9), 41 (53.5), 39 (44.3), 28 (66.2).

Compound (7c): Anal. Calcd for C₁₄H₁₁NO₃ (241.42); calcd.: C, 69.65; H, 4.59; N, 5.80; found: C, 69.57; H, 4.53; N, 5.71; IR (KBr, cm⁻¹): 1640 (C=O), 2830, 2961 (CH), 3225 (NH). ¹H-NMR (400 MHz, CDCl₃, δ/ppm): 6.05 (s, 2H), 6.38 (m, 1H), 6.87 (d, 1H), 7.11 (m, 3H), 7.15 (d, 1H), 7.20 (d, 1H, C₂-H; *J*=15.63), 7.94 (d, 1H, C₃-H; *J*=15.62), 10.47 (s, 1H). ¹³C-NMR (75 MHz, CDCl₃, δ/ppm): 103.25 (CH₂), 105.65 (CH), 107.60 (CH), 109.84 (CH), 116.20 (CH), 119.48 (C₂-H), 124.21 (CH), 129.43 (C), 133.10 (C), 142.52 (C₃-H), 148.25 (C), 148.30 (C), 178.85 (C=O). ¹³C-NMR (CDCl₃, 75 MHz): 30.8, 41.4, 101.3, 110.2, 117.2, 125.8, 126.7, 128.1, 132.5, 137.1, 138.8, 146.6, 148.4, 190.4. MS (*m/z*, (relative abundance, %)): 241 (M⁺, 30.1), 147 (48.9), 117 (59.7), 94 (74.6), 41 (69.7), 39 (35.6), 28 (41.1).

Compound (8c): Anal. Calcd for C₁₅H₁₆N₂O (240.30); calcd.: C, 74.98; H, 6.71; N, 11.58; found: C, 74.92; H, 6.65; N, 11.53. ¹³C-NMR (75 MHz, CDCl₃, δ/ppm): 34.6, 40.1, 41.4, 110.8, 112.9, 125.5, 128.8, 131.1, 132.8, 148.6, 190.4; IR (KBr, cm⁻¹): 1635 (C=O), 2906 (CH), 3240 (NH). ¹H-NMR (400 MHz, CDCl₃, δ/ppm): 3.02 (s, 6H), 6.35 (m, 1H), 6.70 (d, 2H), 7.08 (m, 2H), 7.16 (d, 1H, C₂-H; *J*=15.58), 7.55 (d, 2H), 7.80 (d, 1H, C₃-H; *J*=15.53), 10.39 (s, 1H). MS (*m/z*, (relative abundance, %)): 240 (M⁺, 15.2), 146 (54.3), 107 (23.8), 94 (39.7), 41 (53.8), 39 (44.7), 28 (51).

Compound (1d): Anal. Calcd for C₁₄H₁₂OS (228.31); calcd.: C, 73.65; H, 5.30; S, 14.04; found: C, 73.58; H, 5.27; IR (KBr, cm⁻¹): 1590 (C=C), 1645 (C=O), 2919, 3085 (CH). ¹H-NMR (400 MHz, CDCl₃, δ/ppm): 2.40 (s, 3H), 7.17 (m, 1H), 7.20 (d, 2H), 7.40 (d, 1H, C₂-H; *J*=15.65), 7.55 (d, 2H), 7.66 (d, 1H), 7.85 (d, 1H, C₃-H; *J*=16.13), 7.87 (d, 1H). ¹³C-NMR (75 MHz, CDCl₃, δ/ppm): 21.60 (CH₃), 120.59 (CH), 128.20 (CH), 128.55 (2xCH), 129.72 (2xCH), 131.70 (C₂-H), 131.95 (C), 133.78 (CH), 141.22 (C), 144.20 (C₃-H), 145.68 (C), 182.16 (C=O). MS (*m/z*, (relative abundance, %)): 228 (M⁺, 14.0), 213 (56.4), 124

(46.7), 117 (35.6), 111 (81.2), 58 (34.4), 41 (32.1), 39 (29.0).

Compound (**2d**): Anal. Calcd for $C_{13}H_9ClOS$ (248.73); calcd.: C, 62.78; H, 3.65; S, 12.89; found: C, 62.66; H, 3.62; IR (KBr, cm^{-1}): 1593 (C=C), 1647 (C=O), 3091 (CH). 1H -NMR (400 MHz, $CDCl_3$, δ/ppm): 7.20 (m, 1H), 7.23 (d, 2H), 7.40 (d, 1H, C_2 -H; $J=15.65$), 7.64 (d, 2H), 7.72 (d, 1H), 7.87 (d, 1H, C_3 -H; $J=15.79$), 7.95 (d, 1H). ^{13}C -NMR (75 MHz, $CDCl_3$): 121.95 (CH), 128.26 (CH), 129.25 (2xCH), 129.62 (2xCH), 131.90 (C_2 -H), 133.14 (C), 134.10 (CH), 136.45 (C), 142.53 (C_3 -H), 145.30 (C), 181.74 (C=O). MS (m/z , relative abundance, %): 248 (M^+ , 22.7), 213 (32.4), 137 (56.4), 124 (43.5), 111 (81.1), 58 (23.7), 41 (44.3), 39 (31.7).

Compound (**3d**): Anal. Calcd for $C_{13}H_9BrOS$ (293.18); calcd.: C, 53.26; H, 3.09; S, 10.94; found: C, 53.19; H, 3.05; IR (KBr, cm^{-1}): 1580 (C=C), 1647 (C=O), 3025 (CH). 1H -NMR (400 MHz, $CDCl_3$, δ/ppm): 7.20 (m, 1H), 7.46 (d, 1H, C_2 -H; $J=15.58$), 7.50 (d, 2H), 7.57 (d, 2H), 7.73 (d, 1H), 7.80 (d, 1H, C_3 -H; $J=15.58$), 7.87 (d, 1H). ^{13}C -NMR (75 MHz, $CDCl_3$, δ/ppm): 122.05 (CH), 124.85 (C), 128.29 (CH), 128.76 (2xCH), 131.96 (C_2 -H), 132.18 (2xCH), 133.55 (C), 134.12 (CH), 142.60 (C_3 -H), 145.31 (C), 181.70 (C=O). MS (m/z , relative abundance, %): 292 (M^+ , 31.2), 213 (37.6), 181 (42.8), 124 (29.7), 58 (56.8), 41 (43.6), 39 (42.6).

Compound (**4d**): Anal. Calcd for $C_{14}H_{12}O_2S$ (244.31); calcd.: C, 68.83; H, 4.95; S, 13.13; found: C, 68.77; H, 4.90; IR (KBr, cm^{-1}): 1594 (C=C), 1645 (C=O), 3022 (CH). 1H -NMR (400 MHz, $CDCl_3$, δ/ppm): 3.85 (s, 3H), 6.95 (d, 2H), 7.24 (m, 1H), 7.30 (d, 1H, C_2 -H; $J=15.62$), 7.39 (d, 1H), 7.66 (d, 2H), 7.77 (d, 1H), 7.89 (d, 1H, C_3 -H; $J=15.62$). ^{13}C -NMR (75 MHz, $CDCl_3$, δ/ppm): 34.6, 41.4, 55.8, 110.7, 114.4, 117.3, 125.6, 129.9, 132.8, 133.7, 190.3. MS (m/z , relative abundance, %): 244 (M^+ , 16.1), 213 (56.9), 133 (42.4), 124 (34.7), 65 (53.2), 58 (46.7), 41 (38.6), 39 (54.5).

Compound (**5d**): Anal. Calcd for $C_{15}H_{14}O_3S$ (274.34); calcd.: C, 65.67; H, 5.14; S, 11.69; found: C, 65.58; H, 5.07; IR (KBr, cm^{-1}): 1565 (C=C), 1637 (C=O), 3021 (CH). 1H -NMR (400 MHz, $CDCl_3$, δ/ppm): 3.85 (s, 3H), 3.91 (s, 3H), 6.50 (d, 2H), 7.16 (m, 1H), 7.48 (d, 1H, C_2 -H; $J=15.62$), 7.57 (d, 1H), 7.63 (m, 1H), 7.85 (s, 1H), 8.07 (d, 1H, C_3 -H; $J=15.62$). ^{13}C -NMR (75 MHz, $CDCl_3$, δ/ppm): 25.7, 41.5, 55.9, 56.6, 100.4, 111.1, 117.3, 125.5, 132.4, 159.0, 190.1. MS (m/z , relative abundance, %): 274 (M^+ , 41.2), 243 (56.5), 212

(34.4), 163 (29.7), 124 (38.6), 111 (76), 58 (67.5), 41 (53.4), 39 (43.1).

Compound (**6d**): Anal. Calcd for $C_{15}H_{14}O_3S$ (274.34); calcd.: C, 65.67; H, 5.14; S, 11.69; found: C, 65.61; H, 5.10; IR (KBr, cm^{-1}): 1575 (C=C), 1648 (C=O), 2987 (CH). 1H -NMR (400 MHz, $CDCl_3$, δ/ppm): 3.86 (s, 3H), 3.95 (s, 3H), 6.85 (d, 1H), 6.98 (s, 1H), 7.12 (d, 1H), 7.17 (m, 1H), 7.35 (d, 1H, C_2 -H; $J=15.64$), 7.59 (d, 1H), 7.67 (d, 1H, C_3 -H; $J=15.64$), 7.69 (d, 1H). ^{13}C -NMR (75 MHz, $CDCl_3$, δ/ppm): 30.6, 41.4, 56.3, 11.1, 112.4, 117.2, 122.2, 132.5, 147.2, 149.8, 190.4. MS (m/z , relative abundance, %): 258 (M^+ , 17.2), 147 (43.7), 124 (56.9), 111 (76.5), 58 (64.9), 41 (42.3), 39 (39.0).

Compound (**7d**): Anal. Calcd for $C_{14}H_{10}O_3S$ (258.30); calcd.: C, 65.10; H, 3.90; S, 12.41; found: C, 64.96; H, 3.85; IR (KBr, cm^{-1}): 1589 (C=C), 1646 (C=O), 2989 (CH). 1H -NMR (400 MHz, $CDCl_3$, δ/ppm): 6.05 (s, 2H), 6.77 (d, 1H), 7.19 (d, 1H), 7.29 (m, 2H), 7.34 (d, 1H, C_2 -H; $J=15.62$), 7.62 (d, 1H), 7.78 (d, 1H, C_3 -H; $J=15.69$), 7.85 (d, 1H). ^{13}C -NMR (75 MHz, $CDCl_3$, δ/ppm): 101.62 (CH_2), 106.67 (CH), 108.65 (CH), 119.83 (CH), 125.35 (C_2 -H), 128.20 (CH), 129.18 (C), 131.56 (CH), 133.65 (CH), 143.90 (C_3 -H), 145.67 (C), 148.35 (C), 149.95 (C), 181.94 (C=O). MS (m/z , relative abundance, %): 220 (M^+ , 16.3), 148 (67.8), 137 (73.3), 109 (43.7), 58 (52.1), 41 (41.5), 39 (23.7).

Compound (**8d**): Anal. Calcd for $C_{11}H_8OS_2$ (220.32); calcd.: C, 59.97; H, 6.10; S, 29.11; found: C, 59.91; H, 6.07; IR (KBr, cm^{-1}): 1574 (C=C), 1640 (C=O), 3095 (CH). 1H -NMR (400 MHz, $CDCl_3$, δ/ppm): 7.08 (d, 1H), 7.19 (m, 1H), 7.27 (d, 1H, C_2 -H; $J=15.72$), 7.41 (s, 1H), 7.51 (m, 1H), 7.76 (m, 1H), 7.89 (s, 1H), 8.09 (d, 1H, C_3 -H; $J=15.63$). ^{13}C -NMR (75 MHz, $CDCl_3$, δ/ppm): 120.38 (CH), 128.27 (CH), 128.36 (CH), 128.85 (C_2 -H), 131.67 (C_3 -H), 132.28 (CH), 133.86 (CH), 136.49 (CH), 141.52 (C), 149.99 (C), 181.59 (C=O). MS (m/z , relative abundance, %): 274 (M^+ , 15.2), 243 (45.6), 212 (54.9), 163 (49.0), 124 (65.9), 111 (78.9), 58 (49.0), 41 (56.7), 39 (63.2).

Compound (**1e**): Anal. Calcd for $C_{14}H_{10}ClNO$ (243.69); calcd.: C, 69.00; H, 4.14; N, 5.75; found: C, 68.91; H, 4.09; N, 5.70; IR (KBr, cm^{-1}): 1568, 1605 (C=C, C=N), 1676 (C=O), 3046 (CH). 1H -NMR (400 MHz, $CDCl_3$, δ/ppm): 7.38 (d, 2H), 7.52 (m, 1H), 7.67 (d, 2H), 7.89 (d, 1H, C_2 -H; $J=16.15$), 7.87 (d, 1H), 8.20 (d, 1H), 8.29 (d, 1H, C_3 -H; $J=16.15$), 8.77 (d, 1H). ^{13}C -NMR (75 MHz, $CDCl_3$, δ/ppm): 121.30 (CH), 122.99 (CH), 127.17 (C_2 -H), 129.19 (CH), 129.98 (CH), 133.65 (C), 136.44 (C),

137.09 (C₃-H), 143.18 (CH), 148.88 (CH), 154.09 (C), 189.29 (C=O). MS (*m/z*, (relative abundance, %)): 243 (M⁺,12.1), 208 (54.7), 137 (75.4), 119 (34.6), 106 (56.8).

Compound (**2e**): Anal. Calcd for C₁₅H₁₃NO₂ (239.27); calcd.: C, 75.30; H, 5.48; N, 5.85; found: C, 75.22; H, 5.43; N, 5.76; IR (KBr, cm⁻¹): 1572, 1596 (C=C, C=N), 1664 (C=O), 3050 (CH). ¹H-NMR (400 MHz, CDCl₃, δ/ppm): 3.85 (s, 3H), 6.97 (d, 2H), 7.49 (m, 1H), 7.71 (d, 2H), 7.89 (m, 1H), 7.97 (d, 1H, C₂-H; *J*=15.95), 8.19 (d, 1H, C₃-H; *J*=15.89), 8.21 (d, 1H), 8.78 (d, 1H). ¹³C-NMR (75 MHz, CDCl₃, δ/ppm): 55.42 (CH₃), 114.31 (CH), 118.47 (CH), 122.85 (CH), 126.74 (CH), 126.95 (C₂-H), 127.92 (C), 130.66 (CH), 136.99 (C₃-H), 144.70 (CH), 148.77 (CH), 154.45 (C), 161.71 (C), 189.42 (C=O). MS (*m/z*, (relative abundance, %)): 239 (M⁺,14.2), 133 (64.6), 119 (78.8), 106 (56.3).

Compound (**3e**): Anal. Calcd for C₁₅H₁₁NO₃ (253.26); calcd.: C, 71.14; H, 4.38; N, 5.53; found: C, 71.08; H, 4.34; N, 5.47; IR (KBr, cm⁻¹): 1581 (C=C, C=N), 1655 (C=O), 3012 (CH). ¹H-NMR (400 MHz, CDCl₃, δ/ppm): 6.02 (s, 2H), 6.87 (d, 1H), 7.23 (d, 1H), 7.29 (s, 1H), 7.49 (m, 1H), 7.85 (d, 1H), 7.87 (d, 1H, C₂-H; *J*=15.88), 8.06 (d, 1H, C₃-H; *J*=15.93), 8.16 (m, 1H), 8.74 (d, 1H). ¹³C-NMR (75 MHz, CDCl₃, δ/ppm): 101.60 (CH₂), 107.07 (CH), 108.60 (CH), 111.84 (CH), 118.90 (CH), 122.86 (CH), 125.65 (CH), 126.80 (C₂-H), 129.71 (C), 137.06 (C₃-H), 144.67 (CH), 148.35 (C), 148.80 (CH), 149.96 (C), 154.34 (C), 189.30 (C=O). MS (*m/z*, (relative abundance, %)): 253 (M⁺, 19.5), 147 (57.7), 119 (45.9), 106 (62.1).

Compound (**4e**): Anal. Calcd for C₁₂H₁₀N₂O (198.22); calcd.: C, 72.71; H, 5.08; N, 14.13; found: C, 72.64; H, 5.06; N, 14.08; IR (KBr, cm⁻¹): 1575 (C=C, C=N), 1653 (C=O), 3091 (CH), 3302 (NH). ¹H-NMR (400 MHz, CDCl₃, δ/ppm): 6.34 (m, 1H), 6.73 (d, 1H), 7.02 (d, 1H), 7.28 (s, 1H), 7.51 (m, 1H), 7.89 (d, 1H, C₂-H; *J*=16.26), 7.98 (m, 1H), 8.39 (d, 1H, C₃-H; *J*=16.28), 8.79 (d, 1H), 8.98 (s, 1H). ¹³C-NMR (75 MHz, CDCl₃, δ/ppm): 111.45 (CH), 113.92 (CH), 116.80 (CH), 122.88 (CH), 123.27 (CH), 126.62 (C₂-H), 134.12 (CH), 136.29 (C), 137.07 (C₃-H), 148.59 (CH), 153.94 (C), 193.20 (C=O). MS (*m/z*, (relative abundance, %)): 198 (M⁺,14.0), 119 (56.9), 118 (67.8), 92 (49.8).

Compound (**5e**): Anal. Calcd for C₁₂H₉NOS (215.28); calcd.: C, 69.51; H, 4.21; N, 6.51; S, 14.90; found: C, 69.47; H, 4.19; N, 6.43; IR (KBr, cm⁻¹): 1580 (C=C, C=N), 1665 (C=O), 3031 (CH), 3319 (NH). ¹H-NMR (400 MHz, CDCl₃, δ/ppm): 7.05 (m, 1H), 7.47 (m, 2H), 7.52 (m, 1H), 7.89 (d,

1H, C₂-H; *J*=15.54), 8.09 (s, 2H), 8.19 (d, 1H, C₃-H; *J*=15.52), 8.77 (d, 1H). ¹³C-NMR (75 MHz, CDCl₃, δ/ppm): 119.75 (CH), 122.85 (CH), 126.83 (C₂-H), 128.22 (CH), 129.17 (CH), 132.15 (CH), 136.96 (C₃-H), 137.20 (CH), 140.98 (C), 148.84 (CH), 155.30 (C), 193.22 (C=O). MS (*m/z*, (relative abundance, %)): 215 (M⁺,16.1), 131 (67.9), 119 (75.4), 106 (56.8), 58 (8.7), 41 (44.6), 39 (43.8).

Compound (**1f**): Anal. Calcd for C₁₆H₁₄O₂ (238.11): C, 80.64; H, 5.93; Found: C, 80.56; H, 5.88 Anal. Calcd for C₁₆H₁₃ClO₂ (272.56): C, 70.44; H, 4.81; Found: C, 70.37; H, 4.75; IR (KBr, cm⁻¹): 1596 (C=C), 1656 (C=O), 2933, 3055 (CH); ¹H-NMR (400 MHz, CDCl₃, δ/ppm): 3.86 (s, 3H), 6.99 (d, 2H, *J*=7.6), 7.43 (m, 3H), 7.55 (d, 1H, C₂-H, *J*=15.7), 7.65 (d, 2H, *J*=5.7), 7.99 (d, 1H, C₃-H, *J*=15.7), 8.06 (d, 2H, *J*=7.6); ¹³C-NMR (75 MHz, CDCl₃, δ/ppm): 56.20, 114.01, 121.11, 127.56, 131.20, 135.56, 145.80, 166.84. MS (*m/z*, (relative abundance, %)): 238 (M⁺,26.4), 148 (75.3), 135 (45.9), 119 (41.2), 107 (32.3).

Compound (**2f**): Anal. Calcd for C₁₆H₁₃ClO₂ (272.56): C, 70.44; H, 4.81; Found: C, 70.37; H, 4.75; IR (KBr, cm⁻¹): 1600 (C=C), 1656 (C=O), 2925, 3012 (CH); ¹H-NMR (400 MHz, CDCl₃, δ/ppm): 3.91 (s, 3H), 6.99 (d, 2H, *J*=8.6), 7.41 (d, 2H, *J*=8.3), 7.50 (d, 1H, C₂-H, *J*=15.7), 7.55 (d, 2H, *J*=8.3), 7.77 (d, 1H, C₃-H, *J*=15.7), 8.06 (d, 2H, *J*=8.6); ¹³C-NMR (75 MHz, CDCl₃, δ/ppm): 55.7, 114.6, 121.1, 128.5, 129.1, 131.0, 133.4, 145.4, 166.6, 189.8. MS (*m/z*, (relative abundance, %)): 272 (M⁺, 22.7), 237 (45.8), 148 (67.8), 137 (54.3), 135 (39.7).

Compound (**3f**): Anal. Calcd for C₁₇H₁₆O₃ (268.13): C, 76.08; H, 6.01; Found: C, 76.01; H, 5.95; IR (KBr, cm⁻¹): 1597 (C=C), 1656 (C=O), 2960, 3015, 3067 (CH); ¹H-NMR (400 MHz, CDCl₃, δ/ppm): 3.84 (s, 3H), 3.89 (s, 3H), 6.97 (dd, 4H, *J*=8.3), 7.44 (d, 1H, C₂-H, *J*=15.5), 7.62 (d, 2H, *J*=8.4), 7.79 (d, 1H, C₃-H, *J*=15.6), 8.06 (d, 2H, *J*=8.4); ¹³C-NMR (75 MHz, CDCl₃, δ/ppm): 55.6, 115.1, 121.4, 127.7, 130.2, 130.9, 135.6, 145.4, 159.7, 166.7, 189.9. MS (*m/z*, (relative abundance, %)): 268 (M⁺,16.1), 148 (67.9), 137 (54.1), 135 (34.6).

Compound (**4f**): Anal. Calcd for C₁₇H₁₄O₄ (282.11): C, 72.31; H, 5.00; Found: C, 72.26; H, 4.95; IR (KBr, cm⁻¹): 1584 (C=C), 1655 (C=O), 2920, 3035 (CH); ¹H-NMR (400 MHz, CDCl₃, δ/ppm): 3.88 (s, 3H), 6.04 (s, 2H), 6.87 (d, 1H, *J*=8.0), 6.99 (d, 2H, *J*=8.6), 7.18 (m, 2H), 7.37 (d, 1H, C₂-H, *J*=15.4), 7.75 (d, 1H, C₃-H, *J*=15.4), 8.04 (d, 2H, *J*=8.6); ¹³C-NMR (75 MHz, CDCl₃, δ/ppm):

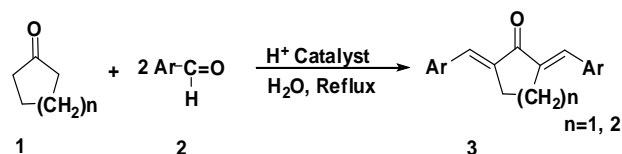
55.6, 106.5, 108.2, 114.7, 122.4, 127.4, 131.1, 145.3, 148.0, 148.8, 166.1, 189.8. MS (*m/z*, (relative abundance, %)): 282 (*M*⁺, 26.2), 148 (65.9), 147 (52.9), 135 (23.8).

RESULTS AND DISCUSSION

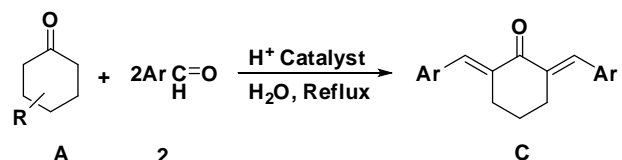
We wish to report an efficient and selective method for condensation of cyclic and acyclic ketones with aromatic and non-aromatic aldehydes in aqueous medium, free of organic solvents. Different types of ketones were subjected to condensation with aromatic and non-aromatic aldehydes, containing either electron-releasing or electron-withdrawing groups, in the presence of the reagent under free of organic solvents conditions (Schemes 1, 2).

The results of crossed-aldol condensation of aromatic and non-aromatic aldehydes are summarized in Tables 1 and 2. The reactions were

completed within 1.5-6 h and high yields of α,α' -bis(substituted benzylidene and cinnamylidene) cyclopentanones and cyclohexanones were obtained (Table 1, entries 1-12).



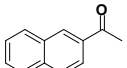
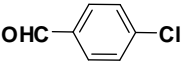
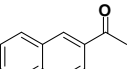
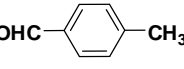
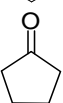
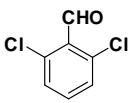
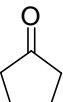
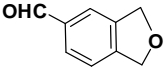
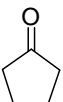
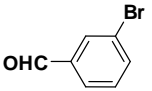
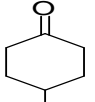
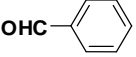
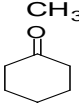
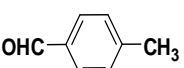
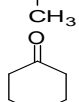
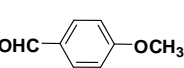
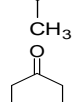
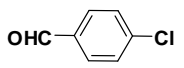
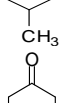
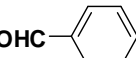
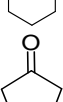
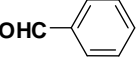
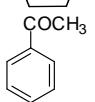
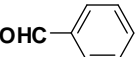
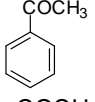
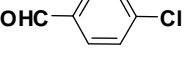
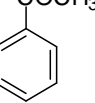
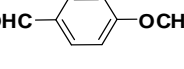
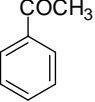
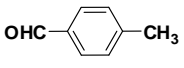
Scheme 1. Crossed-aldol condensation of ketones with aromatic aldehydes (1)



Scheme 2. Crossed-aldol condensation of ketones with non-aromatic aldehydes (A)

Table 1. Crossed-aldol condensation of ketones with aromatic aldehydes (1) in the presence of silica-supported Preyssler heteropolyacids catalyst under organic solvent-free and reflux conditions

Entry	Ketone	Aldehyde	Time, h	^{a,b} Yield, %	M p (°C)	
					Found	Reported
1a		C ₆ H ₅ CH=CH-CHO	2	97	225–227	222–224 ^{17a}
2a			2	98.5	217–219	220 ^{17b}
3a			2.5	95.5	229–230	230–231 ^{17a}
4a			1.5	97	212–214	210–211 ^{17a}
5a			2	96.5	223–225	225 ^{17b}
6a			1.5	96, 96 ^d , 95 ^d , 94 ^d	190–191	188–191 ^{17a}
7a		C ₆ H ₄ CH=CH-CHO	3	92	181–183	180 ^{17a}
8a			2.5	94.5	167–169	170 ¹⁸
9a			3	92.5	160–162	159 ^{17a}
10a			3	93	201–203	203–204 ^{17a}
11a			2.5	94, 93 ^d , 93 ^d , 92 ^d	146–148	147–148 ^{17a}
12a			2	95, 94 ^d , 93 ^d , 93 ^d	115–118	117 ^{17a}

13 a			1.5	97	162–164	163–165 ^{17b}
14 a			1.5	98	143–145	142–143 ^{17b}
15 a			1.5	82	182–188°C (accomp. by decomp.)	–
16 a			1.5	91	247–249	
17 a			2.5	89	208–210	–
18 a			4	93.5	97–99	–
19 a			4.5	94	125–127	–
20 a			4	93	137–139	–
21 a			5	96	156–160	–
22 a			6	^c 28	115–118	117 ^{17a}
23 a			5	^c 30	190–191	188–191 ^{17a}
24 a			2.5	92.5	54–57	55–58 ^{17c}
25 a			2.5	98	108–110	107–109 ^{17b}
26 a			2.5	96.5	74–76	75–77 ^{17c}
27 a			2.5	98	95–97	97–98 ^{17c}

^aIsolated yield; ^bProducts were characterized by comparison of their spectroscopic data (¹H-NMR and IR) and mps with those reported in the literature; ^cThe reaction was performed in the absence of the catalyst; ^dThe same catalyst was used for each of the four runs.

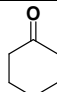
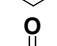

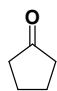
The results of crossed-aldol condensation of cyclic ketones with non-aromatic aldehydes in the presence of silica-supported Preyssler HPAs

catalyst under free of organic solvents conditions was investigated at appropriate times and under reflux (Table 2). In the crossed-aldol condensation

of cyclopentanone with hexanal the reaction yield is good (Table 2, entry 2b), but in similar reactions for other cyclic ketones and with non-aromatic aldehydes the yields are lower (40-51%), (Table 2, entries 1b, 3b and 4b).

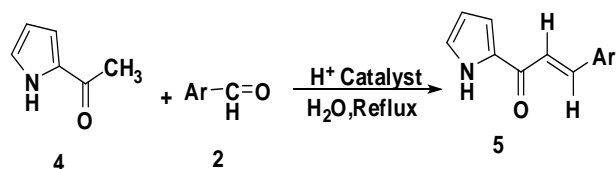
Reactions were also performed for acyclic ketones like 2-acetylnaphthalene and the corresponding products were obtained in excellent yields within 1.5 h (Table 1, entries 13-14, 24-27). The promoting effect of silica-supported Preyssler HPAs catalyst in these reactions was shown by

Table 2. Crossed-aldol condensation of ketones with non-aromatic aldehydes (A) in the presence of silica-supported Preyssler heteropolyacids catalyst under organic solvent-free and reflux conditions

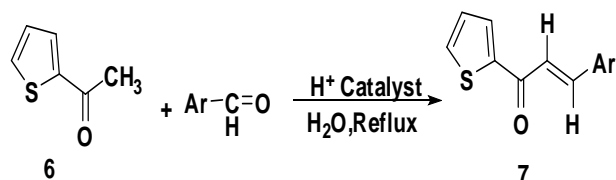
Entry	Ketone	Aldehyde	Time, h	Yield, % ^{a,b}	Bp (°C)	
					Found	Reported
1b		CH ₃ CHO	6	40	130	87-89 ⁴⁰
2b		<i>n</i> -C ₅ H ₁₁ CHO	5	81	140	–
3b		C ₂ H ₅ CHO	5	47	156	–
4b		<i>n</i> -PrCHO	6	51	170	–

^aIsolated yield; ^bProducts were characterized by comparison of their spectroscopic data (¹H-NMR and IR).

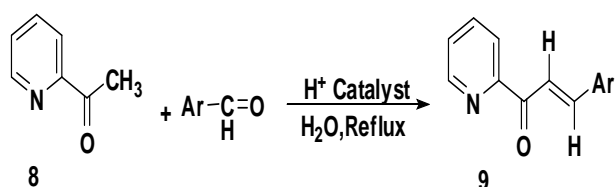
performing some reactions in the absence of the catalyst (Table 1, entries 22, 23). In these experiments the product was isolated and the remaining catalyst was washed and reloaded with fresh substrates for further runs. No decrease in the yield was observed, demonstrating that silica-supported Preyssler HPAs catalyst can be reused in crossed-aldol condensation (Table 1, entries 6 and 11, 12). We continued our research in this paper on the crossed-aldol condensation of some hetarylmethyl ketones with a variety of different aromatic aldehydes in water at reflux temperature and in the presence of silica-supported Preyssler HPAs as a catalyst for the synthesis of (*E*)-3-aryl-1-hetarylprop-2-en-1-ones (5, 7, 9 in Schemes 3, 4, 5) and 1,3-disubstituted propenones (11, Scheme 6) in excellent yields with high stereoselectivity (11, Scheme 6).



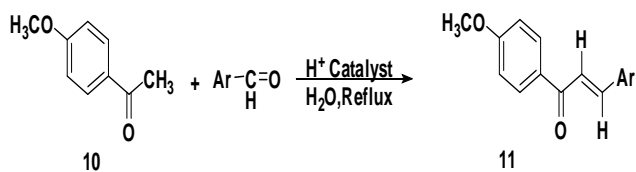
Scheme 3. Crossed-aldol condensation of 2-acetylpyrrole (4) with aromatic aldehydes and synthesis of (*E*)-3-aryl-1-(pyrrol-2'-yl)prop-2-en-1-ones (5, 1-8c).



Scheme 4. Crossed-aldol condensation of 2-acetylthiophene (6) with aromatic aldehydes and synthesis of (*E*)-3-aryl-1-(thien-2'-yl)prop-2-en-1-ones (7, 1-8d).



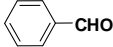
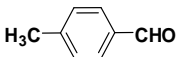
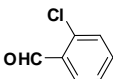
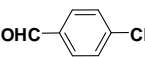
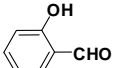
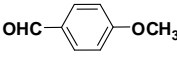
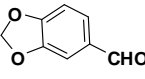
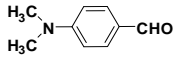
Scheme 5. Crossed-aldol condensation of 2-acetylpyridine (8) with aromatic aldehydes and synthesis of (*E*)-3-aryl-1-(pyrid-2'-yl)prop-2-en-1-ones (9, 1-5e).



Scheme 6. Crossed-aldol condensation of 4-methoxyacetophenone (10) with aromatic aldehydes and synthesis of (*E*)-3-aryl-1-(4'-methoxyphenyl)prop-2-en-1-ones (11, 1-4f).

By efficient stirring of an equimolar amount of 2-hetarylmethyl ketones, 4-methoxyacetophenone (4, 6, 8, 10) and aromatic aldehydes in aqueous acidic (H⁺) solution in the presence of silica-supported Preyssler catalysts as acidic catalyst at reflux temperature, stereoselective crossed-aldol condensation took place with precipitation of 3-aryl-1-hetarylprop-2-en-1-ones (5, 7, 9 in Schemes 3, 4, 5) and 1,3-disubstituted propenones in high yields within a short reaction time as shown in Tables 3, 4, 5, 6.


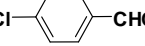
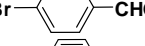
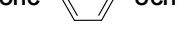
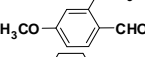
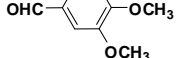
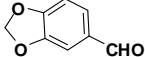
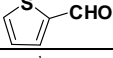
Table 3. Crossed-aldol condensation of 2-acetylpyrrol (4) with aromatic aldehydes in the presence of silica-supported Preyssler heteropolyacids catalyst and water as a solvent at reflux conditions

Entry	Aldehyde	Time, min	^{a,b} Yield, %	Mp (°C)	
				Found	Reported
1c		100	78	136–138	–
2c		110	82	148–150	–
3c		94	88	121–123	–
4c		86	92	154–156	–
5c		135	69	167–168	–
6c		20	94, 94 ^c , 93 ^c , 91 ^c	60–80	–
7c		15	98	140–142	–
8c		15	95	192–194	–

^aIsolated yield; ^bProducts were characterized by comparison of their spectroscopic data (¹H-NMR and IR);

^cThe same catalyst was used for each of the four runs.

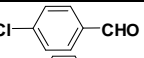
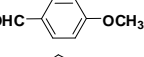
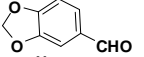
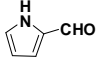
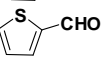
Table 4. Crossed-aldol condensation of 2-acetylthiophene (6) with aromatic aldehydes in the presence of silica-supported Preyssler heteropolyacids catalyst under organic solvent-free and reflux conditions

Entry	Aldehyde	Time, min	^{a,b} Yield, %	Mp (°C)	
				Found	Reported
1d		100	84	112–114	–
2d		76	81	118–120	–
3d		71	77	131–133	–
4d		30	94	144–146	–
5d		12	96	113–115	–
6d		21	93.5	119–121	–
7d		23	92, 90 ^c , 90 ^c , 89 ^c	117–119	–
8d		89	80.5	136–138	–

^aIsolated yield; ^bProducts were characterized by comparison of their spectroscopic data (¹H-NMR and IR);

^cThe same catalyst was used for each of the four runs.

Table 5. Crossed-aldol condensation of 2-acetylpyridine (8) with aromatic aldehydes in the presence of silica-supported Preyssler heteropolyacids catalyst under organic solvent-free and reflux conditions

Entry	Aldehyde	Time, min	^{a,b} Yield, %	Mp (°C)	
				Found	Reported
1e		30	88	103–105	–
2e		36	97, 96 ^c , 96 ^c , 95 ^c	120–122	–
3e		16	98, 97 ^c , 96 ^c , 96 ^c	148–150	–
4e		69	80.5	124–126	–
5e		51	83	76–78	–

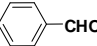
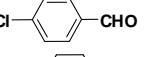
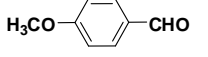
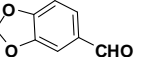
^aIsolated yield; ^bProducts were characterized by comparison of their spectroscopic data (¹H-NMR and IR);

^cThe same catalyst was used for each of the four runs.

It is seen from Tables 3, 4, 5, 6 that electron-donating substituents of aromatic aldehydes reduce the reaction period and increase the yield of these ketones.

We found that the reaction proceeds efficiently and with good yields in the crossed-aldol condensation of 2-acetylpyrrol (4) with aromatic aldehydes (Table 3, 1c-4c and 6c-8c) having electron-withdrawing and electron-donating substituents. In the crossed-aldol condensation of 2-acetylpyrrol (4) with 2-hydroxybenzaldehyde

Table 6. Crossed-aldol condensation of 4-methoxyacetophenone (10) with aromatic aldehydes in the presence of silica-supported Preyssler heteropolyacids catalyst under organic solvent-free and reflux conditions

Entry	Aldehyde	Time, min	^{a,b} Yield, %	Mp (°C)	
				Found	Reported
1f		88	70.5	119–121	–
2f		120	72, 71 ^c , 71 ^c , 69 ^c	120–122	–
3f		28	89.5	89–91	–
4f		26	92.5	24–126	–

^aIsolated yield; ^bProducts were characterized by comparison of their spectroscopic data (¹H-NMR and IR);

^cThe same catalyst was used for each of the four runs.

(Table 3, entry 5c) the reaction yields are lower, and probably an interaction between the ketone substituent and the hydroxyl group occurs (OH group in intermediate conditions of these reactions) (Table 3, entry 5c).

CONCLUSIONS

The present method is very suitable and efficient for crossed-aldol condensation of ketones, 2-acetylthiophene, 2-acetylpyrrole and 2-acetylpyridine with aromatic aldehydes. The synthesis of α,α' -bis(substituted benzylidene) cycloalkanones, (2*E*)-3-aryl-1-(thien-2'-yl)prop-2-en-1-ones, (2*E*)-3-aryl-1-(pyrrol-2'-yl)prop-2-en-1-ones and (2*E*)-3-aryl-1-(pyrid-2'-yl) prop-2-en-1-ones takes place with high yields in the presence of a reusable and environmentally benign catalyst. Simple work-up procedure, including washing the mixture followed by evaporation of the solvent, is another advantage of this method. $H_{14}[NaP_5W_{30}O_{110}]$, Preyssler type HPAs catalyst, is eco-friendly, inexpensive and efficient. High yields, relatively short reaction times, simplicity of operation and easy work-up procedure are some advantages of this protocol. $H_{14}[NaP_5W_{30}O_{110}]$ offers the advantages of higher hydrolytic and thermal stability. The salient features of Preyssler's anion are availability, non-toxicity and reusability. We believe this methodology can find usage in organic synthesis.

Acknowledgements. The authors are thankful to Agricultural Researches & Services Center, Mashhad, Feyzabad, Iran, to Mashhad Islamic Azad University, to Chemistry Department, University of Oslo, Norway and to National Research Council of Canada for the support of this work. Special thanks are due to Professor. Dr. J. (Hans) W. Scheeren from the Organic Chemistry Department, Radboud University Nijmegen, The Netherlands.

REFERENCES

- C. H. Heathcock, *Comp. Org. Syn.*, Oxford: Pergamon, **1991**, pp. 133–179.
- T. Mukaiyama, *Org. React.*, **28**, 203 (1982).
- I. Paterson, *Chem. Ind.*, **12**, 390 (1988).
- D. N. Dhar, *Chemistry of chalcones and related compounds*, Wiley N. Y., **1981**.
- J. H. Wu, X. H. Wang, Y. H. Yi, K. H. Lee, *Bioorg. & Med. Chem. Lett.*, **13**, 1813 (2003).
- N. H. Nam, Y. Kim, Y. J. You, D. H. Hong, H. M. Kim, B. Z. Ahn, *Eur. J. Med. Chem.*, **38**, 179 (2003).
- G. Saydam, H. H. Aydin, F. Sahin, Kucukoglu, O. E. Erciyas, E. Terzioglu, F. Buyukkececi, S. B. Omay, *Leukemia Res.*, **27**, 57 (2003).
- X. Wu, P. Wilairat, M. L. Go, *Bioorg. & Med. Chem. Lett.*, **12**, 2299 (2002).
- J. N. Dominguez, J. E. Charris, G. Lobo, N. G. Dominguez, M. M. Moreno, F. Riggione, E. Sanchez, J. Olson, P. J. Rosenthal, *Eur. J. Med. Chem.*, **36**, 555 (2001).
- P. Tuchinada, V. Reutrakul, P. Claeson, U. Pongprayoon, T. Sematong, T. Santisuk, W. C. Taylor, *Phytochemistry.*, **59**, 169 (2002).
- F. Herencia, M. L. Ferrandiz, A. Ubeda, J. N. Dominguez, J. E. Charris, G. M. Lobo, M. J. Alcaraz, *Bioorg. & Med. Chem. Lett.*, **8**, 1169 (1998).
- Y. Xia, Z. Y. Yang, P. Xia, K. F. Bastow, Y. Nakanishi, K. H. Lee, *Bioorg. & Med. Chem. Lett.*, **10**, 699 (2000).
- S. Ducki, R. Forrest, J. A. Hadfield, A. Kendall, N. J. Lawrence, A. T. McGown, D. Rennison, *Bioorg. & Med. Chem. Lett.*, **8**, 1051 (1998).
- C. J. Li, *Chem. Rev.*, **93**, 2023 (1993).
- C. Reichardt, *Solvent and Solvent Effects in Organic Chemistry*, 2nd ed. VCH, 1988.
- R. Breslow, *Acc. Chem. Res.*, **24**, 159 (1991).
- M. Zheng, L. Wang, J. Shao, Q. Zhong, *Synth. Commun.*, **27**, 351 (1997).
- N. Iranpoor, F. Kazemi, *Tetrahedron.*, **54**, 9475 (1998).
- S. X. Wang, J. T. Li, L. J. Geng, *J. Chem. Res.*, (S), 370 (2003).
- M. B. Smith, J. March, *Advanced Organic Chemistry, Reactions, Mechanisms, and Structure*; John Wiley & Sons: New York, 2001, pp.1218-1224
- J. Deli, T. Lorand, D. Szabo, A. Foldesi, *Pharmazie.*, **39**, 539 (1984).
- B. A. Hathaway, *J. Chem. Educ.*, **64**, 367 (1987).
- T. Nakano, S. Irifune, S. Umamo, A. Inada, Y. Ishii, M. Ogawa, *J. Org. Chem.*, **52**, 2239 (1987).
- M. Misono, L. Ono, G. Koyano, A. Aoshima, *Pure Appl. Chem.*, **72**, 1305 (2000).
- M. T. Pope, A. Muller, *Polyoxometalates: from Platonic Solids to Anti-Retroviral Activity*; Kluwer Academic Publishers: Dordrecht, The Netherlands, 1994.
- M. M. Heravi, G. Rajabzadeh, F. F. Bamoharram, N. Seifi, *J. Mol. Catal. A: Chem.*, **256**, 238 (2006).
- M. M. Heravi, K. Bakhtiari, F. F. Bamoharram, *Catal. Commun.*, **7**, 499 (2006).
- M. M. Heravi, F. F. Bamoharram, G. Rajabzadeh, N. Seifi, M. Khatami, *J. Mol. Catal. A: Chem.*, **259**, 213 (2006).
- M. T. Pope, *Heteropoly and Isopoly Oxometalates*; Springer: Berlin, 1983.
- M. M. Heravi, K. Bakhtiari, F. F. Bamoharram, *Commun.*, **7**, 373 (2006).
- F. F. Bamoharram, M. M. Heravi, M. Roshani, A. Gharib, M. Jahangir, *J. Mol. Catal. A: Chem.*, **252**, 90 (2006).
- M. M. Heravi, R. Motamedi, N. Seifi, F. F. Bamoharram, *J. Mol. Catal. A: Chem.*, **249**, 1 (2006).
- F. F. Bamoharram, M. M. Heravi, M. Roshani, M. Akbarpour, *J. Mol. Catal. A: Chem.*, **255**, 193 (2006).
- T. Okuhara, N. Mizuno, M. Misono, *Advances in Catalysis.*, **41**, 113 (1996).

35. I. V. Kozhevnikov, *Russ. Chem. Rev.*, **56** (9) 811 (1987).
36. J. B. Moffat, *Metal–Oxygen Clusters: The Surface and Catalytic Properties of Heteropoly Oxometalates*, Kluwer, New York, **2001**
37. R. Hekmatshoar, S. Sajadi, M. M. Heravi, F. F. Bamoharram, *Molecules.*, **12**, 2223 (2007).
38. M. H. Alizadeh, S. P. Harmalker, Y. Jeannin, J. Martin-Frere, M. T. Pope, *J. Am. Chem. Soc.*, **107**, 2662 (1985).
39. W. Shanshan, Z. Weihong, W. Jum, R. Xiaoqian, *Catal. Lett.*, **123**, 276 (2008).
40. J. J. English, V. Lamberti, *J. Am. Chem. Soc.*, **74**, 1909 (1952).

КРЪСТОСАНА АЛДОЛНА КОНДЕНЗАЦИЯ НА КЕТОНИ С АРОМАТНИ И НЕ-АРОМАТНИ АЛДЕХИДИ С PREYSSLER‘ОВ ХЕТЕРОКИСЕЛИНЕН КАТАЛИЗАТОР ВЪРХУ СИЛИЦИЕВ ДИОКСИД КАТО НОСИТЕЛ

А. Гариб^{1,2}, М. Джахангир¹, М. Рошани¹, Й. В. Схеерен³

¹Департамент по химия, Ислямски университет „Азад“, Маишад, Иран

²Земеделски център за изследвания и услуги, Маишад, Иран

³Клъстер за молекулярна химия, Департамент по органична химия, Университет Радбуд, Наймехен, Нидерландия

Постъпила на 4 март, 2012 г.; коригирана на 17 аептември, 2012 г.

(Резюме)

Съобщава се за синтезите на α,β -ненаситени алдолни продукти чрез кръстосана алдолна кондензация в присъствие на катализатор от хетерополикиселини (HPAs) при условия на рефлукс и без използванена органични разтворители. Алдолната кондензация на 2-ацетилтиофен, 2-ацетилпирол и 2-ацетилпиридин с различни ароматни алдехида е извършвана във вода в присъствие на Preyssler‘ов катализатор (HPAs) при обикновена температура. Всички реакции протичат с отлични добиви на стереоселективни хет-арилпропанони във вода кат екологично съвместим разтворител.

Total phenolics, flavonoids and antioxidant activity of different apple cultivars

S.S. Mitić, B.T. Stojanović*, M.B. Stojković, M.N. Mitić, J.Lj. Pavlović

Faculty of Sciences and Mathematics, Department of Chemistry, University of Niš, Višegradska 33, P.O.Box 224, 18000 Niš, Serbia

Received April 24, 2012; Revised October 3, 2012

The concentration of polyphenolic compounds and the antioxidant activity in apples seem to differ with cultivar, maturity storage, environmental conditions and part of the fruit. In this work, the total phenolic and flavonoid content and the antioxidant activity were measured in the whole fruit from 15 apple cultivars cultivated in Serbia. Total phenolic content (TP) was assayed by Folin-Ciocalteu method, flavonoid (TF) by colorimetric method with $AlCl_3$. Total antioxidant activity (TAA) of selected apples was determined using 2,2-azinobis(3-ethylbenzothiazoline-6-sulfonic acid) radical cation (ABTS), 2,2-diphenyl-1-picrylhydrazyl radical scavenging capacity (DPPH), ferric ion reducing power (FRP) and ferric ion reducing antioxidant power (FRAP). Polyphenolic content for the whole apple was in the range of 72.80 – 217.37 mg GAE/100 g fresh weight. The apple extracts had different TAA in relation to the method applied, and the different TAA of apples can be ascribed to their TP and TF content. A ripping correlation between TP and TAA was observed using FRAP method.

Keywords: phenolics; flavonoids; antioxidant capacity; apple.

INTRODUCTION

There is strong evidence that free radicals are responsible for the damage of lipids, proteins and nucleic acids in cells [1] leading to several physiological and pathological abnormalities, such as inflammation, cardiovascular diseases and ageing. Recent studies indicate that frequent consumption of fruits is associated with lower risk of stroke and cancer [2,3]. This protective effect is related to the content of plant antioxidant microconstituents. Different fruits exhibit different antioxidant capacities according to their contents of polyphenols, vitamins C, E, carotenoids and flavonoids [4,5].

Apple consumption has been associated with reduced risk of degenerative diseases, such as cancer and cardiovascular diseases [6,7]. The association is often attributed to the polyphenolic antioxidants contained in apples which can protect the human body against oxidative stress by scavenging oxygen free radicals [8]. Apples also contain ascorbic acid but it can explain less than 0.4% of the antioxidant activity, indicating that other factors, such as phenolics, are the main contributors [9]. Many studies show that the concentration of phenolic compounds, such as flavanols and anthocyanins in apple differ with

cultivar, maturity stage, environmental conditions and part of the fruits [10].

Several characterization studies of different apple parts in cultivars grown in the United States [11], Italy [10], Poland [12], Brazil [8] and Czech Republic [13] have been carried out on the basis of their phenolic profiles. However, little attention has been given to apple cultivars grown in Serbia. Therefore, the objective of this study was to determine the total phenolic content, the flavonoid content and the antioxidant capacity in the whole fruit from 15 apple cultivars grown in Serbia.

EXPERIMENTAL PROCEDURES

MATERIALS

Standards and reagents

All chemicals used were analytical reagent grade from well-reputed companies. Trolox (6-hydroxy-2,5,7,8-tetramethylchroman-2-carboxylic acid), iron(II) sulphate, 2,4,6-tri(2-pyridyl)-s-triazine (TPTZ), 2,2'-azinobis(3-ethylbenzothiazoline-6-sulfonic acid) (ABTS), 2,2'-diphenyl-1-picrylhydrazyl (DPPH), Folin-Ciocalteu's reagent, gallic acid, catechin were obtained from Fluka (UK).

Raw materials

Fifteen apple cultivars: Jonathan, Gloster, Melrose, Red Delicious, Golden Delicious, Granny Smith, Sharunka, Gala, Jonagold, Idared, Braeburn, Mutsu, Chadel, Kozara and Red Chief were picked

* To whom all correspondence should be sent:
E-mail: : brankastojanovic81@gmail.com

at commercial maturity during the 2010 harvest season in southern Serbia, and stored at -20°C . Prior to analysis apple was thawed at room temperature, pitted and mixed in a house blender.

Extraction of Phenolics

The phenolics were extracted by using an ultrasound-assisted method [14]. Briefly, phenolics were extracted from 20 g sample using 100 ml of methanol. The mixture was sonicated for 20 min with a continual stream of nitrogen gas purging to prevent possible degeneration of phenolics, filtered through Whatman No. 2 filter paper using chilled Buchner funnel, and rinsed with 50 ml of 100% methanol. Extraction of the residue was repeated under the same conditions. The two filtrates were combined and transferred into 1 l evaporating flask with additional 50 ml of 80% aqueous methanol. The solvent was evaporated in a rotary evaporator at 40°C . The remaining phenolic concentrate was first dissolved in 50 ml of 100% methanol and was diluted to final volume of 100 ml with methanol.

Total Phenolic Content (TP)

Total phenolic content (TP) of the apple extracts was determined using Folin-Ciocalteu (FC) assay described by Singleton and Rossi [15]. Apple extracts (0.15 ml) were mixed with 0.5 ml of FC reagent. After standing for 5 min at room temperature 2.0 ml of (20% w/v) sodium carbonate solution were added and deionized water was added to a final volume of 10.0 ml. The solutions were mixed and allowed to stand for 1 h at room temperature. Then, the absorbance was measured at 760 nm, using a UV-visible spectrophotometer (Agilent 8453). A calibration curve was prepared, using a standard solution of gallic acid (20, 40, 60, 80 and 100 mg/l, $r=0.99978$). Results were expressed on fresh weight basis (fw) as mg gallic acid equivalents per 100g of sample.

Total Flavonoid Content (TF)

The total flavonoid content of apple methanol extracts was determined by a colorimetric method [16]. A suitable volume of sample was mixed with 2 ml of distilled water and subsequently with 0.3 ml of a NaNO_2 solution (5%). After 5 min, 3 ml of AlCl_3 solution (1%) was added, and the solution was allowed to stand for 5 min at room temperature. Then, 2 ml of NaOH solution (1M) was added to the mixture and water was added to a final volume of 10 ml. The mixture was thoroughly mixed and absorbance was immediately measured at 510 nm *versus* water blank. Results were

expressed on a fresh weight basis as mg catechin equivalents (CE) per 100 g of sample.

ABTS Radical-Scavenging Capacity Assay

The trolox equivalent capacity test developed by Lee et al. [15] was used in this study. In brief, the ABTS radical cation ($\text{ABTS}^{\cdot+}$) solution was prepared by the reaction of 7 mM ABTS and 2.45 mM potassium persulphate, after incubation at 23°C in the dark for 12–16 h. The $\text{ABTS}^{\cdot+}$ solution was then diluted with 80% ethanol to obtain an absorbance of 0.700 ± 0.020 at 734 nm. Solution of $\text{ABTS}^{\cdot+}$ (3.9 ml; absorbance of 0.700 ± 0.005) was added to 0.1 ml of the test sample and mixed thoroughly. The reaction mixture was allowed to stand at 23°C for 6 min and the absorbance was immediately measured at 734 nm. The samples were diluted with 80% ethanol so as to give 20–80% reduction of the blank absorbance with 0.1 ml of sample. Reagent blank reading was taken using 0.1 ml of 80% ethanol. Standard curve was obtained by using trolox standard solution at various concentrations (ranging from 2 to 10 μM , $r=0.9985$) in 80% ethanol. Total antioxidant activity of apples was expressed as mmol trolox equivalents (TE) per 100 g fresh weight [17]. The experiment was carried out in triplicate.

DPPH Free Radical-Scavenging Assay

The antioxidant capacity of the apple extracts was also studied through evaluation of the free radical-scavenging effect on the 1,1-diphenyl-2-picrylhydrazyl (DPPH) radical. The determination was based on the method proposed by Miliauskas *et al.* [15] and De Arcos *et al.* [18]. An aliquot (0.1 ml) of apple extract was mixed with 2.5 ml of 100 mM DPPH methanol solution. The mixture was thoroughly vortex-mixed and kept in the dark for 30 min and the decrease in absorbance was measured at 515 nm. A blank sample containing the same amount of methanol and DPPH solution was prepared daily and its absorbance was measured. A calibration curve was prepared using a standard solution of trolox (ranging from 2 to 10 μM). The results were expressed on a fresh weight basis as mmol trolox equivalents (TE)/100g of sample. The experiment was carried out in triplicate.

Ferric-Reducing Antioxidant Power Assay (FRAP)

The FRAP assay was carried out according to the procedure of Benzil and Strain [19]. Briefly, a 0.1 ml apple extract was mixed with 3.0 ml of FRAP reagent. Then, the reaction mixture was incubated at 37°C for 4 min. After that, the

absorbance was measured at 593 nm against a blank that was prepared using deionized water and incubated for 1h instead of 4 min. FRAP reagent should be pre-warmed at 37°C and should always be freshly prepared by mixing 2.5 ml of a 10 mM 2,4,6-tris (1-pyridyl)-5-triazine (TPTZ) solution in 40 mM HCl with 2.5 ml of 20 mM FeCl₃·6H₂O and 25 ml of 0.3 M acetate buffer, pH 3.6. A calibration curve was prepared, using an aqueous solution of ferrous sulphate FeSO₄·7H₂O (200, 400, 600, 800 and 1000 µM, $r=0,9972$). FRAP values were expressed on a fresh weight basis as mmol of ferrous equivalent Fe (II) per 100 g of sample.

Ferric-Reducing Power assay (FRP)

For assessing ferric-reducing power (FRP), the assay described by Chan *et al.* [20] was adapted. Different dilutions of extracts (1 ml) were added to 2.5 mL of phosphate buffer (0.2 M, pH 6.6) and 2.5 mL of potassium ferricyanide (1%, w/v). The mixture was incubated at 50°C for 20 min. After trichloroacetic acid solution (2.5 ml, 10%, w/v) was added, the mixture was separated into aliquots of 2.5 ml and diluted with 2.5 ml of water. To each diluted aliquot, 0.5 ml of ferric chloride solution (0.1%, w/v) was added. After 30 min, absorbance was measured at 700 nm. FRP of extracts was expressed as mg gallic acid equivalent (GAE) per 100 g of fresh fruit. The calibration equation for gallic acid was $y = 0.31143 x + 0.01061$ ($r = 0.99912$), where y is the absorbance and x is the gallic acid concentration in µg/ml.

Statistical analysis

The data were reported as mean \pm standard deviation (SD) for triplicate determinations. The significance of inter-group differences was determined by the analysis of variance (ANOVA). A value of $p < 0.05$ was considered statistically significant.

RESULTS AND DISCUSSION

Phenolic compounds are generally considered as a very important antioxidant source in fruits. Therefore, TP of 15 apple cultivars were examined by the Folin-Ciocalteu assay and the results are presented in Table 1. The 15 apple cultivar samples investigated exhibited considerable differences in their TP values, varying from 72.80 mg GAE/100g fw for Braeburn apple to 217.37 mg GAE/100 g fw for Kozara apple. Chadel, Idared, Red Chief and Granny Smith apples also had relatively higher TP (> 190 mg GAE/100g fw). The results were lower than the data of Imeh and Khochar [21] (300 – 535

mg GAE/100g fw), but higher than those of Valavanidis *et al.* [22] and Lachman *et al.* [13] (80–196 mg GAE/100g fw, 76–134 mg GAE/100 fw, respectively). This differences may be due to multiple reasons including genetic factors, different environmental conditions, storage of maturity, cultivar or varieties differences, growth stage, soil fertilization and part of the fruit used, amongst other factors that effect quantitative variation in these phytochemicals [23,24]. The total flavonoids (TF) content of these apples was determined. Granny Smith apple had the highest TF content (111.82 mg CE/100 g fw), followed by Golden Delicious apple (106.99 mg CE/100 g fw). The results are presented in Table 1. Correlation analysis was performed on the polyphenolic content analysis methods for the 15 apple cultivars. The correlation between TP and TF assays is at the 0.05 level. These results indicate that the flavonoids are an important phenolic group in apple fruit. Correlation coefficient is 0.790.

There are huge varieties of antioxidants contained in fruits. Therefore, measuring the antioxidant capacity of each compound separately becomes very difficult. Several methods have been developed to estimate the antioxidant capacity of different plant materials [5,25]. Usually these methods measure the ability of antioxidants, in a particular plant material, to scavenge specific radicals, by inhibiting lipid peroxidation or by chelating metal ions.

Depending upon the reaction involved, the antioxidant capacity assays can be based on hydrogen atom transfer reactions and assays based on electron transfer. Hydrogen atom transfer reaction based assays are methods in which antioxidant and substrate compete for thermally generated peroxy radicals through the decomposition of azo compounds. Those are: oxygen radical absorbance capacity (ORAC), total radical trapping antioxidant power (TRAP), β -carotene bleaching assay, inhibition of linolenic acid oxidation, and inhibition of LDL oxidation. Electron transfer based assays measure the capacity of an antioxidant in the reduction of an oxidant which changes color when reduced. Described methods include 2,2'-azino-bis(3-ethylbenzothiazoline-6-sulfonic acid) radical cation assay (ABTS), ferric ion reducing antioxidant power assay (FRAP), 2,2-diphenyl-1-picrylhydrazyl radical scavenging capacity assay (DPPH) [24,26].

In this study the total antioxidant activity of 15 apple cultivar extracts was determined using DPPH radical scavenging activity, ABTS radical cation

Table 1. Total phenol (TP) and total flavonoid (TF) contents of apple samples

Apple Cultivar	TP*	TF*	TF/TP
	mg GAE/100 g f.w.	mg CE/100 g f.w.	
1. Jonathan	134 ± 2 ^h	74.7 ± 0.9 ^d	0.55
2. Gloster	86 ± 2 ^j	53.1 ± 0.9 ^g	0.61
3. Melrose	85 ± 2 ^j	61 ± 2 ^f	0.72
4. Red Deliciose	87 ± 2 ^j	55.8 ± 0.9 ^{gf}	0.64
5. Golden Deliciose	180 ± 1 ^f	107 ± 2 ^a	0.59
6. Greeny Smith	197 ± 1 ^e	112 ± 3 ^a	0.57
7. Sharunka	161 ± 2 ^g	70 ± 5 ^{de}	0.43
8. Gala	94 ± 2 ⁱ	42.0 ± 0.5 ^h	0.45
9. Jonagold	130 ± 1 ^h	59.5 ± 0.7 ^{gf}	0.46
10. Idared	202 ± 2 ^c	67.1 ± 0.8 ^{ef}	0.33
11. Braeburn	73 ± 2 ^k	37.2 ± 0.4 ^h	0.51
12. Mutsu	134 ± 2 ^h	54 ± 2 ^{gf}	0.40
13. Chadel	212 ± 2 ^b	82.57 ± 0.08 ^c	0.39
14. Kozara	217 ± 2 ^a	96 ± 4 ^b	0.44
15. Red Chief	200 ± 2 ^d	76 ± 2 ^{dec}	0.38

*) The data are reported as mean ± standard deviation (n=3); Bars with no letters in common are significantly different (p<0.05) in the same column.

Table 2. DPPH radical scavenging activity. ABTS radical cation activity. ferric-ion reducing antioxidant parameter-FRAP and ferric-reducing power - FRP of apple samples

Apple Cultivar	ABTS*	DPPH*	FRAP*	FRP*
	mmol TE/100g f.w.	mmol TE/100g f.w.	mmol Fe/100g f.w.	mg GAE/100g f.w.
1. Jonathan	0.371 ± 0.009 ^d	0.259 ± 0.002 ^a	0.663 ± 0.017 ^e	40.440 ± 1.214 ^g
2. Gloster	0.245 ± 0.004 ^f	0.231 ± 0.003 ^b	0.460 ± 0.011 ^{gf}	28.670 ± 0.861 ⁱ
3. Melrose	0.250 ± 0.003 ^f	0.236 ± 0.003 ^b	0.432 ± 0.005 ^{gi}	26.590 ± 0.915 ⁱ
4. Red Deliciose	0.257 ± 0.003 ^f	0.240 ± 0.002 ^b	0.486 ± 0.019 ^{gh}	32.910 ± 0.794 ^h
5. Golden Deliciose	0.501 ± 0.009 ^b	0.266 ± 0.001 ^a	0.987 ± 0.019 ^a	53.610 ± 0.736 ^e
6. Greeny Smith	0.504 ± 0.007 ^{ba}	0.256 ± 0.005 ^a	1.003 ± 0.021 ^a	56.820 ± 0.828 ^e
7. Sharunka	0.314 ± 0.006 ^e	0.257 ± 0.004 ^a	0.670 ± 0.016 ^{ed}	75.307 ± 0.609 ^c
8. Gala	0.186 ± 0.003 ^g	0.255 ± 0.004 ^a	0.387 ± 0.007 ⁱ	45.296 ± 0.823 ^f
9. Jonagold	0.367 ± 0.008 ^d	0.253 ± 0.006 ^a	0.773 ± 0.015 ^c	68.782 ± 0.533 ^d
10. Idared	0.382 ± 0.009 ^d	0.256 ± 0.004 ^a	0.846 ± 0.022 ^b	74.764 ± 0.852 ^{bc}
11. Braeburn	0.181 ± 0.003 ^g	0.227 ± 0.004 ^b	0.319 ± 0.009 ^h	42.090 ± 0.745 ^{gf}
12. Mutsu	0.304 ± 0.006 ^e	0.248 ± 0.006 ^a	0.505 ± 0.014 ^f	43.008 ± 0.595 ^{gf}
13. Chadel	0.421 ± 0.008 ^c	0.261 ± 0.004 ^a	1.001 ± 0.012 ^a	77.100 ± 0.657 ^{bc}
14. Kozara	0.536 ± 0.013 ^a	0.276 ± 0.005 ^a	1.003 ± 0.017 ^a	85.510 ± 0.729 ^a
15. Red Chief	0.384 ± 0.011 ^d	0.250 ± 0.007 ^a	0.729 ± 0.015 ^d	76.246 ± 0.670 ^{bc}

*) The data are reported as mean ± standard deviation (n=3); Bars with no letters in common are significantly different (p<0.05) in the same column.

scavenging activity, FRAP ferric ion reducing antioxidant power and FRP ferric reducing power.

The DPPH radical scavenging activities of 15 apple cultivar extracts are shown in Table 2. All extract samples selected exhibited strong DPPH radical scavenging activities at the test concentration. The values of DPPH radical

scavenging activities ranged from 0.227 to 0.276 mmol TE/100g fw.

Different apple cultivars were also measured and compared for the free radical scavenging activity against the ABTS radical cation. Results showed that all apple samples used in this study had significant ABTS radical cation activities (Table 2). The values of ABTS radical cation scavenging

Table 3. Correlations among apple extracts activity evaluation indices and total phenolic content.

	DPPH	ABTS	FRAP	FRP	TP
DPPH	1	0.801	0.806	0.706	0.798
ABTS		1	0.917	0.640	0.880
FRAP			1	0.730	0.914
FRP				1	0.813
TP					1

activities of the 15 apple samples were in the range 0.181 – 0.536 mmol TE/100 g fw. The highest and lower ABTS radical cation scavenging activities among the apple samples studied were found in Kozara and Braeburn apples, respectively. It is important to mention that the TAA values of the same apple obtained by the ABTS assay were consistently higher than those obtained by the DPPH assay. The same phenomena were found in recent studies on antioxidant activity of selected fruits by Dragovic-Uzelac *et al.* [24], and that of red fruit juices by Bermudez-Soto and Tomas-Barberan [27]. Different reaction kinetics between phenol and ABTS radical cation or DPPH radical over a similar range of concentrations might lead to the different results from two methods [28]. Actually, the ABTS radical cation scavenging activity also reflects hydrogen-donating ability.

The FRAP assay involves a single electron reduction of the Fe(TPTZ)₂(III) complex (pale yellow) to the Fe(RPTZ)₂(II) complex (blue) by single electron donor species/antioxidants. The FRAP assay is one of the most simple, rapid, inexpensive tests and is very useful for routine analysis. FRAP assay is developed as a direct test of the total antioxidant power of a sample. The antioxidant activity of apple extracts using FRAP assay is shown in Table 2. The ferric reducing power of apple extracts tested in this investigation ranged from 0.319 mmol Fe²⁺/100 g fw in the case of Braeburn apple to 1.003 mmol Fe²⁺/100 g fw in the case of Kozara and Granny Smith apples.

As shown in Table 2, there are significant variations in reducing power (FRP) for the different apple samples. The reducing power of 15 apple cultivars tested in this investigation ranged from 26.59 mg GAE/100 g fw (Melrose apple) to 85.51 mg GAE/100 g fw (Kozara apple). The results were partly different from those obtained in the assays mentioned above, and this might be due to the different reaction mechanisms of the antioxidant evaluation assays. Reducing power is generally associated with antioxidant activity and may serve as a significant measure of the antioxidant activity.

Compounds with reducing power indicate that they could reduce oxidized intermediates of lipid peroxidation processes and act as primary or secondary antioxidants.

Correlations among apple extract activity assays and total phenolic contents

The Pearson product moment correlation coefficients calculated from four different apple extracts antioxidant activity assays and total phenolic contents are shown in Table 3. Significant positive correlations between the four antioxidant activity assays for apple extracts were observed (ranging from 0.640 to 0.917, $p < 0.05$), especially between FRAP ferric ion reducing antioxidant power and ABTS radical cation scavenging activity suggesting that overall antioxidant activity evaluation results for 15 apple samples using four assays were consistent although these assays involved different reaction mechanisms. The measured antioxidant activity of an apple sample depends on the methodology and on the free radical generator or oxidant used in the measurement. As for correlations between antioxidant activity assays and TP, significant ($p < 0.05$) positive correlations with FRAP ferric ion reducing antioxidant power, ABTS radical cation scavenging activity and relatively good positive correlation with reducing power and DPPH reducing scavenging activity were obtained.

Acknowledgements: *This work was supported by the Serbian Ministry of Education and Science Protection (grant numbers 172047 and TR31060).*

REFERENCES

1. L.P. Leong, G. Shui, *Food Chem.*, **76**, 69 (2002).
2. B.T. Kawasaki, E. M. Hurt, T. Mistree, W.L. Farrar, *Mol. Interv.*, **8**, 174 (2008).
3. M.E. Wright, Y. Park, A.F. Subar, N.D. Freedman, D. Albanes, A. Hollenbeck, M.F. Leitzmann, A. Schatzkin, Intakes of fruit, vegetables, and specific botanical groups in relation to lung cancer risk in the NIH-AARP diet and health study, *Am J Epidemiol* (available online) (2008).
4. F. Saura-Calixto, I. Goni, *Food Chem.*, **94**, 442 (2006).
5. M. Alothman, R. Bhat, A. A. Karim, *Food Chem.*, **115**, 785 (2009).
6. P.F. Di Pietro, N.I. Medeiros, F.G.K. Vieira, M.A. Fausto, A. Bello-Klein, *Nutr Hosp*, **22**, 565 (2007).
7. S. Auclair, M. Silberberg, E. Gueux, C. Morand, A. Mazur, D. Milenkovic, A. Scalbert, *J. Agric. Food Chem.*, **56**, 5558 (2008).
8. F.G.K. Vieira, S. Borges Gda, C. Copetti, L.V. Gonzaga, C. Nunes Eda, R. Fett, *Arch. Latinoam. Nutr.*, **59**, 101 (2009).

9. P. D. Drogoudi, Z. Michailidis, G. Pantelidis, *Sci. Hortic.*, **115**, 149 (2008).
10. B. D'Abrosca, S. Pacifico, G. Cefarelli, C. Mastellone, A. Fiorentino, *Food. Chem.*, **104**, 1333 (2007).
11. K. Wolfe, X. Wu, R. H. Liu, *J. Agric. Food. Chem.*, **51**, 609 (2003).
12. B. Lata, K. Tomala, *J. Agric. Food Chem.*, **55**, 10795 (2007).
13. J. Lachman, M. Šulc, J. Sus, O. Pavlikova, *Hort. Sci.(Prague)*, **33**, 95 (2006).
14. K. W. Lee, Y. J. Kim, D. O. Kim, C. Y. Lee, *J. Agric. Food Chem.*, **51**, 6516 (2003).
21. U. Imeh, S. Khochar, *J. Agric. Food Chem.*, **50**, 6301 (2002).
22. A. Valavanidis, T. Vlachogianni, A. Psomas, A. Zavoioli, V. Siatis, *Int. J. Food Sci. Tech.*, **44**, 1167 (2009).
23. M.G.L. Hertog, P.C. H. Hollman, M.B. Katan, *J. Agric. Food Chem.*, **41**, 2379 (1992).
24. V. Dragović-Uzelac, D. Bursać-Kovačević, B. Levaj, S. Pedesić, I. Radojčić, A. Biško, *Agriculturae Conspectus Scientificus*, **72**, 279 (2007).
15. V.L. Singleton, J.A. Rossi, *Am. J. Enol. Vitic.*, **16**, 144 (1965).
16. G. Miliuskas, P.R. Venskutonis, T.A. Van Beek, *Food. Chem.*, **85**, 231 (2004).
17. S. Surveswaran, Y. Z. Cai, H. Corke, M. Sun, *Food. Chem.*, **102**, 938 (2007).
18. B. De Arcos, S. Sgroppo, L. Plaza, M. P. Cano, *J. Sci. Food Agric.*, **82**, 790 (2002).
19. F.F. Benzil, J.J. Strain, *Methods Enzymol.*, **299**, 15 (1999).
20. E.W.C. Chan, Y.Y. Lim, K.L. Chong, J.B.L. Tan, S.K. Wong, *J. Food Comp. Analysis*, **23**, 185 (2010).
25. C. Guo, J. Yang, J. Wei, Y. Li, J. Xu, Y. Jiang, *Nutr. Res.*, **23**, 1719 (2003).
26. D. Haung, B. Ou, R. L. Prior, *J. Agric. Food Chem.*, **53**, 1841 (2005).
27. M. Bermudez-Soto, F.A. Tomas-Barberan, *Eur. Food Res. Technol.*, **219**, 133 (2004).
28. M. Campos, E.A. Lissi, *Int. J. Chem. Kinet.*, **29**, 219 (1996).

ОБЩИ ФЕНОЛИ, ФЛАВОНОИДИ И АНТИОКСИДАНТНА АКТИВНОСТ НА РАЗЛИЧНИ ЯБЪЛКОВИ СОРТОВЕ

С.С. Митич, Б.Т. Стоянович, М.Н. Стойкович, М.Н. Митич, Ђ.Л. Павлович

Департамент по химия, Факултет за науки и математика, Универзитет в Ниш, ул. Вишеградска 33, П.К. 224, 18000 Ниш, Србија

Постъпила на 24 април, 2012 г.; коригирана на 3 октомври, 2012 г.

(Резюме)

Изглежда, че концентрацията на полифенолните съединения и антиоксидантната активност на ябълките зависи от сорта, зреенето при съхранение, условията на околната среда и отчасти от плода. В настоящата работа са определени общото съдържание на феноли, флавоноиди и антиоксидантната активност на цели плодове от 15 сорта ябълки, отглеждани в Србија. Общото съдържание на феноли (TP) е анализирано по метода на Folin-Ciocalteu; общите флавоноиди (TF)- колориметрично с AlCl₃. Общата антиоксидантна активност (ТАА) на избраните ябълки бе определяна с 2,2-азино-бис(3-етилбензотиазолин-6-сулфонова киселина) като радикал-катион (ABTS), 2,2-дифенил-1-пикрилхидразил радикал-премахващ капацитету (DPPH), редуционната способност спрямо ферийони (FRP) and антиоксидантна способност спрямо ферийони (FRAP). Съдържанието на полифеноли за целите плодове бе в границите на 72.80 – 217.37 mg GAE/100 g fw. Ябълковите екстракти имат различна ТАА във връзка с прилагания метод, а тези разлики в ТАА може да се отдадат на съдържанието на TP и TF. С помощта на метода FRAP е намерена между зреенето и съдържанието на TP и ТАА.

Design and synthesis of two sulfathiazole derivatives using a three-component system

L. Figueroa-Valverde^{1*}, F. Díaz-Cedillo², E. García-Cervera¹, E. Pool Gómez¹, M. Rosas-Nexticapa³, M. López-Ramos¹

¹Laboratory of Pharmaco-Chemistry at the Faculty of Chemical Biological Sciences of the University Autonomous of Campeche, Av. Agustín Melgar s/n, Col Buenavista C.P.24039 Campeche Cam., México.

²Escuela Nacional de Ciencias Biológicas del Instituto Politécnico Nacional. Prol. Carpio y Plan de Ayala s/n Col. Santo Tomas, México, D.F. C.P. 11340.

³Facultad de Nutrición, Universidad Veracruzana, Médicos y Odontólogos s/n C.P. 91010, Unidad del Bosque Xalapa Veracruz, México

Received June 2, 2012; Revised November 5, 2012

Two sulfonamide derivatives were synthesized using a three-component system; in the first stage the compound 4-[[2-hydroxy-naphthalen-1-yl]-phenyl-methyl]-amino}-N-thiazol-2-yl-benzenesulfonamide (**4**) was obtained by the reaction of β -naphthol, benzaldehyde and sulfathiazole (**3**) in ethanol. The second stage was achieved by the reaction of **3** with 1-hexyne and benzaldehyde using cupric chloride as a catalyst to form 4(hex-1-ynyl-phenyl-amino)-N-thiazol-2-yl-benzenesulfonamide (**6**). The structure of the compounds obtained was confirmed by elemental analysis, spectroscopy and spectrometry data. The proposed method offers some advantages such as good yields, simple procedure, low cost, and ease of workup.

INTRODUCTION

Since many years sulfonamide derivatives have been synthesized; for example, a sulfonamide derivative was prepared by the reaction of sulfonic acid salts with amines and alcohols using the reagent triphenylphosphine ditriflate [1]. There are other reports on the synthesis of 1-[4-(N-pyrimidin-2-yl-sulfamoyl)phenyl]-1,11-dihydro-11-oxo-4-methylpyrimido[4',5':4,5]selenolo[2,3-b]quinolone by the reaction of an iminoether with 4-amino-N-pyrimidin-2-ylbenzenesulfonamide under reflux in glacial acetic acid [2]. Other studies described the obtaining of 4-(1,2,3,4-tetrahydro-4,4,6-trimethyl-2-thioxo-1-pyrimidinyl)-N-(2-thiazolyl)-benzene sulfonamide using sulfathiazole and 4-methyl-4-isothiocyanato-2-pentanone [3]. The synthesis of N-(2-anilinopyridin-3-yl)-4-methylbenzenesulfonamide by the reaction of N²-phenylpyridine-2,3-diamine with 4-methylbenzenesulfonyl chloride [4] is also reported.

The sulfamethoxazolato anion is obtained by the reaction of sulfamethoxazole with Ph₃PAuCl and AgCl in methanol/triethylamine [5]. 4-(1,2,3,4-Tetrahydro-4,4,6-trimethyl-2-thioxo-1-pyrimidinyl)-N-(2-thiazolyl)-benzenesulfonamide is synthe-

tized by the reaction of sulfathiazole with 4-isothiocyanato-2-pentanone under reflux [6]. The procedures for synthesis of sulfonamide derivatives described in the literature require, however, expensive reagents and special conditions. Therefore, in this study two new sulfonamide derivatives were synthesized using a three-component system.

MATERIAL AND METHODS

General methods

The compounds used in this study were purchased from Sigma-Aldrich Co., Ltd. The melting points of the different compounds were determined on an Electrothermal (900 model) apparatus. Infrared (IR) spectra were recorded on a Perkin Elmer Lambda 40 spectrometer using KBr pellets. ¹H and ¹³C NMR spectra were recorded on a Varian VXR-300/5 FT NMR spectrometer at 300 and 75.4 MHz in CDCl₃ using TMS as internal standard. EIMS spectra were obtained on a Finnigan Trace GCPolaris Q spectrometer. Elemental analysis data were acquired from a Perkin Elmer Ser. II CHNS/O 2400 elemental analyzer.

Synthesis of 4-[[2-hydroxy-naphthalen-1-yl]-phenyl-methyl]-amino}-N-thiazol-2-yl-

* To whom all correspondence should be sent:
E-mail: : lauro_1999@yahoo.com

benzenesulfonamide (4)

A solution of β -naphthol (100 mg, 0.69 mmol), sulfathiazole (192 mg, 0.69 mmol) and benzaldehyde (70 μ l, 71 mmol) in 10 mL of ethanol was stirred for 72 h at room temperature. The reaction mixture was evaporated to a smaller volume. Then, the mixture was diluted with water and extracted with chloroform. The organic phase was evaporated to dryness under reduced pressure, the residue was purified by crystallization from methanol:water (3:1) yielding 60 % of product, m.p. 118-120 °C; IR (V_{\max} , cm^{-1}): 3530 (OH), 3450 (C-NH-Ar) and 1325 (S=O); ^1H NMR (300 MHz, CDCl_3) δ_{H} : 5.45 (s, 1H), 6.50 (d, 2H, $J = 9.0$ Hz), 7.06 (broad, 3H), 7.08-7.12 (m, 2H), 7.16 (d, 1H, $J = 9.0$ Hz), 7.19(m, 1H), 7.21-7.23 (m, 2H), 7.46-7.52 (m, 2H), 7.57 (d, 1H, $J = 3.5$ Hz), 7.59 (m, 1H), 7.73 (m, 1H), 7.75 (d, 2H, $J = 9.0\text{Hz}$), 7.80 (m, 1H) ppm. ^{13}C NMR (75.4 Hz, CDCl_3) δ_{C} : 56.68 (C-17), 114.11 (C-20), 116.04(C-14, C-12), 116.50 (C-5), 119.70 (C-18), 120.89 (C-24), 123.80 (C-26), 127.02 (C-25) 127.10 (C-11, C-15), 127.36 (C-22), 127.80 (C-31), 128.50 (C-21), 129.68 (C-27), 129.90 (C-30, C-32), 130.66 (C-29, C-33), 132.90 (C-28), 135.42 (C-4), 137.65 (C-10), 137.70 (C-23), 153.70 (C-19), 154.22 (C-13), 168.02 (C-2) ppm. EI-MS m/z : 487.75 (M^+ , 12), 334.27, 169.21. Anal. Calcd for $\text{C}_{26}\text{H}_{21}\text{N}_3\text{O}_3\text{S}_2$: C, 64.04; H, 4.34; N, 8.62; O, 9.84; S, 13.15. Found: C, 64.02; H, 4.33.

Synthesis of 4-(hex-1-ynyl-phenyl-amino)-N-thiazol-2-yl-benzenesulfonamide (6)

A solution of 1-hexyne (80 μ l, 0.70 mmol), sulfathiazole (192 mg, 0.69 mmol) benzaldehyde (75 μ l, 0.70 mmol) and cupric chloride anhydrous (140 mg, 1.04 mmol) in 10 ml of ethanol was stirred for 72 h at room temperature. The reaction mixture was evaporated to a smaller volume. Then, the mixture was diluted with water and extracted with chloroform. The organic phase was evaporated to dryness under reduced pressure, the residue was purified by crystallization from methanol:water (3:1) yielding 45 % of product, m.p. 178-180 °C; IR (V_{\max} , cm^{-1}): 3310 (C \equiv C), 1320 (S=O) and 1170 (C-N); ^1H NMR (300 MHz, CDCl_3) δ_{H} : 0.91 (t, $J = 6.3$ Hz, 3H), 1.47 (m, 4H), 2.21 (t, $J = 6.8$ Hz, 2H), 6.67 (m, 2H), 6.78 (m, 1H), 7.17 (d, $J = 3.4$ Hz, 1H), 7.20 (m, 2H), 7.33 (m, 2H), 7.50 (d, $J = 3.4$ Hz, 1H), 7.88 (m, 2H), 8.98 (broad, 1H) ^{13}C NMR (75.4 Hz, CDCl_3) δ_{C} : 13.60 (C-28), 16.95 (C-25), 21.98 (C-27), 32.03 (C-26), 61.08 (C-24), 75.02 (C-23), 113.10 (C-18, C-22), 116.26 (C-12, C-14), 116.57 (C-5), 119.60 (C-20), 128.37 (C-15),

128.50 (C-21), 135.32 (C-4), 138.80 (C-10), 147.02(C-17), 152.34 (C-13), 166.98 (C-2). EI-MS m/z (M^+ 12): 411.15 (M^+ , 12), 218.08(100), 174.24(60), 103.07 (65), 76.15 (78). Anal. Calcd for $\text{C}_{21}\text{H}_{21}\text{N}_3\text{O}_2\text{S}_2$: C, 61.29; H, 5.14; N, 10.21; O, 7.78, S, 15.58. Found: C, 61.03; H, 5.11.

RESULTS AND DISCUSSION

In many procedures a three-component system is used for the synthesis of several compounds. The most widely practiced method employs boric acid [7], silica sulfuric acid [8], poly(4-vinylpyridine-co-divinylbenzene)-Cu(II) complex [9], H_2SO_4 [10], silica triflate [11] and phosphorus pentoxide [12]. Nevertheless, despite their wide scope, the former protocols suffer from several drawbacks, *e.g.*, limited stability or dangerous preparation of some reagents. In this study we report a straightforward route for the synthesis of **4** using a modification of a method reported by Dabiri and coworkers [13]. According to this procedure, **4** is obtained by reaction of β -naphthol, benzaldehyde and sulfathiazole in ethanol (Figure 1). The ^1H NMR spectrum of **4** shows

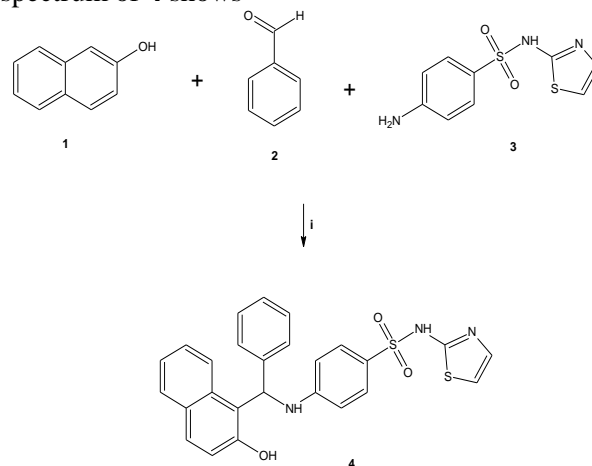


Fig. 1. Synthesis of 4-[(2-hydroxy-naphthalen-1-yl)-phenyl-methyl]-amino-N-thiazol-2-yl-benzenesulfonamide (**4**). Reaction between β -naphthol (**1**), benzaldehyde (**2**) and sulfathiazole (**3**) to form **4** using boric acid as catalyst. i = ethanol/rt.

signals at 5.40 ppm for methylene bound to both phenyl and amine groups; at 6.50 and 7.75 ppm for phenyl group bound to amine group; at 7.08–7.12 and 7.21-7.23 ppm for protons involved in the phenyl group which is bound to the methylene group; at 7.16 ppm for hydrogen of thiazole ring; at 7.19, 7.46-7.73 and 7.80 ppm for naphthol fragment. Finally, another signal at 7.06 ppm for both amino and hydroxyl groups was found. The ^{13}C NMR spectrum contains peaks at chemical shifts of 56.68 ppm for the carbon of the methylene bound to both

phenyl and amine groups. Other signals at 116.50, 135.42 and 168.02 ppm for carbons involved in the thiazole ring; at 127.80 and 129.90–132.90 ppm for phenyl group bound to methylene group; at 114.10, 119.70–127.02, 127.36, 128.50–129.68 and 137.70–153.70 ppm for naphtol fragment; 116.04, 127.10, 137.65 and 154.22 ppm for phenyl group bound to amine group were found. Finally, the presence of **4** was confirmed by the mass spectrum which showed a molecular ion at m/z 487.75.

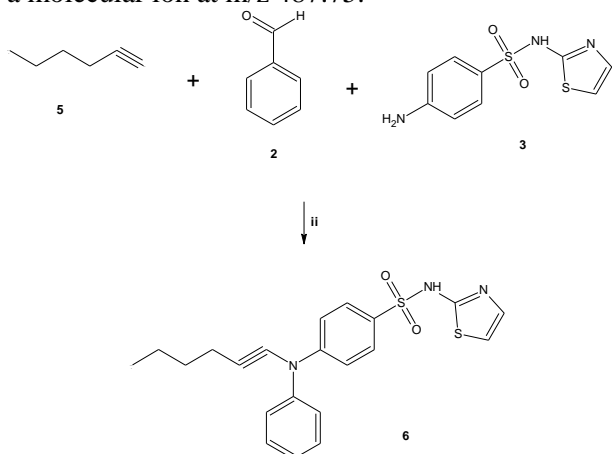


Fig. 2. Synthesis of 4-(hex-1-ynyl-phenyl-amino)-*N*-thiazol-2-yl-benzenesulfonamide (**6**). Reaction between 1-hexyne (**5**), benzaldehyde (**2**) and sulfathiazole (**3**) to form **6** using cupric chloride as catalyst. i = ethanol/rt.

In a second stage the synthesis of 4-(hex-1-ynyl-phenyl-amino)-*N*-thiazol-2-yl-benzenesulfonamide was achieved which has as chemical characteristic an alkyne group bound to amine group (Figure 2). It is important to mention that there are some reports which indicate the synthesis of several alkyne derivatives involving the use of a copper(I) reagent which has been found to be an efficient catalyst for an enantioselective one-pot three-component synthesis between aldehydes, amines and alkynes [14]. Other studies indicate that cupric chloride is a good catalyst for the synthesis of alkyne derivatives [15]. For this reason, in this study the compound **6** was obtained by the reaction of 1-hexyne, sulfathiazole and benzaldehyde using cupric chloride as a catalyst. The ^1H NMR spectrum of **6** shows signals at 0.91 ppm for methyl group; at 1.47–2.21 ppm for methylenes involved in alkyne fragment; at 6.60–7.20, 7.33 and 7.88 ppm for protons of phenyl groups; at 7.17 and 7.50 ppm for methylenes involved in thiazole ring; at 8.98

ppm for amine group. The ^{13}C NMR spectrum of **6** contains chemical shifts at 13.60 ppm for methyl group; 16.95–32.03 ppm for methylenes involved in the arm of alkyne fragment; at 61.08–75.02 ppm for alkyne group; at 113.10–116.26, 119.60–128.50, 138.80–147.02 and 156.34 ppm for phenyl groups; at 116.57, 135.32 and 166.98 ppm for thiazole ring. The presence of **6** was further confirmed by the mass spectrum which showed a molecular ion at m/z 411.15.

In conclusion, the synthesis of sulfonamide derivatives using a three-component system offers some advantages such as good yields, simple procedure, low cost, and ease of workup.

REFERENCES

- 1 S. Caddick, J. Wilden, D. Judd. *J. Am. Chem. Soc.*, **126**, 1024 (2004).
- 2 S. Abdel-Hafez. *Russian J. Bioor. Chem.*, **36**, 370 (2010).
- 3 M. Johar, N. Singhal, S. Dastidar, R. Shukla, R. Raghbir. *Monats. fur Chem.*, **131**, 511 (2000).
- 4 H. Yoshino, N. Ueda, J. Nijima, H. Sugumi, Y. Kotake, N. Koyanagi, K. Yoshimatsu, M. Asada, T. Watanabe. *J. Med. Chem.*, **35**, 2496 (1992).
- 5 L. Marques, G. Manzoni, E. Schulz, M. Matiko, R. Lara. *Inorg. Chem. Comm.*, **10**, 1083 (2007).
- 6 S. Sondhi, M. Johar, N. Singhal, S. Dastidar, R. Shukla, R. Raghbir. *Monats. fur Chem.*, **131**, 511 (2000).
- 7 S. Tu, F. Fang, C. Miao, H. Jiang, Y. Feng, D. Shi, *Tetrahedron Lett.*, **44**, 6153 (2003).
- 8 P. Salehi, N. Fard. *Tetrahedron Lett.*, **44**, 2889 (2003).
- 9 R. Yarapathi, S. Kurva, S. Tammishetti, *Catal. Commun.*, **5**, 511 (2004).
- 10 J. Bussolari, P. McDonnell. *J. Org. Chem.*, **65**, 6777 (2005).
- 11 F. Shirini, K. Marjani, H. Nahzomi. *Arkivoc*, 51 (2007).
- 12 R. Crossland, K. Servis. *J. Org. Chem.*, **35**, 3195 (1970).
- 13 M. Dabiri, A. Sadat, A. Basgir. *Heterocycles*, **71**, 543 (2007).
- 14 N. Gommermann, C. Koradin, K. Polborn, P. Knochel. *Angew. Chem.*, **115**, 5401 (2003).
- 15 L. Figuroa-Valverde, F. Díaz-Cedillo, A. Camacho-Luis, M. López-Ramos, E. García-Cervera. *Asian J. Chem.*, **22**, 7057 (2010).

КОНСТРУИРАНЕ И СИНТЕЗА НА ДВЕ ПРОИЗВОДНИ НА СУЛФОТИАЗОЛА В ТРИ-КОМПОНЕНТНА СИСТЕМА

Л. Фигуроа-Валверде¹, Ф. Диас-Седийо², Е. Гарсия-Сервера¹, Е. Поол Гомес¹, М. Росас-Нехтикапа³, М. Лопес-Рамос¹.

¹Лаборатория по фармацевтична химия, Факултет по биологични науки, Автономен университет в Кампече, Мексико

²Национална школа по биологични науки, Национален политехнически институт, Мексико, D.F. C.P. 11340.

³Факултет по хранително-вкусова промишленост, Университет Веракрусана по медицина и стоматология, Веракрус, Мексико

Постъпила на 2 юни, 2012 г.; коригирана на 5 ноември, 2012 г.

(Резюме)

Синтезирани са две сулфонамидни производни на сулфотиазола при използването на три-компонентна система. В първия етап е получено съединението 4-[(2-хидрокси-нафтален-1-ил)-фенил-метил]-амино}-*N*-тиазол-2-ил-бензенсулфонамид (**4**) чрез реакция с β -нафтол, бензалдеhid и сулфатиазол (**3**) в етанол. Вторият етап се постига чрез реакция на **3** с 1-хексин и бензалдеhid, използвайки меден хлорид като катализатор за образуването на 4(хекс-1-инил-фенил-амино)-*N*-тиазол-2-ил-бензенсулфонамид (**6**). Структурата на получените съединения е потвърдена от елементарен анализ, ИЧ- и ЯМР-спектроскопия и спектрометрия. Предложеният метод предлага някои предимства, като добри добиви, проста процедура, ниски разходи и лесна обработка.

Some aspects of multilayer chitosan electrospun nanofibers web

M. Mohammadian¹, A.K. Haghi^{2*}

¹Department of Textile Engineering, Kashan Branch, Islamic Azad University, Kashan, Iran

²University of Guilan, P.O.Box 3756, Rasht, Iran

Received April 15, 2012; Revised December 18, 2012

The chitosan based nanofibers web is a biocompatible, biodegradable, antimicrobial and non-toxic structure which has both physical and chemical properties to effectively capture and neutralize toxic pollutants from air and liquid media. Despite such potentials, the mechanical properties of nanofibers web is very poor to use in filtration applications. To remedy this defect, nanofibers web could laminate into a strength structure. The purpose of this study is to consider the influence of laminating temperature on nanofibers web/multilayer structure properties. The nanofibers web morphology and multilayer cross-section was observed under an optical microscope and scanning electron microscope, respectively. Also, air permeability experiments were performed to examine the effect of laminating temperature on air transport properties of multilayer structures. Optical microscope images showed that the nanofiber web began to damage when laminating temperature was selected above melting point of adhesive layer. Air permeability decreased with increasing laminating temperature. It is also observed that the adhesive force between layers was increased by increasing laminating temperature.

Keywords: Chitosan, Nanofibers web, Filtration, Lamination

INTRODUCTION

There is an enormous requirement for cleaner air around the world which has activated immense interest in the development of high efficiency filters or face masks. Non-woven nanofibrous media have low basis weight, high permeability, and small pore size that make them appropriate for a wide range of filtration applications. In addition, nanofibers web offers unique properties like high specific surface area (ranging from 1 to 35m²/g depending on the diameter of fibers), good interconnectivity of pores and the potential to incorporate active chemistry or functionality on nanoscale. To date, the most successful method of producing nanofibers is through the process of electrospinning. The electrospinning process uses high voltage to create an electric field between a droplet of polymer solution at the tip of a needle and a collector plate. When the electrostatic force overcomes the surface tension of the drop, a charged, continuous jet of polymer solution is ejected. As the solution moves away from the needle and toward the

collector, the solvent evaporates and jet rapidly thins and dries. On the surface of the collector, a nonwoven web of randomly oriented solid nanofibers is deposited [1]. It has been found that the morphology of the web, such as fiber diameter and its uniformity of the electrospun nanofibers, are dependent on many processing parameters. These parameters can be divided into three main groups: A) solution properties, B) processing conditions, C) ambient conditions. Each of the parameters has been found to affect the morphology of the electrospun fibers.

Solution Properties

Parameters such as viscosity of solution, solution concentration, molecular weight of polymer, electrical conductivity, elasticity and surface tension have an important effect on the morphology of nanofibers.

Viscosity. The viscosity range of a different nanofiber solution which is spinnable is different. One of the most significant parameters influencing the fiber diameter is the solution viscosity. A higher viscosity results in a large fiber diameter. Beads and beaded fibers are less likely to be formed for the more viscous solutions. The bead diameter becomes bigger and the average distance between beads on the fibers become longer as the viscosity

* To whom all correspondence should be sent:
E-mail: Haghi@Guilan.ac.ir

increases.

Solution concentration. In the electrospinning process, for fiber formation to occur a minimum solution concentration is required. As the solution concentration increases, a mixture of beads and fibers is obtained. The shape of the beads changes from spherical to spindle-like when the solution concentration varies from low to high levels. The fiber diameter increases with increasing solution concentration because of the higher viscosity resistance. Nevertheless, at higher concentration the viscoelastic force which usually resists rapid changes in fiber shape may result in uniform fiber formation. However, it is impossible to electrospinning if the solution concentration or the corresponding viscosity become too high due to the difficulty in liquid jet formation.

Molecular weight. Molecular weight also has a significant effect on the rheological and electrical properties such as viscosity, surface tension, conductivity and dielectric strength. It has been observed that too low molecular weight solution tends to form beads rather than fibers and high molecular weight nanofiber solution gives fibers with larger average diameter.

Surface tension. The surface tension of a liquid is often defined as the force acting at right angles to any line of unit length on the liquid surface. By reducing surface tension of a nanofiber solution, fibers could be obtained without beads. The surface tension seems more likely to be a function of solvent compositions, but is negligibly dependent on the solution concentration. Different solvents may contribute different surface tensions. However, a lower surface tension of a solvent will not necessarily always be more suitable for electrospinning. Generally, surface tension determines the upper and lower boundaries of electrospinning window if all other variables are held constant. The formation of droplets, bead and fibers can be driven by the surface tension of solution, and lower surface tension of the spinning solution helps electrospinning to occur at lower electric field.

Solution Conductivity. There is a significant drop in the diameter of the electrospun nanofibers when the electrical conductivity of the solution increases. Beads may also be observed due to low conductivity of the solution, which results in insufficient elongation of a jet by electrical force to produce uniform fiber. In general, electrospun nanofibers with the smallest fiber diameter can be obtained with the highest electrical conductivity.

This indicates that the drop in the size of the fibers is due to the increased electrical conductivity.

Processing Condition

Another important parameter that affects the electrospinning process is the various external factors exerting on the electrospinning jet. This includes the Applied voltage, the feed rate, diameter of nozzle/needle and distance between the needle and collector.

Applied voltage. In the case of electrospinning, the electric current due to the ionic conduction of charge in the nanofiber solution is usually assumed small enough to be negligible. The only mechanism of charge transport is the flow of solution from the tip to the target. Thus, an increase in the electrospinning current generally reflects an increase in the mass flow rate from the capillary tip to the grounded target when all other variables (conductivity, dielectric constant, and flow rate of solution to the capillary tip) are held constant. Increasing the applied voltage (*i.e.*, increasing the electric field strength) will increase the electrostatic repulsive force on the fluid jet, which favors the thinner fiber formation. On the other hand, the solution will be removed from the capillary tip more quickly as jet is ejected from Taylor cone. This results in the increase of the fiber diameter.

Feed rate. The morphological structure can be slightly changed by changing the solution flow rate. When the flow rate exceeded a critical value, the delivery rate of the solution jet to the capillary tip exceeded the rate at which the solution was removed from the tip by the electric forces. This shift in the mass-balance resulted in sustained but unstable jet and fibers with big beads formation. In the first part of this study, the production of electrospun nanofibers was investigated. In another part, a different case study was presented to show how nanofibers can be laminated for application in filter media.

Distance between the needle and collector. When the distance between the tip of needle and the collector is reduced, the jet will have a shorter distance to travel before it reaches the collector plate. Moreover, the electric field strength will also increase at the same time and this will increase the acceleration of the jet to the collector. As a result, there may not have enough time for the solvents to evaporate when it hits the collector.

Diameter of needle. The internal diameter of needle has a certain effect on the electrospinning process. A smaller internal diameter was found to reduce the amount of beads on the electrospun web

and was also found to cause a reduction in the diameter of fibers.

Ambient condition

Since electrospinning is influenced by external electric field, any changes in the electrospinning environment will also affect the electrospinning process. Any interaction between the surrounding and the polymer solution may have an effect on the electrospun fiber morphology. For example, high humidity was found to cause the formation of pores on the surface of the fibers [2-4].

Chitosan. Over the recent years, interest in the application of naturally occurring polymers such as polysaccharides and proteins, owing to their abundance in the environment, has grown considerably. Chitin, the second most abundant polysaccharide found on earth next to cellulose, is a major component of the shells of crustaceans such as crab, shrimp and crawfish. The structural characteristics of chitin are similar to those of glycosaminoglycans. When chitin is deacetylated over about 60% it becomes soluble in dilute acidic solutions and is referred to chitosan or poly(N-acetyl-D-glucosamine). Chitosan and its derivatives have attracted much research because of their unique biological properties such as antibacterial activity, low toxicity, and biodegradability [5-7].

Depending on the chitin source and the methods of hydrolysis, chitosan varies greatly in its molecular weight (MW) and degree of deacetylation (DDA). The MW of chitosan can vary from 30 kDa to well above 1000 kDa and its typical DDA is over 70 %, making it soluble in acidic aqueous solutions. At a pH of about 6–7, the biopolymer is a polycation and at a pH of 4.5 and below, it is completely protonated. The fraction of repeat units which are positively charged is a function of the degree of deacetylation and solution pH. A higher degree of deacetylation would lead to a larger number of positively charged groups on the chitosan backbone [8]. Also, Sorlier *et al.*[9] have studied the effect of pH and DDA on Chitosan solution pKa and found that for varying DDA from 5% to 75%, pKa varies between 6.3 and 7.2.

As mentioned above, chitosan has several unique properties such as the ability to chelate ions from solution and to inhibit the growth of a wide variety of fungi, yeasts and bacteria. Although the exact mechanism with chitosan exerts these properties is currently unknown, it has been suggested that the polycationic nature of this biopolymer that forms from acidic solutions below pH 6.5 is a crucial factor. Thus, it has been

proposed that the positively charged amino groups of the glucosamine units interact with negatively charged components in microbial cell membranes altering their barrier properties, thereby preventing the entry of nutrients or causing the leakage of intracellular contents. Another reported mechanism involves the penetration of low MW chitosan in the cell, the binding to DNA, and the subsequent inhibition of RNA and protein synthesis. Chitosan has been shown also to activate several defense processes in plant tissues, and it inhibits the production of toxins and microbial growth because of its ability to chelate metal ions [10-12].

Electrospinning of chitosan. Chitosan is insoluble in water, alkali, and most mineral acidic systems. However, though its solubility in inorganic acids is quite limited, chitosan is in fact soluble in organic acids, such as dilute aqueous acetic, formic, and lactic acids. Chitosan also has free amino groups, which makes it a positively charged polyelectrolyte. This property makes chitosan solutions highly viscous and complicates its electrospinning [13]. Furthermore, the formation of strong hydrogen bonds in a 3-D network prevents the movement of polymeric chains exposed to the electrical field [14]. Different strategies were used for bringing chitosan in nanofiber form. The three top most abundant techniques include blending of favorite polymers for electrospinning process with chitosan matrix [15, 16], alkali treatment of chitosan backbone to improve electro spinnability through reducing viscosity [17] and employment of concentrated organic acid solution to produce nanofibers by decreasing of surface tension [18]. Electrospinning of polyethylene oxide (PEO)/chitosan [15] and polyvinyl alcohol(PVA)/ chitosan [16] blended nanofiber are two recent studies based on first strategy. In the second protocol, the MW of chitosan decreases through alkali treatment. Solutions of the treated chitosan in aqueous 70-90% acetic acid produce nanofibers with appropriate quality and processing stability [17]. Using concentrated organic acids such as acetic acid¹⁸ and trifluoroacetic acid (TFA) with and without dichloromethane (DCM) [19] has been reported exclusively for producing neat chitosan nanofibers. They similarly reported the decreasing of surface tension and at the same time enhancement of charge density of chitosan solution without significant effect on viscosity. This new method suggests significant influence of the concentrated acid solution on the reducing of the applied field required for electrospinning.

The mechanical properties of neat chitosan electrospun natural nanofibers web can be improved by addition of the synthetic materials including carbon nanotubes (CNTs) [20]. CNTs are one of the important synthetic materials that were discovered by Iijima in 1991 [21]. CNTs, either single-walled nanotubes (SWNTs) or multiwalled nanotubes (MWNTs), combine the physical properties of diamond and graphite. They are extremely thermally conductive like diamond and appreciably electrically conductive like graphite. Moreover, the flexibility and exceptional specific surface area to mass ratio can be considered as significant properties of CNTs. Scientists are becoming more interested in CNTs for existence of exclusive properties such as mechanical strength for various applications [22].

Laminating of electrospun web. While electrospun webs suggest exciting characteristics, it has been reported that they have limited mechanical properties [23, 14]. To compensate this drawback in order to use of them in filtration applications, electrospun nanofibers web could be laminated via an adhesive into a multilayer system [25-28]. The adhesives are as solvent/water-based adhesive or as hot-melt adhesive. At the first group, the adhesives are as solution in solvent or water, and solidify by evaporating of the carrying liquid. Solvent-based adhesives could 'wet' the surfaces to be joined better than water-based adhesives, and also could solidify faster. But unfortunately, they are environmentally unfriendly, usually flammable and more expensive than those. Of course it doesn't mean that the water-based adhesives are always preferred for laminating, since in practice, drying off water in terms of energy and time is expensive too. Besides, water-based adhesives are not resisting to water or moisture because of their hydrophilic nature. At the second group, hot-melt adhesives are environmentally friendly, inexpensive, require less heat and energy, and so are now more preferred. Generally there are two procedures to melt these adhesives; static hot-melt laminating that accomplish by flat iron or Hoffman press and continuous hot-melt laminating that uses the hot calendars. In addition, these adhesives are available in several forms; as a web, as a continuous film, or in powder form. The adhesives in film or web form are more expensive than the corresponding adhesive powders. The web form are discontinuous and produce laminates which are flexible, porous and breathable, whereas, Continuous film adhesives cause stiffening and produce laminates which are not porous and

permeable to both air and water vapour. This behaviour attributed to impervious nature of adhesive film and its shrinkage under the action of heat [29]. Thus, the knowledge of laminating skills and adhesive types is very essential to producing appropriate multilayer structures. Specifically, this subject becomes more highlight as we will laminate the ultrathin nanofibers web, because the laminating process may be adversely influenced on the nanofibers web properties. Lee *et al.* [30] without disclosure of laminating details, reported that the hot-melt method is more suitable for nanofiber web laminating. In this method, laminating temperature is one of the most effective parameters. Incorrect selection of this parameter may lead to change or damage ultrathin nanofiber web. Therefore, it is necessary to find out a laminating temperature which has the least effect on nanofiber web during process.

The purpose of this study is to consider the influence of laminating temperature on the nanofibers web/multilayer structure properties. Multilayer structures were made by laminating of nanofibers web into cotton fabric via hot-melt method at different temperatures. Effects of laminating temperature on the nanofibers web morphology, air transport properties and the adhesive force were discussed.

EXPERIMENTAL

Preparation of chitosan-MWNT solution

Chitosan with DDA of 85% and MW of 5×10^5 was supplied by Sigma-Aldrich. The MWNTs, supplied by Nutrino, have an average diameter of 4 nm and purity of about 98%. All of the other solvents and chemicals were commercially available and used as received without further purification. A Branson Sonifier 250 operated at 30W used to prepare the MWNT dispersion in chitosan/organic acid solution (70/30 TFA/DCM). First, 3mg of as received MWNTs was dispersed into deionized water or DCM using solution sonicating for 10min. Next, chitosan was added to MWNTs dispersion to preparing a 10 wt% solution after sonicating for 5min. Finally, in order to obtain a chitosan/MWNT solution, organic acid solution was added and the dispersion was stirred for 10 hours.

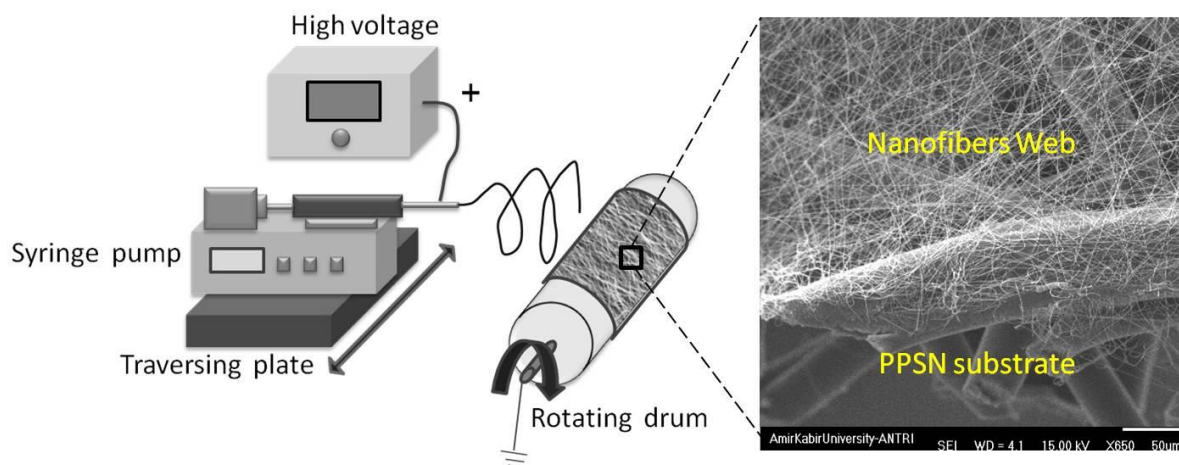


Fig.1. Electrospinning setup and an enlarged image of Nanofibers Web on PPSN

Table1. Electrospinning conditions and layers properties for laminating

Electrospinning conditions		Layers properties	
Polymer concentration	12% w/w	PPSN Thickness	0.19 mm
Feed rate	1 μ l/h	Air permeability	824 $\text{cm}^3/\text{s}/\text{cm}^2$
		Melting point	140°C
Nozzle inner diameter	0.4 mm	Mass	25 g/m^2
Nozzle-Drum distance	7 cm	Electrospun web	
Voltage	11 KV	Mass	3.82 g/m^2
Traversing plate speed	0.4 m/min	Fabric thickness	0.24 mm
Drum speed	9 m/min		
Spinning time	8 hrs	Warp-weft density	25×25 per cm

Electrospinning

After the preparation of spinning solution, it was inserted into a syringe with a stainless steel nozzle and then the syringe was placed in a metering pump from WORLD PRECISION INSTRUMENTS (Florida, USA). Next, this set installed on a homemade plate which it could traverse to left-right direction along drum collector (Fig.1).The electrospinning conditions and layers properties for laminating are summarized in Table 1. The electrospinning process was carried out for 8h and the electrospun fibres were collected on an aluminium-covered rotating drum which was previously covered with a Poly-Propylene Spun-bond Nonwoven (PPSN) substrate. After removing of PPSN covered with electrospun

fibres from drum and attaching another layer of PPSN on it, this set was incorporated between two cotton weft-warp fabrics as a structure of fabric-PPSN- nanofibers web-PPSN-fabric (Fig. 2). Finally, hot-melt laminating performed using a simple flat iron for 1min, under a pressure of 9 gf/cm^2 and at temperatures 85,110,120,140,150°C (above softening point of PPSN) to form multilayer structures.

Characterizations

The morphology of electrospun fibers. The electrospun fibers were characterized using scanning electron microscope (SEM, Seron Technology, AIS-2100, Korea) to study the fiber morphology. The sample was sputter

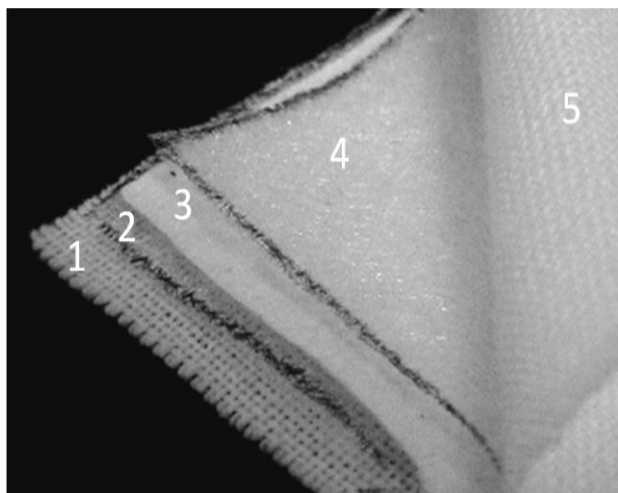


Fig. 2. Multilayer components: (1) Fabric, (2) PPSN, (3) Nanofibers Web, (4) PPSN, (5) Fabric.

coated with Au/Pd to prevent charging during SEM imaging. Image processing software (MICROSTRUCTURE MEASUREMENT) was used to measure the fiber diameter from the SEM micrograph. Fiber diameter was measured at 50 different points for determining the average and distribution of diameter. The Mass per unit area (g/m^2 or gsm) of the electrospun web was measured by dividing the mass of the web by its area.

The morphology of multilayer structure

A piece of each multilayer was freeze fractured in liquid nitrogen and after sputter-coating with Au/Pd, a cross-section image of them captured using a scanning electron microscope.

Also, to consider the nanofiber web surface after hot-melt laminating, other laminations were prepared by a non-stick sheet made of Teflon (0.25 mm thickness) as a replacement for one of the fabrics (fabric/PPSN/nanofibers web/PPSN/Teflon sheet). Laminating process was carried out at the same conditions which mentioned to produce primary laminations. Finally, after removing of Teflon sheet, the nanofibers layer side was observed under an optical microscope (MICROPHOT-FXA, Nikon, Japan) connected to a digital camera.

Measurement of air permeability

The air permeability of multilayer structures, which is a measure of the structural porosity, was measured by air permeability tester (TEXTTEST FX3300, Zürich, Switzerland). It was tested 5 pieces of each sample under air pressure of 125 Pa, at ambient condition (16°C , 70%RH), and then the average air permeability was calculated.

RESULTS AND DISCUSSION

In our previous work, chitosan/MWNTs nanofibers web was fabricated using electrospinning technique, successfully [31]. The goal of this research is to develop chitosan based multilayer structures in order to use of them in filtration applications. In the electrospinning phase, PPSN was chosen as a substrate to provide strength to the nanofiber web and to prevent of its destruction in removing from the collector. In Fig. 1, an ultrathin layer of nanofibers web on PPSN layer is illustrated, which conveniently shows the relative fiber size of nanofiber (326 ± 68 nm) web compared to PPSN fibers. Also, this figure shows that the macropores of PPSN substrate is covered with numerous electrospun nanofibers, which will create innumerable microscopic pores in this system. But in laminating phase, this substrate acts as an adhesive and causes to bond the nanofiber web to the fabric. In general, it is relatively simple to create a strong bond between these layers, which guarantees no delamination or failure in multilayer structures; the challenge is to preserve the original properties of the nanofiber web and fabrics. In other words, the application of adhesive should have minimum affect on the

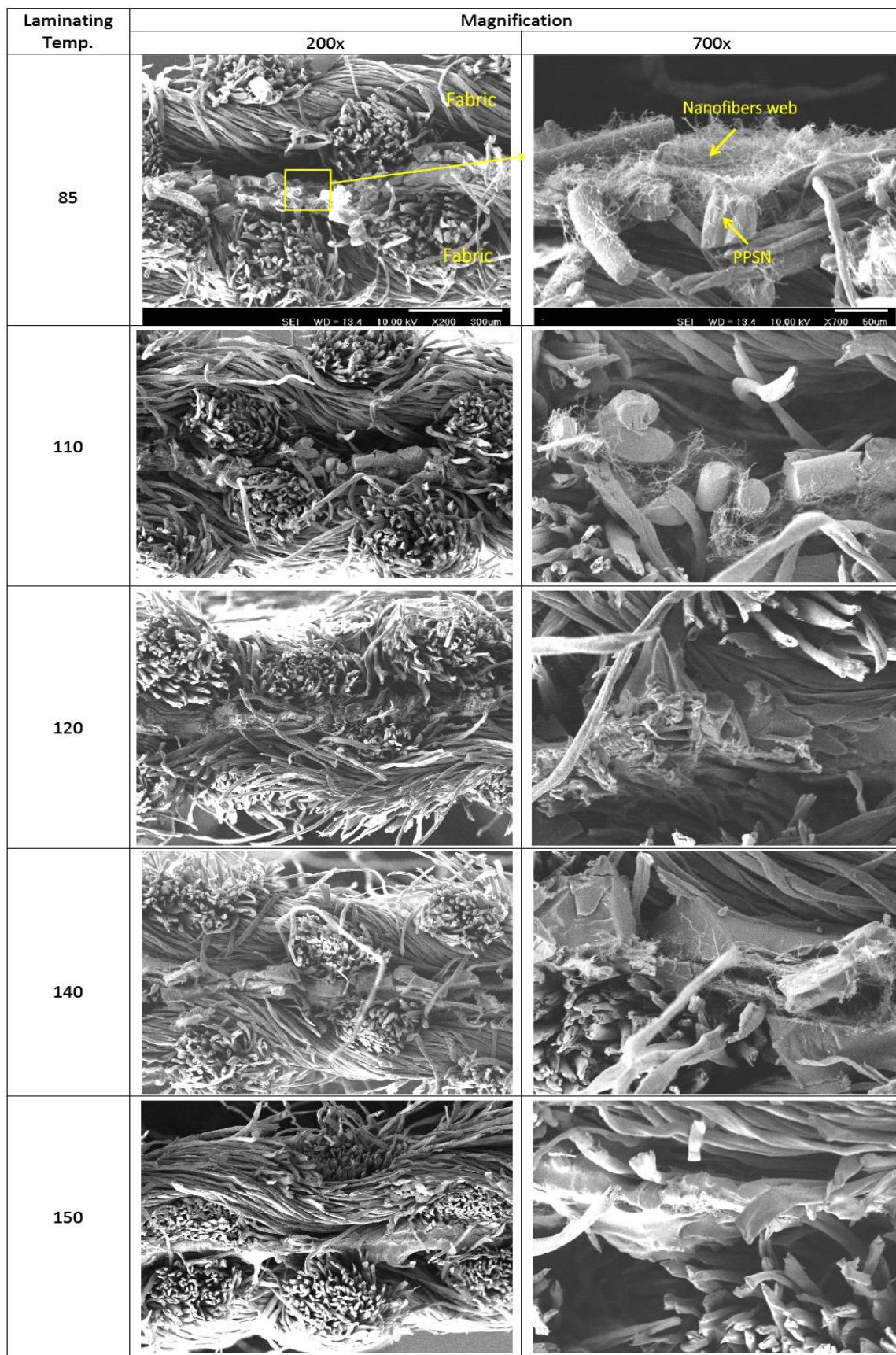


Fig. 3. SEM images of multilayer fabric cross-section at different laminating temperatures.

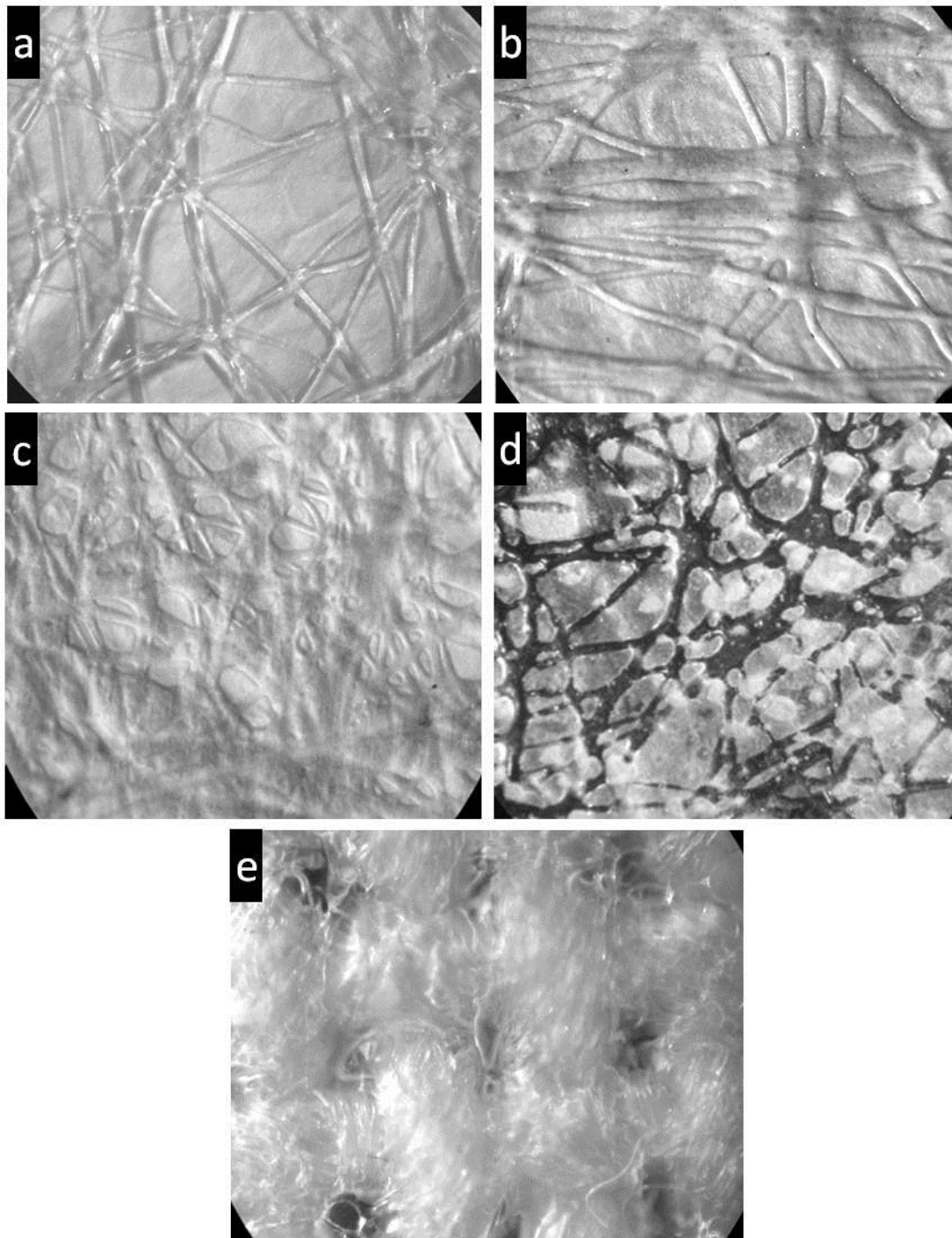


Fig.4. The optical microscope images of nanofiber web surface at different laminating temperatures (100x magnification), a) 85°C, b) 110°C, c) 120°C, d) 140°C and e) 150°C.

fabric or nanofiber web structure. In order to achieve to this aim, it is necessary that: a) the least amount of a highly effective adhesive applied, b) the adhesive correctly cover the widest possible surface area of layers for better linkage between them and c) the adhesive penetrate to a certain extent of the nanofiber web/fabric [29]. Therefore, we selected PPSN,

which is a hot-melt adhesive in web form. As mentioned above, the perfect use of web form adhesive can be lead to produce multilayer fabrics which are porous, flexible and permeable to both air and water vapour. On the other hand, since the melting point of PPSN is low, hot-melt laminating can perform at lower temperatures. Hence, the probability of

shrinkage that may happen on layers in effect of heat becomes smaller; Of course, the thermal degradation of chitosan nanofiber web begins above 250°C [32,33] and the cotton fabrics are intrinsically resistant to heat too. By this description, laminating process performed at five different temperatures to consider the effect of laminating temperature on the nanofiber web/multilayer properties.

The SEM images of multilayer fabric cross-section after laminating at different temperatures are shown in Fig. 3. It is obvious that these images cannot deliver useful information about nanofibers web morphology in multilayer structure, so it becomes impossible to consider the effect of laminating temperature on nanofibers web. Hence, in a novel way, we decided to prepare a secondary multilayer by substitution of one of the fabrics with Teflon sheet. By this replacement, the surface of nanofiber web will become accessible after laminating; because Teflon is a non-stick material and easily separates from the adhesive.

Fig. 4 presents optical microscope images of nanofiber web and adhesive after laminating at different temperatures. It is apparent that the adhesive gradually flattened on nanofiber web (Fig. 4(a-c)) when laminating temperature increased to melting point of adhesive(140 °C). This behaviour is attributed to increment in plasticity of adhesive because of temperature rise and the pressure applied from the iron weight. But, by selection of melting point as laminating temperature, the adhesive completely melted and began to penetrate into the nanofiber web structure instead of spread on it (Fig. 4(d)). This penetration, in some regions, was continued to some extent that the adhesive was even passed across the web layer. The dark crisscross lines in Fig. 4(d) obviously show wherever this excessive penetration is occurred. The adhesive penetration could intensify by increasing of laminating temperature above melting point; because the fluidity of melted adhesive increases by temperature rise. Fig. 4(e) clearly shows the amount of adhesive diffusion in the web which was laminated at 150°C. At this case, the whole diffusion of adhesive lead to create a

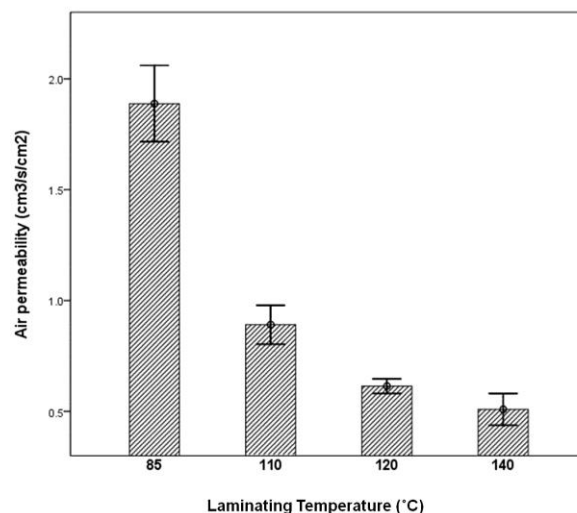


Fig. 5. Air permeability of multilayer structure after laminating at different temperatures.

transparent film and to appear the fabric structure under optical microscope.

Also, to examine how laminating temperature affect the permeability of multilayer structure, air permeability experiment was performed. The bar chart in Fig. 5 indicates the effect of laminating temperature on air transport properties of multilayer. As might be expected, the air permeability decreased with increasing laminating temperature. This procedure means that the air permeability of multilayer fabric is related to adhesive's form after laminating; because at these temperatures, the nanofiber web and cotton fabrics intrinsically are resistant to heat. Of course, it is to be noted that the pressure applied during laminating can leads to compact the web/fabric structure and to reduce the air permeability too. Nevertheless, this parameter didn't have effective role on air permeability variations at this work, because the pressure applied for all samples had the same quantity. As discussed, by increasing of laminating temperature to melting point, PPSN was gradually flattened between layers so that it was transformed from web-form to film-like. It is obvious in Fig. 4(a-c) that the pore size of adhesive layer becomes smaller in effect of this transformation. Therefore, we can conclude that the adhesive layer, as a barrier, resists to convective air flow during experiment and finally reduces the air permeability of multilayer fabric according to

the pore size decrease. But, this conclusion is unacceptable for the samples laminated at melting point (140°C); since the adhesive was missed self layer form in effect of penetration into the web/fabric structures (Fig. 4d). At these samples, the adhesive penetration leads to block the pores of web/fabrics and to prevent of the air pass during experiment. It should be noted that the adhesive was penetrated into the web much more than the fabric because, PPSN structurally had more surface junction with the web (Fig. 3). Therefore, at here, the nanofiber web absorbs the adhesive and forms an impervious barrier to air flow.

Furthermore, we only observed that the adhesive force between layers was improved according to temperature rise. For example, the samples laminated at 85°C were exhibited very poor adhesion between the nanofiber web and the fabrics as much as they could be delaminated by light abrasion of thumb, as illustrated at Fig. 3. Generally, it is essential that no delamination occurs during use of this multilayer structure, because the nanofiber web might be destroyed due to abrasion of other layers. Before melting point, improving the adhesive force according to temperature rise is simultaneously attributed to the more penetration of adhesive into layers and the expansion of bonding area between them, as already discussed. Also at melting point, the deep penetration of adhesive into the web/fabric leads to increase in this force.

CONCLUSION

In this study, the effect of laminating temperature on the nanofibers web/multilayer structures properties investigated to make next generation of filter media. First, we demonstrate that it is impossible to consider the effect of laminating temperature on the nanofiber web morphology by a SEM image of multilayer cross-section. Thus, we prepared a surface image of nanofiber web after laminating at different temperature using an optical microscope. It was observed that nanofiber web was approximately unchanged when laminating temperature was below PPSN melting point. In addition, to compare air transport properties of multilayer fabrics, air permeability tests were performed. It was found that by increasing laminating temperature, air

permeability was decreased. Furthermore, it only was observed that the adhesive force between layers in multilayer was increased with temperature rise. These results indicate that temperature is an effective parameter for laminating of nanofiber web to make a new type of antibacterial filter media.

Acknowledgement: The authors wish to thank the Iran National Science Foundation (INSF) for their financial support under grant No. 90003694.

REFERENCES

- 1.J. S. Kim, D. H. Reneker, *Poly. Eng. Sci.*, **39**, 849 (1999).
- 2.S.A. Theron, E. Zussman, A.L. Yarin, *Polymer*, **45**(6), 2017(2004).
- 3.S. H. Tan, R. Inai, M. Kotaki, S. Ramakrishna, *Polymer*, **46**, 6128 (2005).
- 4.A. K. Haghi, M. Akbari, *Phys. Stat. Sol. A*, **204**, 1830 (2007).
- 5.S. W. Fang, C. F. Li, D. Y. C. Shih, *J. Food Prot.*, **56**, 136 (1994).
- 6.N.M. Angelova, I. Rashkov, V. Maximova, S. Bogdanova, A. Domard, *J. Bioactive Compatible Polymers*, **10**, 285 (1995).
- 7.M. Ignatova, N. Manolova, N. Markova, I. Rashkov, *Macromol. Biosci.*, **9**, 102 (2009).
- 8.K.M. Kim, J.H. Son, S.-K. Kim, C.L. Weller, M.A. Hanna, *J. Food Sci.*, **71**, 119 (2006).
- 9.P. Sorlier, A. Denuziere, C. Viton, A. Domard, *Biomacromolecules*, **2**, 765 (2001).
10. I.M. Helander, E.L. Nurmiaho-Lassila, R. Ahvenainen, J. Rhoades, S. Roller, *Int.l J.Food Microbio.*, **71**, 235 (2001).
11. S.H. Lim, S.M. Hudson, *J. Macromolecular Science-Polymer Reviews*, **C**, **43**, 223 (2003).
12. F. Devlieghere, A. Vermeulen, J. Debevere, *Food Microbiol.*, **21**, 703 (2004).
13. I. Aranaz, M. Mengibar, R. Harris, I. Paños, B. Miralles, N. Acosta, G. Galed, Á. Heras, *Curr. Chem. Biol.*, **3**, 203 (2009).
14. A. Neamnark, R. Rujiravanit, P. Supaphol, *Carbohydr. Polym.*, **66**, 298 (2006).
15. B. Duan, C. Dong, X. Yuan, K. Yao, *J. Biomater. Sci. Polym. Ed.*, **15**, 797 (2004).
16. Y. T. Jia, J. Gong, X. H. Gu, H. Y. Kim, J. Dong, X. Y. Shen, *Carbohydr. Polym.*, **67**, 403 (2007).
17. H. Homayoni, S. A. H. Ravandi, M. Valizadeh, *Carbohydr. Polym.*, **77**, 656 (2009).
18. X. Geng, O.-H. Kwon, J. Jang, *Biomaterials*, **26**, 5427 (2005).
19. S. D. Vrieze, P. Westbroek, T.V. Camp, L.V. Langenhove, *J. Mater. Sci.*, **42**, 8029 (2007).
20. K. Ohkawa, D. Cha, H. Kim, A. Nishida, H. Yamamoto, *Macromol. Rapid Commun.*, **25**, 1600 (2004).
21. S. Iijima, *Nature*, 354, **56** (1991).
22. A. M. K. Esawi, M.M. Farag, *Mater. Design*, **28**, 2394 (2007).

23. A. Pedicini, R. J. Farris, *Polymer*, **44**, 6857 (2003).
24. K. H. Lee, B. S. Lee, C. H. Kim, H. Y. Kim, K. W. Kim, C. W. Nah, *Macromol. Res.* **13**(5), 441(2005).
25. H. Schreuder-Gibson, P. Gibson, K. Senecal, M. Sennett, J. Walker, W. Yeomans, D. Ziegler, P.P. Tsai, *J. Adv.Mater.*, **34**, 44 (2002).
26. L. Liu, Z. M. Huang, C. L. He, X. J. Han, *Mater. Sci. Eng. A* **435-436**, 309 (2006).
27. M. Kanafchian, M. Valizadeh, A. K. Haghi, *Korean J. Chem. Eng.*, **28**(2), 445 (2011).
28. M. Kanafchian, M. Valizadeh, A. K. Haghi, *Korean J. Chem. Eng.*, **28**(3), 763 (2011).
29. W. Fung, In "Coated and laminated textiles", 1st ed, Woodhead Publishing, 2002, p. 63.
30. S. Lee, D. Kimura, K.H. Lee, J. C. Park, I.S. Kim, *Textile Res. J.*, **80**, 99 (2010).
31. Z. M. Mahdiah, V. Mottaghitalab, N. Piri, A. K. Haghi, *Korean J. Chem. Eng.*, **29**(1), 111 (2012).
32. K.Sakurai, T.Maegawa, T. Takahashi, *Polymer*, **41**, 7051 (2000).
33. M.Zeng, Z.Fang, C. Xu, *J. Membr. Sci.*, **230**, 175 (2004).

НЯКОИ АСПЕКТИ НА МРЕЖА ОТ МНОГОСЛОЙНИ ХИТОЗАНОВИ НАНОВЛАКНА, ПОЛУЧЕНИ ПРИ ЕЛЕКТРОПРЕДЕНЕ

М. Мохамадян¹, А.К. Хаги²

¹Департамент по текстилно инженерство, Ислямски университет "Азад", клон Кашан, Кашан, Иран

²Университет Гилан, Рац, Иран

Постъпила на 15 април, 2012 г.; коригирана на 18 декември, 2012 г.

(Резюме)

Мрежите от многослойни хитозанови нановлакна, получени при електропредене са биосъвместими, биоразградими, с анти-микробна и не-токсична структура. Те имат свойствата ефективно да улавят и неутрализират токсични замърсители от газови и течни среди. Въпреки тези качества механичните свойства на мрежите от нановлакна не позволяват използването им за филтруване. За намаляването на този ефект мрежите от нановлакна се ламинират в здрави структури. Целта на настоящата работа е да се определи влиянието на температурата на ламиниране върху свойствата на многослойни влакна, свързани в мрежа. Морфологията на мрежите от нановлакна и напречното сечение на многослойната структура са изследвани с помощта на оптичен микроскоп и сканираща електронна микроскопия. Освен това е изследвана проникваемостта спрямо въздух, за да се изследва ефекта на температурата на ламиниране върху транспортните свойства на многослойните структури. Оптичните образи показват, че мрежите от нановлакна започват да се повреждат при температура на ламиниране по-висока от точката на топене на адхезивния слой. Проницаемостта на въздуха намалява с повишаването на температурата на ламиниране. Освен това силите на адхезия между слоевете нарастват с повишаването на температурата на ламиниране.

Electrochemical characterization of Jordanian coins

M.K. Hourani*, A.I. Wehbeh

Department of Chemistry, The University of Jordan, Amman 11942 – Jordan

Received July 5, 2012; Accepted February 12, 2013

Cyclic voltammetry was applied for characterization of Jordanian coins. Four different Jordanian coins of different composition were investigated by cyclic voltammetry. These are the piaster, the shelling (5-piaster coin), the quarter, and the half-dinar. The coin samples were collected from the market in addition to new coins obtained from the Central Bank of Jordan (CBJ). Each of the investigated coins displayed a distinct voltammogram that can be easily related to the composition of the coin. The voltammograms were, indeed, "electrochemical spectra" or "voltammetric signatures" of the coins. The voltammogram of the piaster which is composed of a copper plated stainless steel shows very close resemblance to the voltammogram of copper. The shelling which is composed of nickel plated stainless steel displayed a voltammogram that shows close similarity to the voltammogram of nickel. The quarter displayed a voltammogram that is very close to the voltammogram of copper. The half-dinar coin is composed of a nickel plated stainless steel disk and a copper alloy ring. The voltammogram of the disk is close to the voltammogram of nickel while the ring showed a voltammogram that shows great resemblance to the voltammogram of copper.

Key words: Characterization of coins, Jordanian coins, Cyclic voltammograms of coins, Electrochemical characterization

INTRODUCTION

Characterization of coins and metal alloys is an important task that was approached by various techniques. These techniques include scanning electron microscopy (SEM) [1], atomic absorption spectrometry (AAS) [2], laser ablation inductively coupled plasma mass spectrometry (LA-ICP-MS) [3], x-ray diffraction (XRD) [4], energy dispersive x-ray spectroscopy (EDX) [5], neutron activation analysis (NAA) [6], proton-induced x-ray emission (PIXE) [7], Mossbauer microscopy [8] and cyclic voltammetry [9]. Cyclic voltammetry proved itself as a simple, inexpensive technique for characterization of metallic surfaces at ambient conditions. In fact, cyclic voltammetry, is the electrochemical analog, of the UHV electron spectroscopies; Auger and X-ray photon spectroscopy and low energy electron diffraction (LEED) [10]. Cyclic voltammogram provides the whole electrochemical picture for the surface and the produced voltammogram, to an extent, resembles the survey scan in X-ray photon spectroscopy [11].

This paper presents an application of cyclic voltammetry to characterization of Jordanian coins. Jordanian coins are metallic alloys of a very

specific well-known composition. Based on the premise that coins as metallic alloys display very distinct voltammetric features depending on their composition, cyclic voltammetry can be used for characterization of coins.

The present work was undertaken with a major goal of application of cyclic voltammetry to analysis of Jordanian coins. Cyclic voltammetry may provide a sensitive, reliable and inexpensive method for characterization of coins as exemplified by Jordanian coins. Simple home-made potentiostats can be constructed and used to pursue this task. The degree of expertise to run the experiment cannot be compared with any of the above-mentioned techniques.

MATERIALS AND METHODS

Cell, Materials and Electrodes

A potentiostat (Model 273A Princeton Applied Research, EG&G) interfaced to a computer via GPIB card (IEEE). M 270 PAR V.4.41 software was used for experiment control and data acquisition (Princeton Applied Research, EG&G). A conventional H-shape, three-electrode cell equipped with a multiple inlet system for admission of supporting electrolyte and for purging and blanketing the solution with oxygen-free nitrogen was used. The reference electrode was

* To whom all correspondence should be sent:
E-mail: mhourani@ju.edu.jo

Ag/AgCl/[Cl⁻] = 1.0 M and all the potentials were measured and referenced to this electrode. The working electrode was the coin or a pure metal wire of platinum (1.0 mm diameter, 99.99% pure, Johnson Matthey), copper (1.0 mm diameter, 99.99% pure, Goodfellow), and nickel (1.0 mm diameter, 99.99% pure, Goodfellow). The wires were rounded at the end which offered a mark for obtaining a reproducible surface area on immersion beneath the surface of the solution in the working electrode compartment. The coins were collected randomly from the market in addition to new coins obtained from the Central Bank of Jordan (CBJ). The auxiliary electrode was made of platinum (99.99% pure, Johnson Matthey).

All the reagents used were of analytical-reagent grade and were used as received without further purification. The nitrogen or argon gases were G5 grade (99.999% minimum purity) products supplied by International Industrial & Medical Liquid Gas, Jordan). Gas cylinders were coupled with Oxosorb cartridges (Supelco) for removal of residual traces, if any, of oxygen. All solutions were prepared from the reagents dissolved in triply distilled water; the second distillation of which was carried out from basic potassium permanganate solution.

Experimental procedures System cleanliness

The electrochemical cell and all the related glassware and PTFE tubing were cleaned by submerging and soaking in chromic acid solution for a minimum of two hours followed by extensive rinsing with triply distilled water. Platinum electrode was cleaned with freshly prepared hot chromic acid followed by thorough rinsing with triply distilled water.

System cleanliness, including the cell, the PTFE tubes, the electrodes, supporting electrolyte solutions, and purging gas as an integrated system was ensured by reproducing the cyclic voltammogram of polycrystalline platinum electrode in 0.5 M H₂SO₄. The resolution of the hydrogen adsorption/desorption and oxygen adsorption/desorption peaks, the width of the double layer region, and the stability of the voltammogram upon potential cyclization provided enough evidence for system cleanliness. This procedure was followed at the beginning of every set of experiments.

Sample pretreatment

The coin samples were collected randomly from the market while new coins were obtained from

Central Bank of Jordan (CBJ). Copper-coated and copper-based samples were cleaned by immersion in 1 M HNO₃ solution for 10 s. Nickel-coated coin samples were cleaned by dipping in chromic acid solution for few seconds. In both cases, the coins were rinsed extensively with triply distilled water.

The working electrode

The working electrode in our measurements was either a highly pure 1.0 mm-diameter copper wire (Goodfellow, 99.99% pure), a 1.0 mm-diameter nickel wire (Goodfellow, 99.99% pure) or the tested coins. The investigated coins were spot welded to the end of a platinum wire. A consistent surface area was produced by allowing the coin to form a hanging meniscus with the solution. Another alternative was based on using a cell with a side arm where the coin electrode was pressed snugly against the side arm of a specially designed electrochemical cell.

In all cases the electrodes were conditioned between the hydrogen and oxygen evolution limits until the stable voltammogram of a clean surface was produced.

RESULTS AND DISCUSSION

The piaster

The piaster according to the data provided by the CBJ [12] is a copper plated steel coin with a mass of 5.5 g and a 22.00 mm diameter. The specific gravity as determined in our laboratory is 7.9±0.8 g/cm³. Figure 1 shows a representative cyclic voltammogram for the piaster electrode.

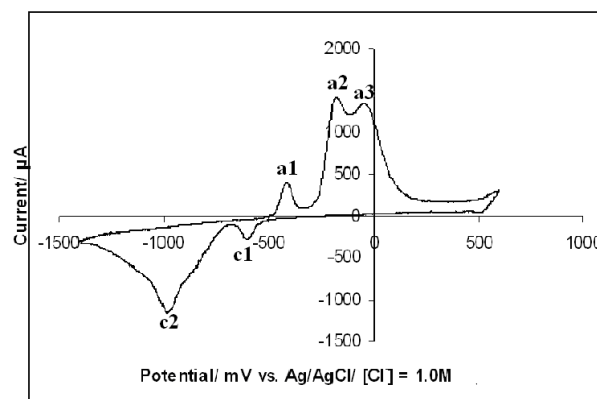


Fig. 1. Cyclic voltammogram of a 1-piaster Jordanian coin in 1.0 M KOH, recorded at scan rate of 50 mV/s.

The variation between the voltammograms of five sample coins was insignificant. The average peak potentials for the three main anodic peaks (peaks labeled a1, a2 and a3 in Figure 1) are -0.417 V, -0.112 V, and -0.050 V respectively. The average cathodic peaks (peaks c1 and c2 in

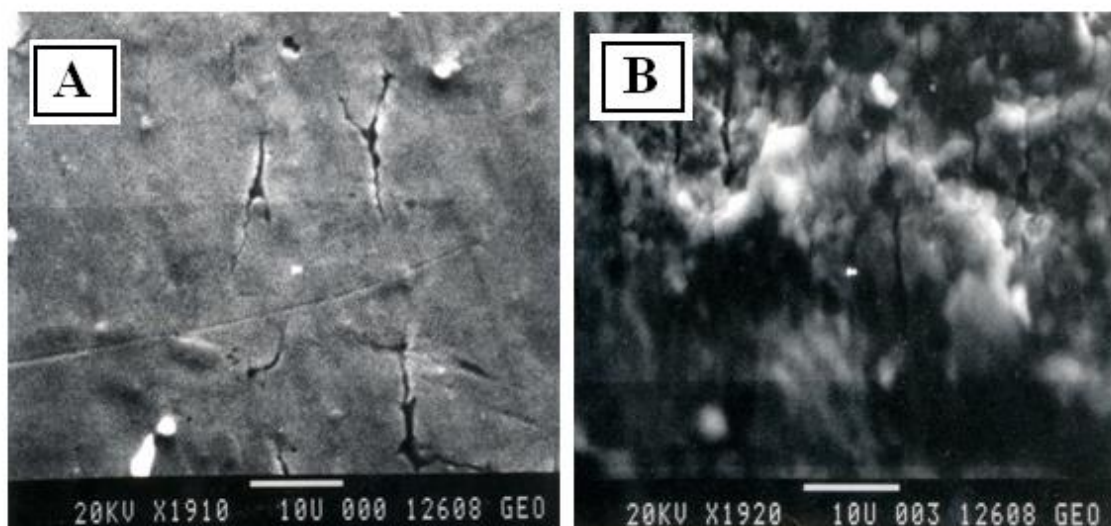


Fig. 2. SEM micrographs of the 1-piaster of A) a new coin surface. B) Old coin surface.

Figure 1) are centered at -0.600 V and -0.991 V respectively. Comparing the voltammograms of the piaster coins with the voltammograms of polycrystalline copper metal revealed that the voltammograms of the piaster coins were very similar to the voltammogram of polycrystalline copper electrode [13].

Investigation of peak current (i_p) as a function of the scan rate revealed that all peak currents are proportional to the scan rate rather than $(\text{scan rate})^{1/2}$ which ensures that all peaks are associated with surface processes [11]. Variation of scan rate between 50 and 150 discloses that the best scan rate in terms of the resolution of the peaks is around 50 mV/s.

Figure 2 shows the SEM micrographs for one of the sample coin collected from the market (referred to as the old coin) and the voltammogram for a coin obtained from CBJ (referred to as the new coin). The micrographs indicate that the surface of the old coin is rougher than the new coin. Chemical etching in nitric acid, however, seems to reduce the variation between the voltammograms of the coin samples.

The 10-piaster, the 5-piaster coins and the 2.5-piaster coins

The composition of the 2.5-, 5-, and 10-piaster coins as declared by CBJ is nickel-plated steel. Since these coins have the same chemical composition, only characterization of the 5-piaster coin was conducted.

The 5-piaster coin weighs 5.00 g, has a disk shape with 26.00 mm diameter.

Figure 3 shows an example voltammogram for the 5-piaster coin. The voltammogram shows two

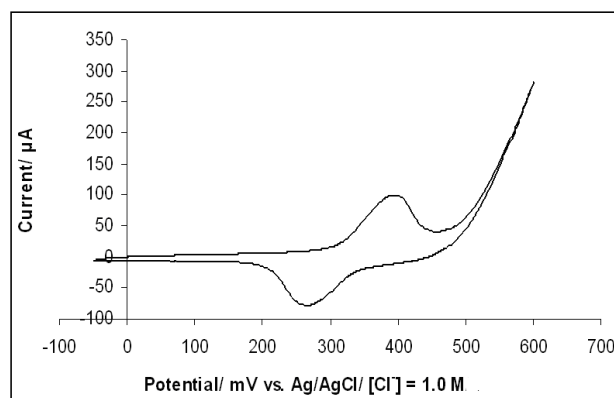


Fig. 3. Cyclic voltammogram of the 5-piaster Jordanian coin in 1.0 M KOH, recorded at scan rate of 50 mV/s.

peaks; an anodic peak and a cathodic peak related to surface oxidation and reduction of the surface oxide. The variation between the peak potentials for the different samples is insignificant. The average peak potential for the anodic peak is 0.399 ± 0.005 V while the average peak potential for the cathodic peak is 0.28 ± 0.01 V.

The voltammogram is similar to the voltammogram of nickel electrode produced under the same experimental conditions. The peak potentials of the sample coins and the nickel wire have the same anodic and cathodic peaks potentials but they differ in the peak sharpness and the peak width. The peak width of the nickel-plated sample coins is larger than that of the pure polycrystalline nickel electrode.

Investigation of the peak heights; the anodic peak current, i_{pa} , and the cathodic peak current, i_{pc} , revealed that i_{pa} and i_{pc} are proportional to the potential scan rate which indicates that the peaks on the voltammograms are associated with surface processes rather than bulk processes.

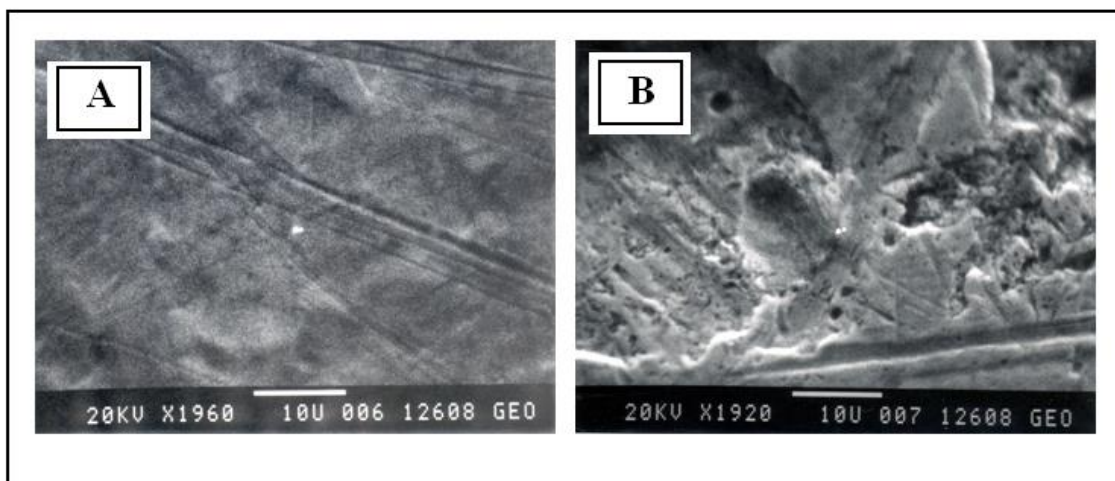


Fig. 4. SEM micrograph of the 5-piaster coin surfaces surface of A) a new 5-Piaster coin.B) an old 5-Piaster coin.

Figure 4 shows the SEM micrographs for an old coin collected from the market along with the SEM voltammogram of a new coin obtained directly from CBJ. The figure shows higher roughness degree for the old coin which is attributed to the effect of oxidation and handling between people hands. Despite the difference between the coins samples in roughness but there was no difference in the voltammograms because the voltammograms are insensitive to macroscopic long-range topographic differences. Moreover, it seems that the outer layers were removed by the applied chemical etching.

The quarter (25-piaster) coin

The quarter (25-piaster coin) is an alloy composed of 5.5% nickel, 24.5% zinc and 70.0% copper. The coin has a diameter of 26.50 mm, a mass of 7.40 and a density of 8.3 ± 0.8 g. Figure 5 shows a representative voltammogram for the quarter coin

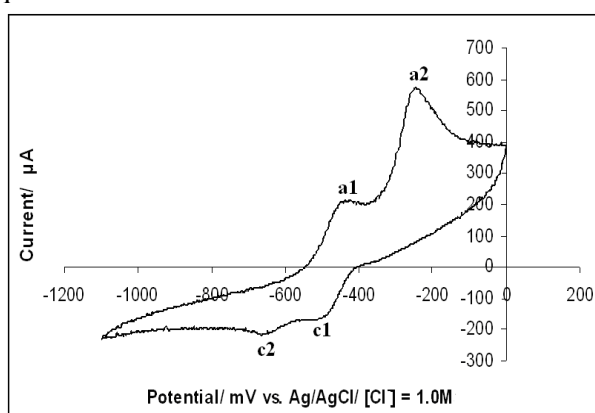


Fig. 5. Cyclic voltammogram of the quarter Jordanian coin in 1.0 M KOH, recorded at scan rate of 20 mV/s

The voltammogram shows two anodic peaks and their counter cathodic peaks. The peak potentials are $E_{pa1} = -0.458$ V, $E_{pa2} = -0.263$ V, $E_{pc1} = -0.660$ V and $E_{pc2} = -0.483$ V). There is an insignificant change between investigated samples in terms of the peak potentials. The standard deviation values for the four peaks E_{pa1} , E_{pa2} , E_{pc1} , and E_{pc2} are 0.003, 0.002, 0.002 and 0.004 respectively. The dependency of i_p for the four peaks was found to be, $i_p \propto v$, where v is the potential scan rate. The optimal scan rate in terms of peak resolution was 20 mV/s.

Figure 6 shows the SEM micrographs of two quarter coin samples, one of them is an old sample, collected from the market and another new sample supplied by CBJ. The surface of the old sample looks very rough compared with the SEM of the new coin. Though there is a difference between the SEM micrographs of the coins, the voltammograms were not affected by the roughness of the samples because cyclic voltammetry is not sensitive to macrotopography of the surface and the chemical etching was efficient in removing the impurities and the oxide from the outer surface layers.

The half-dinar coin

The half-dinar Jordanian coin is composed of an outer ring and an inner disk. The outer ring is composed of 29% copper, 2% nickel and 6% aluminum while the inner ring is composed of 75% copper and 25% nickel. The mass of the half-dinar coin is 9.60 g, its diameter is 29.00 mm and its density is 5.7 ± 0.8 g/cm² for the outer ring and 8.3 ± 0.8 g/cm³ for the inner disk.

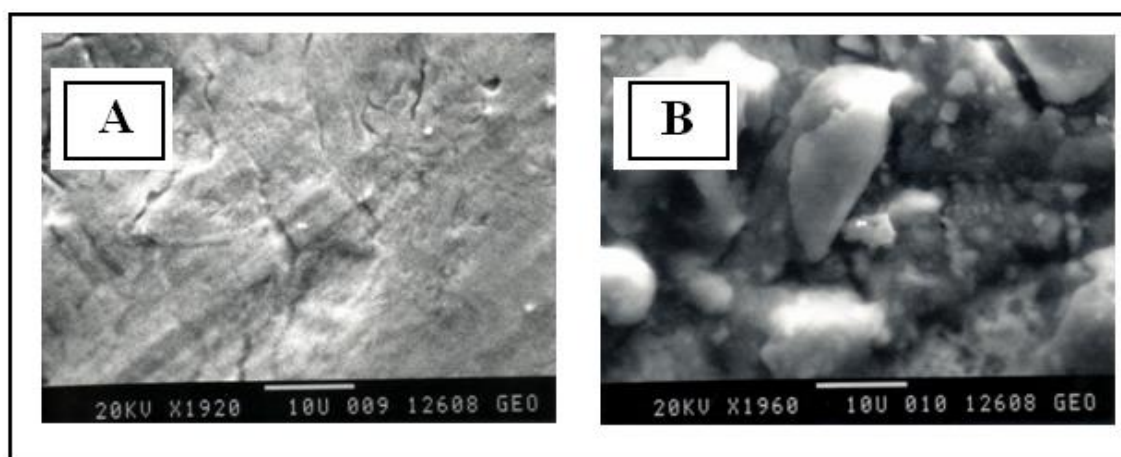


Fig. 6: SEM micrograph of the 25-piaster (quarter) coin surface of A) a new 25-Piaster coin B) an old 25-Piaster coin.

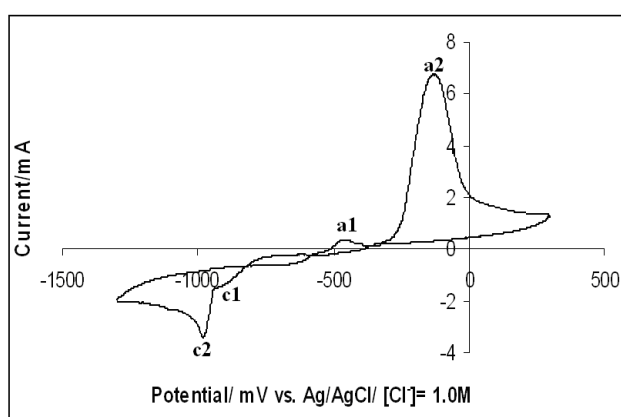


Fig. 7. Cyclic voltammogram of outer ring of the half-dinar Jordanian in 1.0 M KOH, recorded at scan rate of 10 mV/s.

Figure 7 shows a distinct voltammogram of the outer ring of the half-dinar coin. The voltammogram, though displays a similarity to the voltammogram of pure copper electrode, it shows unique distinct voltammetric features of the alloy it represents. There are two anodic peaks, one of them is a small peak appears at -0.450 V (a1) and another prominent anodic peak centered at -0.124 V (a2). On the negative-going scan, two cathodic peaks appear at -0.992 (c1) and -1.098 V (c2). The variation in peak potentials is insignificant as indicated by the standard deviation values, ± 3 , ± 5 , ± 6 , and ± 2 mV for E_{pa1} , E_{pa2} , E_{pc1} , and E_{pc2} respectively. The peak potentials were independent of the scan rate as expected from surface processes while the peak currents were directly proportional to the scan rate, $i_p \propto v$.

Figure 8 shows a representative voltammogram of the inner disk of half-dinar coin. The voltammogram shows only one anodic peak and its counter cathodic peak. The anodic peak is centered

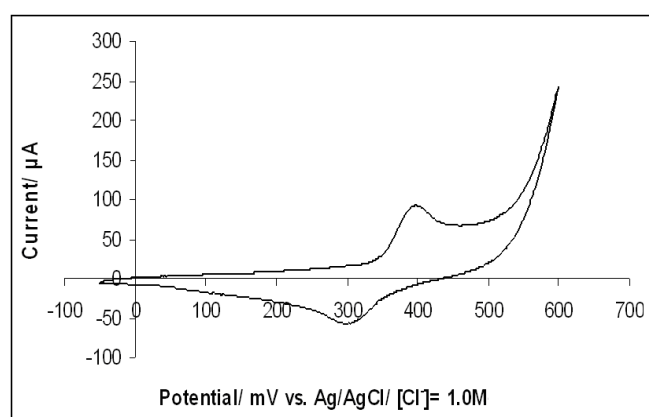


Fig. 8. Cyclic voltammogram of the inner ring of the half-dinar Jordanian coin in 1.0 M KOH, recorded at scan rate of 10 mV/s.

at 0.400 V while the cathodic peak is centered at 0.300 V. The variation between the six tested samples was insignificant as indicated by the values of the standard deviation for the anodic and cathodic peaks, ± 0.005 and ± 0.004 respectively. The peak potentials were also independent of the scan rate while peak currents showed direct proportionality with scan rate which indicates that these peaks are associated with surface rather than bulk processes. Though the coin is composed of 75% copper and 25% nickel, the voltammogram displays great similarity to nickel. This result is not unexpected because nickel is electrochemically more active than copper.

CONCLUSIONS

The cyclic voltammograms for the tested Jordanian coins were obtained under optimized conditions in terms of the composition of the supporting electrolyte and potential scan rates. A distinct voltammogram was obtained for each coin

that is insensitive to the lifetime of introduction of the coin to the market. The voltammetric features were very indicative of the coin. When combined with the other physical properties of the coin like the mass, the diameter, and specific gravity, cyclic voltammetry can be used as an inexpensive, reliable, simple and fast method for characterization of coins.

Acknowledgements: *The authors would like to thank Miss Wafa Hourani for the invaluable comments and revising the manuscript.*

REFERENCES

1. I. Calliari, M. Magrini, A. Zambon, P. Guerriero, R. Martini, *X-Ray Spectrum.*, **28**, 68 – 90 (1999).
2. A. Denker, W. Bohne, J. Opitz-Coutureau, J. Rauschenberg, J. Röhrich, E. Strub, *Nuclear Instr. Methods Physics Research B*, **329**, 65-70 (2005).
3. M. Ponting, J.A. Evans, V. Pashley, *Archaeometry*, **45**, 591 (2003)
4. G. Giovannelli, S. Natali, B. Bozzini, A. Siciliano, G. Sarcinelli, R. Vitale, *Archaeometry*, **47**, 817 (2005)
5. Lei Junfeng, Zeng Libo, Tong Hua, Yu Xiaoming, Liu Juntang, Hu Jiming, *Microchim. Acta*, **142**, 123 (2003).
6. E.H. Bakraji, A. Sarhell, *Nuclear Science Techniques*, **10**, 61 (1999)
7. V. Vijayan, R.K. Choudhury, C.B. Patel, *Int.J. PIXE*, **15**, 323 (2005).
8. A. Kyek, F.E. Wagner, G. Lehrberger, Q.A. Pankhurst, B. Ziehaus, *Hyperfine Interactions*, **126**, 235 (2000).
9. N. Souissi, L. Bousselemi, S. Khosrof, E. Triki, *Materials Corrosion*, **55**, 284 (2004)
10. J. E. Soto, D. Li, J. Sanabria, M.P. Soriaga, *J. Mol. Struct.*, **890**, 298 (2008)
11. A. Bard, L. Faulkner, *Electrochemical Methods: fundamentals and Applications*, Wiley: New York, 2004.
12. www.cbj.gov.jo
13. S.M. Abd el Haleem, Badr Ateya, *J. Electroanal. Chem*, **117**, 309, (1981).

ЕЛЕКТРОХИМИЧНО ОХАРАКТЕРИЗИРАНЕ НА ЙОРДАНСКИ МОНЕТИ

М.К. Хурани , А.И. Уехбе

Департамент по химия, Йордански университет, Аман 1942 – Йордания

Постъпила на 5 юли, 2012 г.; Приета на 12 февруари, 2013 г.

(Резюме)

Използвана е циклична волтаперометрия за охарактеризирането на йордански монети. Четири различни монети с различен състав са изследвани: пиастр, шелинг (от 5 пиастра), куартер и половин динар. Монетите са взети от обращение или са взети като нови от Централната банка на Йордания. Всяка от тях показва различна волтаперограма, което се обяснява с различния им състав. Волтаперограмите представляват “електрохимични спектри” или волтаперични “подписи” на монетите. Волтаперограмата на пиастра, който представлява покрит с мед неръждаема стомана е твърде сходна с тази на медта. Шелингът, който представлява покрит с никел неръждаема стомана има волтаперограма сходна с тази на никела. Останалите монети също показват волтаперограми, сходни на тези на металите, от които са направени.

Molecular iodine catalyzed synthesis of some biologically active dihydroperimidines

A. Mobinikhaledi^{1*}, F. Sasani¹, A. Hamta², S.M. Shariatzadeh³

¹ Department of Chemistry, Faculty of Science, Arak University, Arak 38156-8-8349, Iran

² Department of Biology, Faculty of Science, Arak University, Arak 38156-8-8349, Iran

³ Science and Research Branch of Islamic Azad University, Tehran-Iran

Received March 27, 2012; Revised February 7, 2013

Several perimidines were prepared in good to high yields by reaction of 1,8-diaminonaphthalene and aromatic aldehydes in the presence of molecular iodine as a highly efficient catalyst. This environmentally benign and clean synthetic procedure offers several advantages, such as high yields, short reaction times and easy workup. Antibacterial activity of these compounds was evaluated using *Staphylococcus aureus* (mm) and *E. coli* (mm) bacterial strains.

Keywords: Iodine, Catalyst, Perimidine, Antibacterial

INTRODUCTION

There has special interest in the chemistry of perimidines due to a wide range of biological activities exhibited by these compounds [1-5]. Perimidines have also used as intermediates in organic synthesis [6]. Variety methods have been reported for the synthesis of perimidines in literatures [2, 6-15]. The traditionally synthesis of such compounds is still ordinary alongside modern synthesis methods. The general method for the synthesis of perimidines involves the condensation reaction of 1,8-diaminonaphthalene with a carbonyl group in the presence of a Lewis or mineral acid. However, in spite of their potential utility, many of these methods are associated with some limitations and generally need strong acidic conditions, expensive or non-available reagents, prolonged reaction times and high temperatures. Thus, the introduction of new methods and /or further work on technical improvements to overcome these limitations is still needed

The mild Lewis acidity of molecular iodine as a catalyst increased its applications in organic synthesis. It has received substantial attention as a non-toxic and commercially available catalyst for synthesis of benzothiophens [16], bis indoles [17], quinolines [18], esterification [19], phenanthrimidazoles[20] and indazoles [21].

In view of these reports and also due to continuation of our studies on synthesis of perimidines [13,14], we wish to report a simple,

efficient and eco-friendly one pot practical method for the synthesis of perimidines by reaction of 1,8-diaminonaphthalene and aromatic aldehydes in the presence of molecular iodine. We also report the biological activity of these compounds.

EXPERIMENTAL

Firstly, to evaluate the catalytic efficiency of molecular iodine, the reaction of 1,8-diaminonaphthalene and 4-nitrobenzaldehyde was studied by using 2 mol% molecular iodine, as a catalyst, in ethanol at room temperature. For optimization of the amount of catalyst, this reaction was carried out as a model, and different amounts of catalyst were tested to increase the yield of product under the same conditions. The amount of catalyst less than 7 % wt. could catalyze the reaction, but it needed a longer reaction time and yields are low. On the other hand, the amount of catalyst over 7 % wt. did not improve the yield of product (Table 1). To examine the effect of solvent for this model reaction, the reaction was carried out in some organic solvents including C₂H₅OH, CH₃OH, CH₃CN, DMSO and DMF at room temperature with 7 mol% of catalyst for 7 min. As Table 1 shows, the most suitable solvent for this procedure is ethanol.

To examine the generality of this simple procedure, several aromatic aldehydes were treated with 1,8-diaminonaphthalene in the presence of 7 mol% of the molecular iodine as a catalyst (Figure 1).

* To whom all correspondence should be sent:
E-mail: akbar_mobini@yahoo.com

Table 1. Reaction of 1,8-diaminonaphthalene with 4-nitrobenzaldehyde using different amounts of catalyst and solvent at room temperature.

Entry	Catalyst load	Solvent	Time (min)	Yield (%) ^a
1	2	EtOH	25	55
2	3	EtOH	20	77
3	5	EtOH	27	79
4	7	EtOH	7	93
5	10	EtOH	8	80
6	15	EtOH	6	87
7	7	MeOH	7	61
8	7	CH ₃ CN	7	72
9	7	DMSO	7	63
10	7	DMF	7	65

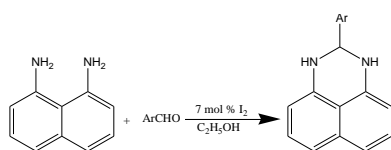
^a Isolated yield

Fig. 1. The scheme preparation of perimidines.

Table 2. Reaction of 1,8-diaminonaphthalene with aromatic aldehydes prompted by 7 mol% molecular iodine catalyst in C₂H₅OH.

Compound	Ar	Time (min)	Yield (%) ^a	M.P (°C)
3a	C ₆ H ₅	40	84	105-106 (101-103) ^b
3b	4-OHC ₆ H ₄	60	85	162-164 (161-163) ^b
3c	4-OCH ₃ C ₆ H ₄	20	65	156-158 (151-152) ^c
3d	2-ClC ₆ H ₄	25	95	115-119 (116-118) ^b
3e	3-ClC ₆ H ₄	30	80	143-146
3f	3-BrC ₆ H ₄	20	55	166-168 (165-166) ^d
3g	4-BrC ₆ H ₄	12	96	115-117 (138-140) ^c
3h	2-NO ₂ C ₆ H ₄	8	98	183-185 (191-192) ^c
3i	3-NO ₂ C ₆ H ₄	10	87	180 (188-190) ^b
3j	4-NO ₂ C ₆ H ₄	7	93	247-249 (>200) ^e
3k	4-FC ₆ H ₄	20	82	182-183 (180-182) ^b
3l	4-CH ₃ C ₆ H ₄	7	62	165 (161-163) ^b
3m	2-OH,4-BrC ₆ H ₃	15	92	112-117 (164-166) ^b
3n	3,4-(OCH ₃) ₂ C ₆ H ₃	45	88	205

a: Isolated yield, b:[ref 13], c:[ref 22], d:[ref 23], e:[ref 24].

The results of this study are presented in Table 2. We were pleased to find that the reaction of different aromatic aldehydes with 1,8-diaminonaphthalene in the presence of molecular iodine afforded corresponding dihydroperimidines **3(a-n)** in good to excellent yields. However, aliphatic aldehydes such as formaldehyde or acetaldehyde were also examined under the same conditions, but the responding products were isolated in low yields (<10%). Almost all synthesized compounds are known and identified

using IR and NMR spectroscopy and also by comparison with their authentic samples.

Melting points were determined using an electro thermal digital apparatus and are uncorrected. NMR spectra were recorded on a Bruker 300 MHz spectrometer. IR spectra were performed on a Galaxy FT-IR 5000 spectrophotometer. Microanalyses were performed by the Elemental Analyzer (Elemental, Vario EL III) at the Arak University. The Microanalyses results were agreed favorably with the calculated values. Reaction progress was routinely monitored by thin layer chromatography using silica gel F₂₅₄ aluminum sheets (Merck).

The microbial strains are identified strains and were obtained from the [Pasteur Institute of Iran](#). The bacterial strains studied are *Staphylococcus aureus* (RTCC, 1885), and *Escherichia Coli* (ATCC, 35922).

Table 3. Zone inhibition of dihydroperimidines (**3a-n**).

E. coli (mm)	Staphylococcus aureus (mm)	Materials
--	9±0.1 mm	3a
--	15±0.2 mm	3b
9±0.1 mm	--	3c
--	--	3d
--	8±0.3 mm	3e
--	--	3f
--	--	3g
--	--	3h
--	--	3i
--	--	3j
--	--	3k
--	--	3l
--	12± 0/2 mm	3m
--	11±0.3 mm	3n
--	--	DMSO
Gentamicin 11 mm	Gentamicin mm 11	Standard drugs

-- indicates resistance of bacteria to compounds. Discs were inoculated with 5 mg of the chemicals dissolved in DMSO. The inhibition zone numbers are the average of three times independent experiments.

Antibacterial activity of synthesized perimidines was tested against *Staphylococcus aureus* (mm) and *E. coli* (mm) bacterial strain and the results presented in Table 3. The verification of antibacterial screening data revealed that compounds **3a**, **3b**, **3e**, **3m**, and **3n** have bactericidal properties against *Staphylococcus aureus*. Also these compounds have bactericidal properties against *E. coli* as a gram negative. The maximum and minimum antibacterial activities

against *Staphylococcus aureus* were related to compounds **3b** and **3e**, respectively.

RESULTS AND DISCUSSION

Antibacterial activities

The agar disk diffusion method was used for this purpose. In each test 5mg of chemically synthesized materials was dissolved in 250 μ l of DMSO as a solvent and 100 μ l of known concentration of the test compounds was introduced onto the disks (0.7 cm) and then allowed to dry. The disk was completely saturated with the test compounds. Then the disk was introduced onto the upper layer of the medium with the bacteria. 100 μ l of solvent (DMSO) was added to the blank disk and implanted as a negative control on each plate along with the standard drugs. The plates were incubated overnight at 37°C. The inhibition zones were measured and compared with the controls. The results are given in Table 3.

Typical procedure for preparation of aryldihydroperimidines (3a-n)

To a solution of 1,8-naphthalenediamine (1 mmol) and corresponding aromatic aldehyde (1 mmol) in ethanol (15–20 mL) was added molecular iodine (7 mol %). The reaction mixture was stirred at room temperature for desired time (Table 2). The progress of reaction was monitored by TLC. After completion of reaction, water (15–20 mL) was added to produce the product, which then filtered and washed with cold water and air dried.

Selected spectra data

4-(2,3-Dihydro-1Hperimidine-2-yl)phenol

(3b). IR (KBr): 3396, 3331, 3045, 1600, 1517, 1412 cm^{-1} . ^1H NMR (DMSO, 300 MHz): δ 5.23 (s, 1H, CH), 6.45–7.41 (m, 12H, CH_{arom} , 2NH), 9.50 (s, 1H, OH). ^{13}C NMR (DMSO, 75 MHz): δ 66.8, 104.7, 112.9, 115.3, 115.6, 127.3, 129.6, 132.4, 134.9, 143.9, 158.2. Anal Calcd for $\text{C}_{17}\text{H}_{14}\text{N}_2\text{O}$: C, 77.84; H, 5.38; N, 10.68%. Found: C, 77.55; H, 5.50; N, 10.64%.

2-(3-Chlorophenyl)-2,3-dihydro-1H-perimidine (3e). IR (KBr): 3393, 3354, 3045, 2806, 1607, 1416 cm^{-1} . ^1H NMR (DMSO, 300 MHz): δ 5.39 (s, 1H, CH), 6.48–7.63 (m, 12H, CH_{arom} , 2NH). ^{13}C NMR (DMSO, 75 MHz): δ 65.8, 104.98, 112.9, 116.0, 127.0, 127.4, 128.2, 128.8, 130.6, 133.4, 134.8, 143.1, 145.1. Anal Calcd for $\text{C}_{17}\text{H}_{13}\text{N}_2\text{Cl}$: C, 72.72; H, 4.68; N, 9.98%. Found: C, 72.86; H, 4.51; N, 10.27%.

2-(2-Nitrophenyl)-2,3-dihydro-1H-perimidine (3h). IR (KBr): 3358, 3231, 2853, 1602, 1519, 1416, 1334 cm^{-1} . ^1H NMR (DMSO, 300 MHz): δ 5.82 (s, 1H, CH), 6.51–8.05 (m, 12H, CH_{arom} , 2NH). ^{13}C NMR (DMSO, 75 MHz): δ 61.4, 105.2, 112.5, 116.2, 124.6, 127.5, 130.0, 130.4, 134.0, 134.7, 136.9, 142.5, 149.4. Anal Calcd for $\text{C}_{17}\text{H}_{13}\text{N}_3\text{O}_2$: C, 70.08; H, 4.51; N, 14.43%. Found: C, 69.98; H, 4.59; N, 14.32%.

2-(3-Nitrophenyl)-2,3-dihydro-1H-perimidine (3i). IR (KBr): 3345, 3227, 1603, 1528, 1416, 1350 cm^{-1} . ^1H NMR (DMSO, 300 MHz): δ 5.56 (s, 1H, CH), 6.53–8.45 (m, 12H, CH_{arom} , 2NH). ^{13}C NMR (DMSO, 75 MHz): δ 65.3, 105.1, 112.9, 116.1, 123.1, 123.7, 127.4, 130.4, 134.8, 135.1, 142.7, 145.0, 148.1. Anal Calcd for $\text{C}_{17}\text{H}_{13}\text{N}_3\text{O}_2$: C, 70.08; H, 4.51; N, 14.43%. Found: C, 70.20; H, 4.53; N, 14.51%.

2-(3,4-Dimethoxyphenyl)-2,3-dihydro-1H-perimidine (3n). IR (KBr): 3350, 2997, 1601, 1416 cm^{-1} . ^1H NMR (DMSO, 300 MHz): δ 3.77 (s, 3H, CH_3), 3.78 (s, 3H, CH_3), 5.29 (s, 1H, CH), 6.47–7.22 (m, 11H, CH_{arom} , 2NH). ^{13}C NMR (DMSO, 75 MHz): δ 55.9, 56.5, 68.8, 104.8, 111.7, 113.0, 115.8, 120.7, 127.3, 134.5, 134.9, 143.8, 149.2, 149.59. Anal Calcd for $\text{C}_{19}\text{H}_{18}\text{N}_2\text{O}_2$: C, 74.49; H, 5.92; N, 9.14%. Found: C, 74.40; H, 5.99; N, 9.20%.

REFERENCES

1. N.M. Starshikoy, F.T. Pozharskii, *Chemistry of Heterocyclic Compounds.*, **9**, 922 (1975).
2. F.T. Pozharskii, V.V. Dalnikovskaya, *Russ. Chem. Rev.*, **50**, 816 (1981).
3. X. Bu, L.W. Deady, G.J. Finlay, B.C. Baguley, W.A. Denny, *J. Med. Chem.*, **44**, 2004 (2001).
4. K.Undheim, T. Benneche, *Comprehensive Heteocyclic Chemistry*, A.R.Katritzky, C.W. Ress, E.F.V. Scriven, Pergamon Oxford, Vol 6, 1996.
5. D.P. Panchasara, S. Pande, *E-J. Chem.*, **6**, S91(2009).
6. A. Mobinikhaledi, M.A. Amrollahi, N. Foroughifar, H. Fathinejad, *Asian. J. Chem.*, **17**, 2411 (2005).
7. I. Yavari, I. M. Adib, F. Jahani-moghaddam, H.R. Bijanzadeh, *Tetrahedron.*, **58**, 6901 (2002).
8. J.J. Van den Eynde, F. Delfosse, A. Mayence, Y.V. Haverbeke, *Tetrahedron.*, **51**, 5813 (1995).
9. J.B. Hendrickson, M.S. Hussoin, *J. Org. Chem.*, **52**, 4137 (1987).
10. L.W. Deady, T. Rodemann, *J. Heterocyclic. Chem.*, **35**, 1417 (1998).
11. U.T. Mueller-Westerhoff, S. Vance, DI. Yoon, *Tetrahedron*, **47**, 909 (1991).
12. A. Mobinikhaledi, N. Foroughifar, R. Goli, *Phosphorus, Sulfur & Silicon.*, **180**, 2549 (2005).

13. A. Mobinikhaledi, N. Foroughifar, N. Basaki, *Turk. J. Chem.* **33**, 1 (2009).
14. A. Mobinikhaledi, J. Stell, *Synth. Reac. Inorg. Mat.* **39**, 133 (2009).
15. Song-Lin, Z., Jun-Min, Z., *Chinese J. Chem.*, **26**, 185 (2008).
16. K.O. Hassian, B.L. Flynn, *Org. Lett.*, **5**, 4377 (2003).
17. B.P. Bandgar, K.A. Shaik, *Tetrahedron. Lett.*, **44**, 1959 (2003).
18. Wu. J, Xia., H.G, Gao.K, *Org. Biomol. Chem.*, **4**, 126 (2006).
19. K. Ramalinga, P. Vijayalakshimi, T.N.B. Kaimal, *Tetrahedron.Lett.*, **43**, 879 (2002).
20. H. Behmadi, M. Roshani, S.M. Saadati, *Chinese. Chem. Lett.*, **20**, 5 (2009).
21. D.D. Gaikwad, S. Abed, P.P. Pawar, *Int. J. Chem. Tech. Res.*, **10**, 442 (2009).
22. D.P. Pop, A. Catala, *J. Heterocyclic. Chem.* **1**, 108 (1964).
23. W. Wasulko, A.C. Noble, F.D. Popp, *J. Med. Chem.* **19**, 599 (1966).
24. O. Maloshitskaya, J. Sinkkonen, V.V. Ovcharenko, K.N. Zelenin, K. Pihaja, *Tetrahedron.*, **60**, 6913 (2004).

СИНТЕЗА НА НЯКОИ БИОЛОГИЧНО-АКТИВНИ ДИХИДРОПЕРИМИДИНИ, КАТАЛИЗИРАНИ ОТ МОЛЕКУЛЕН ЙОД

А. Мобинихаледи¹, М.А. Бодаги Фард¹, Ф. Сасани², М.А. Амролахи³

¹Департамент по химия, Научен факултет, Университет в Арак, Арак, Иран

²Департамент по химия, Научен факултет, Университет в Язд, Язд, Иран

³Научен и изследователски клон на ислямския университет "Азад", Техеран, Иран

Постъпила на 27 март, 2012 г.; коригирана на 7 февруари, 2013 г.

(Резюме)

Получени са няколко перимидини с висок добив при реакцията на 1,8-диаминонафтаден с ароматни алдехиди в присъствие на молекулен йод като високо-ефективен катализатор. Тази екологично издържана и чиста процедура предлага няколко предимства: висок добив, кратко време за реакция и опростена работа. Оценена е анти-бактериалната активност на тези препарати върху бактериалните щамове *Staphylococcus aureus* (mm) и *Escherichia coli* (mm).

Electrodeposition of Ag and Ag-Ni powders in potentiostatic and pulse potential modes

K. Ignatova

University of Chemical Technology and Metallurgy, Sofia 1756, Bulgaria

Received July 24, 2012; Revised September 30, 2012

The kinetics of electrodeposition and the microstructure of pure Ag and alloyed Ag-Ni powders were investigated depending on the type of electrolyte and conditions for deposition. It was found out that in acid nitrate electrolyte the Ag powders are white after deposition and have a more determined crystal structure. In complex ammonia-nitrate electrolyte grey Ag powders with irregularly shaped particles and higher dispersion are formed. In ammonia-citrate electrolyte the deposited Ag powders are dark grey to black in color, with typical dendrite structure of particles and susceptible to agglomeration. Each type of Ag powder consists of a single phase, i.e. silver phase with cubic face-centered lattice (fcc). The advantages of ammonia-citrate electrolyte compared to ammonia-nitrate one for obtaining fine dispersed Ag-Ni powders are proved. The use of higher cathode potentials in potentiostatic mode and pulse frequency up to 1000 Hz in pulse potential mode in the ammonia-citrate electrolyte results in decreasing the average size of particles to approximately 1 μm and increasing the content of nickel up to 12-18%.

Key words: Alloyed metal powders, Pulse potential mode, Morphology, Phase structure

1. INTRODUCTION

Silver powder and alloyed silver-based powders are used in many industrial areas, e.g., in electronics for preparation of electroconductive pastes and solders [1, 2], in silicone solar cells [22], as well as in storage battery manufacturing as active mass in silver-nickel batteries [2]. Silver-nickel powder may be used as a substitute for silver powder, which prolongs its operational life and results in some savings [3].

Electrolysis is a method allowing direct preparation of alloyed metal powders of high purity and dispersibility, controlled phase and composition [4–6]. The application of non-stationary (impulse) current modes [7, 8], the use of complex electrolytes and the introduction of special additives [6, 8] affecting the crystal growth are becoming more and more frequently applied means in order to meet the high requirements for maximum dispersity and morphological homogeneity of the powders. Moreover, electrolysis is the only possible method for obtaining some alloyed metal powders [9].

It is known that Ag is one of the metals easily obtained in powder form [10-13], unlike Ni that belongs to the group of metals that are most difficult to obtain in powder form through electrolysis [9, 23]. The Ag powder precipitates

from acid nitrate electrolyte [12, 13]; there are evidences, however, that very fine powders can be obtained from ammonia solutions of some silver salts [10, 14]. Depending on the conditions for deposition, Ag powders of various morphologies and colors from white to black can be obtained. In solutions free of organic additives the Ag powder is usually black in the beginning and changes its color to white when the current is turned off [14-16]. Additives like gelatin or composition of gelatin and sodium thiosulphate in a ratio of 1:10 [14-16] either impede or partially prevent this transformation. In some sources [16, 17] the change of color upon turning off the current is explained with re-crystallization from hexagonal to cubic singonia with simultaneous aggregation of micro-crystals into larger ones.

Ag-Ni powders can be deposited from ammonia electrolyte [21] and from sulphamin acid electrolyte [24]. The investigations carried out point that in the first case powders with high nickel content (up to 30%) can be obtained, while in the second case the content of Ni in the Ag-Ni powders does not exceed 5%.

This paper aims at studying the effect of three different electrolyte compositions (acid nitrate, ammonia-nitrate and ammonia-citrate) on the kinetics of deposition, morphology and phase structure of pure Ag powder in potentiostatic mode, as well as to examine the kinetics of deposition, morphology and elemental composition of Ag-Ni

*All correspondence should be sent to:
E-mail: katya59ignatova@gmail.com

powder in ammonia-nitrate and ammonia-citrate electrolyte upon application of potentiostatic and

2. EXPERIMENTAL CONDITIONS

The experiments were carried out at ambient temperature ($t=20^{\circ}\text{C}$) in a three-electrode cell with a total volume of 150 ml. Platinum was used as counter-electrode, silver as cathode (1 cm^2 disk surface), and saturated calomel electrode ($E_{\text{SCE}}=0.241\div 0.244\text{ V}$) as reference electrode.

The investigation of the kinetics of processes and electrodeposition of Ag powder was carried out in three different compositions of electrolytes, as follows:

Electrolyte No1 – acid nitrate: 8 g dm^{-3} AgNO_3 ; 15 g dm^{-3} NaNO_3 ; 64% HNO_3 up to $\text{pH}=4.5$;

Electrolyte No2 – ammonia-nitrate: 8 g dm^{-3} Ag (as AgNO_3); 15 g dm^{-3} NH_4NO_3 ; 25% NH_3 up to $\text{pH}=10.0$;

Electrolyte No3 – ammonia-citrate: 8 g dm^{-3} Ag (as AgNO_3); 50 g dm^{-3} Na citrate (from citric acid, $\text{C}_6\text{H}_8\text{O}_7$ and NaHCO_3); 25% NH_3 up to $\text{pH}=10.0$.

The investigation of the kinetics of processes and electrodeposition of Ag-Ni powders was carried out by adding 20 g dm^{-3} $\text{Ni}(\text{NO}_3)_2\cdot 2\text{H}_2\text{O}$ to compositions No2 and No3 (the resulting compositions are designated as Electrolytes No2* and 3*, respectively).

The kinetics of deposition of Ag and Ag-Ni was studied by the method of potentiodynamic polarization dependencies ($v=30\text{ mV s}^{-1}$); the rate of powder formation was determined by the method of chronoamperometry with potentiostatic Wenking (Germany).

The pulse electrodeposition of the coatings was carried out using rectangular pulses of potential generated by a pulse generator connected to the input of a specially designed for the purpose potentiostat connected to the three-electrode cell. The average values of polarization, $\Delta\bar{E}$, (calculated as a difference between the potential at the current and the equilibrium potential) and the average current, I_{av} , were measured using a digital voltmeter with high input resistance and milliammeter. The amplitude values of the polarization, ΔE_p , were measured using an oscilloscope.

The relation between the average ($\Delta\bar{E}$) and amplitude (ΔE_p) polarization values at potentiostatic rectangular pulse conditions is: $\Delta\bar{E} = \Theta\Delta E_p$, where $\Theta = \tau_p / (\tau_p + \tau_z)$, τ_p - pulse time, and τ_z - time between the pulses. At each pulse frequency ($f = 1/T$, Hz; $T = \tau_p + \tau_z$), and $\Theta = 0,5$ the relations $\Delta\bar{E} - I_{\text{av}}$ and $\Delta E_p - I_{\text{av}}$ were calculated. The investigation of morphology and elemental

composition is carried out using SEM and Energy Dispersive Spectral Analysis (EDSA), respectively, on an equipment of Oxford Instruments, JSM-6390-Jeol.

The phase and crystal structure of the deposited coatings were studied using automatic Philips PW 1050 X-Ray diffractometer, equipped with a secondary graphite monochromator for Cu $K\alpha$ radiation, and scintillation counter. The diffractograms were recorded in the 2-theta range from 10° to 100° with a step of 0.04° and a counting time of 1s per step.

3. RESULTS AND DISCUSSION

3.1. Electrodeposition kinetics of Ag and Ag-Ni

3.1.1. Electrodeposition of Ag from electrolytes No 1 to 3

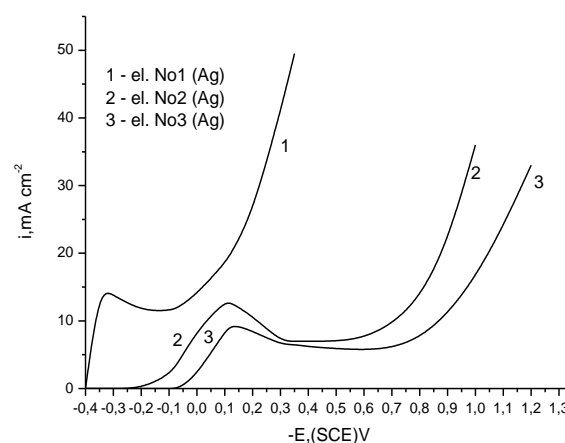


Fig.1. Comparison of the curves of Ag deposition in electrolytes No1 (1); No2 (2); No3 (3), $v=30\text{ mV s}^{-1}$.

In Fig. 1 the potentiodynamically taken polarization dependencies in the three electrolyte compositions for deposition of Ag powder are compared. In electrolyte No1 (acid nitrate) the equilibrium potential of the silver electrode is the most positive one ($E_{\text{eq}} = 0.360\text{V}$ in relation to SCE) compared to the two other electrolytes, i.e. ammonia-nitrate (Fig.1, curve 2) and ammonia-citrate (Fig.1, curve 3), with values of -0.173 V and -0.035V (SCE), respectively. In all three electrolytes (No 1 to 3) the deposition of Ag proceeds with reaching a plateau of the limiting diffusion current, the plateau being shifted to the most negative potentials and covering the widest potential area in the case of ammonia-citrate electrolyte (Fig. 1, curve 3). Obviously, in the presence of Na citrate, deposition of Ag is associated with greatest difficulties.

3.1.2. Co-deposition of Ag and Ni in electrolytes No 2* and 3*.

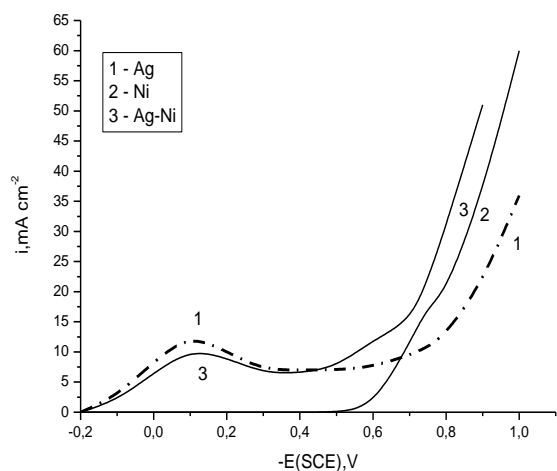


Fig.2. Comparison of the curves of individual deposition ($v = 30 \text{ mV s}^{-1}$) of Ag (1), Ni (2) and co-deposition of Ag-Ni (3) in ammonia-nitrate electrolyte (No 2*).

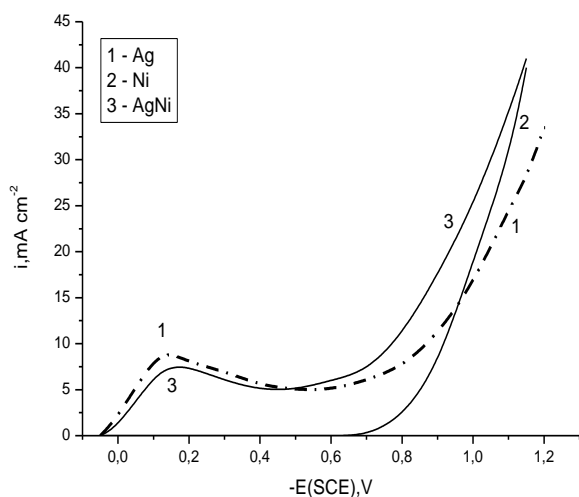


Fig.3. Comparison of the curves of individual deposition ($v = 30 \text{ mV s}^{-1}$) of Ag (1), Ni (2) and co-deposition of Ag-Ni (3) in ammonia-citrate electrolyte (No 3*).

In Figs. 2 and 3 potentiodynamically taken polarization dependencies of independent and joint deposition of Ag and Ni in ammonia-nitrate (Fig. 2) and in ammonia-citrate (Fig. 3) electrolytes (compositions No 2* and No 3*) are presented. In both electrolytes the deposition of Ni is characterized with high initial polarization and absence of plateau, indicating a predominant activation nature of the polarization (curve 2 in Figs. 2 and 3), unlike the deposition of silver discussed above. Silver is always deposited at more positive potentials, i.e. it is the first deposited metal

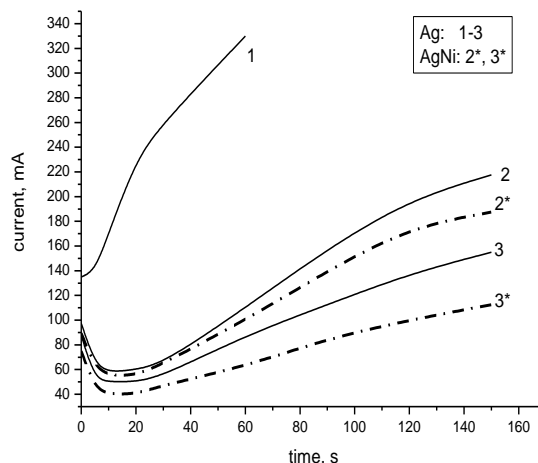


Fig.4. Comparison of I-t dependencies at potentials corresponding to $I=5I_d$ for Ag powders (curves 1-3) in electrolytes No1, No2 and No3, resp. and for Ag-Ni powders (curves 2*, 3*) in electrolytes No2* and No3*, resp.

of the Ag-Ni alloy in the electrolyte investigated. In simultaneous presence of nickel and silver in the electrolyte, the total polarization decreases in comparison to the polarization of each metal in electrolyte No 2* (Fig. 2), while in electrolyte No 3* (Fig. 3) it approaches that for silver deposition.

The strong shift of potential for deposition of nickel to the negative range of potentials in ammonia-citrate electrolyte (Fig. 3) compared to the potentials of its deposition in ammonia-nitrate electrolyte, allows assuming formation of citrate or mixed citrate-ammonia complexes of nickel, which have higher stability than pure ammonia ones [25].

It can be concluded from Figs. 2 and 3 that under the examined conditions the joint deposition of Ag and Ni as Ag-Ni powder is completely possible but it will proceed with less difficulties in ammonia-nitrate electrolyte (Fig. 2).

3.2. Conditions for powder formation of Ag and Ag-Ni

The current-time dependencies taken in electrolytes No 1, 2, and 3 for Ag powder and in No 2* and 3* for Ag-Ni powder at different potentials, are indicative of the growth of the surface area of the electrodes as a result of powder formation. In Fig. 4 the curves taken are compared in such a way that the current corresponds to the same position on the polarization curve (as $I=5I_d$ for all electrolytes selected for the purpose). Through this selection of conditions it is possible to obtain data for the influence of composition on the rate of powder formation from the curves in Fig. 4.

It follows from the data obtained that the powder formation for deposition of Ag powder proceeds at the highest rate in acid nitrate electrolyte (Fig. 4, dashed curve 1), which well agrees with the kinetic data from Fig. 1. In the complex electrolytes 2 and 3 the deposition of pure Ag powder (Fig. 4, dashed curves 2 and 3) proceeds at a lower rate, as the difficulties in citrate-ammonia electrolyte are the greatest. The presence of nickel in the electrolyte results in further decrease of the rate of powder formation (Fig. 4, solid lines 2*, 3*).

3.3. Electrodeposition of Ag-Ni from electrolytes No 2* and 3* in pulse potential mode.

In accordance with the method described in the experimental part, the polarization dependencies in electrolytes 2* and 3* ($\Delta\bar{E}-I_{av}$) and ($\Delta E-I_{av}$) were taken at different frequencies of pulses in the range from 100 Hz to 1000 Hz. These curves are similar by type to the polarization dependencies for joint deposition of metals in c.p.m., but differ for different frequencies. For a more clear comparison based on the data obtained, the dependencies of both average and amplitude polarization on frequency (Fig. 5) were built for the same average value of current $I=5Id$ for electrolytes 2* and 3*. The same comparison could be made for each other value of I/I_d and it will be analogous to the one presented in Fig. 5.

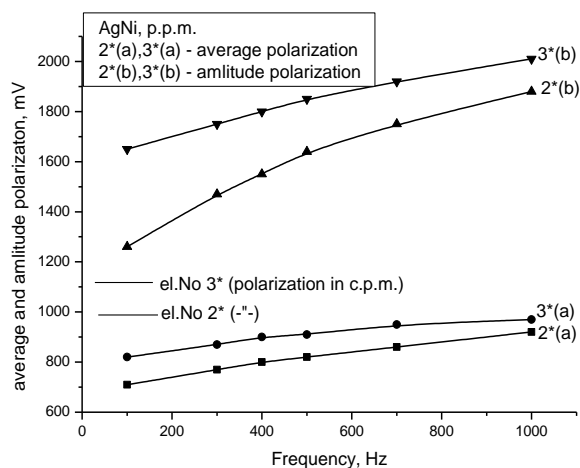


Fig.5. Comparison between dependencies of the average (2*a; 3*a) and the amplitude values of polarization (2*b; 3*b) on the frequencies of pulses (recorded for average current $I=5Id$) in ammonia-nitrate (2*a,2*b) and ammonia-citrate electrolytes (3*a,3*b); the values of polarization for $I=5 Id$ in constant potential potentiostatic mode (c.p.m.) are also indicated.

As seen in Fig. 5, with the increase in pulse frequency from 100 Hz to 1000 Hz, both the

average and the amplitude value of polarization in the two electrolytes increase. The possibility for relaxation of the concentration gradient in the pauses between pulses explains why the average polarization in impulse conditions is lower than that in stationary mode. The increase in frequency of pulses reduces the time of pause, which results in approximating the average polarization pulse to that in c.p.m. (curves 2*a and 3*a). At the same time, as seen from Fig. 5, the values of amplitude polarization remain almost twice as high as the average value for the given frequency, at frequency 1000 Hz the amplitude polarization reaching 1.8-2.0 V (curves 2*b and 3*b). At all pulse frequencies, in ammonia-citrate electrolyte both the average and the amplitude value of polarization are higher than those in ammonia-nitrate electrolyte (curves 3*a, 3b).

3.4. Morphology and phase structure of Ag powder in potentiostatic mode.

As seen from the SEM images of Ag powders (Fig. 6a to 6d), Ag powders deposited from acid nitrate electrolyte (Fig. 6a) have round-shaped crystals, as the average size of particles varies in a wide range from 0.5 μm to 3.5 μm . These powders have white color and metallic luster after deposition. In ammonia-nitrate electrolyte all powders have grey color after deposition and no luster, with much smaller average size of particles (about 0.5-1.0 μm), which witnesses for heavier difficulties during deposition (Fig. 6b). The Ag powders deposited from ammonia-citrate electrolyte remain dark grey to black, as the particles have a typical branched dendrite structure and are susceptible to agglomeration (Fig. 6c). The X-ray diffractogram of the same powders (Fig. 7c) also proves that the "black" Ag powders deposited from electrolyte No 3 (ammonia-citrate) have the greatest dispersion and the dendrites observed consist of agglomerated powder particles.

In Fig. 7a to 7c the X-ray diffractograms of white (Fig. 7a), dark grey (Fig. 7b) and black (Fig. 7c) Ag powders obtained from acid nitrate, ammonia-nitrate and ammonia-citrate electrolyte are compared. The reflexes are closest in the acid nitrate electrolyte (Fig. 7a) and are gradually widening with the increasing dispersion, being widest and of lowest intensity in the ammonia-citrate electrolyte (Fig. 7c). It is seen from the X-ray diffractograms that regardless of the composition of solution, the deposited Ag powders contain a single crystal phase, i.e. that of Ag with face-centered cubic lattice (fcc).

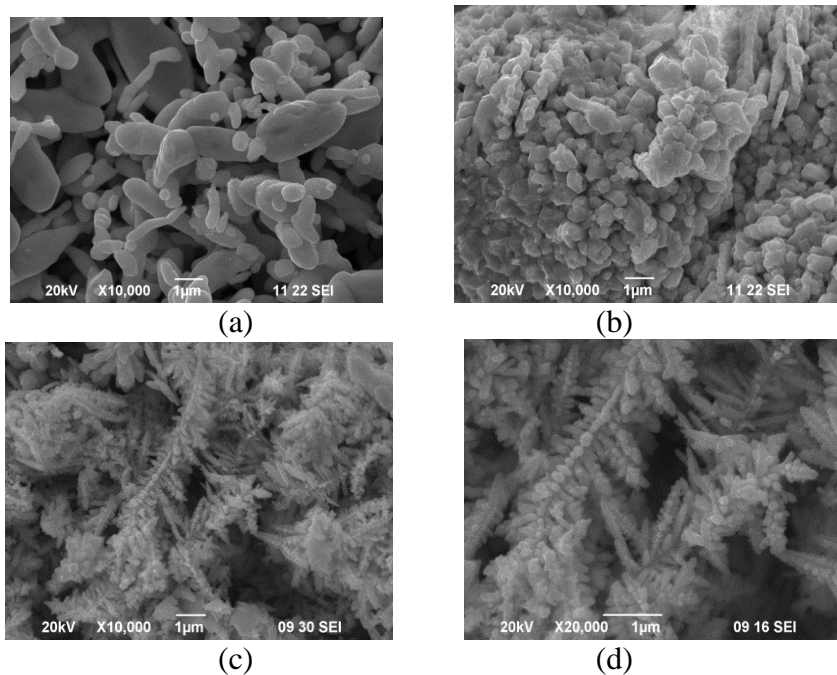


Fig.6. SEM images of Ag powders, deposited at potentials corresponding to $I=5I_d$ in polarization curves for electrolytes No1 (a); No2 (b) and No3 (c,d).

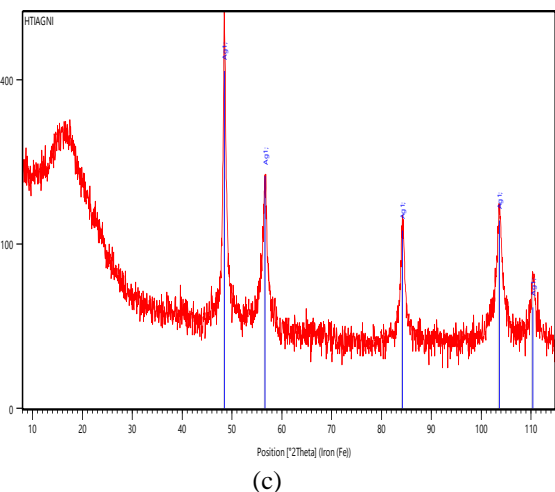
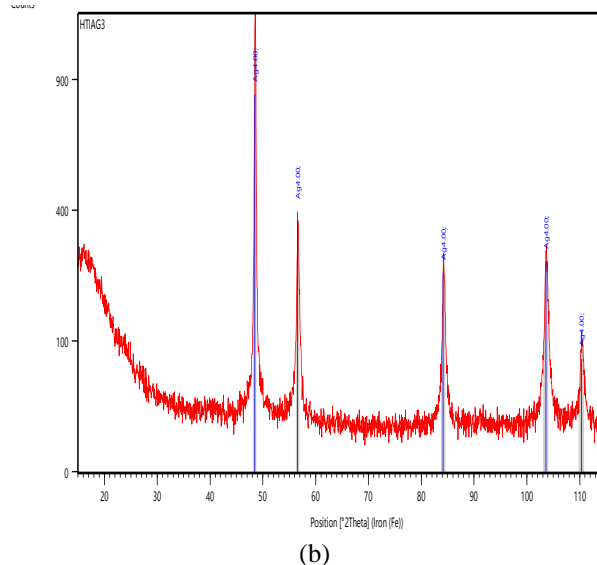
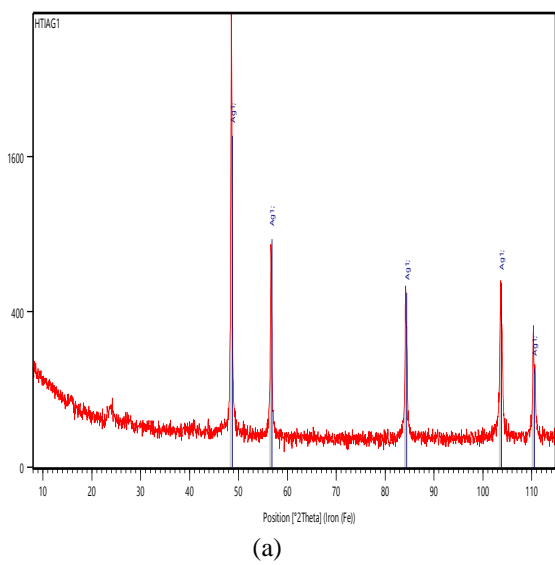


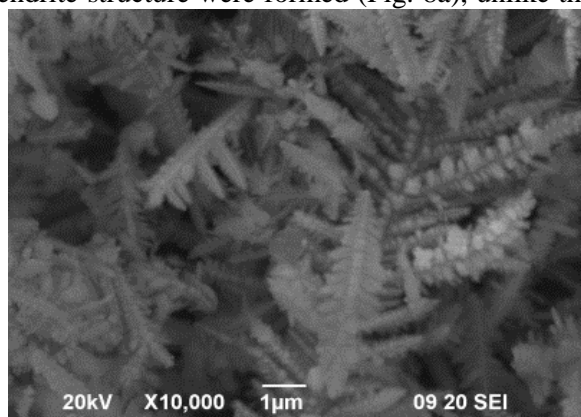
Fig.7 X-ray diffractograms of Ag powders deposited at potentials corresponding to $I=5I_d$ in polarization curves for electrolytes No1 (a); No2 (b) and No3 (c).

3.5. Morphology and elemental composition of Ag-Ni powders in potentiostatic and pulse potential modes.

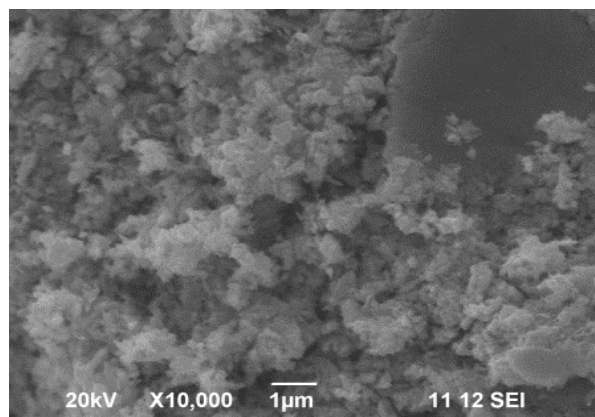
In Fig. 8 SEM images and elemental content of Ag-Ni powder deposited (in figure caption) in potentiostatic and pulse potential modes from ammonia-nitrate electrolyte (composition No 2*) are presented. In potentiostatic mode powders enriched in silver (up to 95%Ag) with typical dendrite structure were formed (Fig. 8a), unlike the

irregular rounded shape of the particles of pure Ag powder deposited from the same composition (Fig. 7b). The application of pulse mode results in strong changes in the morphology of the powders. The particles are strongly shortened, of irregular shape and very small average diameter (less than 1 μm).

In Fig. 9 SEM images and elemental content (in figure caption) of Ag-Ni powder deposited from ammonia-citrate electrolyte (composition No3*) at different cathode potentials in

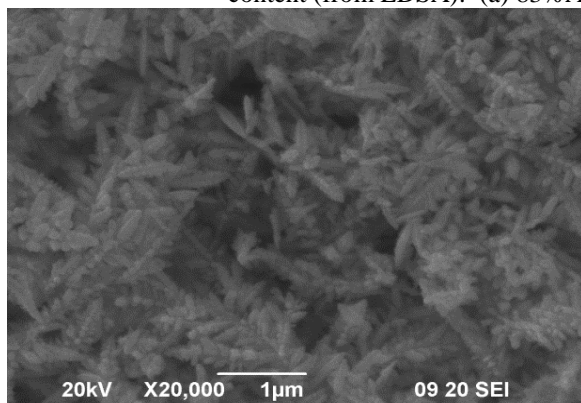


(a)

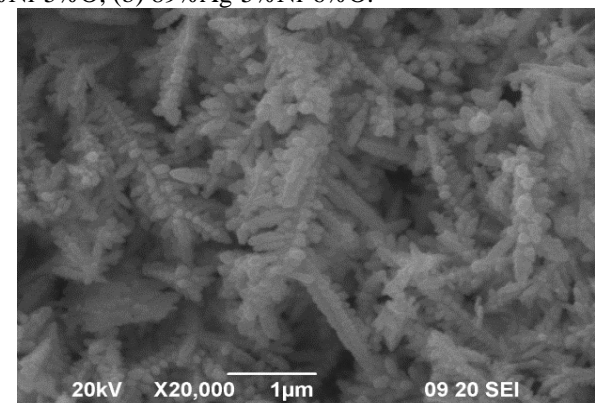


(b)

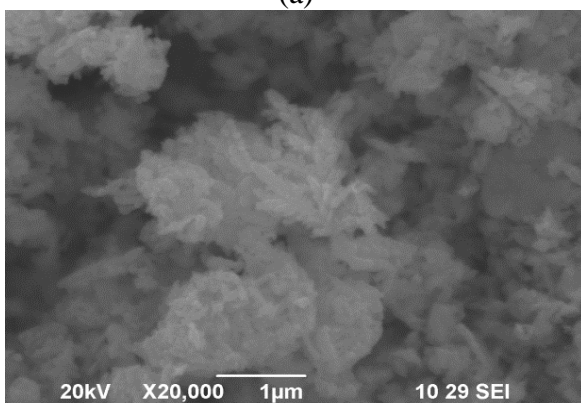
Fig.8. SEM images of Ag-Ni powders deposited at potentials corresponding to $I=5I_d$ in polarization curves for electrolyte No2* in potentiostatic (a) and in pulse potential mode at frequency of pulses $f=500$ Hz (b). Elemental content (from EDSA): (a) 83%Ag-12%Ni-5%O; (b) 89%Ag-5%Ni-6%O.



(a)



(b)

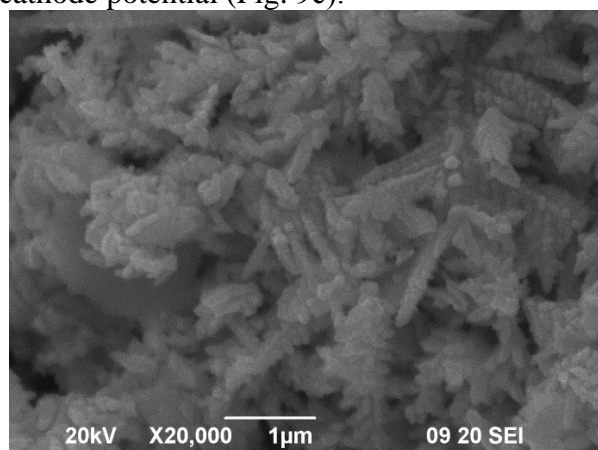


(c)

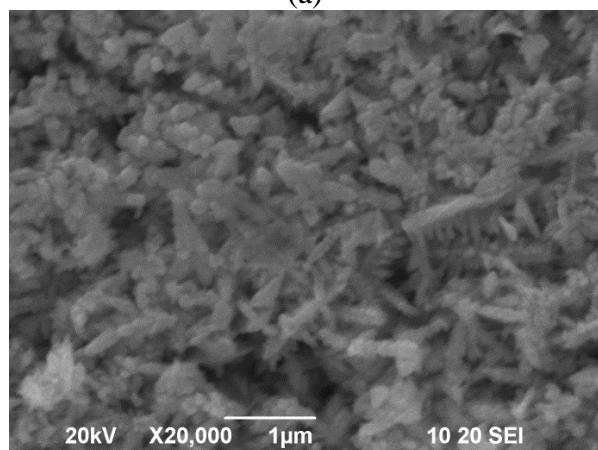
Fig.9. SEM images of Ag-Ni powders deposited from electrolyte No3* in potentiostatic mode at different potentials E (SCE): -1,0V (a); -1,3V (b) and -1,5V (c). Elemental content: (a)95%Ag-5%Ni ; (b) 87%Ag-9%Ni-4%O; (c)76%Ag-18%Ni-6%O.

potentiostatic mode are presented. The higher cathode potential applied leads to powders enriched in nickel (up to maximum 12 % Ni), whilst a decrease of the average size of particles is observed.

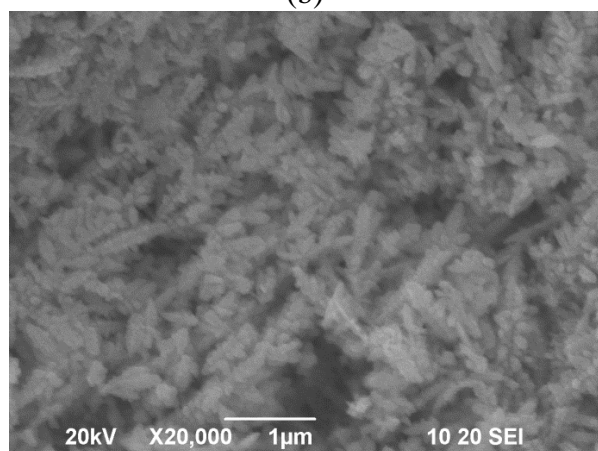
Agglomerates of small particles less than 1 μm are observed on the images at the highest cathode potential (Fig. 9c).



(a)



(b)



(c)

Fig.10. SEM images of Ag-Ni powders deposited from electrolyte No3* in pulse potential mode with different frequencies of pulses: 100 Hz (a); 500 Hz (b) and 1000

Hz (c); the potential values correspond to $I=5I_d$ in polarization curves for each frequency; elemental content: (a) 92%Ag-8%Ni; (b) 91%Ag-9%Ni; (c)83%Ag-12%Ni-5%O.

The comparison between the morphology of powders from the two electrolytes (No 2* and No 3*) in potentiostatic mode that is seen in Figs. 8a and 9a-c proves the advantages of the ammonia-citrate electrolyte (composition No 3*) for obtaining more finely dispersed Ag-Ni powders. That is why the influence of pulse frequency on the change of morphology and elemental content of Ag-Ni powders was precisely studied (Fig.10, a-c) in ammonia-citrate electrolyte (No 3*).

The susceptibility to formation of dendrite structure decreases with the increase of pulse frequency from 100 Hz to 1000 Hz (Fig.10a-c). The Ag-Ni powders obtained at frequencies 500-1000 Hz have either needle-like particles or irregular shaped particles with small lateral branching and average size of particles about or less than 1 μm (Fig.10, b and c).

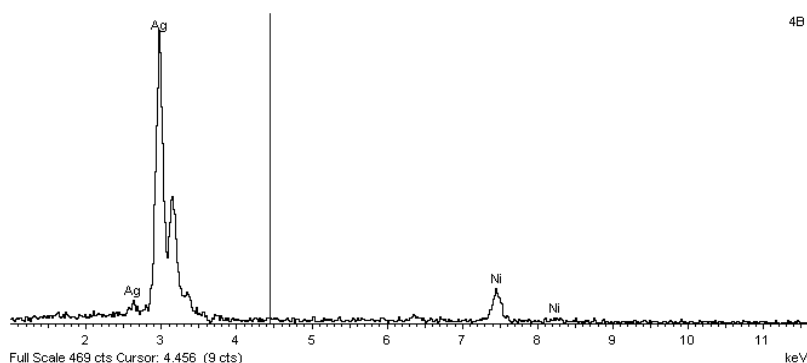
It follows from the data for the elemental content of Ag-Ni powders given in the figure captions that achieving a higher content of Ni up to 18% in ammonia-citrate electrolyte (composition No 2*) and up to 12% in ammonia-citrate electrolyte (composition No 3*) is possible solely in potentiostatic mode at higher cathode potentials. At higher potentials in both electrolytes and at higher frequencies in ammonia-citrate electrolyte, oxides are present in the powders accounted for through the content of oxygen. The most probable reason for oxide formation is that the solution close to the electrode becomes alkaline because of hydrogen evolution at high amplitude values of the polarization at these conditions. The presence of Ni that cannot be found out through regular X-ray analysis is proved through the EDSA spectra of Ag-Ni powders (Fig. 11).

4. CONCLUSIONS

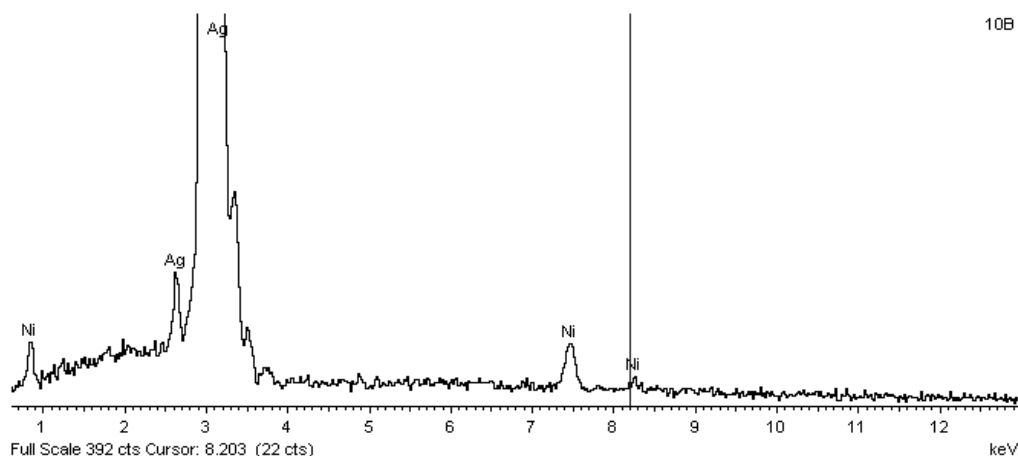
It is found out that the transition from a regular acid electrolyte to complex electrolytes leads to increased dispersion of Ag powders and the deposited powders have different colors – white, dark grey, and black. This is due to the transition from round to dendrite shape of the particles and not to the occurrence of a new structure different from cubic crystal structure (fcc). The advantages of ammonia-citrate electrolyte towards the ammonia-nitrate one are proved, as well as those of pulse potential mode towards the potentiostatic mode for obtaining more finely dispersed Ag-Ni

powders of average size of particles about or less than 1 μm . The maximum content of Ni in Ag-Ni

powders 12-18% is achieved in potentiostatic mode.



(a)



(b)

Fig. 11. EDSA spectra of Ag-Ni powder deposited from electrolyte No2* at $E=-1,0\text{V}$ (a) and from electrolyte No3* at $E=-1,3\text{V}$ (b) in potentiostatic mode.

REFERENCES

- 1.Ch. Cheng, T. Arunagiri, O. Chyan, *American Journal of Undergraduate Research*, **2**, Nr 1, (2003)
- 2.D. Pilone and G. H. Kelsall, *Electrochimica Acta*, **51**, (2006),3802
- 3.D.L. Deborah and Chung at all, *Materials for Electronic Packaning*, London, UK, Butterworth-Heinemann, (1995)
- 4.K.I. Popov, M.G. Pavlovic', in "Modern Aspects of electrochemistry"(Electrodeposition of metal powders with controlled particles grains size and morphology), vol.14, Nr24, Eds. : E.White and J.O'M Bockris, Plenum Press Co, New York, (1993), pp. 299-391
- 5.K.J. Popov, N.D. Nikolic', M.G. Pavlovic', *J. Serbian Chem. Soc.*, **74**, 397 (2006).
- 6.H.M.A. Solimen, H.H. Abdel-Rahman, *J. Braz. Chem.Soc.*, **17**, 705 (2006).
- 7.K.I. Popov, M.D. Maksimovic', S.K. Zecevic', M.R. Stojic', *Surf. Coat. Technol.*, **27**, 117 (1986).
- 8.M.G. Pavlovic', M. D. Maksimovic', K. I. Popov, M. B. Krsul, *J. Appl. Electrochem.*, **8**, 61 (1978).
- 9.A.T. Kuhn, P. Neufeld, K. Young, *J. Appl. Electrochem.*, **14**, 605 (1984).
- 10.V. Maksimovic, M. G. Pavlovic, Lj. J. Pavlovic, M. V. Tomic, V. D. Jovic, *Hydrometallurgy* **86**, 22 (2007).
- 11.C.K. Mital, *J.Electrochem.Soc, India*, **.22**, 251, (1973).
- 12.A.T. Kuhn, P. Neufeld, G.Butler, *Surface Technology*, **16**, 3 (1982).
- 13.A.T. Kuhn, *Oberfläche/Surfaces*, **23**, 279 (1981).
- 14.Yu.M. Polukarov, *Electrochimia (Russian)*, **4**, 568, (1968).
- 15.G.A. Emelyanenko, G. Simulin, *Electrochimia (Russian)*, **4**, 187 (1968).

16. Yu.M. Polikarov, Trud. Ukrainskoi Respubl. Konferencii electrochimii, Novomoskovsk, Dnepropetrovskaya oblast, (Sept. 1977), pp. 116-119
17. Yu.M. Polukarov, *Electrochimia (Russian)*, **2**, 79 (1966).
18. A. Radisic, G.J. Lany, P.M. Hoffman, P.C. Searson, *J. Electrochem. Soc.*, **148**, 41 (2000).
19. P. Borthen, J.B. Hwang, H.H. Strehblow, D.M. Koev, *J. Phys. Chem.*, **104**, 5078 (2000).
20. M.G.Pavlovic, K.I.Popov, Metal powder production by electrolysis. *Electrochemistry Encyclopedia* (2005). Available from <http://electrochem.cwru.edu/ed/encycl/>.
21. O.I.Kuntyi, R.R.Olenych, *Russian Journal of Applied Chemistry*, **78**, 556 (2005).
22. [22*Advance Powder Technology*, (2011), in press
23. N.Ibl, Cl.J.Puippe, *Plating and Surface Finishing*, **6**, 68 (1980).
24. A.W. Pomosov, A.A. Yun, I.W. Muratova, *Poroshkovaya Metalurgiya*, **4**, 1 (1983).
25. T.A. Green, A.E. Russel, S. Roy, *J. Electrochem. Soc.*, **145**, 875, (1998).

ЕЛЕКТРООТЛАГАНЕ НА Ag И НА Ag-Ni ПРАХОВЕ В СТАЦИОНАРЕН И В ИМПУЛСЕН РЕЖИМ

К. Игнатова

Химикотехнологичен и металургичен университет, София 1756, България

Постъпила на 24 юли, 2012 г.; коригирана на 30 септември, 2013 г.

(Резюме)

Изследвани са кинетиката на отлагане, морфологията и състава на чист Ag прах и на AgNi прах в зависимост от вида на електролита и условията на отлагане. Установено е, че в кисел нитратен електролит Ag прахове са бели след отлагане, с по-ясно проявена кристална структура. В комплексен аминитратен електролит се формират сиви Ag прахове с неправилна форма на частиците и по-висока дисперсност. В цитратноамонячен електролит отложените Ag прахове са тъмносиви до черни на цвят, с типично дендритна, склонна към агломериране структура на частиците. Всеки от типовете Ag прахове се състои от една единствена фаза – тази на сребро с кубична стенноцентрирана решетка (fcc). Доказани са предимствата на цитратноамонячния електролит в сравнение с аминитратния за получаване на финодисперсни AgNi прахове. Прилагането на по-високи катодни потенциали в стационарен режим и прилагането на импулсен режим с честота на импулсите до 1000 Hz в цитратноамонячния електролит води до понижение на средния размер на частиците до около и под 1 μm и нарастване на съдържанието на никел до 12-18%.

Gases permeability study in dual membrane fuel cell

E. Mladenova^{1*}, D. Vladikova¹, Z. Stoynov¹, A. Chesnaud², A. Thorel², M. Krapchanska¹

¹*Institute of Electrochemistry and Energy Systems “Acad. E. Budevski” – Bulgarian Academy of Sciences, 10 Acad. G. Bonchev Str., Sofia 1113, Bulgaria*

²*Centre des Matériaux, Mines-ParisTech, BP 87, 91003 Evry Cedex, France*

Received October 30, 2012; Revised March 11, 2013

Gases permeability in a porous mixed (proton and oxide ion) conductive membrane, which is a component of a new high temperature dual membrane fuel cell design is investigated by specially designed testing system based on measurements of the gas flow [ml/min] and pressure P (mm H₂O) when penetrating through porous media. A strong correlation expressed in increase of the permeability with the decrease of the gases molecular weight is registered. The water vapor permeability decreases with the temperature. This is in agreement with data from the literature which show that the viscosity of gases, including water vapor, increases with the temperature. The results obtained suggest optimal porosity in respect to permeability, mechanical stability and conductivity in the range of 35 - 40%. They confirm the need of optimization concerning not only the pores fraction, but also the pores geometry and distribution, as well as the central membrane geometry and the configuration of the cell. This approach can be applied also for optimization of the electrodes porosity (pores concentration, geometry, distribution etc), especially in cases when gas mixtures (including water vapor) are used or produced.

Keywords: gases permeability, dual membrane fuel cell, porous mixed conducting ceramics, electrochemical impedance spectroscopy.

INTRODUCTION

Following the strategic objectives of Europe 2020 for 20% lower greenhouse gas emissions, 20% of energy from renewables and 20% increase of energy efficiency, hydrogen can play an essential role not only as a fuel, but also as an universal energy carrier easy to be integrated in electrical systems. Thus the commercialization of solid oxide fuel cells (SOFC) as extremely efficient device to produce electricity with no deleterious emission if fed by hydrogen is of primary importance.

Classical SOFCs have 50 years of technical history. They operate at high temperatures, use a solid oxide (ceramic) electrolyte to conduct oxide ions created at the cathode to the anode, where they react with hydrogen and produce water as by-product. In our days more than 40 companies and thousands of research groups all over the world are working intensively towards decreases of material costs and operating temperature, improvement of performance stability as well as fuel flexibility and efficiency.

In the last 20 years, due to the discovery of proton conductivity in perovskite-doped cerates

[1–3], more and more attention is drawn to the development of proton conducting fuel cells (pSOFC). They use a solid state proton conducting electrolyte, which transports hydrogen ions created at the anode to the cathode. Since the more mobile proton is transported through the electrolyte, PCFCs have the potential to operate at lower temperatures (500–800°C).

However the dilution of the reacting gases with the exhaust water (at the anode side in SOFC and at the cathode side in PCFC) combined with decrease of their catalytic activity can be regarded as a limiting factor that slows down their marketing. In order to overcome those limitations, innovative Dual Membrane Fuel Cell (DMFC) architecture was proposed [4] and proved [5–8].

The new concept combines the advantages and eliminates the disadvantages of both oxide ion and proton conducting high temperature fuel cells. The main idea is the separation of the hydrogen and oxygen from the exhaust water. It is realized by the introduction of a junction central membrane (CM) layer between a SOFC electrolyte/cathode (cathode compartment) and a PCFC anode/electrolyte (anode compartment). The CM has mixed (H⁺ and O²⁻) conductivity and porous microstructure. Thus protons produced at the anode progress toward the junction membrane where they meet the oxide ions

* To whom all correspondence should be sent:
E-mail: : emiliya@bas.bg

that are created at the cathode and produce water, which is evacuated through the pores of the membrane. Therefore hydrogen, oxygen and exhaust water are located in three independent chambers. The innovative concept has the potential to considerably enhance the overall efficiency and reduce costs of SOFC systems thanks to fine-tuning of the catalytic properties of electrodes, pressurization of both electrode compartments, production of pure water for steam reforming and employment of less sophisticated metallic alloys for interconnects. More details for the concept and its proof are given in [5–8].

The most challenging component of the DMFC design is the composite CM. It should have high anionic and protonic conductivities in the presence of sufficient porosity and proper connectivity among the different phases (proton conductor, oxide ion conductor, open porosity for water evacuation), avoiding tortuous and/or resistive paths. Moreover, both solid phases - the proton conducting BCY15 ($\text{BaCe}_{0.85}\text{Y}_{0.15}\text{O}_{2-\delta}$) and no oxide - ion conducting YDC15 ($\text{Ce}_{0.85}\text{Y}_{0.15}\text{O}_{1.925}$) should percolate towards their respective electrolyte, while porosity must percolate towards the outside of the cell for water evacuation. Thus each triple phase boundary (TPB) segment should be connected to both electrolytes. The CM needs the optimization of two processes with contradictory initial requirements: (i) water vapor formation and evacuation for which a porous structure is needed and (ii) high mixed ion conductivity, favored by higher density. Obviously a compromise between the two targets is needed, since the increase of porosity will improve the water permeability, but will also decrease the conductivity.

For optimization of the CM new research approaches were introduced and developed for deeper insight into the mechanisms and processes of mixed conductivity and water formation and release: X-ray micro-tomography 3D image analysis [9, 10]; “in situ” conductivity measurements of the CM composite matrix components; gas and water vapor permeability studies; capacitive and impedance measurements of water behavior in the CM [8, 11].

This paper aims at summarizing the results of one new and systematic study of gases (including water vapour) permeability in porous ceramic media. Although it is performed for deeper insight into the water permeation in the central membrane of the DMFC design, the applied approaches and

obtained results can be introduced in the electrodes performance optimization procedures.

EXPERIMENTAL

The mixed oxide-ion and proton conductivity of the central membrane was obtained by the application of composite based on the chemically compatible BCY15 and YDC15 electrolytes [6, 7], (YDC15 is a decomposition product of BCY15 [12]). Samples with diameter about 2 cm and thickness about 1 mm were produced by cold pressing and sintering at 1300°C. The ratio of the two ceramic phases was varied in the range from 40/ 60 to 60/40 vol %. Different porosity (25 – 60 v%) was obtained by adjustments of the type (graphite, starch, polyvinyl butyral) and quantity of the pore former.

Morphological studies performed by X-ray micro-tomography 3D image analysis [9, 10] confirmed good percolation rates and tortuosity of the three phases, indicating easy pathways for the ions through the central membrane and for the water evacuation from shaping point of view. Graphite pore former was estimated as the best one.

Since the CM consists of three phases (BCY, YDC and pores), their co-existence influences the way each of them forms and evolves during sintering (the 2 ceramic components have different sintering temperatures). Thus an essential point was to study “in situ” the conductivity behaviour of every ceramic component, i.e. in the presence of the other two phases. This target was successfully realized with the design of a new type of symmetrical CM supported half cells (diameter about 2 cm, thickness about 1 mm) Pt/YDC_{porous}BCY_{porous}/Pt which were measured by electrochemical impedance spectroscopy (EIS). The impedance measurements were carried out with Solartron 1260 FRA in temperature interval 100–750 °C, frequency range from 1 MHz down to 0,1 Hz, density five points/decade and amplitude of the AC signal 50 mV in wet (3%) hydrogen or air/oxygen, which ensured separate information for the conductivity of every component of the composite.

For the performance of the permeability studies a new testing system was specially designed. It is based on measurements of the gas flow q_{flow} [ml/min] and pressure P (mm H₂O) when penetrating through media with different porosity which determine a new characteristic parameter, named permeability resistance R_p (inversely proportional to the permeativity):

$$R_p = P/q_{\text{flow}} \quad (1)$$

The testing system ensures measurements of R_p in the range 0.01 to 600 mm.min/ml. The permeability measurements were carried out with different gases: air, H_2 , O_2 , N_2 , Ar and humidified air. The gas flows varied from 0 to 140 ml/min. The tests with humidified air were performed in temperature range 20 – 600°C at a constant gas flow. The humidity (3% H_2O) was ensured by passing the gas flow through watered vessel at room temperature. The experiments were carried out on samples with different porosity, evaluated by mercury porosimetry. Two configurations of the gas flow set-up were used - lateral, which is similar to the CM configuration in the DMFC, where the water vapor formed in the porous membrane is evacuated through its periphery, and transversal, which represents the gas flows in the porous electrodes layers, cf. Fig. 1.

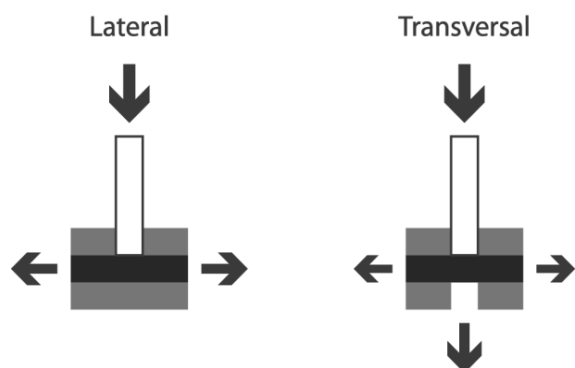


Fig. 1. Different gas flow configurations of the experimental set-up.

Similarly to the ohmic resistance, the permeability resistance can be expressed as:

$$R_p = \rho_p h s^{-n} \quad (2)$$

where “s” is the sample’s surface and “h” is its thickness.

Measurements of gases permeability were calibrated on pipes with varying diameter and length. It was found that for pipes with diameter bigger than 2 mm $n = 1$. However, for internal pipe diameter less than 2 mm the geometrical factor increases, i.e. $n > 1$. For pipes with diameter between 1 and 2 mm it is 1,13. Obviously in porous ceramic media this coefficient should be much bigger.

RESULTS

The impedance measurements of half cells with CM support of different porosity were performed in both air and wet hydrogen atmospheres and thus provided important information about the individual conductivity of each one of the two electrolytes in the real ceramic structure. Results for central membranes with different porosity are presented in Fig. 2. As it could be expected, the porosity increases the resistivity of both electrolytes. It is higher in air/oxygen, where the YDC15 contribution is represented. The influence of the porosity is more pronounced in hydrogen, where the BCY15 resistivity is exhibited.

The obtained results, however, do not give information about the water vapor transport in the CM, which is an important factor in the optimization of the cell performance. For this purpose permeability studies were performed, starting with gases permeability in the CM at room temperature.

As expected, the permeability in the CM is bigger for transversal configuration of the testing rig (Fig. 3). Logically the gas permeability decreases with the decrease of the porosity (Fig. 4). Measurements with different gases at room temperature and constant conditions (set-up configuration and porosity) registered a strong

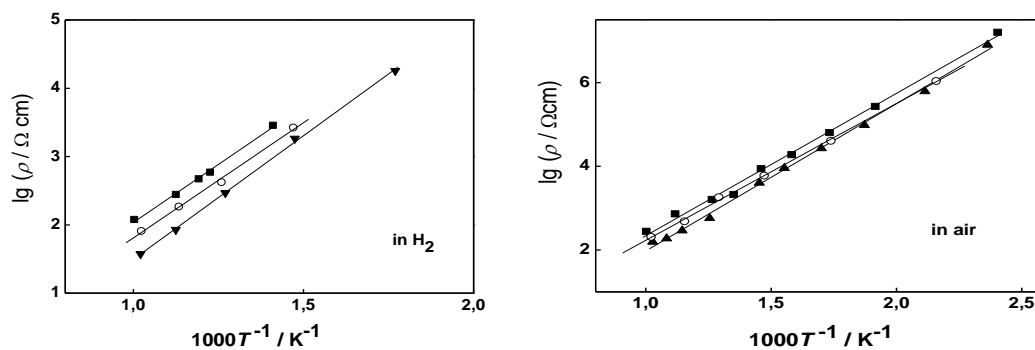


Fig. 2. Arrhenius plots for the resistivity of central membrane with different porosity and 50 v % of BCY15 and YDC15 (■ – 40% porosity; ○ – 35 % porosity; ▼ – 30% porosity).

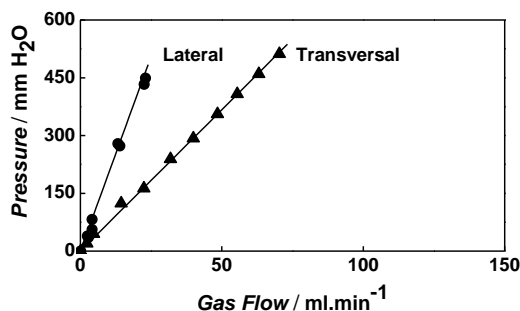


Fig. 3. Permeability measurements of H₂ in CM with 40% porosity at different measurement configurations of the experimental set-up.

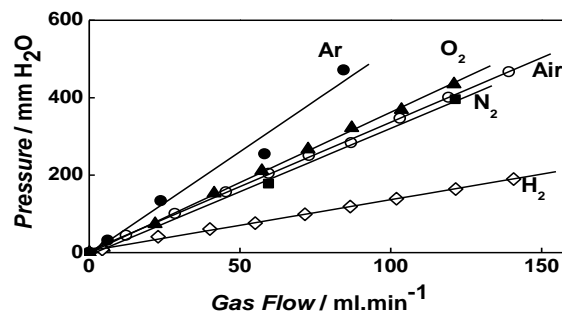


Fig. 5. Gases permeability measurements in CM with 50% porosity at room temperature (transversal configuration).

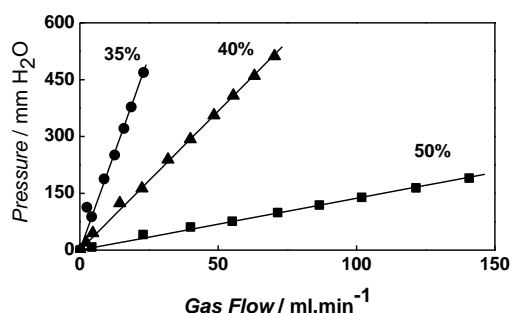


Fig. 4. Permeability measurements of H₂ in CM with different porosity at room temperature (transversal configuration).

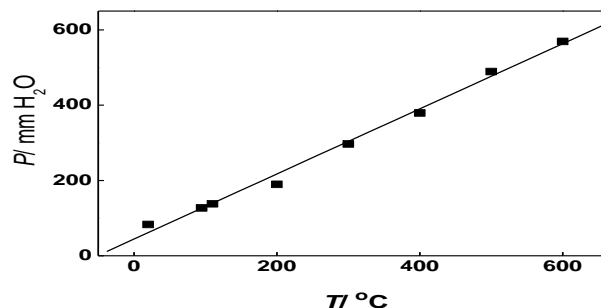


Fig. 6. Temperature dependence of wet air permeability in CM with 40% porosity at constant gas flow.

correlation expressed in increase of the permeability with the decrease of the gases molecular weight (Fig.5).

Water permeability in the CM at elevated temperatures was studied by measurements performed in wet air in the temperature range 20 – 600°C. A decrease of the permeability was registered with the increase of the temperature (Fig. 6). This result is in agreement with data from the literature which show that the viscosity of gases, including water vapor, increases with the temperature (Fig. 5) [13]. Since the available data is up to 300–400°C, the obtained results give important information that at operating temperatures the water produced in the pores of the CM has higher viscosity.

The results obtained from the conductivity and permeability studies showed that the optimal porosity of the mixed ion conducting central membranes in respect to permeability, mechanical stability and conductivity is about 35 – 40%.

CONCLUSIONS

The analysis of the permeability studies shows that the phenomenon is complicated and strongly dependent on the CM porosity, pores geometry,

tortuosity, sample configuration. The obtained results confirm the need of optimization concerning not only the pores fraction, but also the pores geometry and distribution, as well as the CM geometry and configuration in the cell, which brought to the construction of a new cell design [14]. It facilitates the water vapor evacuation from the central membrane.

Gases permeability studies can be applied also for optimization of the electrodes porosity (pores concentration, geometry, distribution etc), in solid oxide fuel cells and electrolyzers especially when gas mixtures (including water vapor) are used, or produced. Obviously the optimal porosity of the cathode and anode will differ since the two electrodes are fed with different gases.

Acknowledgements: The research leading to these results has received funding from the European Community's Seventh Framework Programme (FP7/2007-2013) under grant agreement No 213389. Powders were fabricated and supplied by Marion Technologies (MT).

The authors acknowledge also "Science and Business" BG051PO001/3.3-05-001 for the financial support that made possible the publication of this paper.

REFERENCES

1. H. Iwahara, H. Uchida, K. Ogaki, *J. Electrochem. Soc.*, **135**, 529 (1988).
2. H. Iwahara, *Solid State Ionics*, **168**, 299 (2004).
3. H. Iwahara, Y. Asakura, K. Katahira, M. Tanaka, *Solid State Ionics*, **28-30**, 573 (1988).
4. A. Thorel, *Patent* 0550696000 (2005).
5. <http://www.ideal-cell.eu/content/index.php>.
6. A. Thorel, A. Chesnaud, M. Viviani, A. Barbucci, S. Presto, P. Piccardo, Z. Ilhan, D. Vladikova, Z. Stoynov, in: *Solid Oxide Fuel Cells 11 (SOFC-XI)*, *The Electrochemical Society*, S.C. Singhal, H. Yokokawa (eds), Pennington. ECTS Trans **25**, 753 (2009).
7. S. Presto, A. Barbucci, M. Viviani, Z. Ilhan, S. Ansar, D. Soysal, A. Thorel, J. Abreu, A. Chesnaud, T. Politova, K. Przybylski, J. Prazuch, Z. Zhao, D. Vladikova, Z. Stoynov, in: *Solid Oxide Fuel Cells 11 (SOFC-XI)*, *The Electrochemical Society*, S.C. Singhal, H. Yokokawa (eds), Pennington. ECS Trans **25**, 773 (2009).
8. D. Vladikova, Z. Stoynov, G. Raikova, A. Thorel, A. Chesnaud, J. Abreu, M. Viviani, A. Barbucci, S. Presto, P. Carpanese, *Electrochim. Acta*, **56**, 7955 (2011).
9. D. Jeudin, in: *Advances and Innovations in SOFCs* (Proc. 1th Int. Works., Katarino, 2009.), D. Vladikova, Z. Stoynov (eds.), IEES-BAS, Sofia, 177 (2009).
10. J. Abreu, PhD Thesis, L'École Nationale Supérieure des Mines de Paris, 2011.
11. Z. Stoynov, D Vladikova, E. Mladenova, *Journal of Solid State Electrochemistry*, DOI 10.1007/s10008-012-1916-z (2012)
12. G. Caboche, J.-F. Hochepped, P. Piccardo, K. Przybylski, R. Ruckdäschel, M.-R. Ardigó, E. Fatome, S. Chevalier, A. Perron, L. Combemale, M. Palard, J. Prazuch, T. Brylewski, in: *Solid Oxide Fuel Cells 11 (SOFC-XI)*, *The Electrochemical Society*, S.C. Singhal, H. Yokokawa (eds), Pennington. ECS Trans **25**, 763 (2009).
13. D. Lide (ed), *CRC Handbook of Chemistry and Physics*. CRC Press, Boca Raton (2004)
14. Z. Stoynov, D Vladikova, A. Thorel, A. Chesnaud, M. Viviani, A. Barbucci, *Patent* 1159969 (2011)

ИЗСЛЕДВАНЕ НА ГАЗОВАТА ПРОПУСКЛИВОСТ В ДВОЙНО МЕМБРАННА ГОРИВНА КЛЕТКА

Е. Младенова¹, Д. Владикова¹, З. Стойнов¹, А. Чесно², А. Торел², М. Кръпчанска¹

¹Институт по електрохимия и енергийни системи "Акад. Е. Бudevски" – БАН, ул. "Акад. Г. Бончев", бл. 10,1113, София, България

²Център по материалознание, Миньо-Тех Париж, ВР 87, 91003, Еври, Франция

Постъпила на 30 октомври, 2012 г.; коригирана на 11 март, 2013 г.

(Резюме)

Тествана е нова система за изследване на газова пропускливост, в това число пропускливост и на водни пари, в пореста керамична мембрана (т. н. централна мембрана – ЦМ) със смесена йонна проводимост, която е основен компонент в иновативен дизайн на високо температурен твърдооксиден горивен елемент. Системата за изследване на газова пропускливост се базира на измерването на газовия поток q [ml/min] и налягането P (mm H₂O). Установена е строга корелация между увеличаването на газова пропускливост и намалението на молекулното тегло на газовете. Газовата пропускливост на водни пари намалява с увеличение на температурата. Този резултат е в синхрон с литературните данни, които показват, че вискозитета на газовете се увеличава с повишаването на температурата. Получените резултати дават възможност да се определи оптимално съотношение между газова пропускливост и пористост, механична стабилност и проводимост в диапазон 35 - 40%. Разработеният подход е особено интересен и за оптимизиране микроструктурата на пористостта на електродите - концентрация на порите, тяхната геометрия и разпространение, особено в случаите, когато се използват или произвеждат газови смеси (включително водна пара).

Silica-bonded *N*-propyl sulfamic acid: A recyclable catalyst for microwave-assisted synthesis of spirooxindoles via three-component reaction

A. Gharib^{1,2}, N. N. Pesyan³, B. R. H. Khorasani², M. Roshani¹, J. (HANS) W. Scheeren⁴

¹Department of Chemistry, Islamic Azad University, Mashhad, IRAN

²Agricultural Researches and Services Center, Mashhad, IRAN

³Department of Chemistry, Faculty of Science, Urmia University, 57159 Urmia, Iran

⁴Cluster for Molecular Chemistry, Department of Organic Chemistry, Radboud University Nijmegen, The Netherlands

Received March 13, 2012; Revised January 22, 2013

Silica bonded *N*-propyl sulfamic acid (**SBNPSA**) is employed as a solid acid catalyst for the synthesis of spirooxindoles via three-component reaction in good yields and short reaction times in ethanol under irradiation microwave conditions. Irradiation of the combination of isatin or acenaphthoquinone, an activated methylene reagent, and 1,3-dicarbonyl compounds in the presence of catalytic (**SBNPSA**) was found to be a suitable and efficient method for the synthesis of the biologically important spirooxindoles.

Keywords: Silica-bonded *N*-propyl sulfamic acid (**SBNPSA**); Spirooxindoles; isatin; three-component; Irradiation microwave

INTRODUCTION

Combinatorial chemistry is now routinely applied to find out novel biologically active compounds. In this context, multicomponent reactions (MCRs) are powerful tools in the modern drug discovery process in terms of lead finding and lead optimization [1,2]. However, the range of easily accessible and functionalized small heterocycles is rather limited. The development of new, rapid, and robust routes toward focused libraries of such heterocycles is therefore of great importance. Spirooxindole derivatives are important classes of heterocyclic compounds. The heterocyclic spirooxindole ring system is a widely distributed structural framework that is present in a number of pharmaceuticals and natural products [3], including cytostatic alkaloids like spirotryprostatins and strychnophylline [4]. The unique structural array and the highly pronounced pharmacological activity displayed by this class of spirooxindole compounds have made them attractive synthetic targets [5]. Oxa and azaspiro derivatives are well-known [6], but the preparation of corresponding quinazolinone analogues has not yet evolved. Polyfunctionalized heterocyclic compounds play important roles in the drug discovery process, and analysis of drugs in late development or on the market shows that 68% of them are heterocycles [7,8]. Therefore, it is not

surprising that research on the synthesis of polyfunctionalized heterocyclic compounds has received significant attention.

The quinone moiety is involved in a wide variety of biochemical processes including electron transport and oxidative phosphorylation [3]. Various biological properties including enzyme inhibition, antibacterial, antifungal, and anticancer activities have been reported for quinones and quinone derivatives [9]. The antitumor activity of the quinone moiety has been studied thoroughly, and it is known that they act as topoisomerase inhibitors via DNA intercalation [10]. Quinone-annulated heterocycles are found in nature, and most of them exhibit interesting biological activities. The chemistry of quinone-annulated heterocycles is dependent largely on the substituent being either on the quinone or on adjacent rings [11]. These activities, combined with diverse chemical behavior make quinones attractive targets in organic synthesis. The indole framework is common in a wide variety of pharmacologically and biologically active compounds [12]. Furthermore, it has been reported that sharing of the indole 3-carbon atom during the formation of spiroindoline derivatives enhances the biological activity highly [13]. The spiro-oxindole system is the core structure of some pharmacological agents and natural alkaloids [14]. Similarly, xanthenes have been reported to possess diverse biological and therapeutic properties such as antibacterial, antiviral, and anti-inflammatory activities, as well

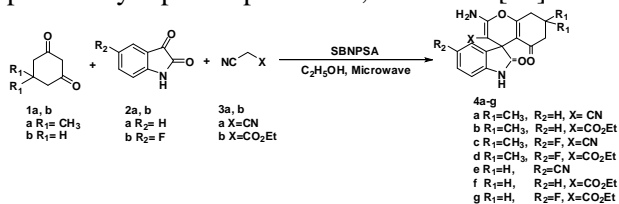
* To whom all correspondence should be sent:

E-mail: aligharib5@yahoo.com

as being used in photodynamic therapy [14]. Other useful applications of these heterocycles are as dyes, fluorescent materials for visualization of biomolecules and in laser technologies [15]. Considering the above reports, and as part of our program aimed at developing new selective and environmentally friendly methodologies for the preparation of heterocyclic compounds [16].

EXPERIMENTAL

All materials and solvents were purchased from Merck and Fluka. Melting points were determined in open capillary tubes in an Electrothermal IA 9700 melting point apparatus. ¹H NMR spectra were recorded on a Bruker-300 MHz instrument using tetramethylsilane (TMS) as an internal standard. IR spectra were recorded on a Shimadzu-IR 470 spectrophotometer. The mass spectra were scanned on a Varian Mat CH-7 instrument at 70 eV. Irradiation was carried out in a domestic microwave oven (Electra, 2450 MHz, 700 W) for optimized time. silica bonded N-propyl sulfamic acid (SBNPSA) was prepared according to our previously reported procedure, Scheme 1 [18].



Scheme 1. Synthesis of spirooxindoles via three-component reaction with isatin (2) in the presence of silica-bonded N-propyl sulfamic acid (SBNPSA) as catalyst under irradiation microwave conditions.

General procedure for the synthesis of spirooxindoles (4a–j):

Silica-bonded N-propyl sulfamic acid (SBNPSA) (0.1 g) was added to a stirred mixture of isatin (1 mmol), malononitrile (1 mmol) and phthalhydrazide (1 mmol) in ethanol (5 mL), and was irradiated in a microwave oven at 700 W for the appropriate time (Table 1). After complete conversion as indicated by TLC, water was added and the product was extracted with ethyl acetate (2 × 15 mL). The combined extracts were dried over anhydrous Na₂SO₄ and concentrated in vacuo. The resulting product was recrystallized from ethanol to afford pure product (4a–j).

3-Amino-5'-nitro-5,10-dioxo spiro[(3'H)-indol-3',1-5,10-dihydro-1(H)-pyrazolo(1,2-b)phthalazin]-(1'H)-2'-one-2-carboxylate (table 1, entry 1, 4a):

Yellow solid. m.p.: 280–282°C. IR (KBr) $\nu_{\max}/\text{cm}^{-1}$: 3377, 3256, 2207, 1710, 1693, 1669,

1609, 1552, 1470, 1437, 1375, 1285, 1255, 1166, 698. ¹H NMR (DMSO-*d*₆, 300 MHz) δ : 7.11 (d, 1H, J = 8.4 Hz), 7.95 (m, 3H), 8.21 (m, 2H), 8.46 (s, 2H, NH₂), 8.62 (d, 1H, J = 7.65 Hz), 11.67 (s, 1H, NH). ¹³C NMR (DMSO-*d*₆, 100 MHz) δ : 64.1, 69.5, 111.0, 114.5, 121.7, 127.6, 128.0, 128.2, 129.5, 135.3, 135.6, 143.5, 148.6, 152.8, 153.0, 157.0, 173.7. MS (m/z): 402 (M⁺). Anal. Calcd. for C₁₉H₁₀N₆O₅: C, 56.72; H, 2.50; N, 20.88%. Found: C, 56.80; H, 2.47; N, 20.82%.

Ethyl 3-amino-1'-allyl-5,10-dioxo spiro[(3'H)-indol-3',1-5,10-dihydro-1(H)-pyrazolo(1,2-b)phthalazin]-(1'H)-2'-one-2-carboxylate (table 1, entry 2, 4b):

Yellow solid. m.p.: 254–256°C. IR (KBr) $\nu_{\max}/\text{cm}^{-1}$: 3385, 3254, 1735, 1709, 1668, 1608, 1572, 1456, 1423, 1377, 1285, 1256, 1178, 692. ¹H NMR (DMSO-*d*₆, 300 MHz) δ : 0.80 (s, 3H), 3.78 (q, 2H, J = 6.9 Hz), 4.25 (2H, J = 17.55 Hz), 5.18 (d, 1H, J = 9.95 Hz), 5.46 (d, 1H, J = 17.55 Hz), 5.83 (m, 1H), 6.90 (t, 1H, J = 7.6 Hz), 6.95 (d, 1H, J = 7.65 Hz), 7.25 (t, 1H, J = 7.65 Hz), 7.36 (d, 1H, J = 6.85 Hz), 7.85 (s, 2H, NH₂), 7.95 (t, 2H, J = 7.65 Hz), 8.05 (d, 1H, J = 9.15 Hz), 8.26 (d, 1H, J = 7.9 Hz). ¹³C NMR (DMSO-*d*₆, 100 MHz) δ : 14.4, 43.7, 59.5, 70.5, 79.7, 111.6, 117.8, 122.7, 124.1, 125.4, 127.1, 127.3, 127.9, 128.5, 130.1, 132.2, 134.7, 135.5, 152.6, 153.1, 157.1, 162.8, 171.8. MS (m/z): 444 (M⁺). Anal. Calcd. for C₂₄H₂₀N₄O₅: C, 64.86; H, 4.54; N, 12.61%. Found: C, 64.75; H, 4.51; N, 12.55%.

3-Amino-1'-allyl-5,10-dioxo spiro[(3'H)-indol-3',1-5,10-dihydro-1(H)-pyrazolo(1,2-b)phthalazin]-(1'H)-2'-one-2-carbonitrile (table 1, entry 3, 4c):

Yellow solid. m.p.: 276–277°C. IR (KBr) $\nu_{\max}/\text{cm}^{-1}$: 3384, 3260, 2200, 1715, 1692, 1665, 1613, 1560, 1469, 1438, 1377, 1285, 1255, 1170, 698. ¹H NMR (DMSO-*d*₆, 300 MHz) δ : 4.35 (2H, J = 13.0 Hz), 5.16 (d, 1H, J = 10.7 Hz), 5.30 (d, 1H, J = 16.8 Hz), 5.81 (m, 1H), 7.00 (d, 1H, J = 7.6 Hz), 7.05 (t, 1H, J = 7.65 Hz), 7.32 (t, 1H, J = 8.4 Hz), 7.54 (d, 1H, J = 7.65 Hz), 7.96 (m, 3H), 8.25 (d, 1H, J = 6.85 Hz), 8.35 (s, 2H, NH₂). ¹³C NMR (DMSO-*d*₆, 100 MHz) δ : 42.5, 60.3, 70.0, 110.2, 114.7, 117.0, 123.9, 125.0, 125.3, 127.5, 128.1, 128.0, 129.1, 131.0, 131.7, 135.0, 135.6, 143.0, 152.4, 153.1, 156.8, 171.5. MS (m/z): 397 (M⁺). Anal. Calcd. for C₂₂H₁₅N₅O₃: C, 66.49; H, 3.80; N, 17.62%. Found: C, 66.57; H, 3.75; N, 17.58%.

Ethyl 3-amino-1'-benzyl-5,10-dioxo spiro[(3'H)-indol-3',1-5,10-dihydro-1(H)-pyrazolo(1,2-

b)phthalazin]-(1*H*)-2'-one-2-carboxylate (table 1, entry 4, 4d):

Yellow solid. m.p.: 290–291°C. IR (KBr) $\nu_{\max}/\text{cm}^{-1}$: 3425, 3317, 1702, 1697, 1529, 1427, 1385, 1299, 1264, 1143, 700. ^1H NMR (DMSO-*d*₆, 300 MHz) δ : 0.63 (m, 3H), 3.41 (m, 2H), 4.86 (t, 2H, *J* = 16.05 Hz), 6.80 (d, 1H, *J* = 7.65 Hz), 6.90 (t, 1H, *J* = 7.65 Hz), 7.18 (t, 1H, *J* = 7.65 Hz), 7.25 (t, 1H, *J* = 6.85 Hz), 7.30 (t, 2H, *J* = 7.65 Hz), 7.38 (d, 1H, *J* = 7.65 Hz), 7.50 (d, 2H, *J* = 7.65 Hz), 7.95 (m, 3H), 8.15 (s, 2H, NH₂), 8.29 (d, 1H, *J* = 9.15 Hz). ^{13}C NMR (DMSO-*d*₆, 100 MHz) δ : 14.1, 43.9, 56.5, 59.1, 70.3, 109.3, 123.1, 124.0, 127.5, 127.8, 127.9, 128.1, 128.9, 129.2, 130.0, 134.8, 135.6, 136.6, 144.5, 152.8, 157.0, 163.6, 172.3. MS (m/z): 494 (M⁺). Anal. Calcd. for C₂₈H₂₂N₄O₅: C, 68.01; H, 4.48; N, 11.33%. Found: C, 67.95; H, 4.42; N, 11.28%.

3-Amino-1'-benzyl-5,10-dioxo spiro[(3'*H*)-indol-3',1-5,10-dihydro-1(*H*)-pyrazolo(1,2-*b*)phthalazin]-(1'*H*)-2'-one-2-carbonitrile (table 1, entry 5, 4e):

Yellow solid. m.p.: 266°C. IR (KBr) $\nu_{\max}/\text{cm}^{-1}$: 3375, 3259, 2198, 1667, 1612, 1469, 1372, 1163, 699. ^1H NMR (DMSO-*d*₆, 300 MHz) δ : 4.95 (t, 2H, *J* = 16.05 Hz), 6.88 (d, 1H, *J* = 8.4 Hz), 7.03 (t, 1H, *J* = 6.85 Hz), 7.25 (d, 2H, *J* = 6.9 Hz), 7.30 (t, 2H, *J* = 7.65 Hz), 7.41 (d, 2H, *J* = 7.6 Hz), 7.55 (d, 1H, *J* = 7.65 Hz), 7.96 (m, 2H), 8.05 (d, 1H, *J* = 6.85 Hz), 8.28 (d, 1H, *J* = 9.15 Hz), 8.40 (s, 2H, NH₂). ^{13}C NMR (DMSO-*d*₆, 100 MHz) δ : 44.0, 60.3, 70.0, 110.2, 115.1, 123.9, 125.1, 125.4, 127.5, 127.7, 128.0, 128.2, 129.1, 129.3, 131.0, 135.0, 135.6, 136.0, 143.1, 152.5, 153.2, 156.8, 171.8. MS (m/z): 447 (M⁺). Anal. Calcd. for C₂₆H₁₇N₅O₃: C, 69.79; H, 3.83; N, 15.65%. Found: C, 69.72; H, 3.78; N, 15.60%.

Ethyl 3-amino-1'-butyl-5,10-dioxo spiro[(3'*H*)-indol-3',1-5,10-dihydro-1(*H*)-pyrazolo(1,2-*b*)phthalazin]-(1'*H*)-2'-one-2-carboxylate (table 1, entry 6, 4f):

Pale yellow solid. m.p.: 258–260°C. IR (KBr) $\nu_{\max}/\text{cm}^{-1}$: 3428, 3320, 2934, 1730, 1704, 1675, 1610, 1528, 1469, 1429, 1377, 1298, 1264, 1142, 757, 699. ^1H NMR (DMSO-*d*₆, 300 MHz) δ : 0.79 (m, 3H), 0.88 (t, 3H, *J* = 6.85 Hz), 1.36 (m, 2H), 1.61 (m, 2H), 3.65 (t, 2H, *J* = 7.65 Hz), 3.80 (m, 2H), 6.91 (t, 1H, *J* = 7.6 Hz), 7.03 (d, 1H, *J* = 8.4 Hz), 7.25 (t, 1H, *J* = 7.65 Hz), 7.35 (d, 1H, *J* = 7.65 Hz), 7.94 (m, 3H), 7.60 (s, 2H, NH₂), 8.26 (d, 1H, *J* = 6.85 Hz). ^{13}C NMR (DMSO-*d*₆, 100 MHz) δ : 14.0, 14.3, 20.1, 29.7, 59.3, 70.0, 80.2, 108.8, 122.7, 124.0, 126.8, 127.6, 128.1, 128.5, 129.0,

130.2, 134.8, 135.5, 144.7, 151.4, 152.7, 157.2, 163.6, 171.8. MS (m/z): 460 (M⁺). Anal. Calcd. for C₂₅H₂₄N₄O₅: C, 65.21; H, 5.25; N, 12.17%. Found: C, 65.27; H, 5.20; N, 12.12%.

3-Amino-1'-butyl-5,10-dioxo spiro[(3'*H*)-indol-3',1-5,10-dihydro-1(*H*)-pyrazolo(1,2-*b*)phthalazin]-(1'*H*)-2'-one-2-carbonitrile (table 1, entry 7, 4g):

Yellow solid. m.p.: 222–223°C. IR (KBr) $\nu_{\max}/\text{cm}^{-1}$: 3384, 3260, 2938, 2197, 1668, 1612, 1562, 1468, 1434, 1375, 1257, 1146. ^1H NMR (DMSO-*d*₆, 300 MHz) δ : 0.85 (t, 3H, *J* = 6.9 Hz), 1.34 (m, 2H), 1.58 (m, 2H), 3.70 (m, 2H), 7.04 (t, 1H, *J* = 7.65 Hz), 7.14 (d, 1H, *J* = 7.65 Hz), 7.36 (t, 1H, *J* = 7.6 Hz), 7.50 (d, 1H, *J* = 6.85 Hz), 7.96 (t, 2H, *J* = 7.6 Hz), 8.00 (d, 1H, *J* = 8.45 Hz), 8.27 (d, 1H, *J* = 7.6 Hz), 8.36 (s, 2H, NH₂). ^{13}C NMR (DMSO-*d*₆, 100 MHz) δ : 14.1, 19.8, 29.7, 60.5, 70.0, 109.8, 114.8, 123.5, 125.0, 125.3, 127.7, 128.1, 128.3, 129.2, 131.3, 134.9, 135.6, 143.6, 152.3, 153.1, 156.9, 171.4. MS (m/z): 413 (M⁺). Anal. Calcd. for C₂₃H₁₉N₅O₃: C, 66.82; H, 4.63; N, 16.94%. Found: C, 66.93; H, 4.58; N, 16.88%.

2.2c 3-Amino-1'-methyl-5,10-dioxo spiro[(3'*H*)-indol-3',1-5,10-dihydro-1(*H*)-pyrazolo(1,2-*b*)phthalazin]-(1'*H*)-2'-one-2-carbonitrile (table 1, entry 8, 4h):

Yellow solid. m.p.: 282–284°C. IR (KBr) $\nu_{\max}/\text{cm}^{-1}$: 3455, 3328, 2197, 1727, 1665, 1610, 1472, 1370, 698 cm⁻¹. ^1H NMR (DMSO-*d*₆, 300 MHz) δ : 3.20 (s, 3H), 7.06 (t, 1H, *J* = 7.65 Hz), 7.10 (d, 1H, *J* = 7.65 Hz), 7.38 (t, 1H, *J* = 8.4 Hz), 7.50 (d, 1H, *J* = 6.9 Hz), 7.96 (m, 3H), 8.25 (d, 1H, *J* = 8.4 Hz), 8.37 (s, 2H, NH₂). ^{13}C NMR (DMSO-*d*₆, 125 MHz) δ : 27.3, 60.1, 69.8, 109.7, 114.9, 123.8, 124.9, 125.3, 127.5, 128.1, 128.3, 129.2, 131.2, 135.0, 135.6, 144.2, 152.4, 153.1, 156.8, 171.5. MS (m/z): 371 (M⁺). Anal. Calcd. for C₂₀H₁₃N₅O₃: C, 64.69; H, 3.53; N, 18.86%. Found: C, 64.63; H, 3.48; N, 18.81%.

Ethyl 3-amino-5,10-dioxo spiro[(3'*H*)-indol-3',1-5,10-dihydro-1(*H*)-pyrazolo(1,2-*b*)phthalazin]-(1'*H*)-2'-one-2-carboxylate (table 1, entry 9, 4i):

Yellow solid. m.p.: 284–286°C. IR (KBr) $\nu_{\max}/\text{cm}^{-1}$: 3439, 3327, 1742, 1700, 1665, 1528, 1294, 1140. ^1H NMR (DMSO-*d*₆, 300 MHz) δ : 0.85 (t, 3H, *J* = 7.65 Hz), 3.80 (m, 2H), 6.80 (d, 1H, *J* = 7.65 Hz), 6.85 (t, 1H, *J* = 6.85 Hz), 7.18 (t, 1H, *J* = 7.65 Hz), 7.28 (d, 1H, *J* = 7.65 Hz), 7.52 (s, 2H, NH₂), 7.93 (m, 3H), 8.25 (d, 1H, *J* = 9.15 Hz), 10.74 (s, 1H). ^{13}C NMR (DMSO-*d*₆, 100 MHz) δ : 14.1, 59.6, 70.5, 81.3, 109.8, 122.1, 124.3, 127.3,

127.5, 128.0, 128.5, 129.1, 130.0, 134.7, 135.5, 143.9, 151.3, 152.6, 157.0, 163.7, 173.5. MS (m/z): 404 (M⁺). Anal. Calcd. For C₂₁H₁₆N₄O₅: C, 62.37; H, 3.99; N, 13.85 %. Found: C, 62.28; H, 3.94; N, 13.78%.

3-Amino-5,10-dioxo spiro[(3'H)-indol-3',1-5,10-dihydro-1(H)-pyrazolo(1,2-b)phthalazin]-(1'H)-2'-one-2-carbonitrile (table 1, entry 10, 4j):

Yellow solid. m.p.: 269–270°C. IR (KBr) $\nu_{\max}/\text{cm}^{-1}$: 3440, 3350, 2207, 1755, 1679, 1654, 1467, 1364, 1258, 1163. ¹H NMR (DMSO-*d*₆, 300 MHz) δ : 6.95 (d, 1H, J = 7.65 Hz), 6.95 (t, 1H, J = 7.65 Hz), 7.26 (t, 1H, J = 7.6 Hz), 7.45 (d, 1H, J = 7.65 Hz), 7.96 (m, 3H), 8.23 (d, 1H, J = 7.65 Hz), 8.34 (s, 2H, NH₂), 10.90 (s, 1H, NH). ¹³C NMR (DMSO-*d*₆, 100 MHz) δ : 60.5, 70.2, 110.9, 114.8, 123.2, 125.2, 125.9, 127.5, 128.1, 128.3, 129.2, 131.0, 134.9, 135.6, 142.7, 152.2, 153.1, 156.9, 173.0. MS (m/z): 357 (M⁺). Anal. Calcd. For C₁₉H₁₁N₅O₃: C, 63.87; H, 3.10; N, 19.60%. Found: C, 63.83; H, 3.06; N, 19.55 %.

Typical procedure for preparation of 2-amino-7,7-dimethyl-20,5-dioxo-5,6,7,8-tetrahydrospiro[chromene-4,30-indoline]-3-carbonitrile (4a):

A mixture of isatin (0.15 g), malononitrile (0.05 g), 5,5-dimethyl-1,3-cyclohexanedione (0.15 g), and silica-bonded N-propyl sulfamic acid (SBNPSA) (0.01 g) in ethanol (6 mL) was stirred and irradiated in a microwave oven at 700 W for the appropriate time (Table 2). Upon completion, monitored by TLC (*n*-hexane/ethyl acetate: 2/1), the reaction mixture was allowed to cool to room temperature. The solid was filtered off and washed with water and cool ethanol to give the desired products. The crude product was recrystallized from EtOH to the yields:

Ethyl-2-amino-50-fluoro-20,5-dioxo-5,6,7,8-tetrahydrospiro[chromene-4,30-indoline]-3-carboxylate (table 2, entry 1, 4a):

White solid. Mp 273–274 °C, IR (KBr) $\nu_{\max}/\text{cm}^{-1}$: 3595, 3366, 3160, 1715, 1695, 1656, 1520, 1295. ¹H NMR (DMSO-*d*₆, 300 MHz) δ : 0.7 (t, 3H, J=7.1 Hz, CH₃), 1.86 (m, 2H, CH₂), 2.19 (m, 2H, CH₂), 2.62 (m, 2H, CH₂), 3.70 (q, 2H, J=6.5 Hz, CH₂), 6.64–6.86 (m, 3H, ArH), 7.90 (s, 2H, NH₂), 10.17 (s, 1H, NH). ¹³C NMR (DMSO-*d*₆, 100 MHz) δ : 13.58, 20.05, 27.45, 37.5, 47.70, 59.36, 76.30, 108.72, 111.7, 113.53, 114.11, 138.30, 140.83, 156.60, 159.65, 165.06, 167.99, 180.34, 195.38. MS, m/z (%): 372 (M⁺, 65), 299 (100), 271

(25), 42 (45). Anal. Calcd for C₁₉H₁₇FN₂O₅: C, 61.29; H, 4.60; N, 7.52%. Found: C, 61.12; H, 4.77; N, 7.69%.

Ethyl-2-amino-20,5-dioxo-5,6,7,8-tetrahydrospiro[chromene-4,30-indoline]-3-carboxylate (table 2, entry 2, 4b):

White solid. Mp 263–265 °C, IR (KBr) $\nu_{\max}/\text{cm}^{-1}$: 3369, 3247, 3160, 1695, 1649, 1524, 1299. ¹H NMR (DMSO-*d*₆, 300 MHz) δ : 0.79 (t, 3H, J=7.1 Hz, CH₃), 1.85 (m, 2H, CH₂), 2.15 (m, 2H, CH₂), 2.62 (m, 2H, CH₂), 3.73 (q, 2H, J=6.1 Hz, CH₂), 6.66–7.05 (m, 4H, ArH), 7.87 (s, 2H, NH₂), 10.15 (s, 1H, NH). ¹³C NMR (DMSO-*d*₆, 100 MHz) δ : 13.57, 20.12, 27.39, 37.58, 47.15, 59.27, 76.80, 108.49, 114.64, 120.98, 122.88, 127.59, 136.56, 144.48, 159.44, 164.69, 168.12, 180.35, 195.29. MS, m/z (%): 354 (M⁺, 40), 281 (100), 253 (25), 55 (30), 39 (30). Anal. Calcd for C₁₉H₁₈N₂O₅: C, 64.40; H, 5.12; N, 7.91%. Found: C, 64.08; H, 5.44; N, 8.23%.

2-Amino-20,5-dioxo-5,6,7,8-tetrahydrospiro[chromene-4,30-indoline]-3-carbonitrile (table 2, entry 3, 4c):

White solid. Mp 251–252 °C, IR (KBr) $\nu_{\max}/\text{cm}^{-1}$: 3365, 3283, 3160, 2195, 17223, 1655, 1347, 1214. ¹H NMR (DMSO-*d*₆, 300 MHz) δ : 1.91 (s, 2H, CH₂), 2.20 (s, 2H, CH₂), 2.65 (s, 2H, CH₂), 6.77–7.10 (m, 4H, ArH), 7.20 (s, 2H, NH₂), 10.38 (s, 1H, NH). ¹³C NMR (DMSO-*d*₆, 100 MHz) δ : 20.25, 27.16, 36.80, 47.30, 57.95, 109.58, 112.30, 122.2, 123.65, 128.58, 134.98, 142.44, 159.06, 166.49, 178.57, 195.47. MS, m/z (%): 307 (M⁺, 50), 251 (100), 209 (50), 140 (55), 39 (30). Anal. Calcd for C₁₇H₁₃N₃O₃: C, 66.44; H, 4.26; N, 13.67%. Found: C, 66.31; H, 4.43; N, 13.84%.

Ethyl-2-amino-50-fluoro-7,7-dimethyl-20,5-dioxo-5,6,7,8-tetrahydrospiro[chromene-4,30-indoline]-3-carboxylate (table 2, entry 4, 4d):

White solid. Mp 240–242 °C, IR (KBr) $\nu_{\max}/\text{cm}^{-1}$: 3395, 3350, 2954, 1707, 1689, 1665, 1487, 1170. ¹H NMR (DMSO-*d*₆, 300 MHz) δ : 0.76 (t, 3H, J=6.5 Hz, CH₃), 0.97 (s, 3H, CH₃), 1.00 (s, 3H, CH₃), 2.05 (d, 1H, J=16.6 Hz), 2.15 (d, 1H, J=15.7 Hz), 2.56 (m, 2H, CH₂), 3.72 (q, 2H, J=6.5 Hz, CH₂), 6.66–6.84 (m, 3H, ArH), 7.90 (s, 2H, NH₂), 10.18 (s, 1H, NH). ¹³C NMR (DMSO-*d*₆, 100 MHz) δ : 13.59, 27.38, 28.07, 31.99, 47.60, 51.08, 59.35, 76.28, 108.87, 110.66, 113.39, 116.67, 138.24, 140.86, 159.63, 163.21, 167.97, 180.23, 195.23. MS, m/z (%): 400 (M⁺, 25), 327 (100), 299 (22), 83 (25), 41 (45). Anal. Calcd for C₂₁H₂₁FN₂O₅: C,

62.99; H, 5.29; N, 7.00%. Found: C, 62.74; H, 5.54; N, 7.25%.

2-Amino-50-fluoro-7,7-dimethyl-20,5-dioxo-5,6,7,8-tetrahydrospiro[chromene-4,30-indoline]-3-carbonitrile (table 2, entry 5, 4e):

Pink solid. Mp 270–273 °C, IR (KBr) $\nu_{\max}/\text{cm}^{-1}$: 3357, 3299, 3160, 2964, 2192, 1725, 1648, 1345, 1225. ^1H NMR (DMSO- d_6 , 300 MHz) δ : 1.00 (s, 3H, CH₃), 1.06 (s, 3H, CH₃), 2.05 (d, 1H, J=15.9 Hz), 2.17 (d, 1H, J=16.0 Hz), 2.53 (m, 2H, CH₂), 6.65–6.77 (m, 3H, ArH), 7.71 (s, 2H, NH₂), 10.25 (s, 1H, NH). ^{13}C NMR (DMSO- d_6 , 100 MHz) δ : 27.36, 28.12, 33.13, 47.37, 51.23, 59.16, 110.17, 112.29, 117.80, 123.09, 124.45, 129.58, 133.80, 144.53, 160.02, 167.52, 179.45, 196.27. MS, m/z (%): 353 (M⁺, 30), 269 (100), 227 (55), 42 (75). Anal. Calcd for C₁₉H₁₆FN₃O₃: C, 64.58; H, 4.56; N, 11.89%. Found: C, 64.27; H, 4.87; N, 12.14%.

Ethyl-2-amino-7,7-dimethyl-20,5-dioxo-5,6,7,8-tetrahydrospiro[chromene-4,30-indoline]-3-carboxylate (table 2, entry 6, 4f):

White solid. Mp 257–258 °C, IR (KBr) $\nu_{\max}/\text{cm}^{-1}$: 3366, 3187, 2926, 1667, 1612, 1223. ^1H NMR (DMSO- d_6 , 300 MHz) δ : 0.79 (t, 3H, J=6.57 Hz, CH₃), 0.95 (s, 3H, CH₃), 1.03 (s, 3H, CH₃), 2.00 (d, 1H, J=15.7 Hz), 2.16 (d, 1H, J=15.7 Hz), 2.57 (m, 2H, CH₂), 3.69 (q, 2H, J=5.2 Hz, CH₂), 6.68–7.04 (m, 4H, ArH), 7.87 (s, 2H, NH₂), 10.15 (s, 1H, NH). ^{13}C NMR (DMSO- d_6 , 100 MHz) δ : 13.56, 27.12, 28.24, 32.0, 47.05, 51.08, 59.30, 76.75, 108.59, 113.53, 120.99, 122.68, 127.63, 136.45, 144.49, 159.56, 162.87, 168.10, 180.26, 195.13. MS, m/z (%): 382 (M⁺, 90), 309 (100), 281 (25), 83 (25), 41 (23). Anal. Calcd for C₂₁H₂₂N₂O₅: C, 65.96; H, 5.80; N, 7.33%. Found: C, 65.72; H, 6.03; N, 7.57%.

2-amino-7,7-dimethyl-20,5-dioxo-5,6,7,8-tetrahydrospiro[chromene-4,30-indoline]-3-carbonitrile (table 2, entry 7, 4g):

white solid. Mp 268–270 °C, IR (KBr) $\nu_{\max}/\text{cm}^{-1}$: 3378, 3314, 2906, 2191, 1722, 1658, 1220. ^1H NMR (DMSO- d_6 , 300 MHz) δ : 0.99 (s, 3H, CH₃), 1.02 (s, 3H, CH₃), 2.08 (d, 1H, J=16.1 Hz), 2.17 (d, 1H, J=15.9 Hz), 2.52 (m, 2H, CH₂), 6.76–7.15 (m, 4H, ArH), 7.22 (s, 2H, NH₂), 10.40 (s, 1H, NH). ^{13}C NMR (DMSO- d_6 , 100 MHz) δ : 27.46, 28.06, 32.40, 47.25, 50.44, 57.89, 109.69, 111.22, 117.81, 122.14, 123.47, 128.63, 134.87, 142.49, 159.22, 164.61, 178.50, 195.37. MS, m/z (%): 335 (M⁺, 50), 251 (100), 210 (25), 83 (23), 66 (23), 39 (35).

Anal. Calcd for C₁₉H₁₇N₃O₃: C, 68.05; H, 5.11; N, 12.53%. Found: C, 67.94; H, 5.23; N, 12.64%.

Ethyl-20-amino-2,50-dioxo-50,60,70,80-tetrahydro-2Hspiro[acenaphthylene-1,40-chromene]-30-carboxylate (table 2, entry 8, 6a):

Yellow solid. Mp 225–227 °C, IR (KBr) $\nu_{\max}/\text{cm}^{-1}$: 3400, 3295, 2989, 1726, 1677, 1520, 1354. ^1H NMR (DMSO- d_6 , 300 MHz) δ : 0.04 (t, 3H, J=7.1 Hz, CH₃), 1.47 (m, 2H, CH₂), 2.65 (t, 2H, J=6.2 Hz, CH₂), 3.45 (q, 2H, J=7.1 Hz, CH₂), 4.52 (t, 2H, J=7.1 Hz, CH₂), 6.58 (s, 2H, NH₂), 7.22–8.48 (m, 6H, ArH). ^{13}C NMR (DMSO- d_6 , 100 MHz) δ : 12.25, 27.43, 36.82, 59.43, 63.40, 75.09, 119.40, 119.90, 122.78, 124.21, 127.80, 127.99, 128.72, 128.83, 129.50, 129.61, 129.71, 132.21, 136.02, 141.23, 164.17, 168.32, 195.60. MS, m/z (%): 389 (M⁺, 20), 316 (100), 176 (80), 149 (40), 55 (25). Anal. Calcd for C₂₃H₁₉NO₅: C, 70.94; H, 4.92; N, 3.60%. Found: C, 70.75; H, 5.12; N, 3.78%.

20-Amino-2,50-dioxo-50,60,70,80-tetrahydro-2Hspiro[acenaphthylene-1,40-chromene]-30-carbonitrile (table 2, entry 9, 6b):

Yellow solid. Mp 245–247 °C, IR (KBr) $\nu_{\max}/\text{cm}^{-1}$: 3372, 3189, 2192, 1718, 1672, 1595, 1344, 1205. ^1H NMR (DMSO- d_6 , 300 MHz) δ : 1.92 (m, 2H, CH₂), 2.15 (m, 2H, CH₂), 2.71 (m, 2H, CH₂), 7.32–8.66 (m, 6H, ArH), 7.92 (s, 2H, NH₂). ^{13}C NMR (DMSO- d_6 , 100 MHz) δ : 20.27, 27.17, 36.50, 51.46, 58.50, 113.55, 117.99, 120.47, 121.81, 124.95, 128.90, 129.33, 130.19, 131.86, 132.67, 140.87, 143.82, 159.10, 166.93, 195.87, 204.06. MS, m/z (%): 342 (M⁺, 23), 230 (70), 202 (50), 175 (40), 84 (30), 42 (100). Anal. Calcd for C₂₁H₁₄N₂O₃: C, 73.68; H, 4.12; N, 8.18%. Found: C, 73.54; H, 4.28; N, 8.34%.

Ethyl-20-amino-70,70-dimethyl-2,50-dioxo-50,60,70,80-tetrahydro-2H-spiro[acenaphthylene-1,40-chromene]-30-carboxylate (table 2, entry 10, 6c):

White solid. Mp 261–263 °C, IR (KBr) $\nu_{\max}/\text{cm}^{-1}$: 3380, 3269, 2953, 1718, 1687, 1519, 1222. ^1H NMR (DMSO- d_6 , 300 MHz) δ : 0.53 (t, 3H, J=7.0 Hz, CH₃), 0.93 (s, 3H, CH₃), 1.01 (s, 3H, CH₃), 1.92 (d, 1H, J=15.9 Hz), 2.07 (d, 1H, J=16.0 Hz), 2.62 (m, 2H, CH₂), 7.22–8.12 (m, 6H, ArH), 7.94 (s, 2H, NH). ^{13}C NMR (DMSO- d_6 , 100 MHz) δ : 12.66, 27.17, 28.23, 32.15, 50.48, 51.16, 58.86, 77.67, 115.32, 119.46, 119.58, 124.23, 128.17, 128.68, 129.71, 129.89, 136.45, 141.09, 145.76, 159.85, 163.41, 167.91, 195.73, 205.65. MS, m/z

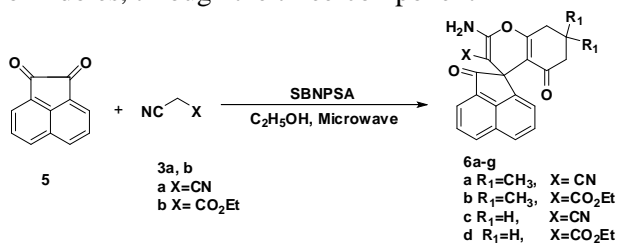
(%): 418 (M^{+1} , 25), 344 (100), 271 (30), 83 (25).
 Anal. Calcd for $C_{25}H_{23}NO_5$: C, 71.93; H, 5.55; N, 3.36%. Found: C, 71.78; H, 5.70; N, 3.95%.

20-Amino-70,70-dimethyl-2,50-dioxo-50,60,70,80-tetrahydro-2H-spiro[acenaphthylene-1,40-chromene]-30-carbonitrile (table 2, entry 11, 6d):

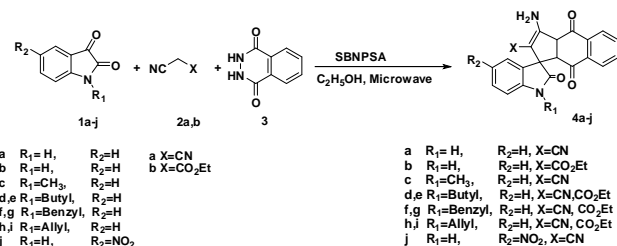
Yellow solid. Mp 260–262 °C, IR (KBr) ν_{max}/cm^{-1} : 3369, 3187, 2953, 2192, 1718, 1666, 1597, 1215. 1H NMR (DMSO- d_6 , 300 MHz) δ : 1.02 (s, 3H, CH_3), 1.04 (s, 3H, CH_3), 2.06 (d, 1H, $J=16.6$ Hz), 2.12 (d, 1H, $J=16.5$ Hz), 2.63 (m, 2H, CH_2), 7.35 (s, 2H, NH_2), 7.38–8.26 (m, 6H, ArH). ^{13}C NMR (DMSO- d_6 , 100 MHz) δ : 27.65, 27.93, 32.50, 50.17, 51.44, 58.48, 112.48, 117.99, 120.28, 121.88, 124.99, 128.94, 129.36, 130.25, 131.90, 132.65, 140.99, 143.66, 159.24, 165.03, 195.77, 204.05. MS, m/z (%): 370 (M^+ , 75), 286 (100), 259 (45), 83 (25), 39 (30). Anal. Calcd for $C_{23}H_{18}N_2O_3$: C, 74.58; H, 4.90; N, 7.56%. Found: C, 74.45; H, 5.15; N, 7.31%.

RESULTS AND DISCUSSION

We wish to report an efficient and green protocol for the three-component synthesis of some chromene derivatives at ambient temperature in excellent yields (Schemes 2 and 3). As part of our endeavour to discover new spirooxindoles of biocidal interest, and guided by the observation that the presence of two or more different heterocyclic moieties in a single molecule often enhances the biocidal profile remarkably, we investigated a three-component reaction of isatin with malononitrile and phthalhydrazide, in order to synthesize a new class of spirooxindoles with fused phthalazines. To the best of our knowledge, there have been no reports on the synthesis of pyrazolophthalaziny spiro-3'-oxindoles. We wish to report here a simple and efficient method for the synthesis of pyrazolophthalaziny spiro-3'-oxindoles, through the three-component

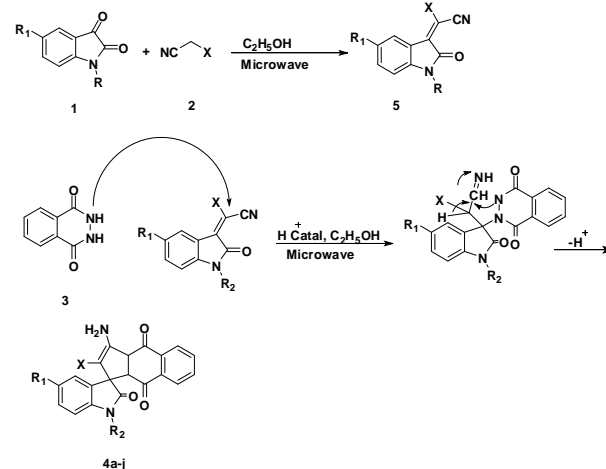


Scheme 2. Synthesis of spirooxindoles via three-component reaction with acenaphthoquinone (5) in the presence of silica-bonded N-propyl sulfamic acid (SBNPSA) as catalyst under irradiation microwave conditions.



Scheme 3. Synthesis of pyrazolophthalaziny spiro-3'-oxindoles 4a–j in the presence of silica-bonded N-propyl sulfamic acid (SBNPSA) as catalyst under irradiation microwave conditions.

condensation of isatin, malononitrile and phthalhydrazide using silica-bonded N-propyl sulfamic acid (SBNPSA) as a catalyst (Scheme 4).



Scheme 4. The mechanism for the synthesis of pyrazolophthalaziny spiro-3'-oxindoles of 4a–j.

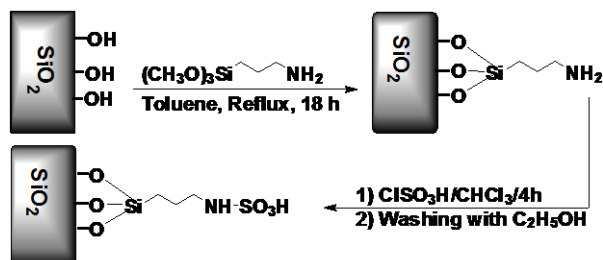
The structures of compounds 4a–j were confirmed by IR, 1H and ^{13}C NMR spectroscopy, mass spectrometry and elemental analysis. The 1H NMR spectrum of 4a exhibited a broad singlet at δ 8.34 due to $-NH_2$, a singlet at δ 10.90 due to $-NH$ isatin and aromatic protons in the range δ 6.95–8.223. Table 1 summarizes our results on the one-pot reaction of various isatin derivatives and malononitrile/ethyl cyanoacetate with phthalhydrazide (scheme 4). All the completed reactions afforded the corresponding pyrazolophthalaziny spiro-3'-oxindoles in good yields.

A possible mechanism for the formation of 4a–j is proposed in Scheme 5. The process represents a typical cascade reaction in which the isatin 1 first condenses with malononitrile/ethyl cyanoacetate 2 to afford isatylidene malononitrile derivative 5. This step can be regarded as a fast Knoevenagel addition. Then, its cyclization affords the corresponding product 4a–j.

Table 1. Synthesis of pyrazolophthalazinyl spiro-3'-oxindoles 4a-j. The reactions were run at microwave conditions and in the presence of silica-bonded *N*-propyl sulfamic acid (**SBNPSA**) as catalyst.

Entry	Product	Time (min)	^a Yield (%)	Mp(°C)
1	4a	35	93(92, 91, 91) ^b	281-283
2	4b	40	89(89, 87, 87) ^b	255-257
3	4c	34	90(89, 88, 88) ^b	276-278
4	4d	34	94(94, 93, 91) ^b	291-292
5	4e	31	97(97, 96, 95.5) ^b	266-267
6	4f	41	91.5(91, 89, 89) ^b	259-261
7	4g	35	94.5(93, 93, 92) ^b	223-224
8	4h	30	95(95, 94, 93) ^b	283-285
9	4i	32	90.5(90, 88, 88) ^b	284-286
10	4j	30	94(93, 93, 92) ^b	268-270

^{a,b} Isolated yield. The reactions were run at microwave conditions and in the presence of silica-bonded *N*-propyl sulfamic acid (**SBNPSA**) catalyst. ^bYield of catalyst recycled three times.

**Scheme 5.** Preparation of silica bonded *N*-propyl sulfamic acid (**SBNPSA**).

The catalyst could be recycled and reused several times without any loss of efficiency. The possibility of recycling the catalyst was examined in the synthesis of pyrazolophthalazinyl spiro-3'-oxindoles (4a-j). When the reaction was completed, the mixture was filtered and the remaining was washed with warm ethanol, and the catalyst reused in the next reaction. The recycled catalyst could be reused three times without any additional treatment. No observation of any appreciable loss in the catalytic activity of **SBNPSA** was observed (Table 1 and Fig 1.). As shown Table 1, the results obtained from the reactions of the malononitrile/ethyl cyanoacetate with isatin indicate that the application of the microwave irradiation can considerably increase the efficiency of these reactions to produce (4a-j) in satisfactory yields (89-97%) and reduce the reaction times when compared with the conventional thermal conditions (Table 1).

We have developed for the synthesis of spirooxindoles. In the present exploration, the reaction of 1,3-dicarbonyl compounds (1a,b), isatin (2a,b), and activated methylene reagents (3a,b) in a molar ratio of 1:1:1 in the presence of catalytic

silica-bonded *N*-propyl sulfamic acid (**SBNPSA**) and ethanol for the appropriate time (Schemes 2,3) furnished spirooxindoles in moderate yields (Table 2).

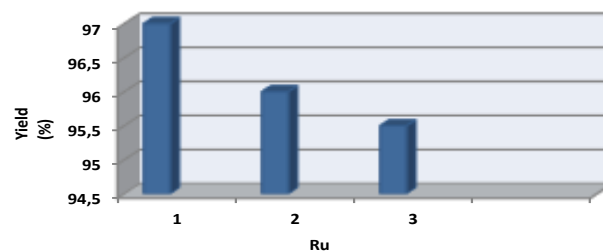
Table 2. Synthesis of compounds 4a-g, 6a-d in EtOH by the reaction of 1,3-diketones (1), isatins (2) or acenaphthenequinone (5), and activated methylene compounds in the presence of silica-bonded *N*-propyl sulfamic acid (**SBNPSA**) as catalyst.

Entry	Product	Time (min)	^a Yield (%)	Mp(°C)
1	4a	10	90	274-275
2	4b	9	89	262-264
3	4c	6	90	250-253
4	4d	6	97	240-242
5	4e	5	85.5	271-273
6	4f	9	91.5	259-260
7	4g	5	94	268-270
8	6a	5	91	226-228
9	6b	10	79.5	244-246
10	6c	9	88	262-264
11	6d	5	95	261-263

^a Isolated yield. The reactions were run at microwave conditions and in the presence of silica-bonded *N*-propyl sulfamic acid (**SBNPSA**) as catalyst.

As shown in Table 2, Two types of substituted isatins and 1,3-cyclohexanediones were used in this reaction (Scheme 2). We examined one-pot reactions involving acenaphthoquinone (5), instead of isatin. Under these conditions, a variety of desired spirochromenes were also produced in excellent yields (Scheme 3, Table 2).

The possibility of recycling the catalyst was examined. For this reason, the reaction of isatin with malononitrile/ethyl cyanoacetate was studied in EtOH in the presence of **SBNPSA**. When the reaction was complete, the mixture was filtered, the residue was washed with warm ethanol and recycled catalyst was reused in the next reaction. No appreciable loss of catalytic activity was observed after twelve cycles (Fig. 1).

**Figure 1.** Recyclability of **SBNPSA** catalyst for the synthesis of compound (Table 1, 4e).

CONCLUSION

In conclusion, we have developed a simple and clean procedure for the synthesis of a series of spirochromene and spirooxindole derivatives catalyzed by silica-bonded *N*-propyl sulfamic acid (SBNPSA) in water starting from commercially available starting materials. The use of inexpensive and available silica-bonded *N*-propyl sulfamic acid (SBNPSA) has made this procedure simple, convenient and practical. The utility of the described methodology in MCRs is highly promising as it allows for the combination of the synthetic virtues of the conventional MCR strategy with the ecological benefits and convenience of the procedure. The microwave irradiation reduced the reaction times in this synthesis. The catalyst was recovered and reused without any noticeable loss of reactivity. The mild reaction conditions and simplicity of the procedure offers improvements over many existing methods.

REFERENCES

- 1 D. Choudhary, S. Paul, R. Gupta, J. H. Clark, *Green Chem.*, **8**, 479 (2000).
- 2 H. Bienayme, C. Hulme, G. Odon, P. Schmidt, *Chem.dEur. J.*, **6**, 3321 (2000).
- 3 J. F. M. Da Silva, S. J. Garden, A. C. Pinto, *J. Braz. Chem. Soc.*, **12**, 273 (2001).
- 4 C.-B. Cui, H. Kakeya, H. Osada, *Tetrahedron*, **52**, 12651 (1996).
- 5 C. Fischer, C. Meyers, E. M. Carreira, *Helv. Chim. Acta*, **83**, 1175 (2000).
- 6 M. Bella, S. Kobbelgaard, K. A. Jorgensen, *J. Am. Chem. Soc.* **127**, 3670 (2005).
- 7 A. Dömling, I. Ugi, *Angew. Chem., Int. Ed.* **39**, 3168 (2000).
- 8 A. Dömling, *Chem. Rev.* **106**, 17 (2006).
- 9 E. B. Skibo, I. Islam, M. J. Hileman, W. G. Schulz, *J. Med. Chem.* **37**, 78 (1994).
- 10 W. A. Denny, B. C. Bagulet, In *Molecular Aspects of Anticancer Drug-DNA Interactions*, 2nd ed.; M. J. Waring, S. Neidle, Eds.; Macmillan: London, (1994) 270.
- 11 M. Tisler, *Advances in Heterocyclic Chemistry. In Heterocyclic Quinones*; Katritzky, A. R., Ed.; Academic: London, **45**, 37 (1989).
- 12 R. J. Sundberg, *The Chemistry of Indoles*; Academic: New York, NY, 1996.
- 13 A. Dandia, R. Sing, S. Khaturia, C. Merienne, G. Morgant, A. Loupy, *Bioorg. Med. Chem.* **14**, 2409 (2006).
- 14 T. Hideu, Jpn. Tokkyo Koho JP 56005480, *Chem. Abstr.*, **95**, 80922b (1981).
- 15 M. Sayyafi, M. Seyyedhamzeh, H. R. Khavasi, A. Bazgir, *Tetrahedron*, **64**, 2375 (2008).
- 16 K. Niknam, D. Saberi, D. *Tetrahedron Lett.*, **50**, 5210 (2009).

N-ПРОПИЛ-СУЛФАМИНОВА КИСЕЛИНА, СВЪРЗАНА СЪС СИЛИЦИЕВ ДИОКСИД: РЕЦИКЛИРУЕМ КАТАЛИЗАТОР ЗА СИНТЕЗА НА СПИРО-ОКСИНДОЛИ ЧРЕЗ ТРИ-КОМПОНЕНТНА РЕАКЦИЯ, СТИМУЛИРАНА ОТ МИКРОВЪЛНИ

А. Гариб^{1,2}, Н. Н. Песян³, Б. Р. Х. Хорасани², М. Рошани¹, Й. В. Схеерен⁴

¹Департамент по химия, Ислямски университет „Азад“, Маишад, Иран

²Земеделски център за изследвания и услуги, Маишад, Иран

³Департамент по химия, Научен факултет, Университет в Урни, 57159 Урния, Иран

⁴Клъстер за молекулярна химия, Департамент по органична химия, Университет Радбуд, Наймехен, Холандия

Постъпила на 13 март, 2012 г.; коригирана на 22 януари, 2012 г.

(Резюме)

N-пропил-сулфаминовата киселина (SBNPSA), свързана със силициев диоксид е използвана като твърд киселинен катализатор за синтезата на спиро-оксиндоли чрез три-компонентна реакция с високи добиви и кратки времена за реакция в среда от етанол. Реакцията е стимулирана от микровълново електромагнитно поле. Най-подходящо е облъчването в комбинация с изагин и аценафтохинон (активиран метиленов реагент) и 1,3-ди-карбонилни съединения в присъствие на катализатор (SBNPSA). Методът е подходящ за синтезиране на биологично значими спиро-оксиндоли.

Ethylene bis (*N*-methyl imidazolium) ditribromide: An efficient and reusable reagent for oxidation of thiols and sulfides

Z. Lasemi^{1,*}, R. Hosseinzadeh², M. Tajbakhsh², M. Mohadjerani³

¹Department of Chemistry, Firoozkooh Branch, Islamic Azad University, Firoozkooh, Iran

²Department of Organic Chemistry, Faculty of Chemistry, University of Mazandaran, Babolsar, Iran

³Department of Biology, Faculty of Science, University of Mazandaran, Babolsar, Iran

Received August 5, 2012; Revised April 30, 2013

Ethylene bis (*N*-methyl imidazolium) ditribromide (EBMIDTB) is an efficient and selective reagent for the oxidation of thiols to their corresponding symmetrical disulfides and sulfides to sulfoxides under mild reaction conditions in good to excellent yields. Selective oxidation of thiols in the presence of sulfides at room temperature is also achieved with this reagent.

Keywords: Ethylene bis (*N*-methyl imidazolium) ditribromide, thiols, sulfides, oxidation, sulfoxides

INTRODUCTION

Disulfides are important compounds possessing unique and diverse chemistry in the synthetic and biochemical areas. Large disulfide-linked aggregates are prevalent in proteins and many other bioactive molecules [1]. Industrially, disulfides find wide applications as vulcanizing agents for rubbers and elastomers, giving them excellent tensile strength. Numerous reagents and catalysts have been applied to oxidize thiols to disulfides under controlled conditions [2]. Disulfides can also be prepared by electrochemical oxidation of thiols in methanol/sodium methoxide solution under constant current [3].

Most of the described methods for oxidation of thiols to disulfides make use of volatile organic solvents [4] and are promoted by molecular bromine supported on silica gel [4a], anhydrous potassium phosphate [4b], PCC [4c], *N*-phenyltriazolinedione [4d], nitric acid [4e], I₂/CeCl₃·7H₂O [4f], VO(acac)₂ [4g], Bu₃SnOMe/FeCl₃ [4h], potassium permanganate [4i], (NH₄)₂S₂O₈ [4j], trichloroisocyanuric acid [4k], montmorillonite K10 [4l], CsF-Celite [4m], and basic alumina [4n].

Although, many of the reported methods are effective, but suffer from drawbacks such as the use of expensive, rare or toxic reagents and metal oxidants, low yields, long reaction times and high temperature, or the risk of overoxidation of the

products. Thus, there is still a demand for simple and efficient oxidative methods that would produce the target disulfides in high yields without above mentioned disadvantages.

On the other hand, selective oxidation of sulfides to the corresponding sulfoxides remains a challenge and is interesting because of the importance of sulfoxides as synthetic intermediates for the construction of various chemically and biologically significant molecules [5], especially for the synthesis of drugs and natural products [6]. There are several reagents available for this key transformation; sulfoxides conventionally prepared using stoichiometric amounts of both organic and inorganic reagents, for example, FeBr₃-nitric acid [7a], *N*-halosuccinimides [7b], NBS/ β -CD/H₂O [7c], *m*-chloroperbenzoic acid [7d], halogens [7e], MnO₂-TMSCl [7f], sodium meta periodate [7g], (*n*-Bu₄N)₂S₂O₈ [7h], CAN [7i], ozone [7j], NaClO₂/Mn (III) catalyst/Alumina [7k], binuclear manganese complex periodic acid [7l], and H[AuCl₄·4H₂O]/H₂O₂ [7m].

Due to importance of sulfoxides in organic synthesis, the introduction of a mild, efficient and selective method to synthesize sulfoxides is still needed.

Tribromide reagents due to their crystalline nature are preferred over some liquid brominating agent such as, liquid bromine, as they are less harmful and can be easily handled and stored, without loss of bromine. These reagents have been recently used as either an oxidant [8] or brominating agent [9] in organic synthesis; for example, tribromides, quinolinium tribromide

* To whom all correspondence should be sent:
E-mail: zlasemi.z@gmail.com

[10a], bipyridinium hydrobromide perbromide [10b], *o*-xylylenebis(triphenylphosphonium tribromide [10c], pyridinium tribromide [10d] and cetyltrimethylammonium tribromide [10e].

EXPERIMENTAL

¹H NMR spectra were measured on Bruker Avance DRX 500 MHz and Bruker Avance 400 MHz spectrometers, using deuterated chloroform (CDCl₃) as solvent. Melting points were determined on Electro Thermal 9100. Materials were purchased from Fluka and Merck companies. All the products were characterized by ¹H NMR, and GC data and also by comparison with authentic samples.

General procedure:

To a solution of thiol or sulfide (1 mmol) in acetonitrile (5 mL), EBMIDTB (0.336 g, 0.5 mmol) was added. The mixture was stirred magnetically at room temperature for the appropriate time (Tables 1, 2). The progress of the reaction was monitored by TLC (eluent: *n*-hexane/ethyl acetate: 5/1) or GC. The reaction mixture was transferred into a separatory funnel, and washed with water (15 mL) and extracted with dichloromethane (20 mL). Organic layer was dried over anhydrous Na₂SO₄ and solvent was concentrated in a rotary evaporator. The crude product was purified by passing it over a column of silica gel, using a mixture of *n*-hexane and ethyl acetate as the eluent. In order to regenerate the reagent, the aqueous layer was concentrated under vacuum and treated with Br₂ in *n*-hexane. All of the products were known compounds and characterized by comparing melting point and ¹H NMR spectra with those reported in the literature. ¹H NMR spectra of some products are given below:

1, 2- Diphenyl disulfide (2a).

Yield 97%; mp 60-61 °C; ¹H NMR (500 MHz, CDCl₃): δ 7.26-7.31 (m, 2H), 7.35-7.40 (m, 4H), 7.57 (d, *J* = 8.3, 2H), 7.61 (d, *J* = 8.3, 2H).

1, 2- Di *p*-tolyl disulfide (2c).

Yield 99%; mp 45-47 °C; ¹H NMR (500 MHz, CDCl₃): δ 2.36 (s, 6H), 7.15 (d, *J* = 8.1, 4H), 7.42 (d, *J* = 8.1, 4H).

1, 2- Bis(4-bromo phenyl) disulfide (2f).

Yield 90%; mp 92-95 °C; ¹H NMR (500 MHz, CDCl₃): δ 7.38 (d, *J* = 8.4, 4H), 7.47 (d, *J* = 8.4, 4H).

1, 2- Bis(benzo thiazolyl) disulfide (2g).

Yield 85%; mp 176-178 °C; ¹H NMR (400 MHz, CDCl₃): δ 7.38 (dt, *J* = 7.7, 1.0, 2H), 7.49 (dt, *J* = 7.7, 1.0, 2H), 7.79 (d, *J* = 8.0, 2H), 7.96 (d, *J* = 8.4, 2H).

1, 2- Dipentyl disulfide (2i).

Yield 85%; ¹H NMR (500 MHz, CDCl₃): δ 0.95 (t, *J* = 7.0, 6H), 1.35-1.44 (m, 8H), 1.69-1.75 (m, 4H), 2.72 (t, *J* = 7.4, 4H).

1, 2- Dicyclohexyl disulfide (2j).

Yield 75%; ¹H NMR (500 MHz, CDCl₃): δ 1.24-1.39 (m, 10H), 1.64-1.67 (m, 2H), 1.81-1.86 (m, 4H), 2.07-2.09 (m, 4H), 2.69-2.74 (m, 2H).

Dibenzyl sulfoxide (4b).

Yield 98%; mp 134-136 °C; ¹H NMR (400 MHz, CDCl₃): δ 3.90 (d, *J* = 13.0, 2H), 3.95 (d, *J* = 13.0, 2H), 7.30-7.33 (m, 4H), 7.35-7.42 (m, 6H).

Benzyl phenyl sulfoxide (4c).

Yield 96%; mp 122-124 °C; ¹H NMR (400 MHz, CDCl₃): δ 4.02 (d, *J* = 12.4, 1H), 4.12 (d, *J* = 12.4, 1H), 7.0 (d, *J* = 7.6, 2H), 7.24-7.33 (m, 4H), 7.38-7.48 (m, 4H).

4-Methyl benzyl phenyl sulfoxide (4d).

Yield 97%; mp 96-98 °C; ¹H NMR (400 MHz, CDCl₃): δ 2.42 (s, 3H), 4.0 (d, *J* = 12.6, 1H), 4.11 (d, *J* = 12.6, 1H), 7.02 (d, *J* = 7.6, 2H), 7.24-7.31 (m, 7H).

RESULTS AND DISCUSSION

Ethylene bis (N-methyl imidazolium) ditribromide is easily prepared from N-methylimidazole, 1,2-dibromoethane and bromine and used for bromination of organic compounds [11]. Herein we report its utility for the oxidation of thiols and sulfides to disulfides and sulfoxides, respectively.

Thiols were oxidized in acetonitrile with EBMIDTB to give the corresponding disulfides at room temperature.

In our first experiments, thiophenol was chosen as a model substrate to determine the optimal reaction conditions. When thiophenol was treated with 0.5 mmol EBMIDTB at room temperature in acetonitrile, complete conversion to the corresponding disulfide achieved within 5 min. This reaction was carried out in different solvents such as CH₂Cl₂, THF, dioxane, ethanol, H₂O and under solvent free condition the best results in

Table 1. Oxidation of thiols with EBMIDTB in acetonitrile
$$\text{R-SH} \xrightarrow[\text{CH}_3\text{CN}]{\text{EBMIDTB}} \text{RS-SR}$$

1a-j 2a-j

Entry	R	Product ^a	Time (min)	Yield % ^b	mp (°C) [Ref]
1	Ph	2a	5	97	60-61 [4e]
2	β -Naphthyl	2b	5	97	143-144 [4e]
3	<i>p</i> -Methyl phenyl	2c	5	99	45-47 [12]
4	<i>p</i> -Methoxy phenyl	2d	5	98	42-43 [13]
5	<i>o</i> -Methyl phenyl	2e	5	60	37-39 [14]
6	<i>p</i> -Bromo phenyl	2f	5	90	92-95 [4e]
7	Benzo thiazolyl	2g	15	85	176-178 [12]
8	Benzyl	2h	15	90	71-72 [4e]
9	<i>n</i> -Pentyl	2i	15	85	Oil [12]
10	Cyclohexyl	2j	15	75	Oil [4e]

^a All the products were identified by comparing of melting point and ¹H NMR spectra with those of authentic samples reported in the literature.

^b Yields refer to isolated products.

Table 2. Oxidation of sulfides with EBMIDTB in acetonitrile.
$$\text{R-S-R}' \xrightarrow[\text{CH}_3\text{CN}]{\text{EBMIDTB}} \text{R-S(=O)-R}'$$

3a-e 4a-e

Entry	R	R'	Product ^a	Time (min)	Yield % ^b	mp (°C) [Ref]
1	Phenyl	Me	4a	20	95	31-33 [15]
2	Benzyl	Benzyl	4b	20	98	134-136 [16]
3	Phenyl	Benzyl	4c	20	96	122-124 [17]
4	<i>p</i> -Methyl benzyl	Phenyl	4d	20	97	96-98 [18]
5	Phenyl	Phenyl	4e	90	-	-

^a All the products were identified by comparing of melting point and ¹H NMR spectra with those of authentic samples reported in the literature.

^b Yields refer to isolated products.

terms of reaction time and yield of the product was obtained, when the reaction conducted in acetonitrile

To show the generality of this procedure, a wide range of aromatic and aliphatic thiols were transformed into the corresponding disulfides by treatment with EBMIDTB in acetonitrile at ambient temperature (Table 1). As it is clear from this table, thiophenol, β -thionaphthol, electron donating and electron withdrawing substituted thiophenols were reacted with EBMIDTB at room temperature to give high yield of the expected disulfides (Table 1, entries 1–6).

p-Methyl and *p*-methoxy thiophenol also under reaction conditions formed the expected disulfide in high yields (Table 1, entries 3 and 4). 2-Mercaptobenzothiazol and aliphatic thiols were converted to their corresponding disulfides in good yields in longer reaction times (Table 1, entries 7–10).

Similarly when sulfides were treated with EBMIDTB in acetonitrile at room temperature, a

high yield of the corresponding sulfoxides were obtained in 20 min (Table 2, entries 1-4). However, diphenylsulfide under the reaction conditions did not afford any sulfoxides even with higher amount of EBMIDTB and at higher temperature (Table 2, entry 5).

In order to study the selectivity of this method, a mixture of equimolar amounts of thiophenol or *p*-methoxythiophenol and phenylmethylsulfide was treated with 0.5 equivalent of EBMIDTB at room temperature. After only 5 min diphenyl and di(*p*-methoxyphenyl)disulfide were formed in 97-98% yield and a trace amount of phenylmethyl sulfoxide was detected (Scheme 1).

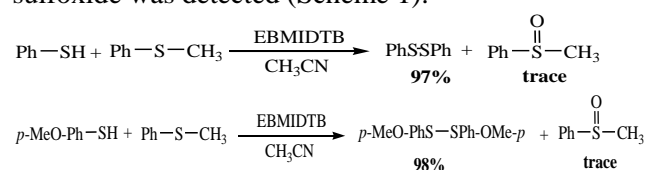
**Scheme 1.** Selective oxidation of thiol in the presence of sulfide.

Table 4. Comparison of EBMIDTB with other tribromide reagents for the oxidation of thiophenol and methyl phenyl sulfide.

Entry	Substrate	Reagent	Reaction Conditions	Time (min)	Yield%	[Ref]
1	Ph-SH	EBMIDTB	CH ₃ CN/rt	5	97	-
2	Ph-SH	phenyltrimethylammonium tribromide	Ethyl acetate	1	95	[19a]
3	Ph-SH	<i>o</i> -xylylenebis (triphenylphosphonium tribromide)	THF/rt	2	98	[10c]
4	Ph-SH	{[K.18-Crown-6]Br ₃ } _n	CH ₃ CN/rt	-	100 (conv.)	[19b]
5	Ph-SH	Benzyl trimethyl ammonium tribromide	NaOH/CH ₂ Cl ₂ /H ₂ O	-	98	[19c]
6	Ph-SH	Quinolinium tribromide	CH ₃ CN/rt	10	95	[10a]
7	Ph-SH	bipyridinium hydrobromide perbromide	rt	10	88	[10b]
8	Ph-S-Me	EBMIDTB	CH ₃ CN/rt	20	95	-
9	Ph-S-Me	<i>o</i> -xylylenebis (triphenylphosphonium tribromide)	THF/rt	5	98	[10c]
10	Ph-S-Me	1,1'-(ethane-1,2-diyl)dipyridinium ditribromide	CH ₂ Cl ₂ /H ₂ O	5	87	[19d]
11	Ph-S-Me	phenyltrimethylammonium tribromide	Ethyl acetate	5	86	[19a]
12	Ph-S-Me	Pyridinium tribromide	CH ₂ Cl ₂ / Hydrated silica gel	25	100	[10d]
13	Ph-S-Me	DBU-hydrobromide-perbromide	H ₂ O ₂ /H ₂ O CH ₃ CN	60	95	[19e]
14	Ph-S-Me	<i>N</i> -methylpyrrolidine-2-one hydrotribromide	CHCl ₃ / H ₂ O 65 °C	180	85	[19f]
15	Ph-S-Me	phenyltrimethylammonium tribromide	Pyridine	180	85	[15]
16	Ph-S-Me	Cetyltrimethyl ammonium tribromide	CH ₃ CN/ H ₂ O/rt	720	93	[10e]

A good feature of this reagent is that it can be regenerated and reused several times without loss of activity. To regenerate the reagent, after completion of the reaction, the mixture was successively washed with water and CH₂Cl₂. The aqueous layer was concentrated and treated with bromine in *n*-hexane to give ethylene bis (*N*-methyl imidazolium) ditribromide, which was identical in all respects with the parent EBMIDTB. This process repeated for three cycles in the oxidation of thiophenol and the yield of the diphenyldisulfide did not change significantly (Table 3). The decrease in conversion can be attributed to the losses during handling of the small amount of reagent during recycle. These results clearly show the stability of EBMIDTB in the reaction media as well its recovery and recycle without any appreciable decrease in its activity.

Table 3. Recycling studies of oxidation of thiophenol to diphenyldisulfide with EBMIDTB.

Entry	Cycle	Time (min)	Yield % ^a
1	fresh	5	97
2	1	5	94
3	2	7	89
4	3	7	87

^a Yields refer to isolated products.

However, in order to show the merits and drawbacks of this reagent, some of our results were compared with other tribromide reagents reported in literature (Table 4). As shown in Table 4, thiophenol and methyl phenyl sulfide were oxidized with EBMIDTB very fast at room temperature in excellent yield in mild conditions (Table 4, entries 1 and 8), which is comparable with some reagents (Table 4, entries 2-5 and 9-11), but in other cases gave better results (Table 4, entries 6-7 and 12-16).

In summary, the method described here is very simple and efficient for the oxidation of thiols and sulfides to the corresponding disulfides and sulfoxides using EBMIDTB. This reagent oxidizes thiols almost quantitatively irrespective of the presence of sulfides. This method is applicable to a wide variety of thiols and sulfides, being a useful alternative of the existing methodologies.

Acknowledgements: We gratefully acknowledge financial support from the Research Council of University of Mazandaran.

REFERENCES

1. M. Bodzansky, *Principles of Peptide Synthesis*, Springer, Berlin, 1984, Chapter 4.

2. (a) G. A. Olah, M. Arvanaghi, Y. D. Vankar, *Synthesis*, 721 (1979). (b) J. P. Mahieu, M. Gosselet, B. Seville, Y. Beuzard, *Synth. Commun.*, **16**, 1709 (1986). (c) H. Firouzabadi, E. Mottghinejad, M. Seddighi, *Synthesis*, 378 (1989). (d) T. Sato, J. Otera, H. Nozaki, *Tetrahedron Lett.*, **31**, 3591(1990). (e) A. Mckillop, D. Koyuncu, *Tetrahedron Lett.*, **31**, 5007 (1990). (f) H. Fujihara, H. Mima, M. Ikemori, N. Furukawa, *J. Am. Chem. Soc.*, **113**, 6337 (1991). (g) H. Suzuki, S. I. Kawato, A. Nasu, *Bull. Chem. Soc. Jpn.*, **65**, 626 (1992). (h) M. Tajbakhsh, R. Hosseinzadeh, A. Shakoori, *Tetrahedron Lett.*, **45**, 1889 (2004). (i) R. Hosseinzadeh, M. Tajbakhsh, H. Khaledi, K. Ghodrati, *Monatsh. Chem.*, **138**, 871 (2007).
3. S. L. S. Leite, V. L. Pardini, H. Viertler, *Synth. Commun.*, **20**, 393 (1990).
4. (a) M. H. Ali, M. Mc Dermott, *Tetrahedron Lett.*, **43**, 6271 (2002). (b) A. V. Joshi, S. Bhusare, M. Baidossi, N. Qafisheh, Y. Sasson, *Tetrahedron Lett.*, **46**, 3583 (2005). (c) P. Salehi, A. Farrokhi, M. Gholizadeh, *Synth. Commun.*, **31**, 2777 (2001). (d) A. Christoforou, G. Nicolaou, Y. Elemes, *Tetrahedron Lett.*, **47**, 9211 (2006). (e) A. K. Misra, G. Agnihotri, *Synth. Commun.*, **34**, 1079 (2004). (f) C. C. Silveira, S. R. Mendes, *Tetrahedron. Lett.*, **48**, 7469 (2007). (g) S. Raghavan, A. Rajender, S. C. Joseph, M. A. Rasheed, *Synth. Commun.*, **31**, 1477 (2001). (h) T. Sato, J. Otera, H. Nozaki, *Tetrahedron. Lett.*, **31**, 3591 (1990). (i) A. Shaabani, F. Tavasoli-Rad, D. G. Lee, *Synth. Commun.*, **35**, 571 (2005). (j) R. S. Varma, H. M. Meshram, R. Dahiya, *Synth Commun.*, **30**, 1249 (2000). (k) P. Zhong, M. P. Guo, *Synth. Commun.*, **31**, 1825 (2001). (l) M. Hirano, S. Yakabe, M. Fukami, T. Morimoto, *Synth. Commun.*, **27**, 2783 (1997). (m) S. T. A. Shah, K. M. Khan, M. Fecker, W. Voelter, *Tetrahedron Lett.*, **44**, 6789 (2003). (n) K. T. Liu, Y. C. Tong, *Synthesis*, 669 (1978).
5. (a) M. C. Carreno, *Chem. Rev.*, **95**, 1717 (1995). (b) G. Solladie, *In Comprehensive Organic Synthesis*, B. M. Trost, I. Fleming, Eds, Academic Press, Oxford, 1991, Vol. 6, p. 148.
6. (a) H. L. Holland, *Chem. Rev.*, **88**, 473 (1988). (b) E. Block, *Angew. Chem., Int. Ed. Engl.*, **31**, 1135 (1992).
7. (a) S. Martin, L. Rossi, *Tetrahedron Lett.*, **41**, 7147 (2001). (b) W. Tagaki, K. Kikukawa, K. Anclo, S. Oac, *Chem. Ind.*, 1624 (1964). (c) K. Surendra, N. S. Krishnaveni, V. P. Kumar, R. Sridhar, K. R. Rao, *Tetrahedron. Lett.*, **46**, 4581 (2005). (d) D. J. Burton, D. M. Wiemers, *J. Fluorine. Chem.*, **18**, 573 (1981). (e) J. Drabowicz, W. Midura, M. Mikolajczyk, *Synthesis*, 39 (1979). (f) F. Bellesia, G. F. Helfi, U. M. Paganoni, A. Pinetti, *Synth. Commun.*, **23**, 1759 (1993). (g) N. J. Leonard, C. R. Johnson, *J. Org. Chem.*, **27**, 282 (1962). (h) F. Chen, J. Wan, C. Guan, J. Yang, H. Zhang, *Synth. Commun.*, **26**, 253 (1996). (i) M. H. Ali, D. R. Leach, C. E. Schmitz, *Synth. Commun.*, **28**, 2969 (1998). (j) R. Varma, R. Sain, H. Meshram, *Tetrahedron Lett.*, **38**, 6525 (1997) and references cited therein. (k) M. Hirano, S. Yakabe, S. Itoh, J. H. Clark, T. Morimoto, *Synthesis*, 1161 (1997). (l) D. Barton, W. Li, *Tetrahedron Lett.*, **39**, 7075 (1998). (m) Y. Yuan, Y. Bian, *Tetrahedron Lett.*, **48**, 8518 (2007).
8. (a) J. K. Joseph, S. L. Jain, B. Sain, *Catal. Commun.*, **8**, 83 (2007). (b) T. Aoyama, T. Takido, M. Kodomari, *Tetrahedron Lett.*, **46**, 1989 (2005).
9. (a) D. Dlugosz, M. Pach, A. Zabrzenska, M. Zegar, B. J. Oleksyn, J. Kalinowska-Tluscik, K. Ostrowska, *Monatsh. Chem.*, **139**, 543 (2008). (b) L. F. Fieser, M. Fieser, *Reagents for Organic Synthesis*, Wiley and Sons Inc, New York, 1967, p. 967. (c) A. Bekaert, O. Provot, O. Rasolojaona, M. Alami, J. D. Brion, *Tetrahedron Lett.*, **46**, 4187 (2005). (d) S. J. Zhang, Z. Le, *Chin. Chem. Lett.*, **16**, 1590 (2005). (e) C. Giordano, L. Coppi, *J. Org. Chem.*, **57**, 2765 (1992).
10. (a) M. Joshaghani, E. Rafiee, F. Shahbazi, H. Jafari, S. Amiri, M. Omid, *Arkivoc*, 164 (2007). (b) M. Joshaghani, A. R. Khosropour, H. Jafary, I. Mohammadpoor-Baltork, *Phosphorus, Sulfur, and Silicon*, **180**, 117 (2005). (c) M. Tajbakhsh, M. M. Lakouraj, K. Yadollahzadeh, A. R. Shakeri, M. A. Khalilzadeh, *J. Chem. Res-S.*, 796 (2005). (d) M. H. Ali, S. Stricklin, *Synth. Commun.*, **36**, 1779 (2006). (e) G. Kar, A. K. Saikia, U. Bora, S. K. Dehury, M. K. Chaudhuri, *Tetrahedron Lett.*, **44**, 4503 (2003).
11. (a) R. Hosseinzadeh, M. Tajbakhsh, M. Mohadjerani, Z. Lasemi, *Monatsh. Chem.*, **140**, 57 (2009). (b) R. Hosseinzadeh, M. Tajbakhsh, M. Mohadjerani, Z. Lasemi, *Synth. Commun.*, **40**, 868 (2010).
12. M. M. Khodaei, I. Mohammadpoor-Baltork, K. Nikoofar, *Bull. Kor. Chem. Soc.*, **24**, 885 (2003).
13. N. Iranpour, B. Zeynizadeh, *Synthesis*, 49 (1999).
14. H. Suzuki, H. Tani, A. Osuka, *Chem. Lett.*, **13**, 139 (1984).
15. J. Rabai, I. Kapovits, B. Tanacs, J. Tamas, *Synthesis*, 847 (1990).
16. C. Caupene, C. Boudou, S. Perrio, P. Metzner, *J. Org. Chem.*, **70**, 2812 (2005).
17. T. Kageyama, Y. Ueno, M. Okamura, *Synthesis*, 815 (1983).
18. H. R. Memarian, I. Mohammadpoor-Baltork, K. Bahrami, *Bull. Korean. Chem. Soc.*, **27**, 106 (2006).
19. (a) A. Ghorbani-Choghamarani, M. Soleiman-Beigi, F. Noormohammadi, *Phosphorus, Sulfur, and Silicon*, **186**, 1665 (2011). (b) M. A. Zolfigol, G. Chehardoli, S. Salehzadeh, H. Adams, M. D. Ward, *Tetrahedron Lett.*, **48**, 7969 (2007). (c) S. Kajigaeshi, K. Murakawa, S. Fujisaki, T. Kakinami, *Chem. Ind. Fac.*, **2**, 129 (1991). (d) A. Ghorbani-Choghamarani, M. A. Zolfigol, T. Azadbakht, *Phosphorus, Sulfur, and Silicon*, **185**, 573 (2010). (e) M. Bakavoli, M. Ghabdian, A. Davoodnia, A. M. Kakhky, A. Shirri, H. Eshghi, M. Khatami, *Chin. Chem. Lett.*, **21**, 651 (2010). (f) J. K. Joseph, S. L. Jain, B. Sain, *Synth. Commun.*, **36**, 2743 (2006).

ЕТИЛЕН БИС-(*N*-МЕТИЛ ИМИДАЗОЛ) ДИ-ТРИБРОМИД: ЕФЕКТИВЕН И МНОГОКРАТНО ИЗПОЛЗВАН РЕАГЕНТ ЗА ОКИСЛЕНИЕТО НА ТИОЛИ И СУЛФИДИ

З. Ласеми¹, Р. Хосеинзаде², М. Таджбакш², М. Мохаджерани³

¹Департамент по химия, клон Фирузку, Ислямски университет "Азад", Фирузку, Иран

²Департамент по органична химия, Факултет по химия, Университет в Мазандаран, Баболсар, Иран

³Департамент по биология, Научен факултет, Университет в Мазандаран, Баболсар, Иран

Постъпила на 5 август, 2012 г.; коригирана на 30 април, 2013 г.

(Резюме)

Етилен бис-(*N*-метил имидазол) ди-трибромидът (ЕВМІДТВ) е ефективен и селективен реагент за окислението на тиоли до съответните симетрични дисулфиди и на сулфиди до сулфоксиди при меки условия с добри до отлични добиви. С този реагент се постига и селективното окисление на тиоли в присъствие на сулфиди при стайна температура.

Synthesis of di-*N*-acetyl- β -chitobiosyl *N*-glycothiazoline

X. Mei, Sh. Shu, F. Cheng, G. Huang*

Chongqing Normal University, Chongqing, 401331, P.R. China

Received May 27, 2013; Accepted June 26, 2013

The synthesis of di-*N*-acetyl- β -chitobiosyl *N*-glycothiazoline **2** was investigated. The synthesis was processed using the *N*-benzyloxycarbonyl (Cbz) protected trichloroacetimidates **11** and **13** as donors, polystyrene as support, and *o*-nitrobenzyl ether tether as linker. The target compound **2** was efficiently yielded by three glycosylations, catalytic hydrogenolysis, acetylation, deacetylation, and photolysis, respectively.

Key words: di-*N*-acetyl- β -chitobiosyl *N*-glycothiazoline, synthesis, glycosylation, analogue

INTRODUCTION

The allosamidin **1** (Fig. 1) is a well-known pseudotrisaccharide, and it is a typical chitinase inhibitor. Compound **1** has the important biological activities, for example, acting as insecticide and fungicide [1]. It has been reported about the synthetic methods of allosamidin **1** and its analogues [2-3], and these compounds mostly were synthesized by the liquid-phase synthesis. The methods have multiple steps and the manufacturing costs are high, which prevents allosamidin **1** and its analogues from being widely utilized in agriculture. The compound **1** was synthesized by the solid/liquid phase methods [1]. However, but the allosamidin **1** must be purified to use column chromatography in the final step. Therefore, it doesn't fully utilize the strongpoint of solid-phase synthesis to synthesize compound **1**. Namely, one can distinctly avoid the purification process if the allosamidin **1** is synthesized by total solid-phase method. So, the redundant reactants or outgrowths can be removed by filtrating and washing. For such point of view, the solid-phase synthesis of di-*N*-acetyl- β -chitobiosyl

N-glycothiazoline **2** was re-studied herein.

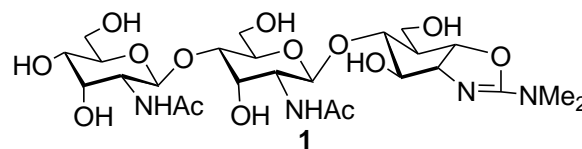
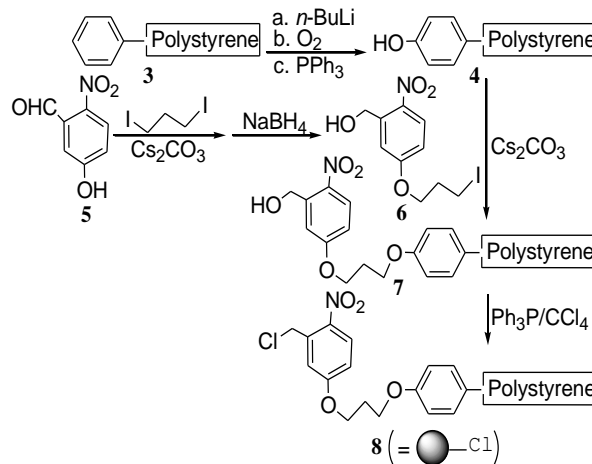


Fig. 1 Structures of allosamidin **1**.

RESULTS AND DISCUSSION



Scheme 1 Preparation of the chlorinated *o*-nitrobenzyl ether polystyrene **8**.

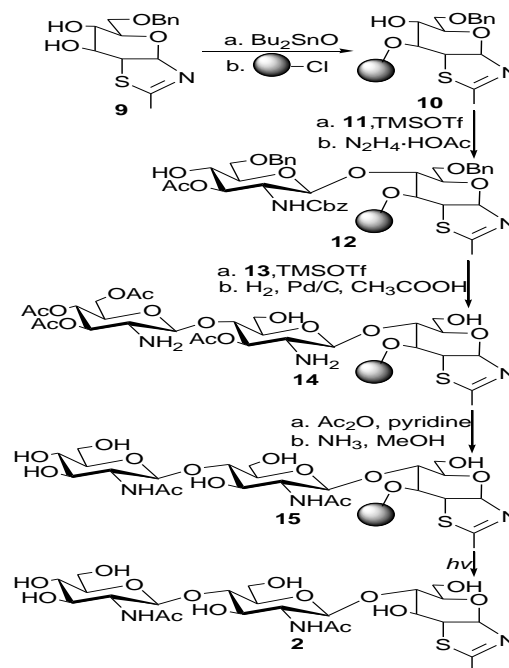
Polystyrene **3** (Scheme 1) was functionalized to phenolic polystyrene **4** by reaction with *n*-BuLi, oxygen, and PPh₃, respectively. The linker, *o*-nitrobenzyl ether tether, was used because it was

* To whom all correspondence should be sent:

easy to attach and cleave. So, the available 5-hydroxy-2-nitrobenzaldehyde **5** was reacted with 1,3-diiodopropane in DMF under the alkaline condition, and then directly was reduced with NaBH₄ to offer iodobenzyl alcohol **6** in 93% yield for the above two steps. Compound **6** was attached to phenolic polystyrene **4** via its linker with Cs₂CO₃ to provide the conjugate **7** in 91% yield based on mass gain of the polymer. Chlorination of compound **7** with Ph₃P/CCl₄ obtained the chloride **8** in 86% yield.

The *N*-glycothiazoline **9** was obtained according to the reported method [4]. The C-3 hydroxyl group of diol **9** was selectively benzylated with chloride **8** and Bu₂SnO [1] to afford the intermediate **10** in 60 % yield (Scheme 2). Glycosylation reactions were gone along using donor (3.0 equiv.) and trimethylsilyl trifluoromethanesulfonate (TMSOTf, 0.1 equiv.) as catalyzer to activate the trichloroacetimidate donor. Under zero temperature, TMSOTf-catalyzed glycosylation of trichloroacetimidate donor **11** under the protection of *N*-benzyloxycarbonyl (Cbz) [5] with the 6-*O*-benzylallosamizoline acceptor **10** yielded the *O*-perprotected β -pseudodisaccharide in 70 % yield. The yield was proved by the analysis of high pressure liquid chromatography (HPLC) after removal of the polystyrene and *o*-nitrobenzyl ether tether by photolysis from the *O*-perprotected β -pseudodisaccharide. This method for yield calculation was analogous to the following process. The levulinoyl ester was removed with hydrazine acetate and MeOH to obtain acceptor **12**. After the acceptor **12** was reacted with trichloroacetimidate donor **13** under the protection of *N*-Cbz [5], the resin-bound saccharide was hydrogenated with Pd/C and acetic acid for removal of Cbz and Bn to provide intermediate **14** in 88 % yield. Whereafter, the resulting mixture was acetylated with Ac₂O-pyridine and deacetylated with NH₃-MeOH, respectively. After above-mentioned reactions were finished, the resin was filtrated and washed, respectively.

Efficient removal of the di-*N*-acetyl- β -chitobiosyl *N*-glycothiazoline **2** moiety from linker was achieved by photolysis of intermediate **15** to offer the target compound **2** [6] in 91 % yield. It wasn't necessary to re-purify di-*N*-acetyl- β -chitobiosyl *N*-glycothiazoline **2** because it had the high purity.



Scheme 2 The synthesis of di-*N*-acetyl- β -chitobiosyl *N*-glycothiazoline **2**.

CONCLUSION

The solid-phase synthesis of di-*N*-acetyl- β -chitobiosyl *N*-glycothiazoline **2** was reported herein. With the support polystyrene and the linker *o*-nitrobenzyl ether tether, the satisfying yield for compound **2** was obtained by three glycosylations, hydrogenation with Pd/C-acetic acid, acetylation, deacetylation, and photolysis, respectively.

Acknowledgments: The work was funded by Natural Science Foundation Project of CQ CSTC (No. cstc2012jjA10101), Open Foundation from Tertiary College of Chongqing Engineering Research Center of Bioactive Substance and Ministry of Education Engineering Research Center of Active Substance & Biotechnology (No. GCZX2012-2), Chongqing University Students'

Training Project of Innovation and Undertaking (Nos. 201210637015 and 201210637010), and Chongqing University Innovation Team Project (No. KJTD201309), China.

Compound 2: ^1H NMR (CD_3OD , 300 MHz): 1.94, 2.01 (2s, 6H, COCH_3), 2.24 (br s, 3H, oxazoline CH_3), 3.17-3.28 (m, 5H), 3.28-3.50 (m, 3H), 3.52-3.71 (m, 6H), 3.82 (d, 1H), 3.88 (d, 1H), 4.27-4.39 (m, 1H, H-2), 4.45, 51 (2d, 2H, H-1", 1"), 4.65 (br s, 1H, H-3), 6.31 (d, 1H, H-1).

REFERENCES

- 1 G.L. Huang, Y.P. Dai, *Synlett*, **21**(10), 1554-1556 (2010).
- 2 G.L. Huang, *Curr. Org. Chem.*, **16**(1), 115-120 (2012).
- 3 G.L. Huang, *Mini-Rev. Med. Chem.*, **12**(7), 665-670 (2012).
- 4 E.M. Reid, E.S. Vigneau, S.S. Gratia, C.H. Marzabadi, and M. De Castro, *Eur. J. Org. Chem.*, **2012**(17), 3295-3303 (2012).
- 5 G.L. Huang, *Lett. Org. Chem.*, **8**(1), 70-72 (2011).

СИНТЕЗА НА ДИ- *N*-АЦЕТИЛ- β -ХИТОБИОЗИЛ *N*-ГЛИКОТИАЗОЛИН

Кс. Мей, Ш. Шу, Ф. Ченг, Г. Хуанг

Университет Чонгкинг, Чонгкинг, 401331, Китайска народна република

Постъпила на 27 май, 2013 г.; приета на 26 юни, 2013 г.

(Резюме)

Изследвана е синтезата на ди- *N*-ацетил- β -хитобиозил *N*-гликотиазолин **2**. Синтезата е извършена използвайки *N*-benzyloxycarbonyl (Cbz), защитени трихлор-ацетимидати **11** и **13** като донори, полистирен като носител и *o*-нитробензил-етер като свързващ агент. Целевото съединение **2** беше получено с високи ефективност и добив съответно чрез три гликолизирания, каталитична хидрогенолиза, ацетилиране, деацетилиране и фотолиза.

Calculation of atomic spectroscopic terms for f^2 and f^{12} orbital configurations, assigning the term symbols and comparative study

P.L. Meena^{1*}, N. Kumar¹, A.S.Meena¹, K.S. Meena², P.K. Jain²

¹Department of Chemistry, M.L.S.University, Udaipur, (Raj.), India-313001

²Department of Chemistry, M.L.V.Govt.College, Bhilwara, (Raj.), India-311001

Received May 20, 2012; Revised September 2, 2012

A term is a particular energy state and term symbol is a label to an energy state. Russell-Saunders (L-S) coupling and j-j coupling schemes are important schemes to determine the terms and to assign the term symbols. In this proposed work computation is done to calculate all possible microstates and atomic spectroscopic terms for f^2 and f^{12} configuration without any long tabulation with mental exercise and a comparative study was carried out between the atomic spectroscopic terms for f^2 and f^{12} orbital configuration. The possible microstates and atomic spectroscopic terms calculated for f^2 and f^{12} orbital configuration are 91 and 7 for each. These terms are triplets (3) and singlet's (4). The ground state term for f^2 and f^{12} configuration is triplet H (3H) and the ground state for f^2 is 3H_4 and for f^{12} is 3H_6 .

Key words: Term symbol, Russell-Saunders coupling, microstate, singlet, triplet.

1. INTRODUCTION

The term refers to the energy associated with the state of an atom involved in a transition. Term symbols are abbreviated descriptions of the energy, angular momentum and spin multiplicity of an atom in a particular state. When only one electron is present at a degenerate energy level or sub shell such as 2p, 3d, 4f, etc., the energy depends on 'l' - the orbital quantum number but when more than one electron is present, they interact with one another with the formation of a ground state and one or more excited states for the atom or ion.

It is found that the Russell-Saunders scheme gives a good approximation for the first row transition series where spin-orbit (j-j) coupling can generally be ignored, however for elements with atomic number greater than thirty, spin-orbit coupling becomes more significant due to the higher nuclear charge and the j-j coupling scheme is used [1-3]. However, for heavier atoms it is still convenient to use the Russell-Saunders scheme [4].

The microstates are expressed by proper term symbols and are defined by new quantum numbers - L, M_L, M_S, S. These quantum numbers for multi electron systems are obtained by vectorial summing of the quantum numbers for the individual electrons [5].

The total number of microstates increases with the increase in the number of electrons in the

orbital. The formulation of a hole can be used for a sub shell that is more than half full. When a sub shell is more than half full, it is simpler and more convenient to work out the terms by considering the holes that are vacancies in the various orbital's rather than the larger number of electrons actually present. By considering the holes, the terms which arise for pairs of atoms with p^n and p^{6-n} , d^n and d^{10-n} and f^n and f^{14-n} arrangements give rise to identical terms [6]. In the f^{12} configuration there are two holes which have the same possible arrangements as the electrons in f^2 configuration. A complete term symbol is $^{(2S+1)}L_J[4,6,7]$.

2. EXPERIMENTAL

2.1. Calculation of the total number of microstates

The question of arranging x electrons in a degenerate set of 'r' orbital's is equivalent to asking how many ways are there to distribute n indistinguishable objects among n boxes (where n would equal 2r). The answer is given by the expression [8]:

Number of ways of filling electrons

$$N = \frac{2(2l+1)!}{x!(2(2l+1)!-x!)} \text{ or } \frac{n!}{x!(n!-x!)}$$

$n = 2(2l+1)$ or two wise of the total number of orbital's,

x = Total number of electrons in sub shell.

* To whom all correspondence should be sent:
E-mail: Parmeshwar1978@gmail.com

So, for f^2 configuration $n= 14$ and $x= 2$

$$N = \frac{14!}{2!(14! - 2!)},$$

$$N = \frac{14 \times 13 \times 12 \times 11 \times 10 \times 9 \times 8 \times 7 \times 6 \times 5 \times 4 \times 3 \times 2 \times 1}{12 \times 11 \times 10 \times 9 \times 8 \times 7 \times 6 \times 5 \times 4 \times 3 \times 2 \times 1 \times 2 \times 1},$$

$N = 91$ Microstates

For f^{12} configuration $n= 14$ and $x=12$

$$N = \frac{14!}{12!(14! - 12!)},$$

$$N = \frac{14 \times 13 \times 12 \times 11 \times 10 \times 9 \times 8 \times 7 \times 6 \times 5 \times 4 \times 3 \times 2 \times 1}{12 \times 11 \times 10 \times 9 \times 8 \times 7 \times 6 \times 5 \times 4 \times 3 \times 2 \times 1 \times 2 \times 1},$$

$N = 91$ Microstates

2.2. Determination of the electronic configuration allowed by the Pauli principle or possible spin conditions for f^2 and f^{12} configuration

It is determined by arranging the possible spin states of electrons in an orbital. Total microstates with possible spin states are given in Tables 1 and 2.

2.3. Determination of orbital angular momentum quantum number (L), l-l coupling

The coupling of orbital momentums of non-equivalent electrons referred to as l-l coupling gives a resultant L of magnitude $[L(L+1)]^{1/2} h/2\pi = L * h/2\pi$. The orientations of l_1 and l_2 for f^2 configuration, which can be taken, are governed by the values that the quantum number L can take. L is

associated with the total orbital angular momentum for the two electrons of the f^2 and the twelve electrons of the f^{12} configuration and is restricted to the values $L= (l_1+l_2), (l_1+l_2 -1), (l_1+l_2 -2) \dots | (l_1-l_2) |$ [4, 6, 7, 9]. The space quantization of L produces $2L+1$ components with $M_L = L, L-1, \dots -L$ analogous of l . In the present case $L= 6,5,4,3,2,1,0$ and the magnitudes of L are $42^{1/2} h/2\pi, 30^{1/2} h/2\pi, 20^{1/2} h/2\pi, 12^{1/2} h/2\pi, 6^{1/2} h/2\pi, 2^{1/2} h/2\pi$ and 0, respectively, which can be drawn by vector diagrams. Some of them are shown in Fig.1, Fig.2 and Fig.1. It follows that the f^2 and f^{12} configurations give rise to S, P, D, F, G, H and I terms corresponding to $L= 0,1,2,3,4,5$ and 6 respectively.

2.4. Determination of total spin angular momentum quantum number (S) s-s coupling

It represents the total spin of an atom while 's' represents the spin state of an electron. The coupling between the spin momentums is referred to as s-s coupling. The vector for each electron is always of magnitude of $3^{1/2} h/2\pi$ according to $[s(s+1)]^{1/2} h/2\pi = s * h/2\pi$. The vectors can only take orientations relative to each other such that the magnitude of the s-s coupling can be as follows: $[S(S+1)]^{1/2} h/2\pi = S * h/2\pi$. $S= (s_1+s_2), (s_1+s_2-1), (s_1+s_2-2) \dots \dots \dots, | (s_1+s_2) |$ [4, 6, 7, 9]. In the case of f^2 and f^{12} configuration for the two and twelve electrons, the values of $S = 1/2$ or zero. The vector sums giving the resultant S vectors of magnitude $2^{1/2} h/2\pi$ or $1^{1/2} h/2\pi$ are drawn in Fig. 2.

Table 1 and 2. Possible spin arrangement of electrons with microstates according to Pauli principle for f^2 and f^{12} configuration.

Table 1 for f^2 configuration

S	Possible spin states	Total Spin	Total M.S
1		+1	21
2		-1	21
3		0	42
4		0	7
Total microstates for f^2 configuration- 91			

Table 2 for f^{12} configuration

S	Possible spin states	Total Spin	Total M.S
1		+1	21
2		-1	21
3		0	42
4		0	7
Total microstates for f^{12} configuration- 91			

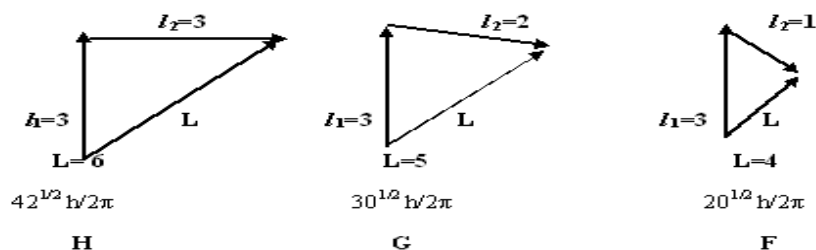


Fig.1. l-l coupling (magnitude of L)

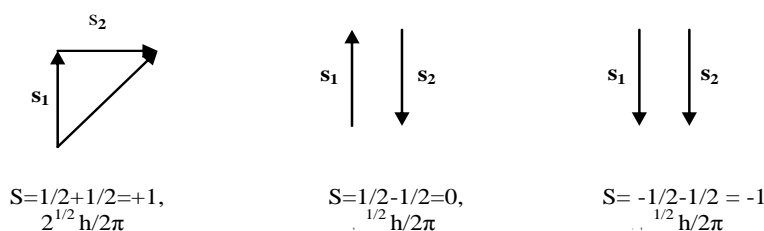


Fig.2. s-s coupling (magnitude of S)

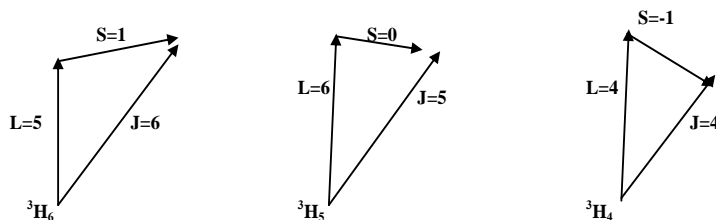


Fig.3. L-S coupling (Magnitude of J)

2.5. Determination of M_L and M_S

$M_L = \sum m_l$ = the components of the total angular momentum along a given axis. The total values of $M_L = 2L+1$, $M_L = +L \dots 0 \dots -L$. The total possible values of M_L for the f^2 and f^{12} configurations are $2 \times 6 + 1 = 13$ $M_L = +6, +5, +4, +3, +2, +1, 0, -1, -2, -3, -4, -5, -6$. $M_S = \sum m_s$. It defines the spin state for a given 'S' value, it is equal to $(2S+1)$. $M_S = +S \dots 0 \dots -S$. $M_S = m_{s1} + m_{s2} + \dots + m_s$. Total M_S values are $2 \times 1 + 1 = 3$ ranging from +1 to -1.

2.6. Determination of (J) L-S coupling

It is a result of the orbital angular momentum vector and the electron spin angular momentum vector. This coupling gives the total angular momentum vector J $[J(J+1)]^{1/2} h/2\pi = J^*h/2\pi$, where J is restricted to the values $J = L+S, L+S-1, \dots, L-S$, from which it follows that if $L \geq S$, J can take $2S+1$ values, but if $L < S$, it can take $2L+1$ values. When $L=0$, J can take only one value, viz., $J=S$. The vector sum can be made only in certain ways and the values of 'J' may be either $1+1/2$ or $1-1/2$. The $1-1/2$ state is of lower energy state since the orbital and spin are opposed [6, 7, 9, 10, 11]. The L-S coupling for 3H term is given in Fig. 3.

2.7. Statistical representation of microstates

All microstates for the f^2 and f^{12} orbital configuration calculated as given above can be represented statistically as given in Tables 3 and 4.

Tables 3 and 4. Microstate chart representing the total number of microstates for f^2 and f^{12} configuration (statistic chart of microstates)

		Table 3			
		M_S			
		+1	0	-1	
M_L	6		1		1
	5	1	2	1	4
	4	1	3	1	5
	3	2	4	2	8
	2	2	5	2	9
	1	3	6	3	12
	0	3	7	3	13
	-1	3	6	3	12
	-2	2	5	2	9
	-3	2	4	2	8
	-4	1	3	1	5
	-5	1	2	1	4
	-6		1		1
Total		21	49	21	91

Table 4

		M_S			
		+1	0	-1	
	6		*		1
	5	*	**	*	4
	4	*	***	*	5
	3	**	****	**	8
	2	**	*****	**	9
	1	***	*****	***	12
M_L	0	***	*****	***	13
	-1	***	*****	***	12
	-2	**	*****	**	9
	-3	**	****	**	8
	-4	*	***	*	5
	-5	*	**	*	4
	-6		*		1
	Total	21	49	21	91

2.8. Resolving the chart of microstates into appropriate atomic spectroscopic terms

An atomic state forms an array of microstates consisting of $2S+1$ columns and $2L+1$ rows. Thus, a 1I state requires one column or (13×1) array and 3H state requires (11×3) array [4, 6]. By removing each state from the microstate table (Table 4) we can draw microstate sub tables for each term [13,18]. The microstate sub tables for each atomic spectroscopic term can be drawn as given in Table 5. The term or energy state (ground and excited) splits up into singlet, doublet, triplet, etc., due to electron-electron coupling and orbit-orbit coupling, which further splits up into different states due to orbit-spin coupling that gives different values of J [19]. The ground state term and the order of stability of other terms can be determined by applying Hund's rule [4, 6, 7, 10, 11, 20].

Table 5. Sub tables representing each atomic spectroscopic term

		M_S	
		0	
	6		
	5		
	4		
	3		
	2		
	1		
M_L	0		
	-1		
	-2		
	-3		
	-4		
	-5		
	-6		
		13	

$L=6, S=0, 2S+1=1,$
Microstates=13,
Term= 1I

Table 5.2

		M_S			
		+1	0	-1	
	5				
	4				
	3				
	2				
	1				
M_L	0				
	-1				
	-2				
	-3				
	-4				
	-5				
		11	11	11	

$L=5, S=1, 2S+1=3,$
Microstates=33, Term= 3H

Table 5.3

		M_S	
		0	
	4		
	3		
	2		
	1		
M_L	0		
	-1		
	-2		
	-3		
	-4		
		9	

$L=4, S=0, 2S+1=1,$
Microstates= 9,
Term= 1G

Table 5.4

		M_S			
		+1	0	-1	
	3				
	2				
	1				
M_L	0				
	-1				
	-2				
	-3				
		7	7	7	

$L=3, S=1, 2S+1=3,$
Microstates=21, Term= 1D

Table 5.5

		M_S	
		0	
	2		
	1		
M_L	0		
	-1		
	-2		
		5	

$L=2, S=0, 2S+1=1,$
Microstates=5,
Term= 3P

Table 5.6

M _s	
	0
M _L 0	
	1
L=0, S=0, 2S+1=1, Microstates=1, Term= ¹ S	

2.9. A complete matrix table for f^2 and f^{12} orbital configuration

It can be drawn as given in Table 6 for f^2 and f^{12} orbital configuration including atomic spectroscopic term, term symbol, microstate, multiplicity, total J values.

3. RESULTS AND DISCUSSION

For the f^2 and f^{12} configuration the total number of atomic spectroscopic terms calculated are 7, out of 7, 3 are triplets and 4 are singlet's. These terms are ³H, ³F, ³P, ¹I, ¹G, ¹D and ¹S. The stability order terms is ³H>³F>³P>¹I>¹G>¹D>¹S. The ground

state term for f^2 and f^{12} is triplet H (³H) which is split up into three energy states due to orbit-spin (interaction) coupling, which are ³H₆, ³H₅, ³H₄.

4. CONCLUSIONS

It is concluded that there are 7 atomic spectroscopic terms for the f^2 and f^{12} configuration which split up into triplets (3) and singlet's (4) due to s-s and l-l coupling. The stability order of the ground state terms for the f^2 configuration is ³H₆<³H₅<³H₄ and for the f^{12} configuration it is ³H₆>³H₅>³H₄, so that the ground state for f^2 configuration is ³H₄ and for f^{12} configuration it is ³H₆. The order of energy of all terms and ground state terms can be drawn as given in fig.4 for f^2 and f^{12} configuration.

5. Acknowledgement: Authors are thankful to all the members of Department of Chemistry M.L.V.Govt. College, Bhilwara and M.L.S. University, Udaipur.

Table 6 A complete matrix table

S. N	L	L Label	S	Multiplicity (2S+1)	Term symbol	Total values of J	Several Possible Terms	Array	Microstates
1	6	I	0	1	¹ I	J=1	¹ I ₆	13x1	13
2	5	H	1	3	³ H	J=3	³ H ₆ , ³ H ₅ , ³ H ₄	11x3	33
3	4	G	0	1	¹ G	J=1	¹ G ₄	9x1	9
4	3	F	1	3	³ F	J=3	³ F ₄ , ³ F ₃ , ³ F ₂	7x3	21
5	2	D	0	1	¹ D	J=1	¹ D ₂	5x1	5
6	1	P	1	3	³ P	J=3	³ P ₂ , ³ P ₁ , ³ P ₀	3x3	9
7	0	S	0	1	¹ S	J=1	¹ S ₀	1x1	1

Total No of Microstates-91

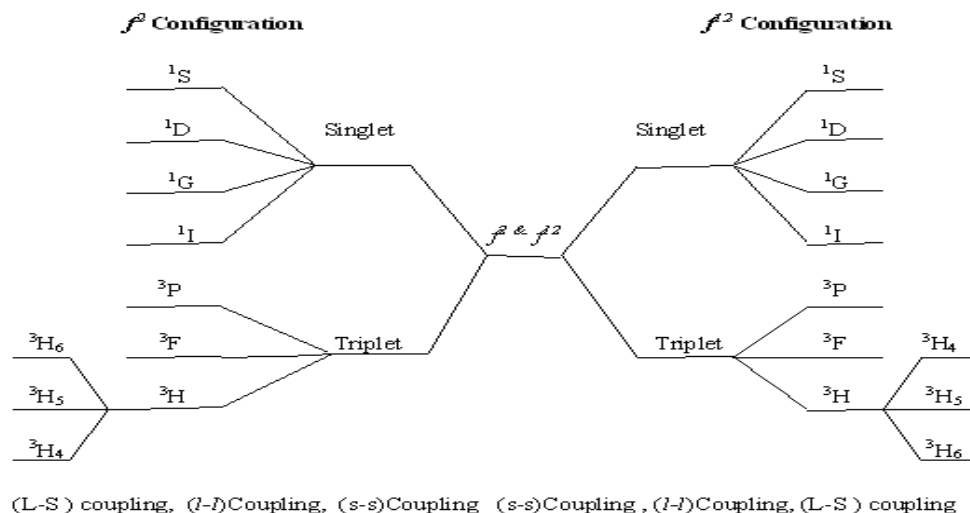


Fig.4. Stability order of different atomic spectroscopic terms

REFERENCES

1. N.J.L. Robert, W.J. Jones, T. Timberlake, *Astrophysics .J.* **61**, 38 (1925).
2. E. Y. Wopg, *J. Chemical Phys.*, **38**, 976 (1963).
3. A.B.P. Lever, *J. Chem. Educ.*, **45**, 711 (1968).
4. B.R.Puri, L.R.Sharma, M.S.Pathania, "Principle of Physical Chemistry", 43rd ed., Vishal Publishing Co. New Delhi, (2008) pp.104, 107.
5. P. K. Jain and R. Goyal, Proc. National Conference, (EVIAC), M. L. V. P.G. Govt. College, Bhilwara, (Raj.), p.75-81 (2010).

- J.D. Lee, Concise Inorganic Chemistry, 5th ed., Chapman and Hall, London, (1996), p. 947.
- W.U.Malik, G.D.Tuli,R.D.Madan, Selected topics in Inorganic Chemistry, S. Chand Group, New Delhi, (1999), pp.22, 24.
- E. Douglas, D.H. McDaniel, Concepts of Model of Inorganic Chemistry, Oxford and IBH Publishing Company, New Delhi, (1970).
- J.E. Huheey, E.A.Keiter, R.L.Keiter, Inorganic Chemistry: Principles of Structure and Reactivity, 4th ed., Harper Collins College New York, (2001), A-8-11.
- D.H. McDaniel, *J. Chem. Ed.*, **54**, 147(1977).
- E.U.Condon, G.H.Shorttley, The theory of atomic spectra, Cambridge, Uni Press, London (1963).
- P. L. Meena, P. K. Jain, N. Kumar, K. S. Meena, R.Goyal, *J. Chem. Bio. Phys. Sci.*, **1.1**, 188 (2011).
- P.L.Meena, N.Kumar, P.K.Jain, Abstracts International Conference AMU, Aligarh (UP) India, 122, IP-51, (2011).
- P.L. Meena , P.K. Jain, N. Kumar, K.S. Meena, *Int. J. Chem. Sci.*, **9**, 1364 (2011).
- P.L. Meena, P.K. Jain, N. Kumar, K.S. Meena, Abstracts National Conference, (NCCSNM), Pacific University, Udaipur (Raj.) India, 10 (2012).
- P.L. Meena , P K. Jain, N. Kumar, K.S. Meena, Abstracts International Conference, (GTER), FET, Gurukul Kangari University, Haridwar (Uttarakhand), India, pp.142,126 (2012)
- P.L. Meena, P.K. Jain, N. Kumar, K.S. Meena, Abstracts International Conference, (ICTSC-2012), Asian Journal of Chemistry ,Udaipur (Raj.) India, AB-284 (2012).
- P.L. Meena, P.K. Jain, N. Kumar, K.S. Meena, *Acta Chim. Pharm. Indica*, **2**, 322 (2012).
- E.M.R. Kiremire, *J. Chem. Educ.*, **64**, 951(1987).
- D.F.Shriver, P.W.Atkins, Inorganic Chemistry, 3rded. Oxford University Press New York (2002) p.4

Изчисляване на атомни спектроскопски нива за f^2 и f^{12} орбитални конфигурации чрез сравнително изследване и символи на нивата

П.Л. Меена¹, Н. Кумар¹, А.С. Меена¹, К.С. Меена², П.К. Джайн²

¹Департамент по химия, М.Л.С.Университет, Удайпур (Раджастан), Индия

²Департамент по химия, М.Л.В. правителствен колеж, Бхилвара, (Раджастан), Индия

Постъпила на 20 май, 2012 г.; коригирана на 2 септември, 2012 г.

(Резюме)

Нивото е особено енергийно състояние, а символът на нивото е означение на това състояние. Свързването по Ръсел-Саундърс (L-S) и j-j – свързването са важни схеми за определянето на нивата и за присвояването на символите към тях. В настоящата работа са изчислени всички възможни микросъстояния и атомни спектроскопски нива за f^2 и f^{12} конфигурации без никакво табулиране. Извършено е сравнително изследване за f^2 и f^{12} орбиталните конфигурации. Възможните микросъстояния и атомни спектроскопски нива, изчислени за f^2 и f^{12} орбитални конфигурации са съответно 91 и 7. Тези нива са триплети (3) и синглети (4). Нивото за основното състояние за f^2 и f^{12} –конфигурациите е триплет Н (3H); основното състояние за f^2 е 3H_4 а за f^{12} е 3H_6

Conversion of free fatty acids in low grade crude palm oil to methyl esters for biodiesel production using chromosulfuric acid

A. Hayyan^{1*}, F.S. Mjalli², M.A. Hashim¹, M. Hayyan¹, I.M. AlNashef³

¹Department of Chemical Engineering, Centre for Ionic Liquids (UMCiL), University of Malaya, Kuala Lumpur 50603, Malaysia

²Petroleum and Chemical Engineering Department, Sultan Qaboos University, Muscat 123, Sultanate of Oman

³Chemical Engineering Department, King Saud University, Riyadh 11421, Saudi Arabia

Received September 29, 2012 ; Revised November 12, 2012

In this study low grade crude palm oil (LGCPO) was proposed as a potential agro-industrial raw material for biodiesel production. Chromosulfuric acid was used as a new homogenous catalyst in the pre-treatment process to reduce the free fatty acids (FFA) content in LGCPO to the acceptable level for producing biodiesel via alkaline transesterification reaction. The results of esterification reaction showed that the FFA of LGCPO was reduced from 7.0 % to less than 1% using optimum operating conditions. The yield of the final product after the alkaline transesterification was 85% with 0.14 % FFA content and ester content 97.5% (mol mol⁻¹) which meets the international standard quality specifications for biodiesel.

Keywords: biodiesel, esterification, free fatty acids, chromosulfuric acid.

INTRODUCTION

The limited resources to produce fuel have driven the attention to biodiesel as an alternative renewable fuel. The production of biodiesel was mainly using vegetable and animal oils [1,2]. Malaysia is one of the biggest palm oil producer and exporter in the world [3]. There has been an increasing interest in the utilization of palm oil for biodiesel raw material as an alternative, renewable, non-toxic, biodegradable and environment friendly one [4-6]. The high value of palm oil as a food product makes its production very expensive [7, 8]. However, many large industrial vegetable oil mill facilities produce low grade crude palm oil (LGCPO). LGCPO is oil with high acidity that can be converted to biodiesel fuel. LGCPO is an attractive feedstock and a significant raw material for biodiesel production. The use of LGCPO can lower the cost of biodiesel production significantly. A number of researchers have worked on a variety of feedstock that have elevated FFA levels [9-12]. LGCPO typically contain 5% to 10% FFAs and this value is high compared to the acceptable level that can be converted to biodiesel fuel [4, 6]. It is reported that the oil should not contain more than 1% FFA for alkaline-catalyst transesterification reactions [2, 5, 12, 13]. Thus, an acid-catalyzed pre-treatment step to convert the FFA to fatty acid

methyl esters (FAME) followed by an alkali-catalyzed step to convert the remaining triacylglycerols (TAG) to FAME and glycerol is the typical process to produce biodiesel fuel from acidic oils [14]. Lipase enzyme was used as a biocatalyst for biodiesel production [15]. Methane-sulfonic acid, ethane-sulfonic acid, and sulfuric acid were used in the esterification reaction for biodiesel production [7-9] while, *p*-toluene sulfonic monohydrate acid (PTSA) was used in the pre-treatment of sludge palm oil (SPO) [6]. Tri-potassium phosphate as a heterogeneous catalyst was studied for biodiesel production by Guan et al [17]. Introducing new type of homogenous acid catalyst is gaining an increasing interest in the development of biodiesel production process. No study was reported in the literature for the esterification of acidic oil using chromosulfuric acid (CSA). Therefore, the main objective of this study was to investigate the potential of using LGCPO as a low-cost feedstock in biodiesel production and to study the influence of operational conditions such as dosage of CSA to LGCPO, molar ratio, reaction temperature, reaction time and stirrer speed for reducing FFAs content to less than 1% in LGCPO and to give high biodiesel yield.

MATERIALS AND METHODS

Raw materials and chemicals

LGCPO was obtained from local mill, Selangor, Malaysia. LGCPO was stored in cool room at 4°C.

* To whom all correspondence should be sent:
E-mail: adeeb.hayyan@yahoo.com

Methyl alcohol anhydrous was purchased from Mallinckrodt Chemicals USA, CSA and potassium hydroxide laboratory grade were purchased from Merck.

Preparation of biodiesel

First, a pre-heating step was performed because LGCPO usually exists in semisolid phase at room temperature similar to sludge palm oil and acidic crude palm oil. The LGCPO was molten in an oven at a temperature of around 70°C and the preheated LGCPO was then transferred into the reactor. The LGCPO was pre-treated by using an acid esterification step. This was followed by an alkaline transesterification under fixed conditions of 10:1 molar ratio, 60°C reaction temperature and 30 min reaction time. The final product was separated and purified to produce high quality biodiesel fuel.

Chemical analysis

The fatty acid composition of LGCPO was determined using a GC/MS (Agilent Technologies 7890A); the capillary column was DB-wax 122-7032, with length of 30 m, film thickness of 0.25 µm and an internal diameter of 0.25 mm. Helium was used as a carrier gas with a flow rate of 36 cm/sec, measured at 50°C; and the experimental run was done for 35 min. A neat sample was diluted in hexane prior to injection into GC. Ester content was analyzed using GC/FID (Perkin Elmer Clarus 500), with a capillary column (Polyethylene glycol wax phase) and an isotherm oven at 250°C.

Monoacylglycerols, diacylglycerols, triacylglycerols, free and total glycerol content were determined using GC/FID (Perkin Elmer Clarus 500). The GC/FID was equipped with an on-column injector, high temperature column with polysiloxo divinyl benzene phase (DB-HT type), and temperature program of oven up to 350°C. The FFA content of LGCPO was tested according to the American Oil Chemists' Society (Ca 5a-40) methods [18]. Product yield is defined as the weight percentage of the final product relative to LGCPO weight at the beginning of experiment [6]. The LGCPO was characterized according to the MPOB test methods [19]. The mean molecular weight of LGCPO was determined based on the saponification value calculated according to Equation 1 [20].

$$S.V. = \frac{3r \cdot 56.1r \cdot 1000}{(\text{mean molecular weight} \cdot 3) + 92.09 - (3r \cdot 18)} \quad (1)$$

where:

S.V. is saponification value defined as mg KOH per g of sample

3 is the number of fatty acids per triacylglycerols

56.1 is molecular mass of KOH (g/mol)

1000 is conversion of units (mg/g)

92.09 is molecular mass of glycerol (g/mol)

18 is molecular mass of water (g/mol)

RESULTS AND DISCUSSION

LGCPO characterization

The study of fatty acid composition is very important to identify properties and the type of carbon chains contained in oil and fat [6]. As shown in Figure 1, the common fatty acids are oleic, palmitic, linoleic and stearic acid.

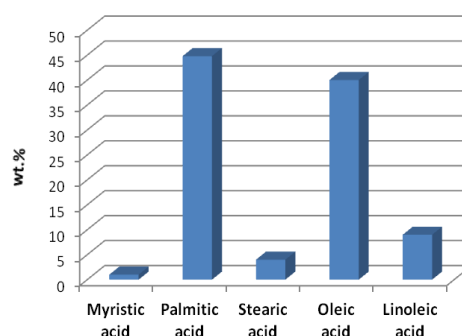


Fig. 1. Fatty acid profile of LGCPO.

The percentage of saturated fatty acids in LGCPO is 44%. Due to the high percentage of saturated fatty acids and FFA, LGCPO exists as a gel phase at room temperature (25±2°C). Higher saturated fatty acids in oils such as LGCPO give a higher cetane number and this type of acidic oil is less prone to oxidation [4]. The vehicle engine works more efficiently with an oil of high cetane number. Table 1 illustrates the characteristics of LGCPO. Based on the saponification value, the average molecular weight calculated was 816.9 g/mol and the LGCPO FFA content used was 7.0 % as shown in Table 1.

Table 1. Characteristics of LGCPO.

Parameters	LGCPO
FFA content (%)	7.0± 0.30
Peroxide value (meq mol/kg)	7.5 ± 0.65
Moisture content (%)	1.03±0.1
Impurities (%)	0.050±0.006
Saponification value (mg KOH/g oil)	198.00 ± 1.70
Unsaponification matter (%)	6.8± 0.22
Ash (%)	0.010± 0.001
Anisidine Value (AV)	3.2± 0.042
DOBI (Index)	1.81± 0.023

The moisture content in LGCPO was found to be 1.03% while the impurities and the ash content were 0.05% and 0.01%. The LGCPO was characterized with high FFA as well as high moisture and impurities content. This indicates that the LGCPO has a lower quality as compared to normal CPO.

Effect of CSA dosage

Using a fixed reaction time (30 min) and fixed molar ratio (10:1), the dosage of CSA was varied in the range of 0.25- 3.5 wt%. The results showed that CSA was a very effective catalyst in the esterification reaction. Figure 2 shows the effect of different dosage of CSA on the reduction of FFA content, conversion of FFA to FAME and yield of treated LGCPO.

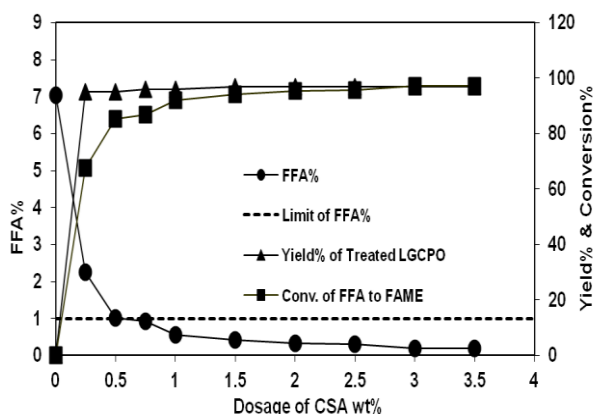


Fig. 2. Effect of CSA dosages on FFA content reduction, conversion of FFA to FAME and yield of treated LGCPO.

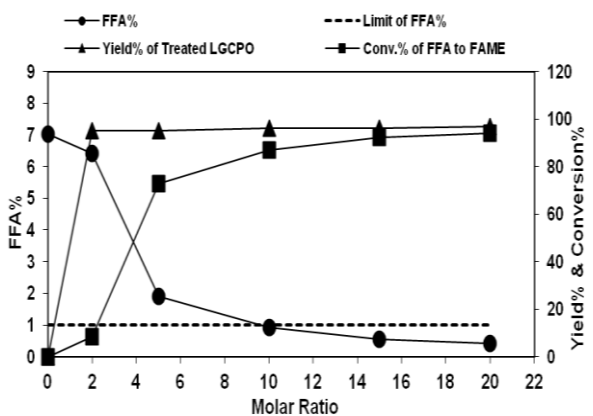


Fig. 3. Effect of molar ratio on FFA content reduction, conversion of FFA to FAME and yield of treated LGCPO.

A FFA content of less than 1% was achieved using a CSA dosage of more than 1 wt%. To minimize catalyst usage, a catalyst dosage value of 0.75% was selected as optimum dosage to reduce the FFA content to the acceptable limit. The conversion of

FFAs to fatty acid methyl ester (FAME) was 86.77% after the esterification process. The FFA content of LGCPO was reduced from 7.0% to 0.92%. In a similar work on SPO, it was reported that 0.75 wt% of the catalyst (such as PTSA) was the optimum dosage needed to reduce the high FFA content [6].

Effect of molar ratio

Molar ratio is one of the important factors affecting the conversion of FFA to FAME, as well as the overall production cost of biodiesel. In this study, the molar ratio of methanol to LGCPO was varied between 2:1 and 20:1. Figure 3 describes the effect of molar ratio on the reduction of FFA content, conversion of FFA to FAME and yield of treated LGCPO. No significant change observed in the reduction of FFA within the molar ratio range of 10:1 to 20:1. On the other hand, a minimum of 10:1 molar ratio were required to reduce the FFA content of LGCPO from 7.0 % to below than 1%, which is the limit of FFA for a successful transesterification reaction. In order to save methanol consumption, a molar ratio of 10:1 was sufficient for the esterification reaction. This ratio was also the optimum ratio reported for the esterification of SPO using PTSA as acid catalyst [6].

Effect of reaction temperature

The reaction temperature during the different steps was reported to range between 40 - 70°C [8, 13]. Figure 4 presents the effect of reaction temperature on the reduction of FFAs content of LGCPO. In this study, it was found that the lowest reaction temperature to reduce the FFA content in LGCPO was 60°C. At this temperature the FFAs content was reduced from 7.0 % to below 1%, with a very high conversion of FFA to FAME. Therefore, a reaction temperature of 60°C was selected for the esterification of LGCPO. It was reported by Leung and Guo [21] that a temperature higher than 50°C had a negative impact on the product yield for neat oil, but had a positive effect for waste oil with higher viscosities. Effect of reaction time

In order to determine the optimum reaction time, esterification reaction time was varied in the range (3-150 minutes). Figure 5 shows the effect of the reaction time on the reduction of FFA content, conversion of FFA to FAME and yield of treated LGCPO. During the course of the reaction and at the first 10–20 minutes, most of FFA was removed as shown in Figure 5. The fast reduction reflects the

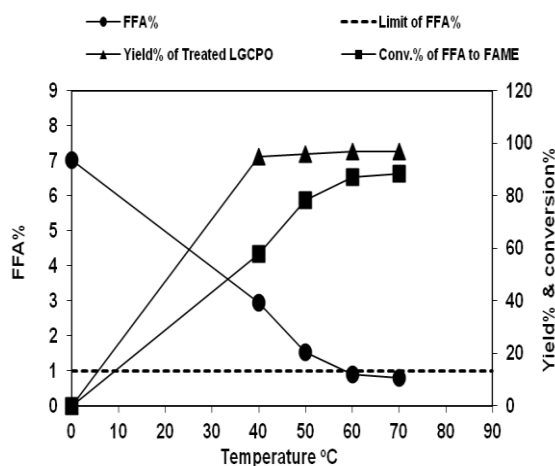


Fig. 4. Effect of reaction temperature on FFA content reduction, conversion of FFA to FAME and yield of treated LGCPO.

catalytic activity of CSA. As shown in Figure 5, the FFA content decreased significantly with the increase in reaction time. A bout 30 to 60 min was sufficient to reduce the FFA content to less than 1%. It was found that after 30 min there was no improvement in the reduction of the acidity along reaction time. Hence, in order to optimize the reaction time, 30 minutes was selected as the shortest reaction time for the pre-treatment of LGCPO. The shortest reaction time can be considered as the optimum value due to the additional cost entailed with longer reaction time. Hashim et al. [22] used trifluoromethanesulfonic acid for the esterification of CPO with high FFA content and the optimum time of reaction was 30 min. The matching between the current study and the mentioned study illustrates that CSA has high catalytic activity compared to super acid (trifluoromethanesulfonic acid).

Effect of stirrer speed

Mixing intensity is a very important operational parameter. Therefore, in order to achieve an effective mass transfer in the esterification reaction, continuous mixing and sufficient reaction time should be used in order to complete the reaction. Mixing intensity affects the kinetics and consequently the whole process. In this study a wide range of mixing speed (100 to 400 rpm) was tested in order to investigate the optimum value for the pre-treatment of LGCPO. Figure 6 shows the effect of stirrer speed on the reduction of FFA content in LGCPO via the esterification reaction. The results revealed that a stirrer speed of 200 was sufficient to reduce FFA content to less than 1%. In order to save energy requirements, lower stirrer speed should be taken as the optimum for LGCPO

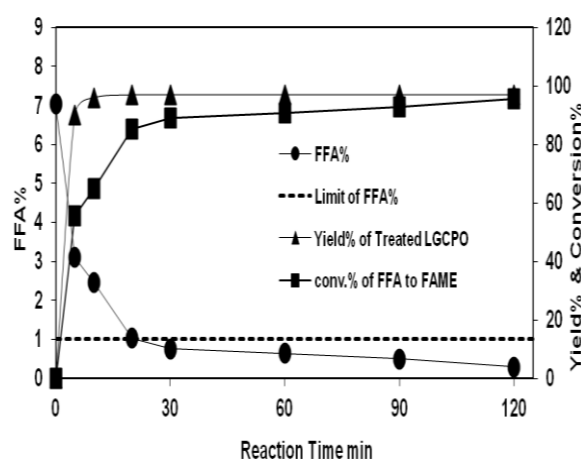


Figure 5. Effect of reaction time on FFA content reduction, conversion of FFA to FAME and yield of treated LGCPO

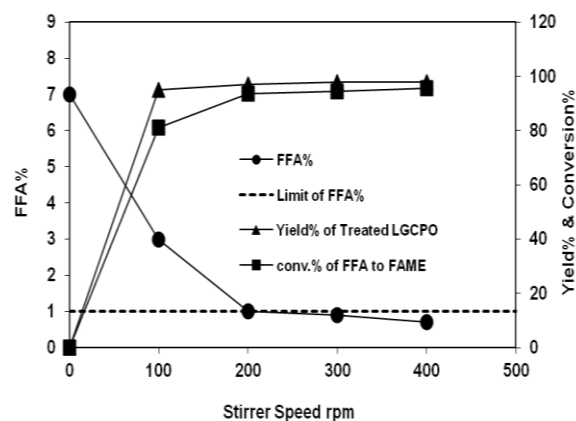


Fig. 6. Effect of stirrer speed on FFA content reduction, conversion of FFA to FAME and yield of treated LGCPO.

esterification. Therefore, a speed of 200 rpm was selected as the optimum mixing intensity. Hayyan et al. [6] used 400 rpm for the pretreatment of SPO due to the high FFA content in SPO compared to LGCPO.

Transesterification reaction

During the esterification reaction, FFA is converted to FAME in the presence of an acid catalyst. The remaining neutral TAG is converted to FAME via transesterification reaction in presence of an alkaline catalyst such as potassium hydroxide. The conditions of biodiesel production were fixed [6,7,23]. The FFA content was less than 0.5% which meets the international standards ASTM D6751-02 and EN 14214. Table 2 shows the fatty acid composition of biodiesel from LGCPO. Using the optimum conditions for the esterification reaction the FFAs were reduced from 7.0 % to less than 1%. The yield of biodiesel was 85% with 0.14 % FFA. The results of this study meet the standard specification for biodiesel fuel as shown in Table 3.

Table 2. Fatty acid composition of biodiesel from LGCPO; results are the average of three replicates \pm standard deviation.

Systematic name of FAME	Carbon chain	Type of fatty acid	FAME content (%)
Dodecanoic acid methyl ester	C12:0	Saturated	0.19 \pm 0.02
Tetradecanoic acid methyl ester	C14:0	Saturated	0.91 \pm 0.02
Hexadecanoic acid methyl ester	C16:0	Saturated	44.1 \pm 1.00
Hexadecenoic acid methyl ester	C16:1	Unsaturated	0.285 \pm 0.002
Octadecanoic acid methyl ester	C18:0	Saturated	4.3 \pm 0.03
<i>cis</i> -9-Octadecenoic acid methyl ester	C18:1	Unsaturated	40.40 \pm 2.40
All- <i>cis</i> -9,12-Octadecadienoic acid methyl ester	C18:2	Unsaturated	9.4 \pm 0.05
All- <i>cis</i> -9,12,15-Octadecatrienoic acid methyl ester	C18:3	Unsaturated	0.28 \pm 0.02
Eicosanoic acid methyl ester	C20:0	Saturated	0.3 \pm 0.003

Table 3. Properties of biodiesel from LGCPO.

Properties	Biodiesel from LGCPO
Ester content	97.5% (mol mol ⁻¹)
Monoacylglycerol content	0.1% (mol mol ⁻¹)
Diacylglycerols content	0.02% (mol mol ⁻¹)
Triacylglycerols content	<0.02% (mol mol ⁻¹)
Free glycerol content	<0.01% (mol mol ⁻¹)
Total glycerol content	0.04% (mol mol ⁻¹)
K content	1 mg kg ⁻¹ max
P content	7.2 mg kg ⁻¹ max
Sulphated ash	<0.005 % (w/w)
Total contamination	0.002 mg kg ⁻¹
FFA content	0.14 %
Copper Strip Corrosion (3hr at 50°C)	Class 1
Cetane Number	77

CONCLUSIONS

This study concludes that LGCPO is a suitable feedstock for biodiesel production with a pre-treatment stage using CSA as a catalyst at 0.75% wt/wt (catalyst to LGCPO) with 10:1 molar ratio and 60° C at 30 min and 200 rpm as stirrer speed. Using these conditions the FFA content was reduced from 7.0 % to less than 1%. The yield of biodiesel was 85% with 0.14 % FFA and ester content 97.5% (mol mol⁻¹). The results attained in the current study meet the international standard specifications for the biodiesel fuel. It is recommended to study the catalytic activity of CSA compared to other conventional homogenous catalysts in the esterification reaction. The comparative study may assist in highlighting the advantages and disadvantages of the different catalysts used for the pre-treatment of acidic oils.

Acknowledgement: The authors would like to express their thanks to University of Malaya HIR-MOHE (D000003-16001), Centre for Ionic Liquids (UMCiL), and the National Plan for Science, Technology, and Innovation at King Saud University (10-ENV1315-02), and Petroleum & Chemical Engineering Department, Sultan Qaboos University for their support to this research.

REFERENCES

1. F. Ma, M.A. Hanna, *Bioresour. Technol.*, **70**, 1 (1999).
2. L.C. Meher, D. Vidya Sagar, S.N. Naik. *Renew. Sustain. Energy Rev.*, **10**, 248 (2006).
3. M.A. Kalam, H.H. Masjuki. *Biomass Bioenerg.*, **23**, 471 (2002).
4. M. Canakci, J. Van Gerpen. *Trans. ASAE.*, **44**, 1429 (2001).
5. M. Canakci., *Bioresour. Technol.*, **98**, 183 (2007).

6. A. Hayyan, M. Z. Alam, M.E.S. Mirghani, N.A. Kabbashi, N.I.N.M. Hakimi, Y.M. Siran, S. Tahiruddin. *Bioresour. Technol.*, **101**, 7804 (2010).
7. A. Hayyan, F. S. Mjalli, M. A. Hashim, M. Hayyan, I. M. AlNashef, S. M. Al-Zahrani, M. A. Al-Saadi. *Bioresour. Technol.* **102**, 9564 (2011).
8. A. Hayyan, M. Z. Alam, M.E.S. Mirghani, N.A. Kabbashi, N.I.N.M. Hakimi, Y.M. Siran, S. Tahiruddin. *Fuel Process. Technol.*, **92**, 920 (2011).
9. A. Hayyan, F.S. Mjalli, M.A. Hashim, M. Hayyan, I. M. AlNashef, S.M. Al-Zahrani, *Chem. Pap.*, **66**, 39 (2012).
10. S. Chongkhong, C. Tongurai, P. Chetpattananondh, C. Bunyakan. *Biomass Bioenerg.*, **31**, 563 (2007).
11. Y.A. Elsheikh, Z. Man, M.A. Bustam, S. Yusup, C.D. Wilfred. *Energy Convers. Manag.*, **52**, 804 (2011).
12. M. Naik, L.C. Meher, S.N. Naik, L.M. Das. *Biomass Bioenerg.*, **32**, 354 (2008).
13. S.V. Ghadge, H. Raheman. *Biomass Bioenerg.*, **28**, 601 (2005).
14. M. Canakci, J.V. Gerpen. *Trans. ASAE.*, **46**, 945 (2003).
15. W.J. Ting, C.M. Huang, N. Giridhar, W.T. Wu. *J. Chinese Inst. Chem. Engineers*, **39**, 203 (2008).
16. G. Guan, K. Kusakabe, S. Yamasaki. *Fuel Process. Technol.*, **90**, 520 (2009).
17. American Oil Chemists' Society (AOCS), Ca 5a-40: free fatty acids. Official Methods and Recommended Practices of the AOCS, 5th ed. American Oil Chemists' Society Press, Champaign, IL. (1997).
18. A. Kuntom, S.W. Lin, T.Y. Ai, N.A. Idris, M. Yusof, T.T. Sue, N.A. Ibrahim. Malaysian Palm Oil Board (MPOB) Test Methods. MPOB, Bangi, Malaysia, (2005).
19. S. Suzanne Nielsen, Food Analysis, Springer, New York Dordrecht Heidelberg London, pp. 247-248 (2010).
20. D.Y.C. Leung, Y. Guo. *Fuel Process Technol.*, **87**, 883 (2006).
21. M.A. Hashim, A. Hayyan, F.S. Mjalli, M. Hayyan, I. M. AlNashef. *Int. J. Sustainable Water Environ. Systems*, **3**, 19 (2011).
22. M. Hayyan, F.S. Mjalli, M.A. Hashim, I.M. AlNashef. *Fuel Process. Technol.*, **91**, 116 (2010).

ИЗПОЛЗВАНЕТО НА ХЛОР-СУЛФОНОВА КИСЕЛИНА ЗА ПРЕВРЪЩАНЕ НА СВОБОДНИТЕ МАСТНИ КИСЕЛИНИ ОТ НИСКО-КАЧЕСТВЕНО ПАЛМОВО МАСЛО В МЕТИЛОВИ ЕСТЕРИ ПРИ ПРОИЗВОДСТВОТО НА БИОДИЗЕЛ

А. Хайян¹, Ф.С. Миджали², М.А. Хашим¹, М. Хайян¹, И.М. АлНашеф³

¹Департамент по инженерна химия, Център за йонни течности (UMCiL), Малайски университет, Куала Лумпур, Малайзия

²Департамент по нефтено и химично инженерство, Университет "Султан Кабус", Мускат, Султанат Оман

³Департамент по инженерна химия, Университет "Крал Сауд", Риад, Саудитска Арабия

Постъпила на 29 септември, 2012 г.; коригирана на 12 ноември, 2012 г.

Предложено е ниско-качествено палмово масло (LGPO) като потенциална растителна суровина за производството на биодизел. Като катализатор на хомогенната химична реакция при предварителното третиране на суровината за намаляване съдържанието на свободните мастни киселини (FFA) в палмовото масло до приемливо ниво преди последващата алкална транс-естерификация е използвана хлор-сулфонова киселина. Резултатите от естерификацията показват, че FFA в палмовото масло са намалели от 7.0 до под 1% при оптимални работни условия. Добивът на крайния продукт след естерификацията е 85% с 0.14 % свободни мастни киселини и съдържание на естери от 97.5% (mol mol⁻¹) което удовлетворява международните изисквания за качеството на биодизел.

BULGARIAN CHEMICAL COMMUNICATIONS

Instructions about Preparation of Manuscripts

General remarks: Manuscripts are submitted in English by e-mail or by mail (in duplicate). The text must be typed double-spaced, on A4 format paper using Times New Roman font size 12, normal character spacing. The manuscript should not exceed 15 pages (about 3500 words), including photographs, tables, drawings, formulae, etc. Authors are requested to use margins of 3 cm on all sides. For mail submission hard copies, made by a clearly legible duplication process, are requested. Manuscripts should be subdivided into labelled sections, e.g. **Introduction, Experimental, Results and Discussion, etc.**

The title page comprises headline, author's names and affiliations, abstract and key words.

Attention is drawn to the following:

a) **The title** of the manuscript should reflect concisely the purpose and findings of the work. Abbreviations, symbols, chemical formulas, references and footnotes should be avoided. If indispensable, abbreviations and formulas should be given in parentheses immediately after the respective full form.

b) **The author's** first and middle name initials, and family name in full should be given, followed by the address (or addresses) of the contributing laboratory (laboratories). **The affiliation** of the author(s) should be listed in detail (no abbreviations!). The author to whom correspondence and/or inquiries should be sent should be indicated by asterisk (*).

The abstract should be self-explanatory and intelligible without any references to the text and containing not more than 250 words. It should be followed by key words (not more than six).

References should be numbered sequentially in the order, in which they are cited in the text. The numbers in the text should be enclosed in brackets [2], [5, 6], [9–12], etc., set on the text line. References, typed with double spacing, are to be listed in numerical order on a separate sheet. All references are to be given in Latin letters. The names of the authors are given without inversion. Titles of journals must be abbreviated according to Chemical Abstracts and given in italics, the volume is typed in bold, the initial page is given and the year in parentheses. Attention is drawn to the following conventions:

a) The names of all authors of a certain publications should be given. The use of “*et al.*” in

the list of references is not acceptable.

b) Only the initials of the first and middle names should be given.

In the manuscripts, the reference to author(s) of cited works should be made without giving initials, e.g. “Bush and Smith [7] pioneered...”. If the reference carries the names of three or more authors it should be quoted as “Bush *et al.* [7]”, if Bush is the first author, or as “Bush and co-workers [7]”, if Bush is the senior author.

Footnotes should be reduced to a minimum. Each footnote should be typed double-spaced at the bottom of the page, on which its subject is first mentioned.

Tables are numbered with Arabic numerals on the left-hand top. Each table should be referred to in the text. Column headings should be as short as possible but they must define units unambiguously. The units are to be separated from the preceding symbols by a comma or brackets.

Note: The following format should be used when figures, equations, *etc.* are referred to the text (followed by the respective numbers): Fig., Eqns., Table, Scheme.

Schemes and figures. Each manuscript (hard copy) should contain or be accompanied by the respective illustrative material as well as by the respective figure captions in a separate file (sheet). As far as presentation of units is concerned, SI units are to be used. However, some non-SI units are also acceptable, such as °C, ml, l, etc.

The author(s) name(s), the title of the manuscript, the number of drawings, photographs, diagrams, etc., should be written in black pencil on the back of the illustrative material (hard copies) in accordance with the list enclosed. Avoid using more than 6 (12 for reviews, respectively) figures in the manuscript. Since most of the illustrative materials are to be presented as 8-cm wide pictures, attention should be paid that all axis titles, numerals, legend(s) and texts are legible.

The authors are asked to submit **the final text** (after the manuscript has been accepted for publication) in electronic form either by e-mail or mail on a 3.5” diskette (CD) using a PC Word-processor. The main text, list of references, tables and figure captions should be saved in separate files (as *.rtf or *.doc) with clearly identifiable file names. It is essential that the name and version of

the word-processing program and the format of the text files is clearly indicated. It is recommended that the pictures are presented in *.tif, *.jpg, *.cdr or *.bmp format, the equations are written using "Equation Editor" and chemical reaction schemes are written using ISIS Draw or ChemDraw programme.

The authors are required to submit the final text with a list of three individuals and their e-mail addresses that can be considered by the Editors as potential reviewers. Please, note that the reviewers should be outside the authors' own institution or organization. The Editorial Board of the journal is not obliged to accept these proposals.

EXAMPLES FOR PRESENTATION OF REFERENCES

REFERENCES

1. D. S. Newsome, *Catal. Rev.–Sci. Eng.*, **21**, 275 (1980).
2. C.-H. Lin, C.-Y. Hsu, *J. Chem. Soc. Chem. Commun.*, 1479 (1992).
3. R. G. Parr, W. Yang, *Density Functional Theory of Atoms and Molecules*, Oxford Univ. Press, New York, 1989.
4. V. Ponec, G. C. Bond, *Catalysis by Metals and Alloys (Stud. Surf. Sci. Catal., vol. 95)*, Elsevier, Amsterdam, 1995.
5. G. Kadinov, S. Todorova, A. Palazov, in: *New Frontiers in Catalysis (Proc. 10th Int. Congr. Catal., Budapest, 1992)*, L. Guzzi, F. Solymosi, P. Tetenyi (eds.), Akademiai Kiado, Budapest, 1993, Part C, p. 2817.
6. G. L. C. Maire, F. Garin, in: *Catalysis. Science and Technology*, J. R. Anderson, M. Boudart (eds), vol. 6, Springer-Verlag, Berlin, 1984, p. 161.
7. D. Pocknell, *GB Patent 2 207 355* (1949).
8. G. Angelov, PhD Thesis, UCTM, Sofia, 2001.
9. JCPDS International Center for Diffraction Data, *Power Diffraction File*, Swarthmore, PA, 1991.
10. *CA* **127**, 184 762q (1998).
11. P. Hou, H. Wise, *J. Catal.*, in press.
12. M. Sinev, private communication.
13. <http://www.chemweb.com/alchem/articles/1051611477211.html>.

CONTENTS

<i>R. Venkatram, V.K. Pai, S. Nagaraj</i> , Novel enantioselective synthesis and dissolution studies on enteric coated pellets of (<i>S</i>)-duloxetine hydrochloride.....	269
<i>K. Shubakar, K.B. Umesha, N. Srikantamurthy, J. Chethan</i> , Synthesis and antimicrobial evaluation of novel derivatives of 1,3,4-thiadiazine incorporated with pyrazole-4-carboxylic acid moiety.....	274
<i>E. Grigorova, M. Khristov, P. Peshev, D. Nihtianova, N. Velichkova, G. Atanasova</i> , Hydrogen sorption properties of a MgH ₂ - V ₂ O ₅ composite prepared by ball milling.....	280
<i>R. Adonyi, E. G. Kirilova, N. Gr. Vaklieva-Bancheva</i> , Systematic approach for designing and activities' scheduling of supply chain network.....	288
<i>M. J. Pourvaghari</i> , Assessing the nano scale variation of the ferritin and iron level following two months of progressively increasing interval physical activity	296
<i>S. Dochev, A. Penkova, P. Retailleau, I. Manolov</i> , Synthesis and crystal structure of an ammonium salt of 4-hydroxy-3-[(2-oxo-2H-chromen-3-yl)-(3,4,5-trimethoxyphenyl)-methyl]chromen-2-one	301
<i>M. Yavari</i> , Permutation symmetry of fullerene isomers of C ₈₂	310
<i>A. Gharib, N. N. Pesyan, M. Jahangir, M. Roshani, J. (Hans) W. Scheeren</i> , A catalytic crossed-aldol condensation of ketones with aromatic and non-aromatic aldehydes by silica supported Preyssler heteropolyacids catalyst.....	314
<i>S. S. Mitić, B. T. Stojanović, M. B. Stojković, M. N. Mitić, J. Lj. Pavlović</i> , Total phenolics, flavonoids and antioxidant activity of different apple cultivars	326
<i>L. Figueroa-Valverde, F. Díaz-Cedillo, E. García-Cervera, E. Pool Gómez, M. Rosas-Nexticapa, M. López-Ramos</i> , Design and synthesis of two sulfathiazole derivatives using a three-component system	332
<i>M. Mohammadian, A. K. Haghi</i> , Some aspects of multilayer chitosan electrospun nanofibers web	336
<i>M. K. Hourani, A. I. Wehbeh</i> , Electrochemical characterization of Jordanian coins	347
<i>A. Mobinikhaledi, F. Sasani, A. Hamta, S.M. Shariatzadeh</i> , Molecular iodine catalyzed synthesis of some biologically active dihydroperimidines	353
<i>K. Ignatova</i> , Electrodeposition of Ag and Ag-Ni powders in potentiostatic and pulse potential modes.	357
<i>E. Mladenova, D. Vladikova, Z. Stoynov, A. Chesnaud, A. Thorel, M. Krapchanska</i> , Gases permeability study in dual membrane fuel cell.....	366
<i>A. Gharib, N. N. Pesyan, B. R. H. Khorasani, M. Roshani, J. W. Scheeren</i> , Silica-bonded N-propyl sulfamic acid: A recyclable catalyst for microwave-assisted synthesis of spirooxindoles via three-component reaction	371
<i>Z. Lasemi, R. Hosseinzadeh, M. Tajbakhsh, M. Mohadjerani</i> , Ethylene bis (N-methyl imidazolium) ditribromide: An efficient and reusable reagent for oxidation of thiols and sulfides	379
<i>X. Mei, Sh. Shu, F. Cheng, G. Huang</i> , Synthesis of di-N-acetyl-β-chitobiosyl N-glycothiazoline	385
<i>P.L. Meena, N. Kumar, A.S.Meena, K.S. Meena, P.K. Jain</i> , Calculation of atomic spectroscopic terms for f ² and f ¹² orbital configuration, assigning the term symbols and comparative study .	388
<i>A. Hayyan, F. S. Mjalli, M. A. Hashim, M. Hayyan, I. M. AlNashef</i> , Conversion of free fatty acids in low grade crude palm oil to methyl esters for biodiesel production using chromosulfuric acid ..	394
INSTRUCTIONS TO THE AUTHORS.....	400

СЪДЪРЖАНИЕ

<i>Р. Венкатрам, В.К. Паи, С. Нагарадж</i> , Нова енантоселективна синтеза и разтваряне на филмови таблетки от (S)-дулоксетин хидрохлорид с ентеро-приложение	273
<i>К. Шубакар, К. Б. Умеша, Н. Срикантамурти, Дж. Четхан</i> , Синтеза и антимикробни свойства на нови производни на 1,3,4-тиадиазин включени в среда от пиразол-4-карбонова киселина	279
<i>Е. Григорова, М. Христов, П. Пешев, Д. Нихтянова, Н. Величкова, Г. Атанасова</i> , Сорбционни свойства по отношение на водород на композит $MgH_2 - V_2O_5$ получен чрез механоактивиране	287
<i>Р. Адоньи, Е.Г. Кирилова, Н.Гр. Ваклиева-Банчева</i> , Редуциране на пиковите въздействия от замърсители върху околната среда за многоцелеви периодични и биохимични производства	295
<i>М. Дж. Пурвагар</i> , Определяне на нивата на феритин и на желязо в наномасшаби след двумесечно прогресивно физическо натоварване	300
<i>С. Дочев, А. Петкова, П. Ретайльо, И. Манолов</i> , Синтез и кристална структура на амониева сол на 4-хидрокси-3-[(2-оксо-2Н-хромен-3-ил)-(3,4,5-триметоксифенил)метил]хромен-2-он	309
<i>Мортеза Явари</i> , Пермутационна симетрия на изомери на фулерен с 82 въглеродни атома	313
<i>А. Гариб, М. Джахангир, М. Рошани, Й. В. Схеерен</i> , У Кръстосана алдолна кондензация на кетони с ароматни и не-ароматни алдехиди с Preyssler'ов хетерокиселинен катализатор върху силициев диоксид като носител.....	325
<i>С.С. Митич, Б.Т. Стоянович, М.Н. Стойкович, М.Н. Митич, Й.Л. Павлович</i> , Общи феноли, флавоноиди и антиоксидантна активност на различни ябълкови сортове	331
<i>М.Л. Фигероа-Валверде, Ф. Диас-Седийо, Е. Гарсия-Сервера, Е. Поол Гомес, М. Росас-Нехтикапа, М. Лопес-Рамос</i> , Конструирание и синтеза на две производни на сулфотиазола в три-компонентна система	335
<i>М. Мохамедиан, А. К. Хаги</i> , Някои аспекти на мрежа от многослойни хитозанови нановлакна, получени при електропредене.....	346
<i>М. К. Хурани, А. И. Уехбе</i> , Електрохимично охарактеризиране на йордански монети	352
<i>А. Мобинихаледи, М. А. Бодаги Фард, Ф. Сасани, М. А. Амролахи</i> , Синтеза на някои биологично-активни дихидроперимидини, катализирани от молекулен йод	356
<i>К. Игнатова</i> , Електроотлагане на Ag и на Ag-Ni прахове в стационарен и в импулсен режим ...	365
<i>Е. Младенова, Д. Владикова, З. Стойнов, А. Чесно, А. Торел, М. Кръпчанска</i> , Изследване на газовата пропускливост в двойно мембранна горивна клетка	370
<i>А. Гариб, Н. Н. Песян, Б. Р. Х. Хорасани, М. Рошани, Й. В. Схеерен</i> , N-пропил-сулфаминова киселина, свързана със силициев диоксид: рециклируем катализатор за синтеза на спиро-оксиндоли чрез три-компонентна реакция, стимулирана от микровълни	378
<i>З. Ласеми, Р. Хосеинзаде, М. Таджбаки, М. Мохаджерани</i> , Етилен бис-(N-метил имидазол) ди-трибромид: ефективен и многократно използван реагент за окислението на тиоли и сулфиди	384
<i>Кс. Мей, Ш. Шу, Ф. Ченг, Г. Хуанг</i> , Синтеза на ди- N-ацетил-β-хитобиозил N-гликотиазолин	387
<i>П.Л. Меена, Н. Кумар, А.С. Меена, К.С. Меена, П.К. Джайн</i> , Изчисляване на атомни спектроскопски термове за f^2 и f^{12} орбитални конфигурации чрез сравнително изследване и символи на термовете	393
<i>А. Хайян, Ф.С. Миджали, М.А. Хашим, М. Хайян, И.М. АлНашеф</i> , Използването на хлор-сулфонова киселина за превръщане на свободните мастни киселини от нискокачествено палмово масло в метилови естери при производството на биодизел ..	399